

Electron Correlation Methodology

ACS SYMPOSIUM SERIES **958**

Electron Correlation Methodology

Angela K. Wilson, Editor
University of North Texas

Kirk A. Peterson, Editor
Washington State University

Sponsored by the
**ACS Divisions of Physical Chemistry and
Computers in Chemistry**



American Chemical Society, Washington, DC

In Electron Correlation Methodology; Wilson, A., et al.;
ACS Symposium Series; American Chemical Society: Washington, DC, 2007.



Electron correlation methodology

Library of Congress Cataloging-in-Publication Data

Electron correlation methodology / Angela K. Wilson, editor, Kirk A. Peterson, editor ; sponsored by the ACS Divisions of Physical Chemistry and Computers in Chemistry.

p. cm.—(ACS symposium series ; 958)

Includes bibliographical references and index.

ISBN 13: 978-0-8412-3843-5 (alk. paper)

1. Electron configuration—Congresses.

I. Wilson, Angela K. II. Peterson, Kirk A. III. American Chemical Society. Division of Physical Chemistry. IV. American Chemical Society. Division of Computers in Chemistry

QC176.8.E4E33 2007
530.4'11—dc22

2006052651

The paper used in this publication meets the minimum requirements of American National Standard for Information Sciences—Permanence of Paper for Printed Library Materials, ANSI Z39.48-1984.

Copyright © 2007 American Chemical Society

Distributed by Oxford University Press

All Rights Reserved. Reprographic copying beyond that permitted by Sections 107 or 108 of the U.S. Copyright Act is allowed for internal use only, provided that a per-chapter fee of \$36.50 plus \$0.75 per page is paid to the Copyright Clearance Center, Inc., 222 Rosewood Drive, Danvers, MA 01923, USA. Republication or reproduction for sale of pages in this book is permitted only under license from ACS. Direct these and other permission requests to ACS Copyright Office, Publications Division, 1155 16th Street, N.W., Washington, DC 20036.

The citation of trade names and/or names of manufacturers in this publication is not to be construed as an endorsement or as approval by ACS of the commercial products or services referenced herein; nor should the mere reference herein to any drawing, specification, chemical process, or other data be regarded as a license or as a conveyance of any right or permission to the holder, reader, or any other person or corporation, to manufacture, reproduce, use, or sell any patented invention or copyrighted work that may in any way be related thereto. Registered names, trademarks, etc., used in this publication, even without specific indication thereof, are not to be considered unprotected by law.

PRINTED IN THE UNITED STATES OF AMERICA

American Chemical Society
Information Resource Center
1155 Sixteenth St NW
Washington DC 20036

Foreword

The ACS Symposium Series was first published in 1974 to provide a mechanism for publishing symposia quickly in book form. The purpose of the series is to publish timely, comprehensive books developed from ACS sponsored symposia based on current scientific research. Occasionally, books are developed from symposia sponsored by other organizations when the topic is of keen interest to the chemistry audience.

Before agreeing to publish a book, the proposed table of contents is reviewed for appropriate and comprehensive coverage and for interest to the audience. Some papers may be excluded to better focus the book; others may be added to provide comprehensiveness. When appropriate, overview or introductory chapters are added. Drafts of chapters are peer-reviewed prior to final acceptance or rejection, and manuscripts are prepared in camera-ready format.

As a rule, only original research papers and original review papers are included in the volumes. Verbatim reproductions of previously published papers are not accepted.

ACS Books Department

Preface

Fundamental challenges in computational chemistry include the high computational cost of ab initio calculations in terms of time, memory, and disk space requirements; difficulties that arise when standard advanced computational treatments are used to describe processes such as bond breaking; determination of the best approach toward functional development in density functional theory, understanding the means for quantitative prediction of thermonuclear kinetics; and computational chemistry treatment of transition metal systems for reliable prediction of molecular properties. This book addresses these important problems, featuring chapters by leading computational chemists and physicists.

Topics include the development of methodology and assessment of approaches used to address bond breaking, including both single- and multireference treatment. The book also discusses improved methods toward the reduction of computational cost, including MP2-R12 and Wigner approaches. An overview of the performance of methods in the prediction of thermochemistry and thermochemical kinetics is discussed. The book also discusses the development of correlation consistent basis sets for transition metal species, including a thorough suite of state-of-the-art benchmark calculations utilizing the newly developed sets; and covers the rationale as to the most suitable form of the exchange-correlation energy in density functional theory.

Acknowledgment

We thank the contributing authors for their manuscripts as well as for their patience through this process. The staff at the American Chemical Society (ACS) Books Department are also thanked for their time and helpfulness. Finally, for financial support of the symposium, we gratefully acknowledge the generosity of the ACS Division of Computers in Chemistry, the Donors of the ACS Petroleum Research

Fund, the ACS Division of Physical Chemistry, Pacific Northwest National Laboratory, and MCNC.

Angela K. Wilson
Department of Chemistry
University of North Texas
Denton, TX 76203–5070

Kirk A. Peterson
Department of Chemistry
Washington State University
Pullman, WA 99164–4630

Chapter 1

Explicitly Correlated Basis Functions for Large Molecules

Claire C. M. Samson and Wim Klopper

Theoretical Chemistry Group, Debye Institute, Utrecht University,
P.O. Box 80052, NL-3508 TB Utrecht, The Netherlands

The MP2-R12 methods are developed further towards applications to spatially extended molecular systems. Firstly, a large auxiliary basis set is employed for the resolution-of-identity approximation (RI approximation, that is, a closure relation) such that smaller standard Gaussian basis sets can be used to expand the wave function. This method yields much better convergence to the limit of a complete basis of second-order Møller–Plesset (MP2) theory than the standard MP2 method using the same correlation-consistent Gaussian basis sets. Secondly, a new correlation factor of the form $r_{12}\exp(-\gamma r_{12}^2)$ is investigated, where the Gaussian geminal dampens the linear r_{12} term at long interelectronic distances. Many long-range integrals then vanish, depending on the magnitude of the adjustable parameter γ . Finally, a similarity-transformed Hamiltonian is investigated using a correlation function $\exp(F)$ similar to the one used for the new MP2-R12 method.

R12 methods: Wave functions linear in r_{12}

One of the main bottlenecks that is encountered when attempting to find approximate solutions of the time-independent Schrödinger equation for many-electron systems is the extremely slow convergence of the computed wave function towards the 'exact' wave function with increasingly large basis sets of atomic orbitals. This major bottleneck arises from the singularity of the Coulomb repulsion at electron–electron coalescence. Figure 1 illustrates the cusp of the He ground-state wave function, which is shown as a function of the angle between the two electrons located on a sphere of radius $0.5 a_0$.

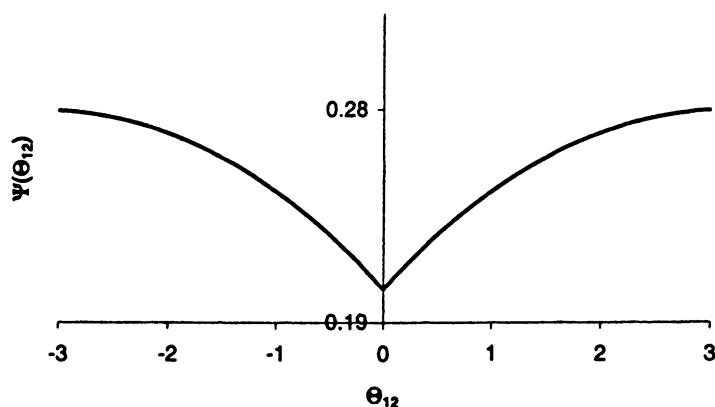


*Figure 1. Coulomb hole of the He ground state.
(Reproduced with permission from Molecular Electronic-Structure Theory
p. 262. Copyright John Wiley and Sons Limited.)*

In the early days of quantum mechanics (1,2), a drastic improvement of the description of the electron correlation was obtained when terms depending explicitly on the interelectronic distances $r_{ij} = |\mathbf{r}_i - \mathbf{r}_j|$ were included into the wave function. Unfortunately, the appearance of such linear r_{12} terms gives rise to arduous integrals to evaluate, making basically impossible the application of these explicitly correlated methods for atoms and molecules with more than four electrons. During the late 1980's and early 1990's (3,4), however new developments based on this fundamental concept have occurred (*i.e.*, the R12 methods), which have extended the application range of the explicitly correlated methods to small and average-sized molecules.

Nevertheless, R12 calculations on very large molecular systems are still computationally very demanding for the following reasons: Firstly, large basis

sets should be employed to satisfy the RI approximation. Secondly, the linear r_{12} term generates a significant number of large two-electron integrals when r_{12} is large, although these integrals don't contribute to the energy calculation. By avoiding the computation of these unnecessary integrals, one should be able to save a considerable amount of computational costs.

Formulation of R12 theory

In the notation of second quantization, the R12 wave function is expressed as follows:

$$\Psi_{R12} = \Phi + \sum_{ia} t_a^i \Phi_i^a + \sum_{ijab} t_{ab}^{ij} \Phi_{ij}^{ab} + \sum_{ijkl} t_{kl}^{ij} \Psi_{ij}^{kl} + \sum_{ijkabc} t_{abc}^{ijk} \Phi_{ijk}^{abc} + \dots, \quad (1)$$

where Φ is the Hartree-Fock determinant, i, j, k, \dots denote occupied spin orbitals, and a, b, c, \dots denote virtual spin orbitals contained in the finite spin orbital basis. The amplitudes $t_a^i, t_{ab}^{ij}, \dots$ represent the expansion coefficients of the respective excitations $\Phi_i^a, \Phi_{ij}^{ab}, \dots$. Each excited determinant can be written as a product of annihilation and creation operators as shown for the single excitations,

$$\Phi_i^a = a_a^+ a_i \Phi. \quad (2)$$

$a_a^+, a_b^+ \dots$ are creation operators and a_i, a_j, \dots are annihilation operators. The only difference between the R12 expansion of the wave function and the conventional configuration-interaction (or coupled-cluster) expansion, is the appearance of a new set of double excitations,

$$\Psi_{ij}^{kl} = \sum_{\alpha\beta} (r_{\alpha\beta}^{kl} - r_{\alpha\beta}^{lk}) a_\beta^+ a_\alpha^+ a_i a_j \Phi, \quad (3)$$

where α, β, \dots denote virtual spin orbitals outside the finite spin orbital basis $\{\varphi_p\}$. Hence, the union of the two sets of p, q, \dots and α, β, \dots spin orbitals represents a complete set,

$$\sum_p |\varphi_p(1)\rangle \langle \varphi_p(1)| + \sum_\alpha |\varphi_\alpha(1)\rangle \langle \varphi_\alpha(1)| = 1. \quad (4)$$

The interelectronic distance is introduced into the wave function through the following two-electron integrals:

$$r_{\alpha\beta}^{kl} = \langle \varphi_{\alpha}(1) \varphi_{\beta}(2) | r_{12} | \varphi_k(1) \varphi_l(2) \rangle. \quad (5)$$

An externally contracted MP2 method

The MP2-R12 method can be regarded as an externally contracted MP2 method with (contracted) double excitations into a complete spin orbital basis. To illustrate this, we shall in the following discuss an externally contracted MP2 method that comprises contracted double excitations into a subspace $\{\varphi_p\}$, which has been orthogonalized against the orbital basis $\{\varphi_p\}$,

$$\Psi_{\text{EC-MP2}} = \Phi + \sum_{ijab} t_{ij}^u \Phi_{ij}^{ab} + \sum_{ijkl} t_{ij}^u \left(\sum_{p'q'} (r_{p'q'}^{kl} - r_{p'q'}^{lk}) \Phi_{ij}^{p'q'} \right), \quad (6)$$

with

$$r_{p'q'}^{kl} = \langle \varphi_{p'}(1) \varphi_{q'}(2) | r_{12} | \varphi_k(1) \varphi_l(2) \rangle = \langle p'q' | r_{12} | kl \rangle. \quad (7)$$

In the following, the latter notation is adopted for simplicity. The only difference between the conventional MP2 and EC-MP2 wave functions is the appearance of a new set of double excitations with expansion coefficients t_{ij}^u . These double excitations are spanned by primitive functions $\Phi_{ij}^{p'q'}$ contracted through the contraction coefficients $(r_{p'q'}^{kl} - r_{p'q'}^{lk})$. If the orthogonal subspace would be the true complementary subspace of the cc-pVnZ basis, the externally contracted MP2 method would be strictly equivalent to the explicitly correlated MP2 method. In Table I, we compare the valence-shell MP2 correlation energies of H₂O obtained from the conventional and externally contracted MP2 methods.

The orthogonal subspace used in Table I is spanned by the large basis O=19s14p8d6f4g3h2i, H=9s6p4d3f2g. The number of basis functions of the large basis that are (nearly) linearly dependent on the cc-pVnZ basis is drastically increased with the cc-pVnZ basis sets. We observe that the externally contracted MP2 calculations converge faster to the MP2 limit. As expected, the energies from the externally contracted MP2 method lie between the standard

Table I. Valence-shell MP2 correlation energy (in mE_h) of H₂O

<i>Basis</i>	<i>MP2</i>	+ <i>Orthogonal subspace</i>	<i>Linearly dependent</i>
cc-pVDZ	-201.6	-231.0	1
cc-pVTZ	-261.5	-273.0	7
cc-p VQZ	-282.8	-287.3	11
cc-pV5Z	-291.5	-293.0	117
Large basis ^{a)}	-296.1		
Limit	-300.5		

a) O= 19s14p8d6f4g3h2i, H=9s6p4d3f2g

SOURCE: Reproduced with permission from *Quantum-Mechanical Prediction of Thermo-Chemical Data* by Cioslowski, 2001; p.21. Copyright 2001 Kluwer.)

MP2 values and the energy obtained in the (uncontracted) large basis. As the size of the orthogonal subspace increases the computational effort of the MP2 calculation, the externally contracted MP2 methods does not appear to be a practicable method. It merely illustrates the explicitly correlated MP2-R12 theory.

Orbital-invariant MP2-R12 method

Contrarily to conventional MP2 theory, the original formulation of MP2-R12 theory (3,4) did not provide the same results when canonical or localized molecular orbitals were used. Indeed, for calculations on extended molecular systems, unphysical results were obtained when the canonical Hartree–Fock orbitals were rather delocalized (5). In order to circumvent this problem, an orbital-invariant MP2-R12 formulation was introduced in 1991, which is the preferred method since then (6),

$$\Psi_{\text{MP2-R12}} = \Phi + \sum_{ijab} t_{ab}^{ij} \Phi_{ij}^{ab} + \sum_{ijkl} t_{kl}^{ij} \left(\sum_{\alpha\beta} (r_{\alpha\beta}^{kl} - r_{\alpha\beta}^{lk}) \Phi_{ij}^{\alpha\beta} \right), \quad (8)$$

with

$$\sum_{\alpha} |\alpha\rangle\langle\alpha| = 1 - \sum_{\text{p}} |\text{p}\rangle\langle\text{p}| = 1 - \hat{\text{P}}. \quad (9)$$

The matrix elements needed for the evaluation of the MP2-R12 energy can be computed as follows:

$$\begin{aligned} \sum_{\alpha\beta} \langle \Phi | \hat{H}^{(1)} | \Phi_{\alpha\beta}^{ab} \rangle \bar{r}_{\alpha\beta}^{-kl} &= \sum_{\alpha\beta} \langle ij - ji | r_{12}^{-1} | \alpha\beta \rangle \langle \alpha\beta | r_{12} | kl - lk \rangle \\ &= \langle ij - ji | r_{12}^{-1} (1 - \hat{P}_1)(1 - \hat{P}_2) r_{12} | kl - lk \rangle, \end{aligned} \quad (10)$$

where $H^{(1)}$ represents the perturbation (*i.e.*, fluctuation potential) to the Hartree-Fock Hamiltonian (*i.e.*, sum of Fock operators). It is difficult to evaluate the integrals of the type of Eq. 10 since three- and four-electron integrals occur. As an example, consider

$$\begin{aligned} \langle ij | r_{12}^{-1} (1 - \hat{P}_1)(1 - \hat{P}_2) r_{12} | kl \rangle &= \langle ij | r_{12}^{-1} r_{12} | kl \rangle - \langle ij | r_{12}^{-1} \hat{P}_1 r_{12} | kl \rangle \\ &\quad - \langle ij | r_{12}^{-1} \hat{P}_2 r_{12} | kl \rangle + \langle ij | r_{12}^{-1} \hat{P}_1 \hat{P}_2 r_{12} | kl \rangle \\ &= S_{ik} S_{jl} - \sum_p \langle ij p | r_{12}^{-1} r_{23} | p l k \rangle \\ &\quad - \sum_p \langle ij p | r_{12}^{-1} r_{13} | k p l \rangle + \sum_{pq} \langle ij | r_{12}^{-1} | p q \rangle \langle p q | r_{12} | kl \rangle. \end{aligned} \quad (11)$$

This inconvenience has been solved by introduction of the resolution-of-identity (RI) approximation,

$$\langle abc | r_{12}^{-1} r_{23} | def \rangle \cong \sum_p \langle ab | r_{12}^{-1} | dp \rangle \langle pc | r_{12} | ef \rangle. \quad (12)$$

However, the introduction of the RI approximation led to the need for large basis sets. In old R12 method, only one single basis was used for both the electronic wave function and the RI approximation. The new formulation of R12 theory presented here uses an independent basis set denoted auxiliary basis set for the RI approximation while we employ a (much) smaller basis set for the MP2 wave function (7). This auxiliary basis set makes it possible to employ standard basis sets in explicitly correlated MP2-R12 calculations.

Examples of R12 calculations

Benchmark calculations of the equilibrium atomization energies (AEs) of the small molecules CH_2 , H_2O , HF , N_2 , CO and F_2 are presented in Table II. The CCSD(T) calculations are performed in systematically increasing correlation-

consistent basis sets (cc-pCVnZ, n=2-6) and compared with the R12 results. In the cc-pCV6Z basis, the mean absolute deviation from the R12 reference values is 2.2 kJ/mol while it is 1.3 kJ/mol for the experimental AEs (corrected for vibrational and relativistic effects). The values illustrate that the cc-pCVnZ results properly converge towards the R12 values, which represent the basis set limit.

In Table III, we list Ne atom pair energies in mE_h . The results obtained with MP2-R12 theory using an auxiliary basis set coincide with the 'exact' atom pair energies. Using this large auxiliary basis is equivalent with computing all three-electron integrals in an exact manner (8).

Table II. Computed equilibrium atomization energies (AEs) at the CCSD(T)/cc-pCVnZ level (kJ/mol)

<i>n</i>	CH_2^a	H_2O	HF	N_2	CO	F_2	Δ_{mad}^b
2	693	875	530	841	1013	112	76.8
3	739	943	574	912	1059	147	25.3
4	751	964	586	936	1076	153	9.8
5	755	971	590	946	1081	157	4.3
6	756	973	592	950	1083	159	2.2
R12	757	975	593	954	1086	161	
Exptl. ^{c)}	757	975	593	956	1087	163	1.3

a) 1A_1 state.

b) Mean absolute deviation from R12 reference values.

c) Experimental AEs corrected for vibrational and relativistic effects.

Table III. Ne atom absolute pair energy / mE_h

<i>Pair</i>	<i>MP2</i>		<i>MP2-R12^{a)}</i>	
	Calc. ^{b)}	Extrap. ^{c)}	'Exact' ^{d)}	Auxiliary basis ^{e)}
$2s^2$	12.00	12.04	12.04	12.04
$2s2p$	86.98	87.19	87.18	87.18
$2p^2$	220.69	220.97	220.95	220.95
Total	319.67	320.20	320.17	320.17

a) In the orbital basis 20s14p11d9f7g5h.

b) $l \geq 12$, taken from Ref. 9.

c) Extrapolated for $1 \rightarrow \infty$, taken from Ref. 9.

d) From Ref. 8.

e) Using the auxiliary basis 32s24p18d15f12g9h6i.

R12 methods augmented with Gaussian geminals

By augmenting the linear correlation factor r_{12} by a Gaussian geminal of the form $\exp(-\gamma r_{12})$, many two-electron integrals become negligible for large distances between two localized molecular orbitals (Figure 2). The Gaussian functions dampen a large number of integrals that are arising in large molecular complexes.

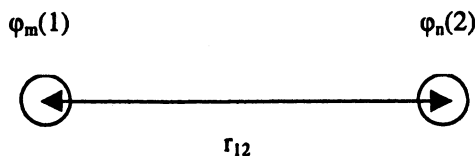


Figure 2. Explicitly correlated basis functions of the form $r_{12} \varphi_m(1) \varphi_n(2)$ that should be avoided in large molecules.

Explicitly correlated Gaussians (ECG) methods have already been developed earlier (10,11,12) and have been used for accurate calculations on small molecules. The main difference between these ECG methods and the use of Gaussian geminals in the framework of R12 theory is that in the latter, their purpose is to dampen the linear r_{12} term more than being a correlation factor on its own.

This new Gaussian function gives rise to five new non-standard two-electron integrals, whose analytical implementation has recently been described (13). They can be summarized as two-electron integrals with operators $r_{12}^k \exp(-\gamma r_{12}^2)$ with $k = 0,1,2,4$ and $c = 1$ or 2. It is remarkable that none of the five nonstandard two-electron integrals that arise from the use of the damped r_{12} factor requires much more effort than the usual two-electron integrals over Gaussian functions. This indicates that the damped-R12 method will be practicable for large systems.

We have explored the effect of the adjustable parameter γ on the number of vanishing integrals corresponding to the operator $r_{12} \exp(-\gamma r_{12}^2)$ by analyzing the behavior of a distribution of normalized s-type Gaussians with exponent $\zeta = 1/a_0^{-2}$. These functions are randomly distributed on the surface of a sphere with radius $R = 2(k-1)a_0$ (Figure 3). The effect of the damping is shown on this graph by the drastic reduction of significant integrals by about a factor of 10 from no damping to a damping of $\gamma = 1.0 a_0^{-2}$ for a distribution of ca. 200 s-type functions. Moreover, linear scaling is reached for $\gamma \geq 0.1 a_0^{-2}$.

The two main conditions on the damping factor γ is that it should be large enough to remove as many integrals as possible while small enough to retain the accuracy of the calculation. The optimum value for γ is yet to be determined.

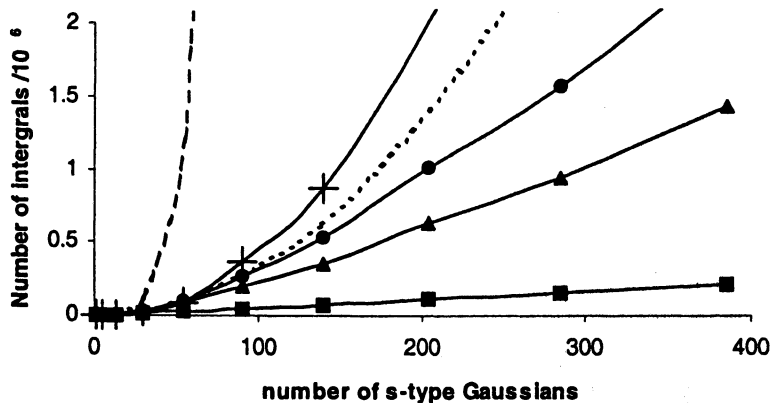


Figure 3. Number of significant integrals ($>10^{-12}$ a.u.) for $\gamma=0.00$ a_0^{-2} (crosses), $\gamma=0.05$ a_0^{-2} (dots), $\gamma=0.1$ a_0^{-2} (triangles), $\gamma=1.0$ a_0^{-2} (squares). The dashed line corresponds to the theoretical number of $n^3/8$ integrals and the dotted line represents the number of significant electron-repulsion integrals.

The aim of this new correlation factor is to associate it with a localization procedure such that it will be possible to predict the vanishing integrals beforehand from the distance between the localized molecular orbitals. This method will allow us to minimize the computational costs considerably since the long-range two-electron integrals represent the major part of the integrals to be computed in a large molecular system. Therefore, this new method in conjunction with auxiliary basis sets for the RI will make it possible to use R12 methods on much larger molecules than is possible today.

Similarity-transformed Hamiltonian

The aim of our similarity-transformed Hamiltonian is to improve the computation of the correlation energy of conventional configuration-interaction (CI) calculations. In this framework, the conventional wave function is multiplied by the correlation function (14,15,16)

$$\Psi = \exp(\mathbf{F})\Phi, \quad (13)$$

with Φ the standard CI-type expansion (*i.e.*, a linear combination of orbital products) and \mathbf{F} a correlation function. Since now the required integrals are

available from the newly developed R12-methods, we found it interesting to investigate the following correlation function:

$$F = \sum_m c_m \sum_{i < j} f_{ij}^m = \sum_m c_m \sum_{i < j} r_{ij} \exp(-\gamma_m r_{ij}^2), \quad (14)$$

where c_m and γ_m are adjustable parameters.

The Schrödinger equation multiplied by $\exp(-F)$ from the left becomes:

$$\exp(-F) \hat{H} \exp(F) \Phi = E \Phi, \text{ that is, } \hat{H}^F \Phi = E \Phi. \quad (15)$$

\hat{H}^F is the non-Hermitian similarity transformed Hamiltonian.

The implementation of the above described correlation function is described in detail in Ref. (17). Figure 4 illustrates the efficiency of the method for the He ground-state energy as a function of the basis sets. Already for basis sets with s- and p-functions, the similarity-transformed Hamiltonian shows a better accuracy than the conventional CI method.

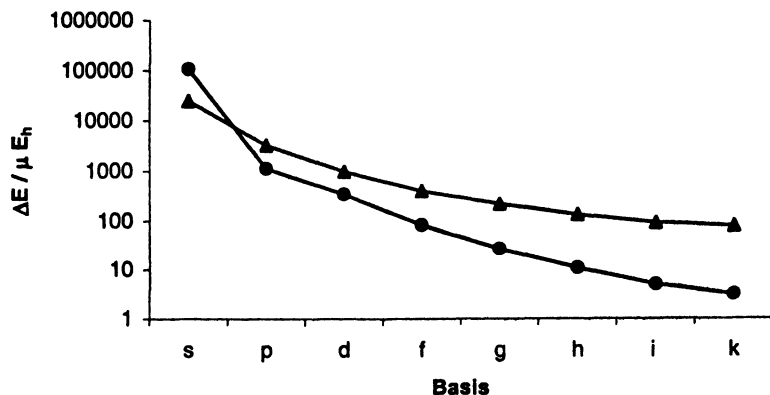


Figure 4. Calculations of the He ground-state energy in subsets of a $19s16p14d12f10g8h6i4k$ basis, $\gamma=0$, $c=1/2$. The circles represent the similarity-transformed results and the triangles the conventional results.

Conclusions

The recent developments in R12 methodology (auxiliary basis sets, damping procedure) seem promising to investigate large molecular systems in the future. All the mentioned methods are implemented in the Dalton (18) source code.

The similarity-transformed Hamiltonian method has so far been applied only to two-electron systems. Using closure (*i.e.*, RI) approximations, this technique will be generalized to many-electron systems (16).

Acknowledgments

The research of W.K. has been made possible by a fellowship of the Royal Netherlands Academy of Arts and Science. This research has been partially supported by COST Chemistry Action D9 (Working Group 13/98). The authors thank Trygve Helgaker (Oslo), Jozef Noga (Bratislava) and Henk J.A. Zweistra (Utrecht) for fruitful collaborations.

References

1. Slater, J.C. *Phys. Rev.* **1928**, *31*, 333.
2. Hylleraas, E.A. *Z. Phys.* **1929**, *54*, 347.
3. Kutzelnigg, W. *Theor. Chim. Acta* **1985**, *68*, 445.
4. Kutzelnigg, W.; Klopper, W. *J. Chem. Phys.* **1991**, *94*, 1985.
5. Klopper, W.; Kutzelnigg, W. *J. Chem. Phys.* **1991**, *94*, 2020.
6. Klopper, W. *Chem. Phys. Lett.* **1991**, *186*, 583.
7. Klopper, W.; Samson, C.C.M. *J. Chem. Phys.* **2002**, *116*, 6397.
8. Wind, P., Klopper, W., Helgaker, T. *Theor. Chem. Acc.* **2002**, *107*, 173.
9. Flores, J.R. *Phys. Rev. A* **1992**, *46*, 6063.
10. Cencek, W., Rychlewski, J. *J. Chem. Phys.* **1995**, *102*, 2533.
11. Bukowski, R., Jeziorski, B., Szalewicz, K. *J. Chem. Phys.* **1999**, *110*, 4165.
12. Persson, B.J.; Taylor, P.R. *J. Chem. Phys.* **1996**, *105*, 5915.
13. Samson, C.C.M.; Klopper, W.; Helgaker, T. *Comp. Phys. Commun.* (in the press).
14. Hirschfelder, J.O. *J. Chem. Phys.* **1963**, *39*, 3145.
15. Handy, N.C. *Mol. Phys.* **1973**, *26*, 169.
16. Hino, O.; Tanimura, Y.; Ten-no, S. *J. Chem. Phys.* **2001**, *115*, 7865.
17. Zweistra, H.J.A.; Samson, C.C.M.; Klopper, W. *Collect. Czech. Chem. Commun.* (submitted).

18. Dalton, *a molecular electronic structure program*, Release 1.2 (2001), written by Helgaker, T.; Jensen, H.J.Aa.; Jørgensen, P.; Olsen, J.; Ruud, K.; Ågren, H.; Auer, A.A.; Bak, K.L.; Bakken, V.; Christiansen, O.; Coriani, S.; Dahle, P.; Dalskov, E.K.; Enevoldsen, T.; Fernandez, B.; Hättig, C.; Hald, K.; Halkier, A.; Heiberg, H.; Hettema, H.; Jonsson, D.; Kirpekar, S.; Kobayashi, R.; Koch, H.; Mikkelsen, K.V.; Norman, P.; Packer, M.J.; Pedersen, T.B.; Ruden, T.A.; Sanchez, A.; Saue, T.; Sauer, S.P.A.; Schimmelpfennig, B.; Sylvester-Hvid, K.O.; Taylor, P.R.; Vahtras, O.

Chapter 2

Uniform Density Limit of Exchange-Correlation Energy Functionals

John P. Perdew, Jianmin Tao, and Stephan Kümmel

Department of Physics and Quantum Theory Group, Tulane University,
New Orleans, LA 70118

We present theoretical and practical reasons why a density functional for the exchange-correlation energy should be essentially exact in the uniform density limit. In this limit, the exchange energy is known exactly, and the correlation energy is known to within less than 1 millihartree in the range of valence-electron or lower densities. Some density functionals perform well in this limit, while others do not. Functionals with many parameters fitted to chemical data tend to fail in this limit, and also for real solids. The spin resolution of the correlation energy of the spin-unpolarized uniform electron gas seems simple but unlike that of the widely-used ansatz of Stoll et al., and its low-density limit brings a surprise: a positive parallel-spin contribution in the spin-unpolarized case.

Why the Uniform Density Limit?

The first density functional for the exchange-correlation energy was the local spin density (LSD) approximation [1, 2]

$$E_{xc}^{LSD}[n_{\uparrow}, n_{\downarrow}] = \int d^3r n(\mathbf{r}) \varepsilon_{xc}(n_{\uparrow}(\mathbf{r}), n_{\downarrow}(\mathbf{r})), \quad (1)$$

where $\varepsilon_{xc}(n_{\uparrow}, n_{\downarrow}) = \varepsilon_x + \varepsilon_c$ is the exchange-correlation energy per particle of an electron gas with uniform spin densities n_{\uparrow} and n_{\downarrow} . This was for decades (and to some extent still is) the standard approximation for electronic structure calculations in condensed matter physics. The generalized gradient approximation (GGA) [3–10]

$$E_{xc}^{GGA}[n_{\uparrow}, n_{\downarrow}] = \int d^3r f(n_{\uparrow}, n_{\downarrow}, \nabla n_{\uparrow}, \nabla n_{\downarrow}) \quad (2)$$

made density functional theory popular in quantum chemistry as well. More recently, meta-GGAs [11–16]

$$E_{xc}^{meta-GGA}[n_{\uparrow}, n_{\downarrow}] = \int d^3r f(n_{\uparrow}, n_{\downarrow}, \nabla n_{\uparrow}, \nabla n_{\downarrow}, \nabla^2 n_{\uparrow}, \nabla^2 n_{\downarrow}, \tau_{\uparrow}, \tau_{\downarrow}) \quad (3)$$

have been developed, where

$$\tau_{\sigma}(\mathbf{r}) = \frac{1}{2} \sum_{\alpha}^{occ} |\nabla \psi_{\alpha\sigma}(\mathbf{r})|^2 \quad (4)$$

is the kinetic energy density of the occupied Kohn-Sham orbitals of spin σ . Hybrid functionals [17–24], which superpose the GGA or meta-GGA form with a fraction of exact exchange, approach chemical accuracy at modest computational cost.

The uniform density limit for any of these functionals is easily evaluated: Just set $\nabla n_{\sigma} = 0, \nabla^2 n_{\sigma} = 0$,

$$\tau_{\sigma} = \frac{3}{10} (6\pi^2)^{2/3} n_{\sigma}^{5/3}, \quad (5)$$

And $E_x^{\text{exact}} = E_x^{\text{LSD}}$. (We use atomic units with energies in hartree and distances in bohr.) The first GGA's (other than Ref. 3) and the first hybrid were designed to be right in the uniform density limit. But some recent functionals have been constructed semi-empirically by fitting to chemical data, and the uniform density limit has been sacrificed to improve the fit.

We argue that the uniform density limit is an important theoretical constraint which should not be sacrificed in a functional that needs to be universal. The density functionals discussed here can be exact *only* for uniform densities. Approximations ought to be exact in those limits where they can be. Moreover, the unexpected success of LSD outside its formal domain of validity

(very slowly-varying densities $n_{\uparrow}(\mathbf{r})$ and $n_{\downarrow}(\mathbf{r})$) has been explained [22,25–27] by the fact that LSD inherits exact constraints on from its underlying model system, the uniform gas, and these constraints plus others have been used to construct non-empirical GGA's [8, 9, 28] and meta-GGA's [16].

On the practical side, we note that nature provides a number of extended systems like solid metals [29, 30], metal clusters [31], and semiconductors [30, 32]. These systems have much in common with the uniform electron gas, and their ground-state properties (lattice constants [29, 30, 32], bulk moduli [29, 30, 32], cohesive energies [29], surface energies [30, 31], etc.) are typically described much better by functionals (including even LSD) which have the right uniform density limit than by those that do not. There is no sharp boundary between quantum chemistry and condensed matter physics. A good density functional should describe all the continuous gradations between localized and delocalized electron densities, and all the combinations of both (such as a molecule bound to a metal surface a situation important for catalysis).

Recent work [16,19–21] suggests that functionals which respect the uniform density limit and other exact constraints can still achieve high accuracy for molecules. Just as the empirical electron-ion pseudopotentials of the 1960's have been replaced by non-empirical ones, we expect that the empirical density functionals of the 1990's will be replaced by ones that are fully or largely non-empirical.

What is Known About the Uniform Density Limit?

The uniform density limit has been well-studied by a combination of analytic and numerical methods. This section will review some (but not all) of what is known about it.

Define the density parameter r_s as the radius of a sphere that on average contains one electron:

$$\frac{4\pi}{3}r_s^3 = \frac{1}{n} \quad \text{where } n = n_{\uparrow} + n_{\downarrow}, \quad (6)$$

and the relative spin polarization ζ as

$$\zeta = \frac{n_{\uparrow} - n_{\downarrow}}{n} \quad (-1 \leq \zeta \leq 1). \quad (7)$$

In the high-density ($r_s \rightarrow 0$) limit, exchange dominates over correlation:

$$\lim_{r_s \rightarrow 0} \frac{\varepsilon_{xc}(r_s, \zeta)}{\varepsilon_x(r_s, \zeta)} = 1. \quad (8)$$

In the low-density limit ($r_s \rightarrow \infty$), correlation and exchange are of comparable strength, and are together independent of ζ . ε_{xc} is then nearly equal to the electrostatic energy per electron of the Wigner crystal [33–36]:

$$\lim_{r_s \rightarrow \infty} \frac{\varepsilon_{xc}(r_s, \zeta)}{\varepsilon_x(r_s, \zeta = 0)} \approx 1.96. \quad (9)$$

The exchange energy is known exactly:

$$\varepsilon_x(r_s, \zeta) = -\frac{3}{4\pi} \left(\frac{9\pi}{4} \right)^{1/3} \frac{1}{2} \left[(1+\zeta)^{4/3} + (1-\zeta)^{4/3} \right] / r_s, \quad (10)$$

so that

$$\varepsilon_x(r_s, \zeta = 0) = -\frac{0.458165}{r_s}, \quad \varepsilon_x(r_s, 1) = 2^{1/3} \varepsilon_x(r_s, 0). \quad (11)$$

Since the uniform electron density is perfectly neutralized by a rigid uniform positive background, the total energy per electron of the uniform gas is just $t_s + \varepsilon_{xc}$, where the non-interacting kinetic energy is

$$t_s(r_s, \zeta) = \frac{3}{10} \left(\frac{9\pi}{4} \right)^{2/3} \frac{1}{2} \left[(1+\zeta)^{5/3} + (1-\zeta)^{5/3} \right] / r_s^2. \quad (12)$$

The correlation energy ε_c is known analytically in the high- and low-density limits. For typical valence electron densities ($1 \leq r_s \leq 10$) and lower densities ($r_s > 10$), it is known numerically from release-node Diffusion Monte Carlo studies [33]. Various parametrizations have been developed to interpolate between the known limits while fitting the Monte Carlo data. The first, simplest and most transparent is that of Perdew and Zunger (PZ) [34]:

$$\begin{aligned} \varepsilon_c(r_s, \zeta = 0) = & \\ & 0.0311 \ln r_s - 0.048 + 0.0020 r_s \ln r_s - 0.0116 r_s \quad (r_s \leq 1) \\ \text{or} & \quad -0.1423 / (1 + 1.0529 \sqrt{r_s} + 0.3334 r_s), \quad (r_s \geq 1) \end{aligned} \quad (13)$$

$$\begin{aligned} \varepsilon_c(r_s, \zeta = 1) = & \\ & 0.01555 \ln r_s - 0.0269 + 0.0007 r_s \ln r_s - 0.0048 r_s \quad (r_s \leq 1) \\ \text{or} & \quad -0.0843 / (1 + 1.3981 \sqrt{r_s} + 0.2611 r_s), \quad (r_s \geq 1) \end{aligned} \quad (14)$$

$$\varepsilon_c(r_s, \zeta) = \varepsilon_c(r_s, 0) + f(\zeta)[\varepsilon_c(r_s, 1) - \varepsilon_c(r_s, 0)], \quad (15)$$

where an exchange-like interpolation between $\zeta = 0$ and $\zeta = 1$ is employed:

$$f(\zeta) = \frac{(1+\zeta)^{4/3} + (1-\zeta)^{4/3} - 2}{2^{4/3} - 2}. \quad (16)$$

Note in Eqs. (10), (13) and (14) the appearance of two length scales: r_s is the radius of the exchange hole, and $\sqrt{r_s}$ is the Thomas-Fermi screening length. Eqs. (13) and (14) have artificial discontinuities in their second derivatives with respect to r_s at $r_s = 1$. The discontinuity was removed and a more realistic ζ -dependence was introduced by Vosko, Wilk and Nusair [35] (VWN5, in the parlance of the Gaussian molecular code). A form simpler than VWN5 and containing additional information about the high-density limit was proposed by Perdew and Wang (PW92) [36], and another parametrization was made recently by Filatov and Thiel (FT) [37].

The first line in Tables I and II presents the PW92 values of $\varepsilon_c(r_s, \zeta)$ for $\zeta = 0$ (Table I) or 1 (Table II) at $r_s = 1, 2, 5, 10$. The next three lines show that, remarkably, VWN5, FT, and PZ never differ from PW92 by more than 0.2 millihartrees.

Analytic or semi-analytic many-body methods provide an independent estimate of $\varepsilon_c(r_s, \zeta)$. Before the Diffusion Monte Carlo work, the best calculation was probably that of Singwi, Sjölander, Tosi and Land (SSTL) [38] which was parametrized by Hedin and Lundqvist (HL) [39] and chosen as the $\zeta = 0$ limit of Moruzzi, Janak and Williams (MJW) [40]. Table I shows that HL agrees within 4 millihartrees with PW92. A more recent calculation along the same lines, but with a more sophisticated exchange-correlation kernel [42], agrees with PW92 to better than 1 millihartree.

The correlation energy can also be found from an approximate self-energy. An early example of this approach was the Gunnarsson-Lundqvist (GL) [41] parametrization, which shows larger deviations (up to 10 millihartree) from PW92 in Tables I and II. Recent and more sophisticated examples [43,44] agree within 2 millihartree with PW92.

The random phase approximation (RPA), to which the SSTL approach reduces when the exchange-correlation kernel is set to zero, is the simplest approximation that is right for the $\ln r_s$ term in the high-density limit of Eqs. (13) and (14). Tables I and II show that three parametrizations of RPA all agree rather well for $1 \leq r_s \leq 10$, although only PW92 gives the correct $r_s \rightarrow \infty$ limit of RPA. The first GGA [3] was an RPA functional. RPA itself is not a good approximation, but it has the interesting feature that *corrections* to full RPA may be described especially well by LSD or GGA [45].

Table I: The essentially-exact PW92 exchange-correlation energy per electron (in hartree) in a spin-unpolarized ($\zeta = 0$) uniform electron gas of density parameter r_s (in bohr), and the deviation (in hartree) of other approximations from PW92. [1 hartree = 27.21 eV = 627.5 kcal/mol.]

$\zeta = 0,$	$r_s =$	1	2	5
ϵ_{xc}^{PW92} [36]	-0.5180	-0.2739	-0.1198	-0.0644
$\epsilon_{xc} - \epsilon_{xc}^{PW92}$:				
VWN5 [35]	-0.0002	0.0000	-0.0001	-0.0001
FT [37]	-0.0001	-0.0001	0.0000	0.0000
PZ [34]	0.0002	-0.0003	-0.0001	0.0000
MJW,HL [40,39]	-0.0027	-0.0036	-0.0033	-0.0024
GL [41]	-0.0142	-0.0097	-0.0045	-0.0017
RPA (VWN) [35]	-0.0195	-0.0176	-0.0149	-0.0124
RPA (PW92) [36]	-0.0189	-0.0170	-0.0143	-0.0121
RPA (VBH) [2]	-0.0187	-0.0174	-0.0141	-0.0106
W [46,47]	0.0098	-0.0001	-0.0062	-0.0061
x-only ($-\epsilon_c^{PW92}$)	0.0598	0.0448	0.0282	0.0186
BLYP [6,7]	0.0204	0.0178	0.0148	0.0111
B3LYP [18]	0.0128	0.0111	0.0091	0.0066
HCTH [10]	-0.0118	0.0017	0.0060	0.0054
VS98 [13]	0.0043	0.0092	0.0086	0.0065
BGGA1 [24]	0.0298	0.0234	0.0153	0.0104
BGGA2 [24]	0.0175	0.0137	0.0090	0.0062

Table II: The essentially-exact PW92 exchange-correlation energy per electron (in hartree) in a spin-polarized ($\zeta = 1$) uniform electron gas of density parameter r_s , (in bohr), and the deviation (in hartree) of other approximations from PW92. [1 hartree = 27.21 eV = 627.5 kcal/mol.]

$\zeta = 1, r_s =$	1	2	5	10
ϵ_{xc}^{PW92} [36]	-0.6089	-0.3125	-0.1309	-0.0682
$\epsilon_{xc} - \epsilon_{xc}^{PW92}$:				
VWN5 [35]	0.0001	0.0000	0.0000	0.0000
FT [37]	0.0002	0.0000	-0.0001	0.0000
PZ [34]	-0.0001	-0.0002	-0.0001	0.0000
MJW [40]	-0.0096	-0.0098	-0.0089	-0.0072
GL [41]	-0.0196	-0.0149	-0.0090	-0.0052
RPA (VWN) [35]	-0.0203	-0.0186	-0.0157	-0.0131
RPA (PW92) [36]	-0.0202	-0.0185	-0.0156	-0.0130
RPA (VBH) [2]	-0.0203	0.0185	-0.0156	-0.0130
W [46,47]	-	-	-	-
x-only $-\epsilon_c^{PW92}$	0.0316	0.0239	0.0154	0.0105
BLYP [6,7]	0.0316	0.0239	0.0154	0.0105
B3LYP [18]	0.0217	0.0158	0.0095	0.0060
HCTH [10]	-0.0292	-0.0083	0.0013	0.0028
VS98 [13]	-0.0094	0.0007	0.0043	0.0040
BGGA1 [24]	0.0296	0.0238	0.0161	0.0112
BGGA2 [24]	0.0259	0.0205	0.0137	0.0094

How Do Energy Functionals Perform in the Uniform Density Limit?

As Tables I and II show, any functional that reduces to PW92, VWN5, FT or PZ in the uniform density limit is correct in that limit. The list of such functionals includes (a) LSD with these inputs, (2) the correlation GGA's P86 [5] (which reduces to PZ) and PW91 [8] or PBE [9, 28] (which reduce to PW92), when used with the exchange GGA's PW86 [4], B88 [6], PW91 [8], or PBE [9, 28], (3) the FT [14], PKZB [15], and PT [16] meta-GGA's (which reduce to FT and PW92, respectively), and (4) the three-parameter Becke hybrid B3PW91 [17], and the one-parameter PBE hybrid [19-21].

Some LSD calculations for solids are still performed with the MJW (HL), GL, and RPA (VBH) parametrizations, or even with the Wigner (W) [46, 47] approximation of 1934. Tables I and II show the extent to which these parametrizations are *not* proper LSD input.

The deviation of the exchange-only (x-only) approximation $\epsilon_x(r_s, \zeta)$ from $\epsilon_{xc}^{PW92}(r_s, \zeta)$ is $-\epsilon_c^{PW92}(r_s, \zeta)$, the magnitude of the PW92 correlation energy, which is also shown in Tables I and II. Although the correlation energy for $1 \leq r_s \leq 10$ is somewhat smaller than the exchange energy, correlation makes a key contribution to the atomization energies of molecules, the cohesive energies of solids, and the surface energies of metals. Thus the size of any other deviation from PW92 is large to the extent that it is comparable to the magnitude of the PW92 correlation energy, and so the deviations shown in Tables I and II should be compared to ϵ_c and not to ϵ_{xc} .

The BLYP [6, 7] and B3LYP [18] functionals are widely and successfully used in quantum chemistry. But, as Tables I and II show, they fail seriously in the uniform density limit, where they underestimate the magnitude of the correlation for $\zeta = 0$ and even more for $\zeta = 1$ (where BLYP reduces to the exchange-only approximation). For uniform densities, B3LYP reduces to a peculiar combination of 81% LYP and 19% RPA (VWN).

The functionals BLYP [6, 7], HCTH [10] and V598 [13] are all successful for molecules but display serious errors (often much worse than true LSD errors) for solids [29-32]. The same problems can be expected for B3LYP [18], and for BGGA1 [24], (a GGA hybrid) and BGGA2 [24] (a meta-GGA hybrid). Note that some of these are heavily parametrized empirical functionals, with 18 (HCTH), 20 (VS98), and 10 (BGGA1, BGGA2) empirical parameters. For the heavily empirical functionals, even the exchange energy is not exact in the uniform density limit, as Table III shows.

Table III: The ratio of approximate to exact exchange energy per electron of a uniform electron gas. For the approximations listed in Tables I and II but not listed here, this ratio is exactly 1. The Becke-Roussel exchange functional is a non-empirical meta-GGA based upon the hydrogen atom.

$\epsilon_x^{\text{approx}}(r_s, \zeta) / \epsilon_x^{\text{exact}}(r_s, \zeta)$	
HCTH [10]	1.093
VS98 [13]	1.053
BGGA1 [24]	1.010
BGGA2 [24]	1.006
Becke-Roussel [12]	0.974

Spin Resolution of the Correlation Energy in the Uniform Density Limit

The correlation energy ϵ_c can in principle be resolved as a sum of contributions from $\uparrow\uparrow$, $\downarrow\downarrow$, and $\uparrow\downarrow$ pair correlations. Such a resolution even in the uniform density limit, is not really needed for the construction of density functional approximations, and no assumption about the spin resolution has been made in any of the functionals from our research group (which are all correct by construction in the uniform density limit).

Spin resolution is however built into Becke's correlation functionals [22, 23, 24], and into many others [10, 13, 48] that have been patterned thereon. Typically these functionals rely upon the ansatz of Stoll et al. [49, 50] for the antiparallel- or opposite-spin contribution to the correlation energy:

$$\text{Stoll: } E_c^{\text{opp}}[n_\uparrow, n_\downarrow] = E_c[n_\uparrow, n_\downarrow] - E_c[n_\uparrow, 0] - E_c[0, n_\downarrow], \quad (17)$$

which is applied to the uniform-gas input to yield

$$\text{Stoll: } \frac{\epsilon_c^{\text{opp}}(r_s, \zeta = 0)}{\epsilon_c(r_s, \zeta = 0)} = 1 - \frac{\epsilon_c(2^{1/3}r_s, \zeta = 1)}{\epsilon_c(r_s, \zeta = 0)} \quad (18)$$

as the fraction of $\zeta = 0$ uniform-gas correlation energy arising from antiparallel spin pairs. The corresponding ratio for $\zeta = 1$ vanishes, of course.

Thus it is of some interest to know if the Stoll ansatz is correct, especially since several other ansätze have been developed and used as input to a spin-resolved pair correlation function. For example, Perdew and Wang (PW) [51, 52] proposed a scaling relation

$$\text{PW: } \frac{\epsilon_c^{\text{opp}}(r_s, \zeta = 0)}{\epsilon_c(r_s, \zeta = 0)} = 1 - 2^{-1/3} \frac{\epsilon_c(r_s, \zeta = 1)}{\epsilon_c(r_s, \zeta = 0)}, \quad (19)$$

Table IV: Spin resolution $\varepsilon_c^{\text{opp}}(r_s, \zeta = 0)/\varepsilon_c(r_s, \zeta = 0)$ of the correlation energy of the spin-unpolarized uniform electron gas, in various approximations described in the text. Shown are *estimates* for the fraction of the correlation energy arising from antiparallel- or opposite-spin correlations.

The GSB value is the best estimate here.

$\zeta = 0, r_s =$	1	2	5	10
GSB [55,56]	0.66	0.68	0.71	0.73
SKTP [53]	0.70	0.70	0.69	0.68
PW [51,52]	0.58	0.58	0.57	0.55
FT [37]	0.54	0.55	0.56	0.56
Stoll [49,50]	0.52	0.52	0.52	0.51

while Schmidt, Kurth, Tao and Perdew (SKTP) [53] proposed a different scaling relation

$$\text{SKTP: } \frac{\varepsilon_c^{\text{opp}}(r_s, \zeta = 0)}{\varepsilon_c(r_s, \zeta = 0)} = 1 - 2^{-5/6} \frac{\varepsilon_c(r_s, \zeta = 1)}{\varepsilon_c(r_s, \zeta = 0)}, \quad (20)$$

and Filatov and Thiel [37] proposed

$$\text{FT: } \frac{\varepsilon_c^{\text{opp}}(r_s, \zeta = 0)}{\varepsilon_c(r_s, \zeta = 0)} = \left\{ 1 + \exp \left[-1.429 r_s^2 / (\sqrt{r_s} + 2.072 r_s)^2 \right] \right\}^{-1}. \quad (21)$$

Table IV compares Eqs. (18)–(21) (using PW92 input) with Monte Carlo data [54] as fitted by Gori-Giorgi, Sachetti and Bachelet (GSB) [55, 56], which we take to be the standard of accuracy here. (The GSB data were kindly provided by Dr. Gori-Giorgi.) In the range $1 \leq r_s \leq 10$, the Stoll decomposition (18) and Eq. (19) seem inaccurate in comparison with the SKTP of Eq. (20), as pointed out by GSB, and so does Eq. (21).

The exact high- and low-density limits can be found from arguments given in Ref. [57]. For $\zeta = 0$ in the high-density limit (where the random phase approximation becomes exact), the parallel-spin and anti-parallel-spin *correlation energies* are equal [57], so

$$\lim_{r_s \rightarrow 0} \varepsilon_c^{\text{opp}}(r_s, \zeta = 0) / \varepsilon_c(r_s, \zeta = 0) = \frac{1}{2}. \quad (22)$$

In the low-density limit, the parallel-spin and anti-parallel-spin *exchange-correlation energies* are equal [57] because this is a classical limit in which spin

does not matter, and this observation plus Eq. (9) leads to the conclusion

$$\lim_{r_s \rightarrow \infty} \varepsilon_c^{\text{opp}}(r_s, \zeta = 0) / \varepsilon_c(r_s, \zeta = 0) = 1.02. \quad (23)$$

(But see the caveat of footnote 37 of Ref. [57].) To derive Eq. (23), note that (for $\zeta = 0$ and $r_s \rightarrow \infty$) $\varepsilon_c^{\text{opp}} = \varepsilon_{xc}^{\text{opp}} = \varepsilon_{xc} / 2 = (1.96\varepsilon_x) / 2 = 0.98\varepsilon_x$, while $\varepsilon_c = \varepsilon_{xc} - \varepsilon_x = 0.96\varepsilon_x$.

Eq. (23) is at first surprising, since it implies that the parallel-spin correlation energy for $\zeta = 0$ is slightly *positive* $[-0.02\varepsilon_c(r_s, \zeta = 0)]$ in the low-density limit. But this cannot be ruled out, since the total correlation energy is of course properly negative. Eqs. (22) and (23) are at least consistent with the increase with r_s of the GSB ratio $\varepsilon_c^{\text{opp}}(r_s, \zeta = 0) / \varepsilon_c(r_s, \zeta = 0)$, as shown in Table IV.

Only the Stoll and FT expressions display the proper $r_s \rightarrow 0$ limit, but neither of these expressions seems correct in the range $1 \leq r_s \leq \infty$. With a satisfactory spin resolution of the correlation energy, it should be possible by the approach of Ref. [57] to construct a satisfactory spin resolution of the pair correlation function of the uniform gas at all r_s (or by the approaches of Refs. [49] and [53] for most r_s of interest). We note that the formula

$$\frac{\varepsilon_c^{\text{opp}}(r_s, \zeta = 0)}{\varepsilon_c(r_s, \zeta = 0)} = \frac{0.5 + A\sqrt{r_s} + 1.02Br_s}{1 + C\sqrt{r_s} + Br_s} \quad (24)$$

has the expected limits, and is accurately fitted to the GSB data for $0.8 \leq r_s \leq 10$ when $A=1.996$, $B=0.1785$, $C=2.857$. The form of Eq. (24) is motivated by the Perdew-Zunger expressions of Eqs. (13) and (14).

For the total correlation energy $\varepsilon_c(r_s, \zeta)$, so much is known about the $r_s \rightarrow 0$ and $r_s \rightarrow \infty$ no limits that accurate values for all r_s and ζ can be found by interpolation [58], without ever using the Monte Carlo or other data. For the spin resolution $\varepsilon_c^{\text{opp}}(r_s, \zeta) / \varepsilon_c(r_s, \zeta)$, however, so little is known about these limits that we must and do rely on the Monte Carlo data. The spin resolution of Eq. (24) has recently been generalized to all ζ [59].

Acknowledgements

This work was supported in part by the National Science Foundation under Grant No. DMR01-35678, and in part by the Deutsche Forschungsgemeinschaft under an Emmy-Noether grant. We thank Dr. Paola Gori-Gorgi for providing the GSB data in Table IV, and the fit parameters for Eq. (24).

References

1. Kohn, W.; Sham, L.J. *Phys. Rev.* **1965**, *140*, A1133.
2. von Barth, U.; Hedin, L. *J. Phys. C: Solid State Phys.* **1972**, *5*, 1129.
3. Langreth, D.C.; Mehl, M.J. *Phys. Rev. B* **1983**, *28*, 1809.
4. Perdew, J.P.; Wang, Y. *Phys. Rev. B* **1986**, *33*, 8800.
5. Perdew, J.P. *Phys. Rev. B* **1986**, *33*, 8822.
6. Becke, A.D. *Phys. Rev. A* **1988**, *38*, 3098.
7. Lee, C.; Yang, W.; Parr, R.G. *Phys. Rev. B* **1988**, *37*, 785.
8. Perdew, J.P.; Chevary, J.A.; Vosko, S.H.; Jackson, K.A.; Pederson, M.R.; Singh, D.J.; Fiolhais, C. *Phys. Rev. B* **1992**, *46*, 6671.
9. Perdew, J.P.; Burke, K.; Ernzerhof, M. *Phys. Rev. Lett.* **1996**, *77*, 3865.
10. Hamprecht, F.A.; Cohen, A.J.; Tozer, D.J.; Handy, N.C. *J. Chem. Phys.* **1998**, *109*, 6264.
11. Perdew, J.P. *Phys. Rev. Lett.* **1985**, *55*, 1665.
12. Becke A.D.; Roussel, M.R. *Phys. Rev. A* **1989**, *39*, 3761.
13. Van Voorhis, T.; Scuseria, G.E. *J. Chem. Phys.* **1998**, *109*, 400.
14. Filatov, M.; Thiel, W. *Phys. Rev. A* **1998**, *57*, 189.
15. Perdew, J.P.; Kurth, S.; Zupan, A.; Blaha, P. *Phys. Rev. Lett.* **1999**, *82*, 2544.
16. Perdew, J.P.; Tao, J.; Scuseria, G.E.; Staroverov, V. work in progress.
17. Becke, A.D. *J. Chem. Phys.* **1993**, *98*, 5648.
18. Stevens, P.J.; Devlin, J.F.; Chabalowski, C.F.; Frisch, M.J. *J. Phys. Chem.* **1994**, *98*, 11623.
19. Perdew, J.P.; Ernzerhof, M.; Burke, K. *J. Chem. Phys.* **1996**, *105*, 9982.
20. Ernzerhof, M.; Scuseria, G.E. *J. Chem. Phys.* **1999**, *110*, 5029.
21. Adamo, C.; Barone, V. *J. Chem. Phys.* **1999**, *110*, 6158.
22. Becke, A.D. *J. Chem. Phys.* **1997**, *107*, 8554.
23. Schmider, H.L.; Becke, A.D. *J. Chem. Phys.* **1998**, *109*, 8188.
24. Becke, A.D. *J. Comp. Chem.* **1999**, *20*, 63.
25. Langreth, D.C.; Perdew, J.P. *Solid State Commun.* **1975**, *17*, 1425; *Phys. Rev. B* **1977**, *15*, 2884.
26. Gunnarsson, O.; Lundqvist, B.I. *Phys. Rev. B* **1976**, *13*, 4274.
27. Burke, K.; Perdew, J.P.; Ernzerhof, M. *J. Chem. Phys.* **1998**, *109*, 3760.
28. Perdew, J.P.; Burke, K.; Wang, Y. *Phys. Rev. B* **1996**, *54*, 16533.
29. Jaffe, J.E.; Lin, Z.; Hess, A.C. *Phys. Rev. B* **1998**, *57*, 11834.
30. Kurth, S.; Perdew, J.P.; Blaha, P. *Int. J. Quantum Chem.* **1999**, *75*, 889.
31. Almeida, L.M.; Perdew, J.P.; Fiolhais, C. *Phys. Rev. B* **2002**, *66*, 075115.
32. Rushton, P.R.; Clark, S.J.; Tozer, D.J. *Phys. Rev. B* **2001**, *63*, 115206.
33. Ceperley, D.M.; Alder, B.J. *Phys. Rev. Lett.* **1980**, *45*, 566.
34. Perdew, J.P.; Zunger, A. *Phys. Rev. B* **1981**, *23*, 5048.

35. Vosko, S.H.; Wilk, L.; Nusair, M. *Can. J. Phys.* **1980**, *58*, 1200.
36. Perdew, J.P.; Wang, Y. *Phys. Rev. B* **1992**, *45*, 13244.
37. Filatov, M.; Thiel, W. *Int. J. Quantum Chem.* **1997**, *62*, 603.
38. Singwi, K.S.; Sjölander, A.; Tosi, M.P.; Land, R.H. *Phys. Rev. B* **1970**, *1*, 1044.
39. Hedin, L.; Lundqvist, B.I. *J. Phys. C* **1971**, *4*, 2064.
40. Moruzzi, V.L.; Janak, J.F.; Williams, A.R. *Calculated Electronic Properties of Metals*; Pergamon Press: NY, 1978.
41. Gunnarsson, O.; Lundqvist, B.J. *Phys. Rev. B* **1976**, *13*, 4274.
42. Lein, M.; Gross, E.K.U.; Perdew, J.P. *Phys. Rev. B* **2000**, *61*, 13431.
43. Holm, B.; von Barth, U.; *Phys. Rev. B* **1998**, *57*, 2108.
44. Garcia-Gonzalez, P.; Godby, R.W. *Phys. Rev. B* **2001**, *63*, 075112.
45. Yan, Z.; Perdew, J.P.; Kurth, S. *Phys. Rev. B* **2000**, *61*, 16430.
46. Wigner, E.P. *Phys. Rev.* **1934**, *46*, 1002; *Trans. Faraday Soc.* **1938**, *34*, 678.
47. Corrected version given in Eq. (3–58) of Pines, D. *Elementary Excitations in Solids*; Benjamin: NY, 1964.
48. Cohen, A.J.; Handy, N.C. *Mol. Phys.* **2001**, *99*, 607.
49. Stoll, H.; Pavlidou, C.M.E.; Preuss, H. *Theoret. Chim. Acta (Berl.)* **1978**, *49*, 143.
50. Stoll, H.; Golka, C.; Preuss, H. *Theoret. Chim. Acta (Berl.)* **1980**, *55*, 29.
51. Perdew, J.P.; Wang, Y. *Phys. Rev. B* **1992**, *46*, 12947.
52. Perdew, J.P.; *Int. J. Quantum Chem.* **1993**, *27*, 93.
53. Schmidt, K.; Kurth, S.; Tao, J.; Perdew, J.P. *Phys. Rev. B* **2000**, *62*, 2227.
54. Ortiz, G.; Harris, M.; Ballone, P. *Phys. Rev. Lett.* **1999**, *82*, 5317.
55. Gori-Giorgi, P.; Sacchetti, F.; Bachelet, G.B. *Phys. Rev. B* **2000**, *61*, 7353.
56. Bachelet, G.B.; Gori-Giorgi, P.; Sacchetti, F. In *Density Functional Theory and its Applications to Materials*; Van Doren, V.E.; Van Alsenoy, K.; Geerlings, P., Eds.; AIP, 2000.
57. Gori-Giorgi, P.; Perdew, J.P. *Phys. Rev. B* **2002**, *66*, 165118.
58. Seidl, M.; Perdew, J.P. work in progress.
59. Gori-Giorgi, P.; Perdew, J.P. unpublished.

Chapter 3

Self-Consistent Hartree–Fock–Wigner Calculations: A Two-Electron-Density Functional Theory

Darragh P. O'Neill and Peter M. W. Gill

Department of Physical Chemistry, University of Nottingham,
University Park NG7 2RD, United Kingdom

We recently presented a correlation method based on the Wigner intracule, in which correlation energies are calculated directly from a Hartree-Fock wavefunction. We now describe a self-consistent form of this approach which we term the Hartree-Fock-Wigner method. The efficacy of the new scheme is demonstrated using a simple weight function to reproduce the correlation energies of the first- and second-row atoms with a mean absolute deviation of $2.5 mE_h$.

Introduction

The electron correlation problem remains a central research area for quantum chemists, as its solution would provide the exact energies for arbitrary systems. Today there exist many procedures for calculating the electron correlation energy (I), none of which, unfortunately, is both robust and computationally inexpensive. Configuration interaction (CI) methods provide a conceptually simple route to correlation energies and a full CI calculation will provide exact energies but only at prohibitive computational cost as it scales factorially with the number of basis functions, N . Truncated CI methods such as CISD (N^6 cost) are more computationally feasible but can still only be used for small systems and are neither size consistent nor size extensive. Coupled cluster

(CC) methods, which have largely superseded CI methods, in the limit can also be used to give exact solutions but again with same prohibitive cost as full CI. As with CI, CC methods are often truncated, most commonly to CCSD (N^6 cost), but as before these can still only be applied to systems of modest size. Finally, Møller-Plesset (MP) perturbation theory, which is usually used to second order (MP2 has a N^5 cost), is more computationally accessible but does not provide as robust results.

We have recently introduced the Wigner intracule (2), a two-electron phase-space distribution. The Wigner intracule, $W(u, v)$, is related to the probability of finding two electrons separated by a distance u and moving with relative momentum v . This reduced function provides a means to interpret the complexity of the wavefunction without removing all of the explicit multi-body information contained therein, as is the case in the one-electron density.

Electron correlation is inherently a multi-electron phenomenon, and we believe that the retention of explicit two-electron information in the Wigner intracule lends itself to its description (3). It has been well established that electron correlation is related to the inter-electronic distance, but it has also been suggested (4) that the relative *momentum* of two electrons should be considered which led us to suggest that the Hartree-Fock (HF) Wigner intracule contains information which can yield the electron correlation energy. The calculation of this correlation energy, like HF, formally scales as N^4 .

Although the HF Wigner intracule can be used to estimate correlation energies, the resulting energy is not variational with respect to the molecular orbital (MO) coefficients, so gradients, which are needed to perform geometry optimizations and frequency calculations, are complicated. The calculation of such gradients is made more straightforward when using a set of MOs which have been self-consistently optimized taking the corrections due to the correlation energy into account. A self-consistent scheme such as this, which we term the Hartree-Fock-Wigner (HFW) method, will now be described.

Theory

We have recently proposed (3) that the correlation energy can be estimated from equations of the form

$$E = \int_0^{\infty} \int W_{\text{HF}}(u, v) G_{\text{HF}}(u, v) du dv \quad (1)$$

where $W_{\text{HF}}(u, v)$ is the Wigner intracule derived from a HF wavefunction and $G_{\text{HF}}(u, v)$ is a weight function. If the MOs are expanded within a basis set, the correlation energy becomes

$$E_{\text{C}} = \frac{1}{2} \sum_{\mu\nu\lambda\sigma} \left[P_{\mu\nu} P_{\lambda\sigma} - P_{\mu\sigma}^{\alpha} P_{\nu\lambda}^{\alpha} - P_{\mu\sigma}^{\beta} P_{\nu\lambda}^{\beta} \right] (\mu\nu\lambda\sigma)_{\text{G}} \quad (2)$$

where $P_{\mu\nu}^{\alpha}$ and $P_{\mu\nu}^{\beta}$ are elements of the α and β HF density matrices, $P_{\mu\nu}$ is an element of the total HF density matrix $P_{\mu\nu} = P_{\mu\nu}^{\alpha} + P_{\mu\nu}^{\beta}$ and $(\mu\nu\lambda\sigma)_{\text{G}}$ is the 10-dimensional correlation integral

$$(\mu\nu\lambda\sigma)_{\text{G}} = \frac{1}{2\pi^2} \int \phi_{\mu}(\mathbf{r}) \phi_{\nu}(\mathbf{r} + \mathbf{q}) \phi_{\lambda}(\mathbf{r} + \mathbf{q} + \mathbf{u}) \phi_{\sigma}(\mathbf{r} + \mathbf{u}) \times v^2 j_0(qv) G(u, v) \, \text{dr} \, \text{dq} \, \text{du} \, \text{dv} \quad (3)$$

where $\phi_i(\mathbf{r})$ is a basis function and $j_0(x)$ is the zeroth-order spherical Bessel function (5).

The HF energy is given by

$$E_{\text{HF}} = \sum_{\mu\nu} P_{\mu\nu} H_{\mu\nu} + \frac{1}{2} \sum_{\mu\nu\lambda\sigma} \left[P_{\mu\nu} P_{\lambda\sigma} - P_{\mu\sigma}^{\alpha} P_{\nu\lambda}^{\alpha} - P_{\mu\sigma}^{\beta} P_{\nu\lambda}^{\beta} \right] (\mu\nu|\lambda\sigma) \quad (4)$$

where $(\mu\nu|\lambda\sigma)$ are the usual Coulomb integrals. This expression may trivially be combined with equation 2 to yield the HFW energy

$$E_{\text{HFW}} = \sum_{\mu\nu} P_{\mu\nu} H_{\mu\nu} + \frac{1}{2} \sum_{\mu\nu\lambda\sigma} \left[P_{\mu\nu} P_{\lambda\sigma} - P_{\mu\sigma}^{\alpha} P_{\nu\lambda}^{\alpha} - P_{\mu\sigma}^{\beta} P_{\nu\lambda}^{\beta} \right] (\mu\nu\lambda\sigma)_{\text{HFW}} \quad (5)$$

where $(\mu\nu|\lambda\sigma)_{\text{HFW}} = (\mu\nu|\lambda\sigma) + (\mu\nu\lambda\sigma)_{\text{G}}$ and $P_{\mu\nu}$ is no longer a HF density matrix element but rather a density matrix element obtained when a self-consistent calculation is performed with the inclusion of the Wigner perturbation.

When implementing the HFW method the extra computational cost incurred is that of evaluating and digesting the correlation integrals. The details (δ) of calculating the $(\mu\nu\lambda\sigma)_{\text{G}}$ integrals depends on the choice of $G(u, v)$, and in this work gaussian weight functions in uv and u , $G(u, v) = Ae^{-\zeta u^2 v^2}$ and $G(u, v) = Be^{-\eta u^2}$, were chosen as these permit the 10-dimensional correlation integral (equation 3) to be reduced to a one-dimensional integral in u . The remaining integration is then performed by quadrature (δ). Several quadrature

schemes have been explored to approximate this final integral and it has been found that the recently introduced MultiExp grid (7) is particularly efficient. The form of the integrand is suitable for use with this grid as it is the product of a power, a gaussian and a modified spherical Bessel function (5) in u , and can be approximated well by a sum of exponentials which MultiExp integrates exactly.

The digestion of the HFW integrals differs from that of HF integrals as the $(\mu\nu\lambda\sigma)_G$ integrals possess lower permutational symmetry than their HF counterparts. Correlation integrals, like the Wigner integrals which make up the Wigner intracule and unlike the conventional Coulomb integrals, have only four-fold permutational symmetry (8)

$$\begin{aligned}(\mu\nu\lambda\sigma)_G &= (\nu\mu\sigma\lambda)_G = (\sigma\lambda\nu\mu)_G = (\lambda\sigma\mu\nu)_G \\ (\mu\nu\sigma\lambda)_G &= (\nu\mu\lambda\sigma)_G = (\sigma\lambda\mu\nu)_G = (\lambda\sigma\nu\mu)_G\end{aligned}\quad (6)$$

and hence an HFW calculation is roughly twice as expensive as the same HF calculation. When the HFW integrals are being assembled, clearly we do not wish to compute the Coulomb integrals twice, so care must be taken to combine the correct Coulomb and correlation integrals. It should also be pointed out that a negligibly small Coulomb integral does not imply that the corresponding correlation integral is negligibly small, so we currently evaluate all of the HFW integrals. A cutoff criterion for discarding correlation integrals, analogous to the Schwarz inequality for Coulomb integrals, would be a desirable tool and is being investigated (9).

After the HFW integrals have been assembled, we then move on to the self-consistent field (SCF) procedure. For the most part this is the same as the HF version (10), with the exception of constructing the Fock matrix. The Fock matrix elements for an unrestricted HFW calculation are analogous to their HF counterparts and are given by

$$F_{\mu\nu}^\alpha = H_{\mu\nu}^{\text{core}} + \sum_{\lambda\sigma} P_{\lambda\sigma} (\mu\nu\lambda\sigma)_{\text{HFW}} - P_{\lambda\sigma}^\alpha (\mu\lambda\nu\sigma)_{\text{HFW}} \quad (7)$$

$$F_{\mu\nu}^\beta = H_{\mu\nu}^{\text{core}} + \sum_{\lambda\sigma} P_{\lambda\sigma} (\mu\nu\lambda\sigma)_{\text{HFW}} - P_{\lambda\sigma}^\beta (\mu\lambda\nu\sigma)_{\text{HFW}} \quad (8)$$

The method usually employed to build the Fock matrix is an integral-driven algorithm in which each integral contributes to six elements of the Fock matrix. Due to the lower symmetry of the HFW integrals, each one contributes to only four elements of the Fock matrix. For a given integral $(\mu\nu\lambda\sigma)_{\text{HFW}}$ the upper or lower diagonal of the α Fock matrix is built up as follows

$$\begin{aligned}F_{\mu\nu}^\alpha &= F_{\mu\nu}^\alpha + P_{\lambda\sigma} (\mu\nu\lambda\sigma)_{\text{HFW}} \\ F_{\lambda\sigma}^\alpha &= F_{\lambda\sigma}^\alpha + P_{\mu\nu} (\mu\nu\lambda\sigma)_{\text{HFW}} \\ F_{\mu\sigma}^\alpha &= F_{\mu\sigma}^\alpha + P_{\nu\lambda}^\alpha (\mu\nu\lambda\sigma)_{\text{HFW}} \\ F_{\nu\lambda}^\alpha &= F_{\nu\lambda}^\alpha + P_{\mu\sigma}^\alpha (\mu\nu\lambda\sigma)_{\text{HFW}}\end{aligned}\quad (9)$$

where the prime indicates that the integrals have been scaled by the number of permutationally equivalent integrals and then by $\frac{1}{4}$. After this Fock matrix is calculated it must be corrected by multiplying the diagonal elements by a factor of two. The β Fock matrix is constructed analogously.

Results

Currently the Hartree-Fock-Wigner method is implemented as a standalone program, but work is underway to integrate this method into the Q-Chem (11) package. Using a gaussian weight function, $(\mu\nu\lambda\sigma)_G$ has been formulated for all *s*- and *p*-type basis functions, and is readily extensible to functions of higher angular momentum. The results that will be considered are those for a $G(u, \nu)$ which aims to reproduce the energies of the atoms of the first and second rows. To accomplish this, the four parameters, *A*, *B*, ζ and η , in the gaussian weight function $G(u, \nu) = Ae^{-\zeta u^2 \nu^2} + Be^{-\eta u^2}$ will be fitted.

We have found that the Wigner intracule is quite insensitive to basis set size and we expect the derived correlation energies to be similarly insensitive. In stark contrast to the post-HF methods mentioned in the introduction, we expect similar Wigner correlation energies from both moderate and large basis sets and thus estimates (made using accurate experimental and theoretical data) to the exact non-relativistic correlation energies (12) are used in the fitting routine. The Hartree-Fock energy, however, is much more sensitive to basis set so the target of the HFW method will be to calculate the sum of the Hartree-Fock energy for a given basis set and the "exact" correlation energy.

We will now examine the results obtained when the parameters of $G(u, \nu)$ are optimized for both non-SCF Wigner correlation and HFW using the 6-311G basis set. The parameters were optimized using the BFGS quasi-Newton method given in ref (13). The two resulting weight functions are as follows

$$G_{\text{HF}}(u, \nu) = -0.135433e^{-0.303089u^2\nu^2} + 0.004183e^{-0.325456u^2} \quad (10)$$

$$G_{\text{HFW}}(u, \nu) = -0.135410e^{-0.303715u^2\nu^2} + 0.004232e^{-0.344968u^2} \quad (11)$$

Table I shows the energies obtained when non-SCF and HFW calculations are performed using each of the functions given in equations 10 and 11. Excellent agreement is seen between the exact and calculated values when using the appropriate function for a given calculation type, with mean absolute deviations of 2.6 mE_h and 2.5 mE_h and the maximum absolute deviations being 6.8 mE_h and 7.1 mE_h in the case of the nitrogen atom.

Table I: Errors in Non-SCF and HFW Energies^a

<i>Calc. Type</i> <i>Function Type^b</i>	<i>Total^c</i>	<i>Non-SCF</i>		<i>HFW</i>	
		<i>G_{HF}</i>	<i>G_{HFW}</i>	<i>G_{HF}</i>	<i>G_{HFW}</i>
He	-2.9019	-0.8	-0.8	-0.8	-0.8
Li	-7.4096	0.8	0.7	1.0	0.9
Be	-14.6662	-0.7	-0.7	-0.6	-0.6
B	-24.6519	0.6	0.6	0.6	0.7
C	-37.8424	3.1	3.3	3.2	3.3
N	-54.5863	6.8	7.0	6.9	7.1
O	-75.0604	-0.6	-0.4	-0.5	-0.3
F	-99.7186	-4.0	-3.9	-3.9	-3.9
Ne	-128.9130	-6.2	-6.3	-6.1	-6.2
Na	-162.2416	-3.7	-4.1	-3.0	-3.4
Mg	-200.0448	2.6	2.1	2.9	2.4
Al	-242.3396	3.0	2.5	3.3	2.8
Si	-289.3528	2.1	1.8	2.3	2.0
P	-341.2476	2.1	2.1	2.3	2.3
S	-398.0999	-2.3	-2.0	-2.1	-1.8
Cl	-460.1355	-3.3	-2.7	-3.2	-2.5
Ar	-527.5287	1.0	1.9	1.2	2.1
Mean^d		2.6	2.5	2.6	2.5
Max^e		6.8	7.0	6.9	7.1

^a Total energies in E_h and errors in mE_h ^b From equations 10 and 11^c Sum of HF/6-311G and exact correlation energies^d Mean Absolute Deviation^e Maximum Absolute Deviation

Table II: Errors in HFW/STO-3G Energies^a

	<i>Total^b</i>	<i>HFW</i>
He	-2.8498	-0.6
Li	-7.3609	5.3
Be	-14.4462	-0.2
B	-24.2738	0.5
C	-37.3548	1.9
N	-53.9073	5.0
O	-74.0621	-1.3
F	-98.311	-3.1
Ne	-126.995	-3.3
Na	-160.064	20.2
Mg	-197.4456	17.4
Al	-239.328	11.8
Si	-285.9712	4.1
P	-337.409	-0.2
S	-393.735	-7.7
Cl	-455.2082	-9.1
Ar	-521.945	-6.9
Mean ^c		5.8
Max ^d		20.2

^a Total energies in E_h and errors in mE_h

^b Sum of HF/STO-3G and exact correlation energies

^c Mean Absolute Deviation

^d Maximum Absolute Deviation

As expected only minor differences are seen between the results obtained when the correct and incorrect fits are used for each calculation type and this is reflected in the similarity of the weight functions.

We predicted above that the Wigner correlation energies should not be very sensitive to the basis set used. The validity of this will now be examined. Table II shows the result of using the HFW weight function optimized for the 6-311G basis set applied to the STO-3G basis set. Again, we cannot expect to reproduce the HF/6-311G energy at the STO-3G level so the total energies now use the HF/STO-3G energy add to the exact correlation energy. Good agreement is seen with the mean absolute deviation increasing to 5.8 mE_h and the maximum absolute deviation being 20.2 mE_h , in the case of the sodium atom.

To investigate the magnitude of the effect that the inclusion of the correlation integrals has, we will look at the change in the density matrix. It is

expected that the change induced on going from HF to HFW will be small so the ratio of a HF density matrix element to its HFW counterpart should be close to unity. Because the maximum deviation in energy occurs in the case of the N atom, it has been chosen to exemplify the change in the density matrix. Our prediction that the induced change will be small is correct with the largest deviation from unity being 0.9854 in the case of the most diffuse p -functions.

Conclusions

We have described a self-consistent field method for calculating correlation energies based on the Wigner intracule. This method involves a perturbation to the usual two-electron integrals. The implementation of this method is very similar to the HF method and complications arise only from the calculation of the new correlation integrals and from the low permutational symmetry of the HFW integrals. It has been shown that HFW, using a simple weight function, can accurately estimate the correlation energies of the first- and second-row atoms with a mean absolute deviation of $2.5 mE_h$. This weight function is used only to highlight some of the features of this new method and we are investing much effort into findings forms of $G(u,v)$ which work more generally. We are considering spin-separated weight functions as it is known that the majority of the correlation energy arises from pairs of electrons with opposite spins. Hence, we use one weight function for the parallel-spin intracule and another for the antiparallel-spin intracule. This a straightforward extension of the method described above. Work is also underway to see how derivatives from the HFW method perform when used to optimize geometries and calculate vibrational frequencies (14).

Acknowledgements

We would like to thank Dr. Nick Besley for useful discussions. This research was partly supported by the Engineering and Physical Sciences Research Council through a project studentship (GR/R81121) to D.P.O.

References

1. Jensen, F. *Introduction to Computational Chemistry*. John Wiley & Sons, 1999.
2. Gill, P.M.W.; O'Neill, D.P.; Besley, N.A. *Theor. Chem. Acc.*, **2003**, *109*, 241.

3. Gill, P.M.W.; O'Neill, D.P.; Besley, N.A., to be submitted.
4. Rassolov, V.A. *J. Chem. Phys.*, **1999**, *110*, 3672.
5. Abramowitz, M.; Stegun, I.A., editors. *Handbook of Mathematical Functions*. Dover, 1972.
6. O'Neill, D.P.; Gill, P.M.W., to be submitted.
7. Gill, P.M.W.; Chien, S.H. *J. Comput. Chem.*, **2003**, *24*, 732.
8. Besley, N.A.; O'Neill, D.P.; Gill, P.M.W. *J. Chem. Phys.*, **2003**, *118*, 2033.
9. O'Neill, D.P.; Gill, P.M.W. to be submitted.
10. Szabo, A.; Ostlund, N.S. *Modern Quantum Chemistry: Introduction to Advanced Electronic Structure Theory*. Dover, 1989.
11. Kong, J.; White, C. A.; Krylov, A. I.; Sherrill, C. D.; Adamson, R. D.; Furlani, T. R.; Lee, M. S.; Lee, A. M.; Gwaltney, S. R.; Adams, T. R.; Ochsenfeld, C.; Gilbert, A. T. B.; Kedziora, G. S.; Rassolov, V. A.; Maurice, D. R.; Nair, N.; Shao, Y.; Besley, N. A.; Maslen, P. E.; Dombroski, J. P.; Daschel, H.; Zhang, W.; Korambath, P. P.; Baker, J.; Byrd, E. F. C.; Voorhis, T. Van; Oumi, M.; Hirata, S.; Hsu, C-P.; Ishikawa, N.; Florian, J.; Warshel, A.; Johnson, B. G.; Gill, P. M. W.; Head-Gordon, M.; Pople, J. A. *J. Comput. Chem.*, **2000**, *21*, 1532.
12. Chakravorty, S.J.; Gwaltney, S.R.; Davidson, E.R.; Parpia, F.A.; Froese Fischer, C. *Phys. Rev. A*, **1993**, *47*, 3649.
13. Press, W.H.; Teukolsky, S.A.; Vetterling, W.T.; Flannery, B.P. *Numerical Recipes in Fortran*. Cambridge University Press UK, second edition, 1992.
14. Dolg, M.; O'Neill, D.P.; Gill, P.M.W. to be submitted.

Chapter 4

New Alternatives for Accurate Electronic Structure Calculations of Potential Energy Surfaces Involving Bond Breaking

Piotr Piecuch^{1,2}, Ian S. O. Pimienta¹, Peng-Dong Fan¹,
and Karol Kowalski¹

¹Department of Chemistry, Michigan State University, East
Lansing, MI 48824

²Alfred P. Sloan Research Fellow

The method of moments of coupled-cluster equations (MMCC) is extended to potential energy surfaces involving multiple bond breaking by developing the quasi-variational (QV) and quadratic (Q) variants of the MMCC theory. The QVMMCC and QMMCC methods are related to the extended CC (ECC) theory, in which products involving cluster operators and their deexcitation counterparts mimic the effects of higher-order clusters. The test calculations for N₂ show that the QMMCC and ECC methods can provide spectacular improvements in the description of multiple bond breaking by the standard CC approaches.

Introduction

Recent years have witnessed a considerable activity towards extending the standard single-reference coupled-cluster (CC) methods (*1-9*) to potential energy surfaces (PESs) involving bond breaking without invoking a multi-reference description (see, e.g., refs *9-31*). Undoubtedly, it would be very useful if we could routinely calculate large portions of molecular PESs with the ease-

of-use and the relatively low cost characterizing the standard CC “black-boxes,” such as CCSD (CC singles and doubles) (32–36), CCSD[T] (37–39), CCSD(T) (40), and CCSD(TQ_f) (41).

The problem is that the CCSD method itself, on which the noniterative CCSD[T], CCSD(T), and CCSD(TQ_f) approaches are based, is inadequate for the description of bond breaking, since it neglects all higher-than-doubly excited clusters, including the important triply and quadruply excited T_3 and T_4 components. The triples and quadruples corrections of the CCSD[T], CCSD(T), and CCSD(TQ_f) methods do not help, since the standard arguments originating from the many-body perturbation theory (MBPT), on which the noniterative CC approximations are based, fail due to the divergent behavior of the MBPT series at larger internuclear separations. In consequence, the ground-state PESs obtained with the CCSD[T], CCSD(T), CCSD(TQ_f), and other noniterative CC approaches are completely pathological if the spin-adapted restricted Hartree-Fock (RHF) configuration is used as a reference (cf., e.g., refs 7, 9–21, 42–45). The iterative analogs of the CCSD[T], CCSD(T), and CCSD(TQ_f) methods, including, for example, the CCSDT- n (39, 46–49) and CCSDTQ-1 (50) approaches, and the noniterative CCSDT + Q(CCSDT) = CCSDT[Q] (50) and CCSDT(Q_f) (41) methods, in which the noniterative corrections due to T_4 clusters are added to the CCSDT (CC singles, doubles, and triples) (51, 52) energies, may improve the description of PES in the bond breaking region (particularly, when the local correlation formalism is employed (53)), but ultimately all of these approaches fail due to the divergent behavior of the MBPT series at larger internuclear distances (see, e.g., refs 11, 12, 16, 42), particularly when multiple bonds are broken (16, 42).

The natural solution to all of the above problems is obtained by switching to the multi-reference CC (MRCC) formalisms, which introduce a concept of a multi-dimensional model space and which are specifically designed to handle general open-shell and quasi-degenerate states, including, at least in principle, various cases of bond breaking (see, e.g., ref 7 for a recent review). However, it is much easier to apply the standard single-reference CC methods of the CCSD or CCSD(T) type, which do not suffer from intruder states and multiple, singular, or unphysical solutions that plague the genuine MRCC theories (see, e.g., refs 54–61). The newly developed state-specific MRCC approaches (cf., e.g., refs 62–71) and the MRCC approach combining the MBPT and MRCC concepts (72, 73) may change this situation, but none of the existing MRCC methods are simple or general enough to be as widely applicable as the standard CCSD or CCSD(T) approaches.

One might, of course, try to resolve the failures of the standard single-reference CC approaches at larger internuclear separations in a brute-force manner by including the triply excited, quadruply excited, pentuply excited, etc. clusters in a completely iterative fashion (a new programming technique developed by Kállay and Surján (74) allows one to write efficient computer codes for CC methods with clusters of any rank). Unfortunately, the resulting

CCSDTQ (CC singles, doubles, triples, and quadruples) (75–78), CCSDTQP (CC singles, doubles, triples, quadruples, and pentuples) (79), etc. approaches are far too expensive for routine applications. For example, the full CCSDTQ method requires iterative steps that scale as $n_o^4 n_u^6$ (n_o (n_u) is the number of occupied (unoccupied) orbitals in the molecular orbital basis). This scaling restricts the applicability of the CCSDTQ approach to very small systems, consisting of $\sim 2 - 3$ light atoms described by small basis sets. For comparison, CCSD(T) is an $n_o^2 n_u^4$ procedure in the iterative CCSD steps and an $n_o^3 n_u^4$ procedure in the non-iterative part related to the calculation of the triples (T) correction. In consequence, it is nowadays possible to perform the CCSD(T) calculations for systems with 10–20 atoms. The application of the local correlation formalism (80–82) enabled Schütz and Werner to extend the applicability of the CCSD(T) approach to systems with ~ 100 atoms (53, 83, 84).

A few single-reference or single-reference-like approaches have been proposed in recent years with an intention of removing the pervasive failing of the standard RHF-based CC approximations at larger internuclear separations, while avoiding the complexity of the genuine multi-reference theory and astronomical costs of the CCSDTQ, CCSDTQP, and similar calculations. The representative examples include the reduced multi-reference CCSD (RMRCCSD) method (7, 85–90), the active-space CC approaches (which can also be classified as the state-selective MRCC methods) (10–12, 15, 43, 78, 91–101) (see refs 102–104 for the excited-state extensions), the orbital-optimized CC methods (22, 23), the noniterative approaches based on the partitioning of the similarity-transformed Hamiltonian (24–28) (cf., also, ref 105), and the renormalized (R) and completely renormalized (CR) CC methods (9, 13–18, 20, 21). The latter approaches are based on the more general formalism of the method of moments of CC equations (MMCC) (9, 13, 14, 18, 19, 21, 45, 106, 107), which can be applied to ground- and excited-state PESs. All of the above methods focus on improving the description of bond breaking, while retaining the simplicity of the single-reference description based on the spin- and symmetry-adapted references of the RHF type. We do not discuss here the spin-contaminated approaches, in which the improvement of the description of bond breaking is accomplished by employing the unrestricted Hartree-Fock (42) or restricted but “spin-flipped” (29, 30) reference configurations.

Of the methods listed above, only the noniterative CC approaches based on the partitioning of the similarity-transformed Hamiltonian (24–28) and the (C)R-CC approaches of refs 9, 13–18, 20, 21, which employ the MMCC formalism (9, 13, 14, 18, 19, 21, 45, 106, 107), retain the simplicity and the “black-box” character of the standard CCSD(T) or CCSD(T_f) methods. One of the two goals of the present work is the development of a new class of the MMCC-based “black-box” methods for multiple bond breaking.

The main idea of the MMCC formalism and of the related R-CC and CR-CC approaches (9, 13–21, 45, 106, 107) is that of the simple, noniterative energy

corrections which, when added to the energies obtained in the standard CC calculations, recover the exact, full configuration interaction (CI), energies of the electronic states of interest. Thus, the MMCC methods and the renormalized and completely renormalized CCSD (T) and CCSD(TQ) approaches, in which we add simple noniterative corrections due to triples or triples and quadruples to the CCSD energies, preserve the conceptual and computational simplicity of the noniterative CC methods, such as CCSD(T) or CCSD(TQ)_f, while offering us a new way of controlling the quality of CC results by focusing on the quantity of interest, which is the difference between the full CI and CC energies. By dealing with the remnant errors that occur in the standard CC calculations, which we estimate by using the explicit relationships between the CC and full CI energies defining the MMCC theory, we can obtain considerable improvements in the results of the standard CC calculations in situations, such as bond breaking, where conventional arguments employing MBPT fail due to the divergent behavior of the MBPT series.

Two different types of the MMCC methods have been considered by us so far, namely, the CI-corrected MMCC schemes (9, 18, 19, 21, 106, 107) and the R-CC and CR-CC methods (9, 13–18, 20, 21). The CI-corrected MMCC schemes have an advantage of being applicable to both the ground states and the excited states, but they require that one performs the *a priori* limited CI calculations in order to construct the noniterative corrections to standard CC energies (9, 18, 19, 21, 106, 107). Although the CI-corrected MMCC methods were already discussed by us in the early MMCC work (9) (cf., also, refs 19, 21, 106, 107) and although they have recently been adopted by others (108–110), we do not discuss them here, since they combine the single-reference CC and the active-space CI or MRCI ideas. The R-CC and CR-CC methods (9, 13–18, 20, 21) do not require any *a priori* non-CC calculations and are as easy to use as the standard CC “black-boxes” of the CCSD(T) or CCSD(TQ)_f type. Thus, they can rather easily be incorporated in any electronic structure package that has the standard CCSD(T) or CCSD(TQ)_f codes in it. The renormalized and completely renormalized CCSD[T] and CCSD(T) methods (the R-CCSD[T], RCCSD(T), CR-CCSD[T], and CR-CCSD(T) methods, respectively) have recently been incorporated (111) in the popular GAMESS package (112). In this chapter, we focus on the new generation of the MMCC methods, termed the quasi-variational (QV) and quadratic (Q) MMCC approaches, that preserve the underlying philosophy of the standard and (completely) renormalized CCSD(T), CCSD(TQ), and similar approaches, which is an idea of adding the noniterative corrections to the CCSD energies that are solely based on the information obtained in the CCSD calculations.

It has been demonstrated in several benchmark calculations that the CR-CCSD(T) (completely renormalized CCSD(T)) and CR-CCSD(TQ) (completely renormalized CCSD(TQ)) methods provide an excellent description of entire PESs involving single and double bond dissociation (9, 13, 15, 17–19, 21, 111), highly-excited vibrational term values near dissociation (17, 18, 21, 111), and

entire PESs for exchange chemical reactions of the general type: closed shell + closed shell \rightarrow doublet + doublet (20, 21). However, the CR-CCSD(T) and CR-CCSD(TQ) results for triple bond breaking (e.g., in N_2) and for certain types of double bond breaking (e.g., in C_2) are somewhat less impressive (14, 18, 21). For example, the relatively small (~ 1 millihartree) errors, relative to full CI, in the CR-CCSD(TQ) results for the double zeta (DZ) (113) model of N_2 near the equilibrium geometry R_e increase to 10–25 millihartree, when $R \geq 1.75 R_e$ (14) (R is the N–N separation). Those are fairly small errors, when compared to the -387.448 , 334.985 , and 426.175 millihartree errors in the CCSD(T), CCSD(TQ_f), and CCSDT(Q_f) results at $R = 2.25 R_e$, but the problem of the 10–25 millihartree errors in the CR-CCSD(TQ) energies for the larger internuclear separations in multiply bonded molecules should, in our view, be addressed. We have recently demonstrated that we can obtain the 1.217–4.552 millihartree errors in the entire $R = 0.75 R_e - 2.25 R_e$ region for a complicated case of N_2 by performing the CI-corrected MMCC calculations (21). In this work, we are addressing the following question: Can one formulate the MMCC approximations that preserve the philosophy of the CCSD(T), CCSD(TQ_f), CR-CCSD(T), CR-CCSD(TQ), and similar approaches, which is an idea of adding noniterative corrections to the CCSD energies that do not require the *a priori* non-CC calculations, and yet obtain the virtually perfect description of triple bond breaking?

The proposed solution, termed the quasi-variational MMCC (QVMMCC) formalism, and its quadratic MMCC (QMMCC) variant, both described in this article, are based on combining the idea of the MMCC noniterative energy corrections with the elements of the extended CC (ECC) (114–124) and expectation value CC (XCC) (124–126) theories, in which products involving cluster operators and their deexcitation counterparts are used to mimic the effects of higher-order clusters, such as T_4 . In designing the QMMCC approach, we were particularly inspired by the recent work by Head-Gordon and coworkers (27, 28, 127–129), who demonstrated that the variational CCD (CC doubles) calculations, based on minimizing the expectation value of the Hamiltonian with the CCD wave function, and the quadratic approximation to the bi-variational ECCD (ECC doubles) method lead to a qualitatively correct description of triple bond breaking in N_2 , eliminating, in particular, the nonvariational collapse of the standard CCD theory at large internuclear separations. As demonstrated in this work, the QMMCC corrections to CCSD energies provide the virtually exact description of the potential energy curve of N_2 with the ease-of-use of the noniterative CC approaches of the CCSD(T) or CCSD(TQ_f) type.

Because of the apparent relationship between the QVMMCC or QMMCC methods and ECC/XCC approaches, we also explore the usefulness of the ECC theory in studies of multiple bond breaking, using N_2 as an example. Instead of the strictly bi-variational ECC method of Arponen and Bishop (114–123), we

use the simplified variant of the ECC theory described by Piecuch and Bartlett in ref 124. We consider the complete ECCSD (ECC singles and doubles) formalism as well as its linear and quadratic approximations. As shown in this article, the complete ECCSD theory and its quadratic QECCSD variant provide an excellent description of the entire potential energy curve of N_2 . The linear ECCSD (LECCSD) theory provides improvements over the standard CCSD results, but those improvements are not sufficient to obtain a good quality potential for N_2 . We also analyze the relationships between the exact wave functions obtained by the full CI method and the approximate wave functions resulting from the CCSD, QECCSD, and ECCSD calculations.

The Method of Moments of Coupled-Cluster Equations: An Overview of the Ground-State Formalism

In the ground-state MMCC theory, we focus on the noniterative energy correction

$$\delta_0^{(A)} \equiv E_0 - E_0^{(A)}, \quad (1)$$

which, when added to the energy $E_0^{(A)}$, obtained in the standard single-reference CC calculations, referred to as method A , recovers the full CI ground-state energy E_0 . The purpose of the approximate MMCC calculations is to estimate correction $\delta_0^{(A)}$, such that the resulting MMCC energy, defined as

$$E_0^{\text{MMCC}} \equiv E_0^{(A)} - \delta_0^{(A)}, \quad (2)$$

is close to the corresponding full CI energy E_0 .

Let us recall that in the single-reference CC theory, the ground-state wave function $|\Psi_0\rangle$ of an N -electron system, described by the Hamiltonian H , is given by the following expression:

$$|\Psi_0\rangle = e^T |\Phi\rangle, \quad (3)$$

where T is the cluster operator and $|\Phi\rangle$ is the independent-particle-model (IPM) reference configuration (e.g., the Hartree-Fock determinant) defining the Fermi vacuum. In all standard CC calculations, we truncate the many-body expansion of cluster operator T at some excitation level $m_A < N$, i.e., the formula for cluster operator $T^{(A)}$ defining the CC method A is

$$T^{(A)} = \sum_{n=1}^{m_A} T_n, \quad (4)$$

where T_n , $n = 1, \dots, m_A$, are the many-body components of $T^{(A)}$. The standard CCSD method is obtained by setting $m_A = 2$ in eq (4). In the CCSDT method,

m_A is set at 3; in the CCSDTQ approach, $m_A = 4$, etc. The explicit equation for the n -body cluster component T_n in terms of the excitation operators $E_{i_1 \dots i_n}^{a_1 \dots a_n}$, which, when acting on reference $|\Phi\rangle$ generate the n -tuply excited configurations $|\Phi_{i_1 \dots i_n}^{a_1 \dots a_n}\rangle$ and the cluster amplitudes $t_{a_1 \dots a_n}^{i_1 \dots i_n}$ is as follows:

$$T_n = \sum_{\substack{i_1 < \dots < i_n \\ a_1 < \dots < a_n}} t_{a_1 \dots a_n}^{i_1 \dots i_n} E_{i_1 \dots i_n}^{a_1 \dots a_n}. \quad (5)$$

As usual, letters i and a designate the occupied and unoccupied spin-orbitals, respectively.

In all standard CC approximations, the cluster operator $T^{(A)}$ or the cluster amplitude $t_{a_1 \dots a_n}^{i_1 \dots i_n}$ that define it are obtained by solving the system of nonlinear, energy-independent, algebraic equations,

$$Q_n \bar{H}^{(A)} |\Phi\rangle = 0, \quad n = 1, \dots, m_A, \quad (6)$$

where

$$\bar{H}^{(A)} = e^{-T^{(A)}} H e^{T^{(A)}} = (H e^{T^{(A)}})_C \quad (7)$$

is the similarity-transformed Hamiltonian of the CC theory and where subscript C designates the connected part of the corresponding operator expression. The Q_n operators entering eq (6) are the projection operators onto the subspaces of the n -tuply excited configurations relative to reference $|\Phi\rangle$, i.e.,

$$Q_n = \sum_{\substack{i_1 < \dots < i_n \\ a_1 < \dots < a_n}} |\Phi_{i_1 \dots i_n}^{a_1 \dots a_n}\rangle \langle \Phi_{i_1 \dots i_n}^{a_1 \dots a_n}|. \quad (8)$$

In particular, the standard CCSD equations for the singly and doubly excited cluster amplitudes $t_{a_1}^{i_1}$ and $t_{a_1 a_2}^{i_1 i_2}$ defining the T_1 and T_2 components, respectively, have the following form:

$$\langle \Phi_{i_1}^{a_1} | \bar{H}^{\text{CCSD}} | \Phi \rangle = 0, \quad (9)$$

$$\langle \Phi_{i_1 i_2}^{a_1 a_2} | \bar{H}^{\text{CCSD}} | \Phi \rangle = 0, \quad i_1 < i_2, \quad a_1 < a_2, \quad (10)$$

where

$$\bar{H}^{\text{CCSD}} = e^{-(T_1+T_2)} H e^{T_1+T_2} = (H e^{T_1+T_2})_C \quad (11)$$

is the similarity-transformed Hamiltonian of the CCSD approach. The system of CC equations, eq (6), is obtained in the following way: We first insert the CC wave function $|\Psi_0\rangle$, eq (3), into the electronic Schrödinger equation,

$$H |\Psi_0\rangle = E_0 |\Psi_0\rangle, \quad (12)$$

and premultiply both sides of eq (12) on the left by e^{-T} to obtain the connected cluster form of the Schrödinger equation (1, 2, 4, 7, 9),

$$\bar{H}|\Phi\rangle = E_0|\Phi\rangle, \quad (13)$$

where

$$\bar{H} = e^{-T} H e^T = (H e^T)_C \quad (14)$$

is the similarity-transformed Hamiltonian. Next, we project eq (13), in which T is replaced by its approximate form $T^{(A)}$, onto the manifold of excited configurations generated by $T^{(A)}$ (represented in eq (6) by the projection operators Q_n with $n = 1, \dots, m_A$). Once the system of equations, eq (6), is solved for $T^{(A)}$, the CC energy corresponding to the standard method A is calculated as follows:

$$E_0^{(A)} = \langle \Phi | \bar{H}^{(A)} | \Phi \rangle. \quad (15)$$

Eq (15) can be obtained by projecting the connected cluster form of the Schrödinger equation on the reference configuration $|\Phi\rangle$.

Piecuch and Kowalski proved that one can obtain the full CI energy E_0 if the following noniterative correction $\delta_0^{(A)}$ is added to the CC energy $E_0^{(A)}$ (9, 13):

$$\delta_0^{(A)} = \sum_{n=m_A+1}^N \sum_{k=m_A+1}^n \langle \Psi_0 | Q_n C_{n-k}(m_A) M_k(m_A) | \Phi \rangle / \langle \Psi_0 | e^{T^{(A)}} | \Phi \rangle \quad (16)$$

Here,

$$C_{n-k}(m_A) = (e^{T^{(A)}})_{n-k} \quad (17)$$

are the $(n-k)$ -body components of the CC wave operator $e^{T^{(A)}}$, defining method A , $|\Psi_0\rangle$ is the exact ground-state wave function, and

$$M_k(m_A) |\Phi\rangle \equiv Q_k \bar{H}^{(A)} |\Phi\rangle = \sum_{\substack{i_1 < \dots < i_k \\ a_1 < \dots < a_k}} \mathcal{M}_{a_1 \dots a_k}^{i_1 \dots i_k}(m_A) |\Phi_{i_1 \dots i_k}^{a_1 \dots a_k}\rangle \quad (18)$$

are the quantities defined through the coefficients

$$\mathcal{M}_{a_1 \dots a_k}^{i_1 \dots i_k}(m_A) = \langle \Phi_{i_1 \dots i_k}^{a_1 \dots a_k} | \bar{H}^{(A)} | \Phi \rangle \quad (19)$$

representing the projections of the single-reference CC equations of method A on all k -tuply excited configurations $|\Phi_{i_1 \dots i_k}^{a_1 \dots a_k}\rangle$ with $k > m_A$. The $C_{n-k}(m_A)$ quantities are trivial to generate. The zero-body term, $C_0(m_A)$, equals 1; the one-body term, $C_1(m_A)$, equals T_1 ; the two-body term, $C_2(m_A)$, equals $T_2 + \frac{1}{2}T_1^2$ if $m_A \geq 2$. The $\mathcal{M}_{a_1 \dots a_k}^{i_1 \dots i_k}(m_A)$ coefficients, eq (19), define the generalized moments of CC equations. They can be easily calculated for the basic CC approximations, such as CCSD (the $m_A = 2$ case). As pointed out in our earlier work (9, 13), the

$\mathcal{M}_{a_1 \dots a_k}^{h \dots k}(m_A)$ moments represent the fundamental quantities for the CC theory. For example, the system of equations defining method A , eq (6), can be obtained by requiring that all $\mathcal{M}_{a_1 \dots a_k}^{h \dots k}(m_A)$ moments with $k=1, \dots, m_A$ vanish.

Eq (16) can be derived in several different ways. The original derivation of eq (16), presented in ref 9, has been based on the analysis of the mathematical relationships between multiple solutions of nonlinear equations representing different CC approximations (CCSD, CCSDT, etc.). An elementary derivation of eq (16), based on applying the resolution of identity to an asymmetric energy expression,

$$\langle \Psi_0 | (H - E_0^{(A)}) e^{T^{(A)}} | \Phi \rangle / \langle \Psi_0 | e^{T^{(A)}} | \Phi \rangle = E_0 - E_0^{(A)} \equiv \delta_0^{(A)} \quad (20)$$

defining the so-called MMCC functional, has been given in Appendix A of ref 13 (cf., also, refs 21, 106).

Eq (16) is the basic equation of the ground-state MMCC formalism. The meaning of eq (16) is as follows: If we want to obtain the exact, full CI, energy by adding the noniterative correction $\delta_0^{(A)}$ to the energy $E_0^{(A)}$ obtained in the standard CC calculations with method A , we must calculate the generalized moments $\mathcal{M}_{a_1 \dots a_k}^{h \dots k}(m_A)$ corresponding to projections of CC equations on all excited configurations that are not included in method A . Thus, if we want to recover the full CI energy by adding the correction $\delta_0^{(A)}$ to the CCSD energy (the $m_A = 2$ case), we have to calculate the generalized moments of the CCSD equations corresponding to projections of these equations on triply, quadruply, pentuply, and hextuply excited configurations, i.e.,

$$\mathcal{M}_{a_1 \dots a_k}^{h \dots k}(2) = \langle \Phi_{a_1 \dots a_k} | \bar{H}^{\text{CCSD}} | \Phi \rangle, \quad k = 3 - 6. \quad (21)$$

We do not have to consider the projections of the CCSD equations on higher-than-hextuply excited configurations, since for Hamiltonians containing up to two-body interactions the $\mathcal{M}_{a_1 \dots a_k}^{h \dots k}(2)$ moments with $k > 6$ vanish. Once the generalized moments of the CCSD equations are known, we can define the quantities $M_k(2)|\Phi\rangle$, using eq (18), to calculate the non-iterative MMCC correction

$$\delta_0^{\text{CCSD}} = \sum_{n=3}^N \sum_{k=3}^{\min(n,6)} \langle \Psi_0 | \mathcal{Q}_n C_{n-k}(2) M_k(2) | \Phi \rangle / \langle \Psi_0 | e^{T_1+T_2} | \Phi \rangle \quad (22)$$

to the CCSD energy.

The remaining issue is what do we do with the wave function $|\Psi_0\rangle$ in eqs (16) or (22), which in the exact MMCC theory represents the full CI ground state. In the approximate MMCC methods considered in our earlier work, the wave functions $|\Psi_0\rangle$ were evaluated either by using the low-order MBPT

expressions (9, 13–18, 20, 21) or by performing the inexpensive limited CI calculations (9, 18, 19, 21, 106, 107). The use of the low-order MBPT expressions is particularly interesting, since it leads to the renormalized (R) and completely renormalized (CR) CC approaches, which represent simple computational “black-boxes” capable of describing bond breaking with the ease-of-use of the standard CC calculations of the CCSD(T) or CCSD(TQ_f) type. For example, if we replace $|\Psi_0\rangle$ in eq (22) by

$$|\Psi^{\text{CCSD[T]}}\rangle = (1 + T_1 + T_2 + T_3^{[2]})|\Phi\rangle, \quad (23)$$

we obtain the CR-CCSD[T] approach, in which we calculate the energy as follows (9, 13–15, 17, 18, 21):

$$E_0^{\text{CR-CCSD[T]}} = E_0^{\text{CCSD}} + \langle \Psi^{\text{CCSD[T]}} | Q_3 M_3(2) | \Phi \rangle / \langle \Psi^{\text{CCSD[T]}} | e^{T_1+T_2} | \Phi \rangle \quad (24)$$

Here, T_1 and T_2 are the singly and doubly excited clusters obtained by solving the CCSD equations, E_0^{CCSD} is the CCSD energy, and

$$T_3^{[2]}|\Phi\rangle = R_0^{(3)}(V_N T_2)_C|\Phi\rangle \quad (25)$$

is a CCSD analog of the connected triples contribution to the MBPT(2) (second-order MBPT) wave function ($R_0^{(3)}$ designates the three-body component of the MBPT reduced resolvent and V_N represents the two-body part of the Hamiltonian in the normal-ordered form). If $|\Psi_0^{\text{CCSD[T]}}\rangle$ in eq (24) is replaced by

$$|\Psi^{\text{CCSD(T)}}\rangle = |\Psi^{\text{CCSD[T]}}\rangle + R_0^{(3)}V_N T_1|\Phi\rangle, \quad (26)$$

we obtain the CR-CCSD(T) method (9, 13–15, 17, 18, 20, 21). The CR-CCSD(TQ) approaches are obtained in a similar way (9, 13–15, 17, 18, 21).

The CR-CCSD[T], CR-CCSD(T), and CR-CCSD(TQ) methods remove the failing of the CCSD[T], CCSD(T), and CCSD(TQ_f) approaches at larger internuclear separations and often provide an excellent description of PESs involving single and double bond dissociation (9, 13, 15, 17–21, 111). However, the CR-CCSD(T) and CR-CCSD(TQ) results for triple bond breaking and for certain types of double bond breaking (e.g., in C₂) are somewhat less accurate (14, 18, 21). It is, therefore, interesting to examine if it is possible to develop new MMCC approximations, which would improve the description of triple bond breaking and preserve, at the same time, the philosophy of the CR-CCSD[T], CR-CCSD(T), and CR-CCSD(TQ) approaches and their standard counterparts, which is an idea of adding the noniterative corrections to the CCSD energies that are solely based on the T_1 and T_2 cluster components obtained in the CCSD calculations.

The Quasi-Variational and Quadratic MMCC Methods

Our recent numerical experiments with the CI-corrected MMCC methods indicate that in looking for the extensions of the CR-CCSD[T], CRCCSD(T), and CR-CCSD(TQ) methods that would provide an accurate description of triple bond breaking one may have to consider the approximations that use the pentuply and hexuply excited moments of the CCSD equations, $\mathcal{M}_{a_1 \dots a_k}^{h_1 \dots h_k}(2)$, $k = 5$ and 6 , respectively (21). The CR-CCSD[T] and CR-CCSD(T) methods use only the triexcited CCSD moments $\mathcal{M}_{a_1 a_2 a_3}^{h_1 h_2 h_3}(2)$, whereas the CR-CCSD(TQ) approaches use the tri- and tetraexcited moments, $\mathcal{M}_{a_1 a_2 a_3}^{h_1 h_2 h_3}(2)$ and $\mathcal{M}_{a_1 a_2 a_3 a_4}^{h_1 h_2 h_3 h_4}(2)$, respectively. In our initial attempt, we tried to extend the CR-CCSD[T], CR-CCSD(T), and CR-CCSD(TQ) approaches by replacing $|\Psi_0\rangle$ in eq (22) by the MBPT(3)-like wave function, which is the lowest-order wave function that has the pentuply and hexuply excited contributions that could engage the pentuply and hexuply excited moments, $\mathcal{M}_{a_1 a_2 a_3 a_4 a_5}^{h_1 h_2 h_3 h_4 h_5}(2)$ and $\mathcal{M}_{a_1 a_2 a_3 a_4 a_5 a_6}^{h_1 h_2 h_3 h_4 h_5 h_6}(2)$, respectively. Unfortunately, we have not succeeded in improving the CRCCSD(TQ) results for triple bond breaking, reported in ref 14, with the resulting methods. A different strategy, described in this section, is required if we want to improve the CR-CCSD(TQ) results for triple bond breaking by adding noniterative “black-box” corrections to the CCSD energies.

Theoretical Considerations

Since the MBPT(3)-like wave functions $|\Psi_0\rangle$ proved to be rather ineffective in constructing the highly accurate corrections δ_0^{CCSD} for multiple bond breaking, we decided to consider an alternative approach, in which $|\Psi_0\rangle$ in eqs (16) or (22) has a CC-like exponential form,

$$|\Psi_0^{\text{QVMMCC}}\rangle = e^{\Sigma} |\Phi\rangle, \quad (27)$$

where Σ is an approximation to the exact cluster operator T . The use of the wave function $|\Psi_0^{\text{QVMMCC}}\rangle$, eq. (27), instead of $|\Psi_0\rangle$ in calculating the MMCC correction $\delta_0^{(A)}$, eq (16), or δ_0^{CCSD} , eq (22), with various forms of the cluster operator Σ , leads to the hierarchy of the quasi-variational MMCC (QVMMCC) approximations. The QVMMCC energy correction to the CC energy $E_0^{(A)}$ has the following general form (cf. eq (16)):

$$\delta_0^{(A)}(\text{QVMMCC}) \equiv \sum_{n=m_A+1}^N \sum_{k=m_A+1}^n \frac{\langle \Phi | e^{\Sigma^\dagger} \mathcal{Q}_n C_{n-k}(m_A) M_k(m_A) | \Phi \rangle}{\langle \Phi | e^{\Sigma^\dagger} e^{T^{(A)}} | \Phi \rangle} \quad (28)$$

In particular, if method A represents the CCSD theory, the corresponding QVMMCC energy is calculated by adding the correction (cf. eq (22))

$$\delta_0^{\text{CCSD}}(\text{QVMMCC}) = \sum_{n=3}^N \sum_{k=3}^{\min(n,6)} \langle \Phi | e^{\Sigma^\dagger} Q_n C_{n-k}(2) M_k(2) | \Phi \rangle / \langle \Phi | e^{\Sigma^\dagger} e^{T+T_2} | \Phi \rangle \quad (29)$$

to the CCSD energy. The CC-like wave functions $|\Psi_0^{\text{QVMMCC}}\rangle$ eq (27), should be more effective in introducing the higher-order terms, needed in accurate calculations for multiple bond breaking, into eqs (16) or (22) than the finite-order MBPT expressions used in the existing CR-CCSD[T], CR-CCSD(T), and CR-CCSD(TQ) approaches. Moreover, the use of the exponential form of $|\Psi_0\rangle$ in eqs (16) and (22) guarantees the strict size extensivity of the resulting energies.

The name “quasi-variational”, in reference to all MMCC methods based on eqs (28) or (29), originates from the fact that by inserting the wave function $|\Psi_0^{\text{QVMMCC}}\rangle$, eq (27), into eq (16) or into the equivalent MMCC functional, eq (20), and by assuming that $\Sigma = T^{(A)}$, we obtain the expectation value of the Hamiltonian with the CC wave function $e^{T^{(A)}}|\Phi\rangle$, which is an upper bound to the exact ground-state energy. Indeed, by replacing $|\Psi_0\rangle$ in eqs (16) and (20) by $|\Psi_0^{\text{QVMMCC}}\rangle$ eq (27), we obtain,

$$\delta_0^{(A)}(\text{QVMMCC}) = \langle \Phi | e^{\Sigma^\dagger} H e^{T^{(A)}} | \Phi \rangle / \langle \Phi | e^{\Sigma^\dagger} e^{T^{(A)}} | \Phi \rangle - E_0^{(A)} \quad (30)$$

so that the corresponding QVMMCC energy, defined by adding $\delta_0^{(A)}(\text{QVMMCC})$ to $E_0^{(A)}$, becomes

$$\begin{aligned} E_0^{\text{QVMMCC}} &\equiv E_0^{(A)} + \delta_0^{(A)}(\text{QVMMCC}) \\ &= \langle \Phi | e^{\Sigma^\dagger} H e^{T^{(A)}} | \Phi \rangle / \langle \Phi | e^{\Sigma^\dagger} e^{T^{(A)}} | \Phi \rangle. \end{aligned} \quad (31)$$

When $\Sigma = T^{(A)}$, the QVMMCC energy, eq (31), reduces to the expectation value of the Hamiltonian with the CC wave function $e^{T^{(A)}}|\Phi\rangle$.

Based on the above considerations, one might propose an approximation, in which $\Sigma = T_1 + T_2$ in eq (29), with T_1 and T_2 obtained in the standard CCSD calculations. When added to the CCSD energies, the resulting corrections $\delta_0^{\text{CCSD}}(\text{QVMMCC})$ would provide upper bounds to the exact energies and, in analogy to the variational CCD theory (28, 127), the choice of $\Sigma = T_1 + T_2$ in eq (29) would lead to a qualitatively correct description of triple bond breaking in N_2 , eliminating, in particular, the nonvariational collapse of the standard CCSD approach at larger N–N separations (14, 16, 18, 21, 42, 44). Our numerical tests indicate, however, that the calculations of correction $\delta_0^{\text{CCSD}}(\text{QVMMCC})$, eq (29), with $\Sigma = T_1 + T_2$, although providing the upper bounds to the exact ground-state energies, do not lead to the desired improvements in the quantitative

description of multiple bond breaking by the QVMCC theory. This is a consequence of the fact that the choice of $\Sigma = T_1 + T_2$ in eq (29) does not bring any meaningful information about the connected triexcited clusters T_3 , which are essential for a quantitative description of bond breaking.

The simplest way of introducing the approximate T_3 clusters into the correction δ_0^{CCSD} (QVMCC) is obtained by considering the following form of the cluster operator Σ in eq (29):

$$\Sigma = T_1 + T_2 + T_3^{[2]} \quad (32)$$

where $T_3^{[2]}$ is an MBPT(2)-like estimate of T_3 defined by eq (25). It should be noticed that Σ , eq (32), represents an approximation to the exact cluster operator T , which is correct through the second order of the MBPT wave function (T_1 and T_3 contribute, for the first time, in the second order and T_2 contributes, for the first time, in the first order; T_4 , T_5 , etc. do not contribute in the first two orders). We could, of course, contemplate other, more elaborate, forms of Σ in eq (29), but our numerical experience to date indicates that a simple definition of Σ given by eq (32) is sufficient to provide very good results for triple bond breaking.

There is only one problem associated with the use of the wave function $|\Psi_0^{\text{QVMCC}}\rangle$ eq (27), in calculations of corrections δ_0^{CCSD} , namely, the use of the exponential wave function $|\Psi_0^{\text{QVMCC}}\rangle$ requires that we consider all many-body terms resulting from e^{Σ} in eq (29), including the N -body ones, where N is the number of electrons, which is impractical. In order to eliminate this bottleneck, we decided to consider simple approximations, in which the power series expansion for $|\Psi_0^{\text{QVMCC}}\rangle$,

$$|\Psi_0^{\text{QVMCC}}\rangle = \sum_{\ell=0}^n \frac{\Sigma^\ell}{\ell!} |\Phi\rangle, \quad (33)$$

or the analogous power series expansion for e^{Σ} with Σ defined by eq (32), is truncated in eqs (22) or (29) at a given power of Σ . The following two approximations are particularly important, namely, the linearized QVMCC (LMMCC) model, in which

$$|\Psi_0^{\text{QVMCC}}\rangle \approx |\Psi_0^{\text{LMMCC}}\rangle = (1 + \Sigma) |\Phi\rangle, \quad (34)$$

and the quadratic QVMCC (QMMCC) model, in which

$$|\Psi_0^{\text{QVMCC}}\rangle \approx |\Psi_0^{\text{QMMCC}}\rangle = (1 + \Sigma + \frac{1}{2}\Sigma^2) |\Phi\rangle. \quad (35)$$

The motivation behind the LMMCC approximation stems from the success of the CR-CCSD[T] and CR-CCSD(T) methods in describing single bond breaking

(9, 13, 15, 17–21, 111). As shown in the previous section, the CR-CCSD[T] and CR-CCSD(T) approximations are based on the formulas for $|\Psi_0\rangle$ that are linear in cluster amplitudes or their perturbative estimates (see eqs (23) and (26) for $|\Psi_0^{\text{CCSD[T]}}\rangle$ and $|\Psi_0^{\text{CCSD(T)}}\rangle$, respectively). As a matter of fact, the LMMCC approach using Σ defined by eq (32) is equivalent to the CR-CCSD[T] method defined by eqs (23) and (24). Indeed, the $|\Psi_0^{\text{LMMCC}}\rangle$ wave function, eq (34), with Σ defined by eq (32), is identical to the $|\Psi_0^{\text{CCSD[T]}}\rangle$ wave function defined by eq (23). In consequence, the LMMCC energy equals the CR-CCSD[T] energy, eq (24).

The LMMCC or CR-CCSD[T] and CR-CCSD(T) methods cannot describe multiple bond breaking (cf., e.g., ref 14) because of the absence of the quadratic $\frac{1}{2}T_2^2$ terms in the wave functions $|\Psi_0\rangle$ defining the relevant energy corrections δ_0^{CCSD} . These terms are present in the wave function $|\Psi_0\rangle$ defining variant “b” of the CR-CCSD(TQ) theory (the CRCCSD(TQ),b approach of ref 14). In consequence, the CR-CCSD(TQ),b results for multiple bond breaking are considerably better than the CRCCSD[T] and CR-CCSD(T) results (14). The $\frac{1}{2}T_2^2$ and other bilinear terms in cluster amplitudes, such as $T_2T_3^{[2]}$, are also present in the wave function $|\Psi_0^{\text{QMMCC}}\rangle$, eq (35), defining the QMMCC theory. Thus, we can expect further improvements in the description of multiple bond breaking by the QMMCC method. This statement parallels similar findings by Head-Gordon *et al.* (27, 28, 128, 129), who considered the quadratic variant of the ECC theory of Arponen and Bishop (114–123), in which the energy is calculated by imposing the stationary conditions for the asymmetric, doubly connected, energy functional

$$E^{\text{ECC}}(\Sigma, T) = \langle \Phi | e^{\Sigma^\dagger} e^{-T} H e^T | \Phi \rangle = \langle \Phi | e^{\Sigma^\dagger} \bar{H} | \Phi \rangle = \langle \Phi | [e^{\Sigma^\dagger} (H e^T)_c]_c | \Phi \rangle, \quad (36)$$

Where \bar{H} is the similarity-transformed Hamiltonian, eq (14), with respect to two independent cluster operators T and Σ or, more precisely, with respect to the excitation operator T and the deexcitation operator Σ^\dagger . The advantage of eq (36) over the expectation value of the Hamiltonian with the CC wave function, which can also improve the results for multiple bond breaking (28, 127), is the fact that $E^{\text{ECC}}(\Sigma, T)$ is a finite series in T and Σ^\dagger . Unfortunately, the power series expansions of $E^{\text{ECC}}(\Sigma, T)$, eq (36), in terms of T and Σ^\dagger contain higher powers of T and Σ^\dagger that cause the ECC calculations to become prohibitively expensive, even at the lowest-order ECCD level (124, 128). For this reason, Van Voorhis and Head-Gordon considered the QECCD (quadratic ECCD) or QCCD approximation, in which the power series expansion of $E^{\text{ECC}}(\Sigma, T)$, with $T = T_2$ and $\Sigma = \Sigma_2$, is terminated at the quadratic terms in Σ^\dagger (128) (cf., also, refs 27, 28, 129). In analogy to the QMMCC approach vs. full QVMMCC theory, the QCCD approximation is considerably less expensive than the full ECCD approach using higher powers of Σ^\dagger and yet it leads to a correct description of

triple bond breaking in N_2 , eliminating the nonvariational collapse of the standard CCD theory at larger N–N separations (128). We should emphasize, however, the difference between the QCCD approximation of ref 128, in which operators T and Σ are treated independently and optimized by imposing, for example, the stationarity conditions on the quadratic approximation to the full ECC functional, i.e.,

$$E^{\text{QECC}}(\Sigma, T) = \langle \Phi | [1 + \Sigma^\dagger + \frac{1}{2}(\Sigma^\dagger)^2] \bar{H} | \Phi \rangle, \quad (37)$$

and our QMMCC methods, in which T is obtained in the standard CC calculations, such as CCSD, and Σ is defined via the cluster components of this T (cf. eq (32)).

Let us now examine the contents of the QMMCC theory, in a somewhat greater detail, by discussing the QMMCC equations for the special case, where the QMMCC corrections are added to the CCSD energy ($T^{(A)} = T_1 + T_2$) and Σ is defined by eq (32). The truncation of the power series expansion of e^{Σ^\dagger} in eq (29) at the quadratic $(\Sigma^\dagger)^2$ terms, with Σ defined by eq (32), greatly simplifies eq (29)

by reducing the summation over n from $\sum_{n=3}^N$ to $\sum_{n=3}^6$. The resulting energy expression, defining the complete QMMCC theory within the $T^{(A)} = T_1 + T_2$ and $\Sigma = T_1 + T_2 + T_3^{[2]}$ approximation, referred here and elsewhere in this work to as the QMMCC(2,6) method, has the following form:

$$E_0^{\text{QMMCC}(2,6)} = E_0^{\text{CCSD}} + \delta_0^{\text{CCSD}}(\text{QMMCC}(2,6)), \quad (38)$$

where

$$\delta_0^{\text{CCSD}}(\text{QMMCC}(2,6)) = N^{\text{QMMCC}(2,6)} / D^{\text{QMMCC}(2,6)}, \quad (39)$$

with the numerator

$$\begin{aligned} N^{\text{QMMCC}(2,6)} &= \sum_{n=3}^6 \sum_{k=3}^n \langle \Psi_0^{\text{QMMCC}} | \rho_n C_{n-k}(2) M_k(2) | \Phi \rangle \\ &= \langle \Phi | [T_1^\dagger T_2^\dagger + (T_3^{[2]})^\dagger] M_3(2) \\ &\quad + [\frac{1}{2}(T_2^\dagger)^2 + T_1^\dagger (T_3^{[2]})^\dagger] [M_4(2) + T_1 M_3(2)] \\ &\quad + T_2^\dagger (T_3^{[2]})^\dagger [M_5(2) + T_1 M_4(2) + (T_2 + \frac{1}{2} T_1^2) M_3(2)] \\ &\quad + \frac{1}{2} [(T_3^{[2]})^\dagger]^2 [M_6(2) + T_1 M_5(2) + (T + \frac{1}{2} T_1^2) M_4(2) \\ &\quad + (T_1 T_2 + \frac{1}{6} T_1^3) M_3(2)] | \Phi \rangle, \end{aligned} \quad (40)$$

and the denominator

$$D^{\text{QMMCC}(2,6)} = \langle \Psi_0^{\text{QMMCC}} | e^{T_1 + T_2} | \Phi \rangle$$

American Chemical Society
Information Resource Center
1155 Sixteenth St NW
Washington DC 20036

$$\begin{aligned}
&= 1 + \langle \Phi | T_1^\dagger T_1 | \Phi \rangle + \langle \Phi | [T_2^\dagger + \frac{1}{2}(T_1^\dagger)^2] (T_2 + \frac{1}{2}T_1^2) | \Phi \rangle \\
&\quad + \langle \Phi | [T_1^\dagger T_2^\dagger + (T_3^\dagger)^\dagger] (T_1 T_2 + \frac{1}{6}T_1^3) | \Phi \rangle \\
&\quad + \langle \Phi | [\frac{1}{2}(T_2^\dagger)^2 + T_1^\dagger (T_3^{[2]})^\dagger] (\frac{1}{2}T_2^2 + \frac{1}{2}T_1^2 T_2 + \frac{1}{24}T_1^4) | \Phi \rangle \\
&\quad + \langle \Phi | T_2^\dagger (T_3^{[2]})^\dagger (\frac{1}{2}T_1 T_2^2 + \frac{1}{6}T_1^3 T_2 + \frac{1}{120}T_1^5) | \Phi \rangle \\
&\quad + \langle \Phi | \frac{1}{2} [(T_3^{[2]})^\dagger]^2 (\frac{1}{6}T_2^3 + \frac{1}{4}T_1^2 T_2^2 + \frac{1}{24}T_1^4 T_2 + \frac{1}{720}T_1^6) | \Phi \rangle. \quad (41)
\end{aligned}$$

As we can see, the QMMCC(2,6) method represents a considerable improvement over the LMMCC or CR-CCSD[T], CR-CCSD(T), and CR-CCSD(TQ),b methods. In addition to the linear terms in Σ^\dagger that are already present in the LMMCC or CR-CCSD[T] and CR-CCSD(T) models and that engage the triply excited moments $\mathcal{M}_{a_1 a_2 a_3}^{i_1 i_2 i_3}(2)$ (see eqs (23)–(26)) and in addition to the quadratic $\frac{1}{2}(T_2^\dagger)^2$ terms that are present in the CR-CCSD(TQ),b energy expression and that engage the tetraexcited moments $\mathcal{M}_{a_1 a_2 a_3 a_4}^{i_1 i_2 i_3 i_4}(2)$ (14), the QMMCC(2,6) energy contains the $T_2^\dagger (T_3^{[2]})^\dagger$ and $\frac{1}{2} [(T_3^{[2]})^\dagger]^2$ components that originate from the $(\Sigma^\dagger)^2$ quadratic terms and that lead to the appearance of the $M_5(2)|\Phi\rangle$ and $M_6(2)|\Phi\rangle$ quantities in eq (40). In consequence, the QMMCC(2,6) energy expression involves the complete set of the generalized moments of the CCSD equations, including the pentuply and hexuply excited moments, $\mathcal{M}_{a_1 a_2 a_3 a_4 a_5}^{i_1 i_2 i_3 i_4 i_5}(2)$ and $\mathcal{M}_{a_1 a_2 a_3 a_4 a_5 a_6}^{i_1 i_2 i_3 i_4 i_5 i_6}(2)$, respectively. The presence of the $\mathcal{M}_{a_1 a_2 a_3 a_4 a_5}^{i_1 i_2 i_3 i_4 i_5}(2)$ and $\mathcal{M}_{a_1 a_2 a_3 a_4 a_5 a_6}^{i_1 i_2 i_3 i_4 i_5 i_6}(2)$ moments in the QMMCC(2,6) energy should help us to obtain an accurate description of triple bond breaking.

Even if we ignore the presence of the $D^{\text{QMMCC}(2,6)}$ denominator in eq (39) (denominators of this type are characteristic to all MMCC expressions; they always play a vital role in improving the results of the MMCC calculations in the bond breaking region; cf., e.g., refs 9, 13, 14, 21), the QMMCC(2,6) energy correction δ_0^{CCSD} (QMMCC(2,6)), eq (39), has an interesting many-body structure, which is characterized by a nonstandard combination of the lower- and higher-order terms. The usual fourth-order-like terms, such as

$$E_T^{[4]} = \langle \Phi | (T_3^{[2]})^\dagger (V_N T_2)_C | \Phi \rangle, \quad (42)$$

which originate from the $\langle \Phi | (T_3^{[2]})^\dagger M_3(2) | \Phi \rangle$ contribution and which define the noniterative triples corrections of the standard (37–40) and renormalized (9,13–15, 17, 18, 20, 21) CCSD[T] and CCSD(T) methods, and the familiar fifth-order-like terms, such as

$$E_{QQ}^{[5]} = \frac{1}{4} \langle \Phi | (T_2^\dagger)^2 (V_N T_2)_C | \Phi \rangle \quad (43)$$

and

$$E_{TQ}^{[5]} = \frac{1}{2} \langle \Phi | (T_3^{[2]})^\dagger (V_N T_2)_C | \Phi \rangle, \quad (44)$$

which originate from the $\frac{1}{2}\langle\Phi|(T_2^\dagger)^2 M_4(2)|\Phi\rangle$ and $\langle\Phi|(T_3^{[2]})^\dagger M_3(2)|\Phi\rangle$ contributions and which define the standard (see ref (41) and references therein) and renormalized (9, 13–15, 18, 21) CCSD(TQ) methods (cf. refs 130–132 for detailed information about all fifth-order $E^{[5]}$ terms), are combined in eq (40) with several higher-order terms, including, for example, the sixth-order-like $\langle\Phi|T_2^\dagger(T_3^{[2]})^\dagger T_2(V_N T_2)_C|\Phi\rangle$ term, originating from the $\langle\Phi|T_2^\dagger(T_3^{[2]})^\dagger T_2 M_3(2)|\Phi\rangle$ contribution, or the eighth-order-like $\frac{1}{48}\langle\Phi|[(T_3^{[2]})^\dagger]^2(V_N T_2^4)_C|\Phi\rangle$ term, originating from $\frac{1}{2}\langle\Phi|[T_3^{[2]})^\dagger]^2 M_6(2)|\Phi\rangle$. The order-by-order analysis, based on the conventional MBPT formalism, used to design the standard CC approximations, would never allow us to write the expressions of the type of eq (40). This observation, combined with the success of the QMMCC(2,6) theory in describing triple bond breaking in N_2 (see the next subsection), is a clear demonstration of the new possibilities offered by the MMCC formalism, which allows us to formulate new and useful types of the noniterative corrections to CC energies that are characterized by the nonstandard selections of higher-order terms.

Along with the complete QMMCC(2,6) method, defined by eqs (38)–(41), we decided to test the approximate QMMCC schemes, in which the high-order terms involving the most expensive hexuply or pentuply and hexuply excited moments of the CCSD equations are ignored. For example, we can neglect the $\frac{1}{2}[(T_3^{[2]})^\dagger]^2$ term in eq (40) by reducing the summation over n to $\sum_{n=3}^5$ and we can simultaneously ignore a similar term in eq (41). This leads to the QMMCC(2,5) method, which does not require the calculation of the hexuply excited moments $\mathcal{M}_{a_1 a_2 a_3 a_4 a_5 a_6}^{h_1 h_2 h_3 h_4 h_5 h_6}(2)$. As shown in the next subsection, the absence of the $\mathcal{M}_{a_1 a_2 a_3 a_4 a_5 a_6}^{h_1 h_2 h_3 h_4 h_5 h_6}(2)$ moments and $\frac{1}{2}[(T_3^{[2]})^\dagger]^2$ components in the QMMCC(2,5) energy expression has no detrimental effect on the results of QMMCC calculations for triple bond breaking in N_2 . We can also propose the QMMCC(2,4) and QMMCC(2,3) approximations. The QMMCC(2,4) method is obtained by ignoring the $T_2^\dagger(T_3^{[2]})^\dagger$ terms in eqs (40) and (41) defining the QMMCC(2,6) energy formula, in addition to the $\frac{1}{2}[(T_3^{[2]})^\dagger]^2$ terms that have already been neglected in the QMMCC(2,5) approach. The QMMCC(2,4) method, just like its CR-CCSD(TQ),b counterpart of ref 14, requires that we only consider the tri- and tetraexcited moments of the CCSD equations, $\mathcal{M}_{a_1 a_2 a_3}^{h_1 h_2 h_3}(2)$ and $\mathcal{M}_{a_1 a_2 a_3 a_4}^{h_1 h_2 h_3 h_4}(2)$, respectively. In the QMMCC(2,3) approximation, we go one step further by neglecting the $[\frac{1}{2}(T_2^\dagger)^2 + T_1^\dagger(T_3^{[2]})^\dagger]$ terms in eqs (40) and (41), in addition to all the other terms ignored in the QMMCC(2,4) and QMMCC(2,5) approximations. The resulting QMMCC(2,3) energy formula is almost identical to the energy expressions defining the CR-CCSD[T] or CR-CCSD(T) approximations. In particular, the only moments of the CCSD equations that need to be considered in the QMMCC(2,3) calculations are the triexcited moments $\mathcal{M}_{a_1 a_2 a_3}^{h_1 h_2 h_3}(2)$.

Neither the QMMCC(2,3) method nor its CR-CCSD[T] and CR-CCSD(T) counterparts are capable of describing multiple bond breaking (cf. ref 14). Thus, in the present work we focus on the QMMCC(2,4), QMMCC(2,5), and QMMCC(2,6) approximations. In particular, we consider the QMMCC(2,4) approach, which allows us to understand the significance of the CR-CCSD(TQ) methods, when compared with the lower-order LMMCC and higher-order QMMCC models. A direct comparison of the QMMCC(2,4) and CR-CCSD(TQ),b energy expressions indicates that the CR-CCSD(TQ),b approach can be viewed as a slightly modified QMMCC(2,4) theory, in which the only bilinear term of the $\frac{1}{2}(\Sigma^\dagger)^2$ type, multiplying $[M_4(2) + T_1M_3(2)]$ in eq (40) and $(\frac{1}{2}T_2^2 + \frac{1}{2}T_1^2T_2 + \frac{1}{24}T_1^4)$ in eq (41), is the lowest-order $\frac{1}{2}(T_2^\dagger)^2$ term. This is reflected in the similarity of the QMMCC(2,4) and CR-CCSD(TQ),b results (see the next subsection). At the same time, the LMMCC approach is equivalent to the CR-CCSD[T] method, which is, in turn, only slightly less accurate than the CR-CCSD(T) approach (9, 13, 21) and considerably less accurate than the CR-CCSD(TQ),b method in applications involving multiple bond breaking (14, 18, 21). Finally, the QMMCC(2,4) approach is an approximation to the more complete QMMCC(2,5) and QMMCC(2,6) models. This means that the CR-CCSD(TQ),b or QMMCC(2,4) approaches can be regarded as the intermediate steps between the less accurate LMMCC = CR-CCSD[T] or CR-CCSD(T) methods, which work great for the ground-state PESs involving single bond breaking (9, 13, 15, 17, 18, 20, 21), and the more accurate QMMCC(2,5) and QMMCC(2,6) approaches, which are capable of providing an accurate description of the PESs involving multiple bond breaking. We expect, therefore, to observe the following accuracy patterns in the actual calculations for bond breaking:

$$\begin{aligned} \text{LMMCC} &\equiv \text{CR-CCSD[T]} \lesssim \text{CR-CCSD(T)} \\ &< \text{CR-CCSD(TQ),b} \approx \text{QMMCC(2,4)} \\ &< \text{QMMCC(2,5)} \lesssim \text{QMMCC(2,6)} \equiv \text{QMMCC} \lesssim \text{Full CI.} \end{aligned} \quad (45)$$

Numerical Example: Bond Breaking in N₂

The primary motivation behind the QMMCC approximations is the need to improve the CR-CCSD(TQ) description of more complicated types of multiple bond breaking, such as triple bond breaking in N₂. The CR-CCSD[T], CR-CCSD(T), and CR-CCSD(TQ) methods are capable of providing an excellent description of PESs involving single and double bond dissociation (9, 13, 15, 17–21, 111), but the CR-CCSD(T) and CR-CCSD(TQ) results for triple bond breaking are less accurate (14, 18, 21). This can be seen by analyzing the CR-

CCSD(T) and CR-CCSD(TQ),b results for the potential energy curve of the N_2 molecule, as described by the DZ basis set (113), shown in Table I and Figure 1.

The CR-CCSD(T) method improves the standard CCSD(T) results for N_2 at larger internuclear separations R , but the level of improvement offered by the CR-CCSD(T) approach is not sufficient to make the CR-CCSD(T) method a reasonable alternative for calculating PESs involving multiple bond breaking (see Table I). The CR-CCSD(TQ),b approach performs much better in this regard, eliminating almost all pathologies observed in the standard single-reference CC calculations for N_2 , but the 10–25 millihartree differences between the CR-CCSD(TQ),b and full CI energies at the intermediate and larger values of R are still too large for many applications. Clearly, it would be desirable to reduce the 10–25 millihartree errors in the CR-CCSD(TQ),b results at larger values of R to a few millihartree. It would also be useful to reduce or, at the very least, shift away the small, ~ 4.9 millihartree, hump on the CR-CCSD(TQ),b potential energy curve obtained for the DZ model of N_2 towards larger N–N separations.

The QMMCC results for the N_2 molecule, as described by the DZ basis set, obtained by adding the QMMCC(2,6), QMMCC(2,5), and QMMCC(2,4) corrections to the CCSD energies (all obtained with the ground-state RHF determinant as a reference), are shown in Table I and Figure 1. As we can see, the QMMCC(2,6) and QMMCC(2,5) methods provide an excellent description of the entire $R = 0.75R_e - 2.25R_e$ region (recall that $R_e = 2.068$ bohr is the equilibrium bond length of N_2). The more complete QMMCC(2,6) theory reduces the very large negative errors in the CCSD results for N_2 in the $R > 1.75R_e$ region and the 13.517, 25.069, and 14.796 millihartree errors in the CR-CCSD(TQ),b results at $R = 1.75R_e$, $2R_e$, and $2.25R_e$ to 1.380, 6.230, and -3.440 millihartree, respectively. For the smaller values of R , the errors in the QMMCC(2,6) results are $\sim 1 - 2$ millihartree (they are smaller than the errors obtained in the full CCSDT calculations).

As shown in Figure 1, the QMMCC(2,6) potential energy curve for N_2 is very close to the exact potential energy curve obtained with the full CI approach. The hump on the QMMCC(2,6) potential energy curve is smaller than the hump on the CR-CCSD(TQ),b curve. The QMMCC(2,6) potential is a monotonically increasing function in the entire $2.068 \text{ bohr} \leq R \leq 4.35 \text{ bohr}$ region. The QMMCC(2,6) energies begin to decrease only when $R \approx 2.25R_e$, but even there the errors in the QMMCC(2,6) results, relative to full CI, are less (in absolute value) than 3.5 millihartree (cf. Table I). The approximate dissociation energy D_e , calculated by forming the difference between the QMMCC(2,6) energies at $R = 4.35 \text{ bohr}$ and $R = R_e$, is 6.59 eV, is in excellent agreement with the full CI value of D_e of 6.61 eV. The QMMCC(2,6) potential energy curve is located above the full CI curve in the entire $R < 2.25R_e$ region, in spite of the apparently nonvariational behavior of the CCSD method at larger N–N separations.

Table I. Ground-state energies of the N₂ molecule, as described by the DZ basis set (113), for a few internuclear separations R^a

Method	$0.75R_e$	R_e^b	$1.25R_e$	$1.5R_e$	$1.75R_e$	$2R_e$	$2.25R_e$
CCSD	3.132	8.289	19.061	33.545	17.714	-69.917	-120.836
CCSDT ^c	0.580	2.107	6.064	10.158	-22.468	-109.767	-155.656
CCSD(T) ^c	0.742	2.156	4.971	4.880	-51.869	-246.405	-387.448
CCSD(TQ) _f ^c	0.226	0.323	0.221	-2.279	-14.243	92.981	334.985
CCSDT(Q) _f ^d	0.047	-0.010	-0.715	-4.584	3.612	177.641	426.175
CR-CCSD(T) ^c	1.078	3.452	9.230	17.509	-2.347	-86.184	-133.313
CR-CCSD(TQ) _f ^c	0.451	1.302	3.617	8.011	13.517	25.069	14.796
QMMCC(2,4)	0.458	1.384	3.916	8.362	13.074	22.091	10.749
QMMCC(2,5)	0.384	1.012	2.365	3.756	1.415	6.672	-2.638
QMMCC(2,6)	0.384	1.012	2.373	3.784	1.380	6.230	-3.440
QMMCC(2,6)	0.384	1.013	2.397	3.782	1.378	6.240	-3.418
$(M_{a_1 a_2 a_3 a_4 a_5 a_6}^{1^1 2^1 3^1 4^1 5^1 6} (2) = 0$							
QMMCC(2,6)	0.387	1.040	2.533	4.317	2.062	4.674	-6.499
$(M_{a_1 a_2 a_3 a_4 a_5}^{1^1 2^1 3^1 4^1 5} (2) = 0,$							
$(M_{a_1 a_2 a_3 a_4 a_5 a_6}^{1^1 2^1 3^1 4^1 5^1 6} (2) = 0$							

^a The CC and QMMCC energies are in millihartree relative to the corresponding full CI energy values, which are -108.549027, -109.105115, -109.054626, -108.950728, -108.889906, -108.868239, and -108.862125 hartree for $R = 0.75R_e$, R_e , $1.25R_e$, $1.5R_e$, $1.75R_e$, $2R_e$, and $2.25R_e$, respectively. The lowest two occupied and the highest two unoccupied orbitals were frozen in the correlated calculations.

^b The equilibrium bond length, $R_e = 2.068$ bohr.

^c From ref 14.

^d From ref 16.

Based on the nature of the triple bond in N₂, which requires, at least in principle, some hextuple excited configurations in the CI expansion of the ground-state wave function, one might expect that the lower-order QMMCC methods, such as QMMCC(2,5), should not work well at larger N–N separations. Interestingly enough, this is not the case. As demonstrated in Table I, the QMMCC(2,5) approach, which does not require the calculation of the hextuple excited $\mathcal{M}_{a_1 a_2 a_3 a_4 a_5 a_6}^{1^1 2^1 3^1 4^1 5^1 6} (2)$ moments, provides the results of the QMMCC(2,6) quality. The QMMCC(2,5) method reduces the large, 30–120 millihartree, unsigned errors in the CCSD results in the $R \geq 1.5R_e$ region to 3.756 millihartree at $R = 1.5R_e$, 1.415 millihartree at $R = 1.75R_e$, 6.672 millihartree at $R = 2R_e$, and 2.638 millihartree at $R = 2.25R_e$. We have, in fact, discovered that we can completely ignore the most expensive $\mathcal{M}_{a_1 a_2 a_3 a_4 a_5}^{1^1 2^1 3^1 4^1 5} (2)$ and $\mathcal{M}_{a_1 a_2 a_3 a_4 a_5 a_6}^{1^1 2^1 3^1 4^1 5^1 6} (2)$ moments in the QMMCC(2,6) energy expression, eq (38), without changing the excellent description of the N₂ potential energy curve by

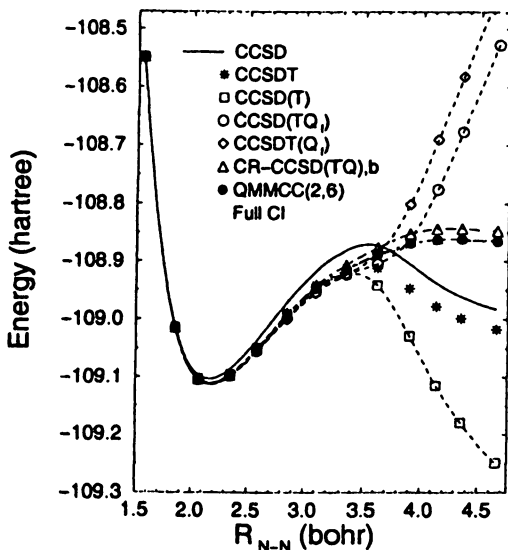


Figure 1. Potential energy curves for the N_2 molecule, as described by the DZ basis set (113) (see refs 14, 16 and Table I for the numerical data; see the text for further details).

the QMMCC(2,6) method. The errors in the QMMCC(2,6) results for N_2 , in which the hextuple excited $M_{a_1 a_2 a_3 a_4 a_5 a_6}^{h^1 2^1 3^1 4^1 5^1 6}$ (2) moments are ignored, are virtually identical to the small errors obtained in the complete QMMCC(2,6) calculations (see Table I). There is a slight increase in the magnitude of errors when the pentuply and hextuple excited moments are neglected, but the overall performance of the QMMCC(2,6) approximation, in which $M_{a_1 a_2 a_3 a_4 a_5}^{h^1 2^1 3^1 4^1 5}$ (2) $M_{a_1 a_2 a_3 a_4 a_5 a_6}^{h^1 2^1 3^1 4^1 5^1 6}$ (2) = 0, is very good. The potential energy curve of N_2 , obtained by performing the QMMCC(2,6) calculations in which the pentuply and hextuple excited moments are zeroed, is a monotonically increasing function in the entire $R_e \leq R \leq 2R_e$ region. The approximate dissociation energy D_e obtained by forming the difference between the QMMCC(2,6) $M_{a_1 a_2 a_3 a_4 a_5}^{h^1 2^1 3^1 4^1 5}$ (2) = 0, $M_{a_1 a_2 a_3 a_4 a_5 a_6}^{h^1 2^1 3^1 4^1 5^1 6}$ (2) = 0) energies at $R = 2R_e$ and $R = R_e$, is 6.54 eV, in very good agreement with the full CI D_e value of 6.61 eV. The somewhat more complete QMMCC(2,6) calculations, in which only the hextuple excited $M_{a_1 a_2 a_3 a_4 a_5 a_6}^{h^1 2^1 3^1 4^1 5^1 6}$ (2) moments are zeroed, and the QMMCC(2,5) calculations produce the D_e values, which are only slightly more accurate than the value of D_e resulting from the QMMCC(2,6) $M_{a_1 a_2 a_3 a_4 a_5}^{h^1 2^1 3^1 4^1 5}$ (2) = 0, $M_{a_1 a_2 a_3 a_4 a_5 a_6}^{h^1 2^1 3^1 4^1 5^1 6}$ (2) = 0) calculations (6.59 and 6.61 eV, respectively). Those are important and potentially very useful

observations, since by neglecting the pentuply and hexuply excited moments of the CCSD equations in the QMMCC(2,6) calculations, we are largely preserving the relatively low cost of the CR-CCSD(TQ),b or QMMCC(2,4) calculations, while considerably improving the results for large values of R .

As expected, the QMMCC(2,4) method does not provide any significant improvements in comparison with the CR-CCSD(TQ),b approach. As shown in Table I, the QMMCC(2,4) and CR-CCSD(TQ),b results are essentially identical. In other words, we cannot ignore the $T_2^\dagger(T_3^{[2]})^\dagger$ terms in the QMMCC(2,6) energy expressions, although we can certainly ignore the corresponding $M_{a_1 a_2 a_3 a_4 a_5}^{i_1 i_2 i_3 i_4 i_5}$ (2) moments in eq (40). Our QMMCC(2,5) calculations imply that we can also neglect the $\frac{1}{2}[(T_3^{[2]})^\dagger]^2$ terms and the corresponding hexuply excited $M_{a_1 a_2 a_3 a_4 a_5 a_6}^{i_1 i_2 i_3 i_4 i_5 i_6}$ (2) moments. The calculations for the N_2 molecule, reported in this work, clearly reflect the accuracy patterns described by eq (45).

The above example demonstrates that the new QMMCC theory may allow us to preserve the "black-box" character of the noniterative CC methods, while giving us an opportunity to obtain a highly accurate description of ground-state PESs involving multiple bond breaking. Interestingly enough, the QMMCC formalism is powerful enough to provide us with the desired improvements in the description of triple bond breaking in N_2 , in spite of the poor description of the N_2 potential energy curve by the CCSD method. At this point we can only speculate about this, but one might expect that the improvements in the results offered by the QMMCC methods might be even more substantial if the values of the T_1 and T_2 cluster amplitudes, used to construct the QMMCC corrections to the CCSD energies, were more accurate than the CCSD values. The alternative methods of calculating the T_1 and T_2 cluster components, which may help us to develop the noniterative energy corrections that are even better than the QMMCC corrections, are discussed in the next section.

Improving the T_1 and T_2 Components by the Extended Coupled-Cluster Theory

We have recently begun experimenting with the alternative sources of information about the T_1 and T_2 clusters that are needed to construct the standard and MMCC or QMMCC noniterative energy corrections. One such source might be provided by the ECC theory (114–123) or by its modified variant described in ref 124. The ECC methods are based on the idea of optimizing the cluster operator T along with the auxiliary operator Σ by considering the energy functional $E^{\text{ECC}}(\Sigma, T)$, eq (36).

As mentioned in the previous section, the major advantage of eq (36) over the expectation value of the Hamiltonian with the CC wave function, which

might also be considered as a way to find the optimum cluster operator T (28, 127), is the fact that the doubly connected expression $E^{\text{ECC}}(\Sigma, T)$, eq (36), is a finite series in T and Σ^\dagger (the expectation value of the Hamiltonian with the CC wave function is a nonterminating series in T and T^\dagger). There are several other advantages of using eq (36) and the related equations for T and Σ as means to determine the cluster operator T . For example, the ECC methods (114–124) and the related XCC approaches (124–126) are capable of describing various higher-order effects, including the effect of T_4 clusters, even at the low levels of approximation, such as ECCD or ECCSD. Those effects are being brought into the ECC formalism as products of the low-order many-body components of Σ^\dagger and T and their powers. For example, an important part of the fifth-order effect due to T_4 clusters, described by the $E_{\text{QQ}}^{[5]}$ energy contribution, eq (43), appears in the ECC theory in the form of the $\frac{1}{4}\langle\Phi|(\Sigma_2^\dagger)^2(V_N T_2^2)_C|\Phi\rangle$ term, where Σ_2 is a two-body component of Σ . This is possible, since the lowest-order MBPT estimates of Σ and T are identical (see, e.g., refs 133, 134; cf., also, refs 124, 135, 136). The $\frac{1}{4}\langle\Phi|(\Sigma_2^\dagger)^2(V_N T_2^2)_C|\Phi\rangle$ term, which mimics the $E_{\text{QQ}}^{[5]}$ contribution, is present in the ECC energy, eq (36), already at the lowest ECCD level, in which $T = T_2$ and $\Sigma = \Sigma_2$. As pointed out in the Introduction, the effects of high-order cluster components, such as T_4 , become very important in the bond breaking region. We can, therefore, expect that the ECCD or ECCSD methods provide improvements in the results of the standard CCSD calculations at larger internuclear separations. Another advantage of the ECC theory over the standard CC formalism is the fact that the cluster operator T of the ECC theory is determined by solving a coupled system of equations for T and Σ , which are treated as completely independent operators. This additional flexibility of the ECC theory may help us to improve the T_1 and T_2 components in the bond breaking region.

In this section, we examine the possibility of improving the quality of T_1 and T_2 components in the bond breaking region by solving the ECCSD equations described in ref 124. The ECC formalism introduced in ref 124 is based on the idea of rewriting the electronic Schrödinger equation for the CC wave function $|\Psi_0\rangle$ eq (3), in the following doubly connected form:

$$\bar{\bar{H}}|\Phi\rangle = E_0|\Phi\rangle, \quad (46)$$

where $|\Phi\rangle$ is the IPM reference configuration and

$$\bar{\bar{H}} = e^{\Sigma^\dagger} (e^{-T} H e^T) e^{-\Sigma^\dagger} = e^{\Sigma^\dagger} \bar{H} e^{-\Sigma^\dagger} = (e^{\Sigma^\dagger} \bar{H})_C = [e^{\Sigma^\dagger} (H e^T)_C]_C \quad (47)$$

is the doubly transformed Hamiltonian, obtained by transforming the CC similarity transformed Hamiltonian \bar{H} , eq (14), with e^{Σ^\dagger} . Eq (46) is obtained

by multiplying both sides of the connected cluster form of the electronic Schrödinger equation, eq (13), on the left by e^{Σ^\dagger} inserting $e^{-\Sigma^\dagger} e^{\Sigma^\dagger} = 1$ between \bar{H} and $|\Phi\rangle$ in eq (13), and replacing $e^{\Sigma^\dagger} |\Phi\rangle$ in the resulting equation by $|\Phi\rangle$ (this is possible since the deexcitation operator Σ^\dagger and its positive powers annihilate $|\Phi\rangle$).

Eq (46) alone is not sufficient to determine two different cluster operators T and Σ . Thus, in addition to the right eigenvalue problem involving \bar{H} , eq (46), we consider the corresponding left eigenvalue problem,

$$\langle \Phi | \bar{H} = E_0 \langle \tilde{\Phi} |. \quad (48)$$

The doubly transformed Hamiltonian \bar{H} , eq (47), being non-Hermitian, has the left-hand (bra) eigenstates, which may be different from the corresponding right-hand (ket) eigenstates. In particular, the left-hand and right-hand ground states of \bar{H} , $\langle \tilde{\Phi} |$ and $|\Phi\rangle$, respectively, are, for the general operators T and Σ , the completely different states. We can, however, impose an additional condition that for the specific cluster operators T and Σ , used to construct \bar{H} in the ECC theory, $\langle \tilde{\Phi} | = \langle \Phi |$. This leads to the desired second equation for T and Σ ,

$$\langle \Phi | \bar{H} = E_0 \langle \Phi |, \quad (49)$$

which is the left-hand analog of eq (46).

Eqs (46) and (49) are the basic equations of the ECC theory described in ref 124. The approximate ECC methods, such as ECCSD, are obtained by truncating the many-body expansions of cluster operators T and Σ at some excitation level $m_A < N$, so that T is replaced by $T^{(A)}$, eq (4), and Σ is replaced by

$$\Sigma^{(A)} = \sum_{n=1}^{m_A} \Sigma_n, \quad (50)$$

where

$$\Sigma = \sum_{\substack{i_1 < \dots < i_n \\ a_1 < \dots < a_n}} \sigma_{a_1 \dots a_n}^{i_1 \dots i_n} E_{i_1 \dots i_n}^{a_1 \dots a_n}, \quad (51)$$

$n = 1, \dots, m_A$, are the many-body components of $\Sigma^{(A)}$, and by projecting eqs (46) and (49), with $T = T^{(A)}$ and $\Sigma = \Sigma^{(A)}$, onto the manifolds of excitations generated by $T^{(A)}$ and $\Sigma^{(A)}$. For example, the ECCSD equations for the cluster amplitudes $t_{a_1}^{i_1}$, $t_{a_1 a_2}^{i_1 i_2}$, $\sigma_{a_1}^{i_1}$, and $\sigma_{a_1 a_2}^{i_1 i_2}$ defining T_1 , T_2 , Σ_1 , and Σ_2 (the $m_A = 2$ case), can be given the following form:

$$\langle \Phi_{i_1}^{a_1} | \bar{H}^{ECCSD} | \Phi \rangle = 0 \quad (52)$$

$$\langle \Phi_{i_1 i_2}^{a_1 a_2} | \bar{H}^{ECCSD} | \Phi \rangle = 0, \quad i_1 < i_2, \quad a_1 < a_2, \quad (53)$$

$$\langle \Phi | \bar{\bar{H}}^{\text{ECCSD}} | \Phi_{i_1}^{a_1} \rangle = 0 \quad (54)$$

$$\langle \Phi | \bar{\bar{H}}^{\text{ECCSD}} | \Phi_{i_1 i_2}^{a_1 a_2} \rangle = 0, \quad i_1 < i_2, \quad a_1 < a_2, \quad (55)$$

where

$$\begin{aligned} \bar{\bar{H}}^{\text{ECCSD}} &= e^{\Sigma_1^\dagger + \Sigma_2^\dagger} (e^{-T_1 - T_2} H e^{T_1 + T_2}) e^{-\Sigma_1^\dagger - \Sigma_2^\dagger} \\ &= e^{\Sigma_1^\dagger + \Sigma_2^\dagger} \bar{H}^{\text{CCSD}} e^{-\Sigma_1^\dagger - \Sigma_2^\dagger} = (e^{\Sigma_1^\dagger + \Sigma_2^\dagger} \bar{H}^{\text{CCSD}})_C, \end{aligned} \quad (56)$$

with \bar{H}^{CCSD} defined by eq (11), is the doubly transformed Hamiltonian of the ECCSD approach. Once the system of equations for $t_{a_1}^{i_1}$, $t_{a_1 a_2}^{i_1 i_2}$, $\sigma_{a_1}^{i_1}$, and $\sigma_{a_1 a_2}^{i_1 i_2}$ is solved, the ECCSD energy is calculated as follows (124):

$$E_0^{\text{ECCSD}} = \langle \Phi | \bar{\bar{H}}^{\text{ECCSD}} | \Phi \rangle. \quad (57)$$

Eq (57) can be obtained by projecting eq (46), with $T = T_1 + T_2$ and $\Sigma = \Sigma_1 + \Sigma_2$, on reference $|\Phi\rangle$.

A direct inspection indicates that the ECC theory of ref 124 and the original ECC formalism of Arponen and Bishop (114–123) are based on the same energy expression (cf., e.g., eqs (36) and (57)). The difference between both theories is in the method of obtaining T and Σ . The original ECC formalism of Arponen and Bishop is based on making the functional $E^{\text{ECC}}(\Sigma, T)$, eq (36), stationary with respect to T and Σ , which is not the case in the ECC theory of ref 124. The ECC theory of Arponen and Bishop is rigorously bi-variational, which is a very useful feature in the calculations of energy derivatives and molecular properties (see, e.g., refs 128, 137–145). The ECC theory of Piecuch and Bartlett (124) is no longer bi-variational, but it has several other interesting features, including the completely symmetric treatment of the right-hand and left-hand ground states of \bar{H} (cf. eqs (46) and (49)). Those features are particularly useful in extending the ECC theory to excited states (see ref 124 for further details).

As already mentioned, the applicability of the ECC theory, in which $T = T_2$ and $\Sigma = \Sigma_2$ (the ECCD case) and in which the power series expansion of $E^{\text{ECC}}(\Sigma, T)$, eq (36), is terminated at the quadratic terms in Σ^\dagger (the QECCD or QCCD (128) approximation; cf. eq (37)), to triple bond breaking in N_2 and other systems has recently been examined by Head-Gordon *et al.* (27, 28, 128, 129). The analogous quadratic and cubic ECCSD schemes, in which $T = T_1 + T_2$ and $\Sigma = \Sigma_1 + \Sigma_2$, have been investigated for several years by Pal and others (141–145), primarily in the context of property calculations. There are unanswered questions though. For example, although the termination of the power series expansion of $E^{\text{ECC}}(\Sigma, T)$, eq (36), at the quadratic terms in Σ^\dagger might be necessary, since this reduces the scaling of the ECCD and ECCSD methods to n^6 (28, 128), other ways of simplifying the ECC functional, obtained by truncating the many-body expansion of the doubly transformed Hamiltonian \bar{H} , eq (47),

defining the ECC energy (cf. eq (57)), are possible and may very well have to be explored in the future (see ref 124 for the examples of the ECCSD methods based on truncating the many-body expansion of \bar{H}). For the development of those alternative ECC methods, it is important to know first how accurate the complete ECCSD theory is in the calculations for multiple bond breaking. A comparison of the complete and quadratic ECCSD (QECCSD) approximations is important, too. In fact, it is useful to compare the entire sequence of the linear (LECCSD), quadratic (QECCSD), and full ECCSD approximations. Since in this preliminary study, we test the ECCSD method of ref 124, described by eqs (52)–(57), we define the LECCSD and QECCSD approximations by replacing the doubly transformed Hamiltonian \bar{H}^{ECCSD} , eq (56), in eqs (52)–(55) and (57) by

$$\bar{H}^{\text{ECCSD}} = [1 + (\Sigma^{\text{CCSD}})^\dagger] \bar{H}^{\text{CCSD}} [1 - (\Sigma^{\text{CCSD}})^\dagger] \quad (58)$$

and

$$\begin{aligned} \bar{H}^{\text{QECCSD}} = & \{1 + (\Sigma^{\text{CCSD}})^\dagger + \frac{1}{2}[(\Sigma^{\text{CCSD}})^\dagger]^2\} \bar{H}^{\text{CCSD}} \\ & \times \{1 - (\Sigma^{\text{CCSD}})^\dagger + \frac{1}{2}[(\Sigma^{\text{CCSD}})^\dagger]^2\}, \end{aligned} \quad (59)$$

respectively, where $\Sigma^{\text{CCSD}} = \Sigma_1 + \Sigma_2$. In the preliminary calculations for N_2 , reported in this paper, we compare the LECCSD and QECCSD results, based on eqs (58) and (59), respectively, with the results of the full ECCSD calculations, employing eqs (52)–(57). We should emphasize that our QECCSD Hamiltonian brings some additional terms, compared to other quadratic ECC approximations studied earlier (27, 28, 128, 129, 141, 145). On the other hand, the LECCSD method defined by eq (58) is not as rich in various nonlinear terms involving Σ^\dagger as the ECC approximations studied previously, so that it is interesting to examine how effective the above LECCSD and QECCSD methods are in improving the standard CCSD results for triple bond breaking in N_2 . Finally, in their original QCCD calculations for N_2 and a few other systems, Head-Gordon and co-workers used the Brueckner orbitals obtained by maximizing the overlap of the reference configuration $|\Phi\rangle$ with the exact, full CI, wave function (28, 128). Clearly, the full CI Brueckner orbitals will never be used in any practical calculations. Thus, it is worthwhile to examine how the full ECCSD, LECCSD, and QECCSD methods perform when the standard RHF configuration is used as a reference.

As in the recent QCCD study by Head-Gordon *et al.* (28, 128), we tested the ECCSD, LECCSD, and QECCSD methods, based on eqs (52)–(59), using the minimum basis set STO-3G (146) model of N_2 . In all correlated calculations, the lowest two core orbitals were kept frozen. As in the earlier section, our discussion of the results focuses on the bond breaking region, where the standard CCSD approach displays, using a phrase borrowed from ref 128, “a colossal failure” (see Table II and Figure 2).

Table II. Ground-state energies of the N₂ molecule, as described by the STO-3G basis set (146)^a

R^b	Full CI	CCSD	QECCSD	ECCSD	$\langle \text{CCSD} \rangle^c$	$\langle \text{QECCSD} \rangle^c$	$\langle \text{ECCSD} \rangle^c$
1.0	-5.208400	0.319	0.298	0.298	0.298	0.298	0.298
1.5	-0.279883	1.102	0.885	0.885	0.890	0.888	0.888
2.0	0.623240	3.295	1.897	1.897	2.004	1.946	1.946
2.5	0.651880	9.220	3.442	3.428	4.316	3.775	3.775
3.0	0.546614	13.176	3.908	3.758	5.288	4.160	4.161
3.5	0.473442	-38.645	5.322	4.746	16.755	3.387	3.388
4.0	0.447822	-140.376	15.968	14.122	80.696	7.206	7.145
4.5	0.441504	-184.984	27.769	24.039	95.003	11.506	11.277
5.0	0.439549	-200.958	35.732	30.390	91.561	13.877	13.327
5.5	0.438665	-206.974	40.491	33.867	86.652	14.931	14.224
6.0	0.438265	-209.538	43.227	35.746	83.037	15.356	14.553
7.0	0.438054	-211.915	45.595	37.306	79.607	15.571	14.724
8.0	0.438029	-213.431	46.320	37.799	78.563	15.578	14.758

^a The CC and ECC energies are in millihartree relative to the corresponding full CI energy values. The full CI energies E are reported as $-(E + 107)$ in hartree. The lowest two occupied orbitals were frozen in the correlated calculations.

^b The N–N separation in bohr. The equilibrium R value is 2.068 bohr.

^c $\langle X \rangle$ ($X = \text{CCSD}, \text{QECCSD}, \text{ECCSD}$) is the expectation value of the Hamiltonian with the $e^{T_1+T_2}|\Phi\rangle$ wave function, where T_1 and T_2 are obtained with method X (cf. eq (60)).

The results in Table II and Figure 2 demonstrate that the complete ECCSD formalism of ref 124, in which all nonlinear terms in Σ and T are included, and its quadratic QECCSD variant, defined by the truncated Hamiltonian \bar{H}^{QECCSD} , eq (59), provide great improvements in the poor description of the potential energy curve of N₂ by the standard CCSD approach. The huge negative errors in the CCSD results at larger internuclear separations $R \geq 4.5$ bohr, of about -200 millihartree reduce to the relatively small positive, 24–38 millihartree (ECCSD) or 28–46 millihartree (QECCSD), errors. The considerable reduction of errors is also observed for the intermediate and small values of R , including the equilibrium, $R \approx 2.0$ bohr, region (see Table II). The QECCSD and ECCSD methods are capable of eliminating the unphysical behavior of the CCSD method at larger N–N distances, restoring, in particular, the variational description of the potential energy curve of N₂ at all internuclear separations (see Figure 2). The fact that the ECCSD method of Piecuch and Bartlett is not rigorously bi-variational seems to be of the secondary importance, since our

QECCSD results are of the same quality as the bi-variational QCCD results for N_2 reported by Van Voorhis and Head-Gordon (128). The presence of the

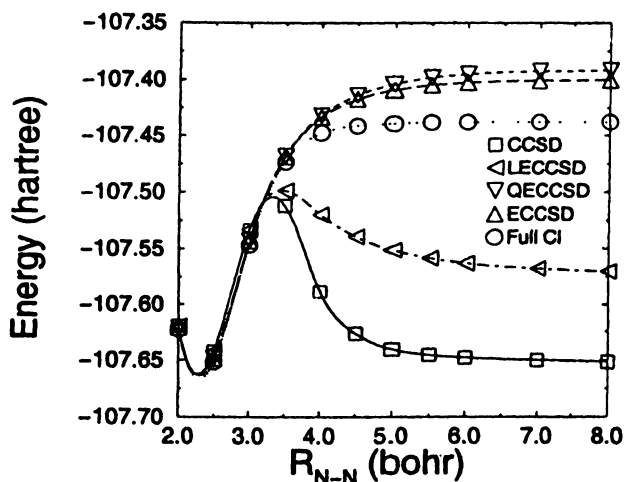


Figure 2. Potential energy curves for the N_2 molecule, as described by the STO-3G basis set (146) (see Table II for the numerical data).

quadratic terms in Σ^\dagger in \bar{H}^{ECCSD} and \bar{H}^{QECCSD} , eqs (56) and (59), respectively, and the flexibility of the ECC theory, resulting from the fact that there are two independent cluster operators in the ECC formalism, T and Σ , are a lot more important for improving the description of the bond breaking region by the ECCSD and QECCSD methods than the particular way of obtaining the $t_{a_1}^1$, $t_{a_1 a_2}^{1/2}$, $\sigma_{a_1}^1$, and $\sigma_{a_1 a_2}^{1/2}$ amplitudes that defines the ECC formalism of Piecuch and Bartlett. The importance of the quadratic terms, such as $\frac{1}{2}[(\Sigma^{\text{CCSD}})^\dagger]^2 \bar{H}^{\text{CCSD}}$ and $\frac{1}{2} \bar{H}^{\text{CCSD}} [(\Sigma^{\text{CCSD}})^\dagger]^2$, can be seen by comparing the QECCSD and LECCSD results. The LECCSD method does not have the $\frac{1}{2}[(\Sigma^{\text{CCSD}})^\dagger]^2 \bar{H}^{\text{CCSD}}$ and $\frac{1}{2} \bar{H}^{\text{CCSD}} [(\Sigma^{\text{CCSD}})^\dagger]^2$ terms in the corresponding Hamiltonian \bar{H}^{LECCSD} , eq (58), and, in consequence, the LECCSD potential energy curve of N_2 has the same type of hump for the intermediate values of R as the CCSD curve (see Figure 2). On the other hand, we observe a considerable reduction of errors at larger N–N separations, when the CCSD approach is replaced by the LECCSD method. This shows once again that the use of two independent cluster operators, T and Σ , in the ECC theory is very important for improving the poor CCSD results at larger internuclear separations.

The considerable improvements in the description of triple bond breaking in N_2 , offered by the QECCSD and ECCSD approaches, suggest that the T_1 and T_2

clusters obtained in the QECCSD and ECCSD calculations must be much better than the T_1 and T_2 clusters obtained by solving the standard CCSD equations. This can be seen by calculating the expectation values of the Hamiltonian with the normalized CCSD-like wave functions

$$|\Psi_0^X\rangle = N^X e^{T_1^X + T_2^X} |\Phi\rangle, \quad (X = \text{CCSD, QECCSD, ECCSD}), \quad (60)$$

designated by $\langle X \rangle$, where T_1^X and T_2^X , $X = \text{CCSD, QECCSD, and ECCSD}$, are the T_1 and T_2 clusters obtained with the CCSD, QECCSD, and complete ECCSD methods, respectively, and $N^X = \langle \Phi | e^{(T_1^X)^\dagger + (T_2^X)^\dagger} e^{T_1^X + T_2^X} | \Phi \rangle^{-1/2}$. Clearly, all three expectation values, $\langle \text{CCSD} \rangle$, $\langle \text{QECCSD} \rangle$, and $\langle \text{ECCSD} \rangle$, corresponding to the T_1 and T_2 clusters obtained in the CCSD, QECCSD, and complete ECCSD calculations, respectively, are upper bounds to the full CI energies. However, as shown in Table II, the (CCSD) energies remain poor at larger N–N separations, whereas the expectation values of the Hamiltonian calculated with the QECCSD and ECCSD wave functions, $|\Psi_0^{\text{QECCSD}}\rangle$ and $|\Psi_0^{\text{ECCSD}}\rangle$, respectively, are very close to the corresponding full CI energies. When the QECCSD and ECCSD energy expressions, based on eq (57), are replaced by the expectation values of H calculated with the QECCSD and ECCSD wave functions, the 28–46 and 24–38 millihartree errors in the QECCSD and ECCSD energies in the $R \geq 4.5$ bohr region reduce to 11–16 millihartree (see Table II). Thus, by solving the QECCSD or ECCSD equations and by simply replacing the QECCSD and ECCSD energy expressions by the expectation values of the Hamiltonian calculated with the QECCSD and ECCSD wave functions, $|\Psi_0^{\text{QECCSD}}\rangle$ and $|\Psi_0^{\text{ECCSD}}\rangle$, respectively, we can obtain the potential energy curves of N_2 , which are not only qualitatively correct, but which are also close to the full CI curve.

The fact that the T_1 and T_2 clusters obtained by solving the QECCSD and ECCSD equations are significantly better than the T_1 and T_2 clusters resulting from the standard CCSD calculations can also be seen by calculating the overlaps of the normalized CCSD, QECCSD, and ECCSD wave functions $|\Psi_0^{\text{CCSD}}\rangle$, $|\Psi_0^{\text{QECCSD}}\rangle$, $|\Psi_0^{\text{ECCSD}}\rangle$, and, respectively, as defined by eq (60), with the normalized full CI wave function $|\Psi_0^{\text{Full CI}}\rangle$ for different values of R (see Figure 3 (a)). As shown in Figure 3 (a), the overlap between the CCSD and full CI wave functions, which is close to 1.0 in the vicinity of the equilibrium geometry ($R \approx 2.0$ bohr), decreases to ~ 0.93 for larger N–N separations. This should be compared with the fact that the overlap between the QECCSD or ECCSD and full CI wave functions varies between 0.98 and 1.00 in the entire R region.

The significant differences between the CCSD and ECCSD (or QECCSD) values of the T_1 and T_2 clusters at larger internuclear distances that result in the observed huge differences between the behavior of the CCSD and ECCSD (or QECCSD) methods in the bond breaking region are shown in Figure 3 (b). In general, if Y and Z are two excitation operators, defined by the amplitudes y_j

and z_J , respectively ($t_{a_1}^{i_1}$ and $t_{a_1 a_2}^{i_1 i_2}$ for the T operator and $\sigma_{a_1}^{i_1}$ and $\sigma_{a_1 a_2}^{i_1 i_2}$ for the Σ operator), we can define the quantity

$$d(Y, Z) = \sqrt{\sum_J (y_J - z_J)^2}, \quad (61)$$

which provides us with a measure of how different or how similar the two operators Y and Z are. When $Y = Z$, we obtain $d(Y, Z) = 0$. For operators Y and Z , which are characterized by the similar values of amplitudes y_J and z_J , $d(Y, Z)$ is close to 0. Otherwise, the value of $d(Y, Z)$ is considerably greater than 0.

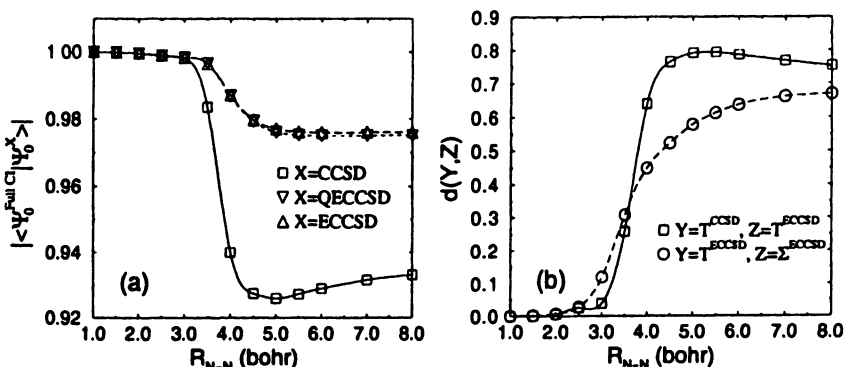


Figure 3. (a) The overlaps of the CCSD (\square), QECCSD (∇), and ECCSD (\triangle) wave functions with the full CI wave function, for the STO-3G (146) model of N_2 . (b) The difference between the CCSD and ECCSD cluster operators T (\square) and the difference between the ECCSD cluster operators T and Σ (\circ), as defined by eq (61), for the STO-3G (146) model of N_2 .

As shown in Figure 3 (b), the CCSD and ECCSD cluster operators T are very similar only for smaller values of R . This explains why the CCSD and ECCSD wave functions, $|\Psi_0^{\text{CCSD}}\rangle$ and $|\Psi_0^{\text{ECCSD}}\rangle$ respectively, and the corresponding energies (particularly, the expectation values of the Hamiltonian calculated with $|\Psi_0^{\text{CCSD}}\rangle$ and $|\Psi_0^{\text{ECCSD}}\rangle$) are virtually identical for smaller values of R . The ECCSD method provides slightly better results in the equilibrium region, when compared to the standard CCSD approach (primarily due to the presence of selected higher-order terms, such as $E_{\text{QQ}}^{[5]}$, eq (43), in the ECCSD energy), but the differences between the overall performance of the CCSD and ECCSD methods for $R \approx 2.0$ bohr are rather small (see Table II and Figure 2). The situation changes when the triple bond in N_2 is stretched. For $R > 3.0$ bohr, the difference between the CCSD and ECCSD operators T dramatically increases (see Figure 3 (b)). This results in a completely different behavior of the CCSD and ECCSD theories for stretched nuclear geometries: the CCSD method

completely fails, whereas the ECCSD approach provides reasonable results. Figure 3 (b) illustrates another important feature of the ECCSD theory, namely, the similarity of the T and Σ operators in the equilibrium region and the significant difference between the T and Σ operators obtained in the ECCSD calculations in the region of stretched nuclear geometries. As already mentioned, the lowest-order MBPT estimates of Σ and T are identical, so that $\Sigma \approx T$ in the $R \approx 2.0$ bohr region, where the MBPT series rapidly converges. The situation changes, when the convergence of the MBPT series is slow or when the MBPT series diverges, as is the case when the N–N bond is stretched. In this case, the operators Σ and T can be quite different. The optimization of two different cluster operators T and Σ in the ECCSD calculations allows us to obtain much better results than those provided by the conventional CCSD method, in which only one cluster operator is considered. This additional flexibility of the ECCSD theory results in much better T_1 and T_2 values, when compared with their CCSD counterparts, and significant differences between T and Σ shown in Figure 3 (b).

We can summarize our preliminary findings by stating that the QECCSD and ECCSD approaches, based on the general ECC formalism of ref 124, represent interesting new alternatives for accurate electronic structure calculations of molecular PESs involving bond breaking. The QECCSD and ECCSD methods remove the failing of the standard CCSD approach at larger internuclear separations and provide reasonable values of the T_1 and T_2 cluster amplitudes in the bond breaking region, in spite of using the poor RHF reference. The fact that the QECCSD method provides the results of the full ECCSD quality implies that we may be able to come up with practical computational schemes for molecular PESs involving bond breaking, based on the ECC formalism of ref 124, by simply dropping higher-order nonlinear terms in the ECCSD equations. In the future, we will consider other ways of simplifying the ECCSD formalism by truncating the many-body expansion of the doubly transformed operator $\bar{\bar{H}}^{\text{ECCSD}}$, eq (56).

Summary and Concluding Remarks

We described a new hierarchy of the QVMCC and QMMCC approximations, which, in analogy to the renormalized and completely renormalized CC methods (9, 13–18, 20, 21), represent “black-box” approaches for the ground-state PESs involving bond breaking. The QMMCC methods are based on the idea of adding the relatively simple noniterative corrections to the standard CCSD energies. The QMMCC corrections are constructed using the T_1 and T_2 clusters obtained in the CCSD calculations. By performing the test calculations for the potential energy curve of N_2 , we showed that the QMMCC approximations can provide considerable improvements in the standard CC and CR-CC results for more complicated cases involving multiple bond breaking.

We will continue testing the QMMCC methods by performing the calculations for other systems and larger basis sets.

The new QVMCC and QMMCC methods are related to the ECC theory, in which products involving cluster operators and their deexcitation counterparts are used to mimic the effects of higher-order clusters. We examined the performance of the ECCSD theory of ref 124 and its linear and quadratic variants. We showed that the complete and quadratic ECCSD methods, employing the ground-state RHF determinant as a reference, provide great improvements in the poor description of multiple bond breaking by the standard CCSD approach. We demonstrated that the QECCSD and ECCSD potential energy curves for N_2 have qualitatively correct shapes and that we can reduce the ~ 200 millihartree unsigned errors in the CCSD results for stretched geometries of N_2 by a factor of 4–5 by performing the complete or quadratic ECCSD calculations. We discovered that the T_1 and T_2 cluster amplitudes resulting from the QECCSD and ECCSD calculations provide a very good description of the electronic wave function, independent of the nuclear geometry. The QECCSD and ECCSD values of the T_1 and T_2 cluster amplitudes turned out to be so accurate that the potential energy curves of N_2 , obtained by calculating the expectation values of the Hamiltonian with the corresponding wave functions $e^{T_1+T_2}|\Phi\rangle$, are qualitatively as well as quantitatively very good. This intriguing finding shows that we may be able to further improve the quality of the ECC results by exploiting the energy expressions, which are not necessarily related to the equations used to determine the cluster operators T and Σ .

Our results imply that the ECC methods may allow us to formulate new classes of accurate and easy-to-use single-reference methods for bond breaking. By having an access to very good T_1 and T_2 cluster amplitudes, resulting from the QECCSD or ECCSD calculations, we should be able to propose simple noniterative corrections to the ECCSD or QECCSD energies, which may provide further improvements in the results in the bond breaking region. We may be able to suggest the desired corrections by employing the MMCC formalism. As shown in this study, the MMCC theory is capable of describing multiple bond breaking, even when the T_1 and T_2 cluster amplitudes originate from the failing CCSD approach. It is, therefore, logical to expect that more accurate values of the T_1 and T_2 cluster amplitudes, originating from the ECCSD calculations, will help us to improve the CR-CC and QMMCC results at larger internuclear separations in multiply bonded systems.

Acknowledgements

This work has been supported by the Department of Energy, Office of Basic Energy Sciences, SciDAC Computational Chemistry Program (Grant No. DE-FG02-01ER15228) and by the Alfred P. Sloan Foundation.

References

1. Čížek, J. *J. Chem. Phys.* **1966**, *45*, 4256.
2. Čížek, J. *Adv. Chem. Phys.* **1969**, *14*, 35.
3. Čížek, J.; Paldus, J. *Int. J. Quantum Chem.* **1971**, *5*, 359.
4. Paldus, J. In *Methods in Computational Molecular Physics*; Wilson, S.; Diercksen, G.H.F., Eds.; NATO Advanced Study Institute, Series B: Physics, Vol. 293; Plenum: New York, 1992; pp. 99-194.
5. Bartlett, R.J. In *Modern Electronic Structure Theory*; Yarkony, D.R., Ed.; World Scientific: Singapore, 1995; Part I, pp. 1047-1131.
6. Lee, T.J.; Scuseria, G.E. In *Quantum Mechanical Electronic Structure Calculations with Chemical Accuracy*; Langhoff, S.R., Ed.; Kluwer: Dordrecht, 1995; (Dordrecht: Kluwer), pp. 47-108.
7. Paldus, J.; Li, X. *Adv. Chem. Phys.* **1999**, *110*, 1.
8. Crawford, T.D.; Schaefer III, H.F. *Rev. Comp. Chem.* **2000**, *14*, 33.
9. Piecuch, P.; Kowalski, K. In *Computational Chemistry: Reviews of Current Trends*; Leszczyński, J., Ed.; World Scientific: Singapore, 2000; Vol. 5, pp. 1-104.
10. Adamowicz, L.; Piecuch, P.; Ghose, K.B. *Mol. Phys.* **1998**, *94*, 225.
11. Piecuch, P.; Kucharski, S.A.; Bartlett, R.J. *J. Chem. Phys.* **1999**, *110*, 6103.
12. Piecuch, P.; Kucharski, S.A.; Špirko, V. *J. Chem. Phys.* **1999**, *111*, 6679.
13. Kowalski, K.; Piecuch, P. *J. Chem. Phys.* **2000**, *113*, 18.
14. Kowalski, K.; Piecuch, P. *J. Chem. Phys.* **2000**, *113*, 5644.
15. Kowalski, K.; Piecuch, P. *Chem. Phys. Lett.* **2001**, *344*, 165.
16. Piecuch, P.; Kucharski, S.A.; Kowalski, K. *Chem. Phys. Lett.* **2001**, *344*, 176.
17. Piecuch, P.; Kucharski, S.A.; Špirko, V.; Kowalski, K. *J. Chem. Phys.* **2001**, *115*, 5796.
18. Piecuch, P.; Kowalski, K.; Pimienta, I.S.O.; Kucharski, S.A. In *Low-Lying Potential Energy Surfaces*; Hoffmann, M.R.; Dyal, K.G., Eds.; ACS Symposium Series, Vol. 828; American Chemical Society: Washington, D.C., 2002; pp. 31-64.
19. Piecuch, P.; Kowalski, K.; Pimienta, I.S.O. *Int. J. Mol. Sci.* **2002**, *3*, 475.
20. McGuire, M.J.; Kowalski, K.; Piecuch, P. *J. Chem. Phys.* **2002**, *117*, 3617.
21. Piecuch, P.; Kowalski, K.; Pimienta, I.S.O.; McGuire, M.J. *Int. Rev. Phys. Chem* **2002**, *21*, 527.
22. Sherrill, C.D.; Krylov, A.I.; Byrd, E.F.C.; Head-Gordon, M. *J. Chem. Phys.* **1998**, *109*, 4171.
23. Krylov, A.I.; Sherrill, C.D.; Byrd, E.F.C.; Head-Gordon, M. *J. Chem. Phys.* **1998**, *109*, 10669.
24. Gwaltney, S.R.; Head-Gordon, M. *Chem. Phys. Lett.* **2000**, *323*, 21.
25. Gwaltney, S.R.; Sherrill, C.D.; Head-Gordon, M.; Krylov, A.I. *J. Chem. Phys.* **2000**, *113*, 3548.
26. Gwaltney, S.R.; Head-Gordon, M. *J. Chem. Phys.* **2001**, *115*, 2014.

27. Gwaltney, S.R.; Byrd, E.F.C.; Van Voorhis, T.; Head-Gordon, M. *Chem. Phys. Lett.* **2002**, *353*, 359.
28. Head-Gordon, M.; Van Voorhis, T.; Gwaltney, S.R.; Byrd, E.F.C. In *Low-Lying Potential Energy Surfaces*; Hoffmann, M.R.; Dyall, K.G., Eds.; ACS Symposium Series, Vol. 828; American Chemical Society: Washington, D.C., 2002; pp. 93-108.
29. Krylov, A.I. *Chem. Phys. Lett.* **2001**, *338*, 375.
30. Krylov, A.I.; Sherrill, C.D. *J. Chem. Phys.* **2002**, *116*, 3194.
31. Slipchenko, L.V.; Krylov, A.I. *J. Chem. Phys.* **2002**, *117*, 4694.
32. Purvis III, G.D.; Bartlett, R.J. *J. Chem. Phys.* **1982**, *76*, 1910.
33. Scuseria, G.E.; Schemer, A.C.; Lee, T.J.; Rice, J.E.; Schaefer III, H.F. *J. Chem. Phys.* **1987**, *86*, 2881.
34. Scuseria, G.E.; Janssen C.L.; Schaefer III, H.F. *J. Chem. Phys.* **1988**, *89*, 7382.
35. Lee, T.J.; Rice, J.E. *Chem. Phys. Lett.* **1988**, *150*, 406.
36. Piecuch, P.; Paldus, J. *Int. J. Quantum Chem.* **1989**, *36*, 429.
37. Urban, M.; Noga, J.; Cole, S.J.; Bartlett, R.J. *J. Chem. Phys.* **1985**, *83*, 4041.
38. Cole, S.J.; Bartlett, R.J. *J. Chem. Phys.* **1987**, *86*, 873.
39. Piecuch, P.; Paldus, J. *Theor. Chim. Acta* **1990**, *78*, 65.
40. Raghavachari, K.; Trucks, G.W.; Pople, J.A.; Head-Gordon, M. *Chem. Phys. Lett.* **1989**, *157*, 479.
41. Kucharski, S.A.; Bartlett, R.J. *J. Chem. Phys.* **1998**, *108*, 9221.
42. Laidig, W.D.; Saxe, P.; Bartlett, R.J. *J. Chem. Phys.* **1987**, *86*, 887.
43. Ghose, K.B.; Piecuch, P.; Adamowicz, L. *J. Chem. Phys.* **1995**, *103*, 9331.
44. Piecuch, P.; Špirko, V.; Kondo, A.E.; Paldus, J. *J. Chem. Phys.* **1996**, *104*, 4699.
45. Kowalski, K.; Piecuch, P. *J. Mol. Struct.: THEOCHEM* **2001**, *547*, 191.
46. Lee, Y.S.; Bartlett, R.J. *J. Chem. Phys.* **1984**, *80*, 4371.
47. Lee, Y.S.; Kucharski, S.A.; Bartlett, R.J. *J. Chem. Phys.* **1984**, *81*, 5906; *ibid.* **1985**, *82*, 5761 (Erratum).
48. Noga, J.; Bartlett, R.J.; Urban, M. *Chem. Phys. Lett.* **1987**, *134*, 126.
49. Trucks, G.W.; Noga, J.; Bartlett, R.J. *Chem. Phys. Lett.* **1988**, *145*, 548.
50. Kucharski, S.A.; Bartlett, R.J. *Chem. Phys. Lett.* **1989**, *158*, 550.
51. Noga, J.; Bartlett, R.J. *J. Chem. Phys.* **1987**, *86*, 7041; *ibid.* **1988**, *89*, 3401 (Erratum).
52. Scuseria, G.E.; Schaefer III, H.F. *Chem. Phys. Lett.* **1988**, *152*, 382.
53. Schütz, M. *J. Chem. Phys.* **2002**, *116*, 8772.
54. Paldus, J.; Pylypow, L.; Jeziorski, B. In *Many-Body Methods in Quantum Chemistry*; Kaldor, U., Ed.; Lecture Notes in Chemistry, Vol. 52; Springer: Berlin, 1989; pp. 151-170.
55. Paldus, J.; Piecuch, P.; Jeziorski, B.; Pylypow, L. In *Recent Progress in Many-Body Theories*; Ainsworthy, T.L.; Campbell, C.E.; Clements, B.E.; Krotschek, E., Eds.; Plenum: New York, 1992; Vol. 3, pp. 287-303.

56. Paldus, J.; Piecuch, P.; Pylypow, L.; Jeziorski, B. *Phys. Rev. A* **1993**, *47*, 2738.
57. Piecuch, P.; Paldus, J. *Phys. Rev. A* **1994**, *49*, 3479.
58. Piecuch, P.; Paldus, J. *J. Chem. Phys.* **1994**, *101*, 5875.
59. Kowalski, K.; Piecuch, P. *Phys. Rev. A* **2000**, *61*, 052506.
60. Jankowski, K.; Paldus, J.; Grabowski, I.; Kowalski, K. *J. Chem. Phys.* **1992**, *97*, 7600; *ibid.* **1994**, *101*, 1759 (Erratum).
61. Jankowski, K.; Paldus, J.; Grabowski, I.; Kowalski, K. *J. Chem. Phys.* **1994**, *101*, 3085.
62. Mahapatra, U.S.; Datta, B.; Mukherjee, D. *Mol. Phys.* **1998**, *94*, 157.
63. Mahapatra, U.S.; Datta, B.; Mukherjee, D. *J. Chem. Phys.* **1999**, *110*, 6171.
64. Mach, P.; Mášik, J.; Urban, J.; Hubač, I. *Mol. Phys.* **1998**, *94*, 173.
65. Mášik, J.; Hubač, I. *Adv. Quantum Chem.* **1999**, *31*, 75.
66. Pittner, J.; Nachtigall, P.; Čársky, P.; Mášik, J.; Hubač, I. *J. Chem. Phys.* **1999**, *110*, 10275.
67. Hubač, I.; Pittner, J.; Čársky, P. *J. Chem. Phys.* **2000**, *112*, 8779.
68. Sancho-Garcia, J.C.; Pittner, J.; Čársky, P.; Hubač, I. *J. Chem. Phys.* **2000**, *112*, 8785.
69. Pittner, J.; Nachtigall, P.; Čársky, P.; Hubač, I. *J. Phys. Chem. A* **2001**, *105*, 1354.
70. Nooijen, M.; Lotrich, V. *J. Mol. Struct.: THEOCHEM* **2001**, *547*, 253.
71. Nooijen, M.; Lotrich, V. *J. Chem. Phys.* **2000**, *113*, 4549.
72. Kowalski, K.; Piecuch, P. *Chem. Phys. Lett.* **2001**, *334*, 89.
73. Piecuch, P.; Kowalski, K. *Int. J. Mol. Sci.* **2002**, *3*, 676.
74. Kállay, M.; Surján, P.R. *J. Chem. Phys.* **2001**, *115*, 2945.
75. Kucharski, S.A.; Bartlett, R.J. *Theor. Chim. Acta* **1991**, *80*, 387.
76. Kucharski, S.A.; Bartlett, R.J. *J. Chem. Phys.* **1992**, *97*, 4282.
77. Oliphant, N.; Adamowicz, L. *J. Chem. Phys.* **1991**, *95*, 6645.
78. Piecuch, P.; Adamowicz, L. *J. Chem. Phys.* **1994**, *100*, 5792.
79. Musiał, M.; Kucharski, S.A.; Bartlett, R.J. *J. Chem. Phys.* **2002**, *116*, 4382.
80. Pulay, P. *Chem. Phys. Lett.* **1983**, *100*, 151.
81. Saebø, S.; Pulay, P. *Chem. Phys. Lett.* **1985**, *113*, 13.
82. Saebø, S.; Pulay, P. *Annu. Rev. Phys. Chem.* **1993**, *44*, 213.
83. Schütz, M. *J. Chem. Phys.* **2000**, *113*, 9986.
84. Schütz, M.; Werner, H.-J. *Chem. Phys. Lett.* **2000**, *318*, 370.
85. Li, X.; Paldus, J. *J. Chem. Phys.* **1997**, *107*, 6257.
86. Li, X.; Paldus, J. *J. Chem. Phys.* **1998**, *108*, 637.
87. Li, X.; Paldus, J. *Chem. Phys. Lett.* **1998**, *286*, 145.
88. Li, X.; Paldus, J. *J. Chem. Phys.* **1999**, *110*, 2844.
89. Li, X.; Paldus, J. *Mol. Phys.* **2000**, *98*, 1185.
90. Li, X.; Paldus, J. *J. Chem. Phys.* **2000**, *113*, 9966.
91. Oliphant, N.; Adamowicz, L. *J. Chem. Phys.* **1991**, *94*, 1229.
92. Oliphant, N.; Adamowicz, L. *J. Chem. Phys.* **1992**, *96*, 3739.
93. Oliphant, N.; Adamowicz, L. *Int. Rev. Phys. Chem.* **1993**, *12*, 339.

94. Piecuch, P.; Oliphant, N.; Adamowicz, L. *J. Chem. Phys.* **1993**, *99*, 1875.
95. Piecuch, P.; Adamowicz, L. *Chem. Phys. Lett.* **1994**, *221*, 121.
96. Piecuch, P.; Adamowicz, L. *J. Chem. Phys.* **1995**, *102*, 898.
97. Ghose, K.B.; Adamowicz, L. *J. Chem. Phys.* **1995**, *103*, 9324.
98. Ghose, K.B.; Piecuch, P.; Pal, S.; Adamowicz, L. *J. Chem. Phys.* **1996**, *104*, 6582.
99. Olsen, J. *J. Chem. Phys.* **2000**, *113*, 7140.
100. Krogh, J.W.; Olsen, J. *Chem. Phys. Lett.* **2001**, *344*, 578.
101. Kállay, M.; Surján, P.R.; Szalay, P. *J. Chem. Phys.* **2002**, *117*, 980.
102. Kowalski, K.; Piecuch, P. *J. Chem. Phys.* **2000**, *113*, 8490.
103. Kowalski, K.; Piecuch, P. *J. Chem. Phys.* **2001**, *115*, 643.
104. Kowalski, K.; Piecuch, P. *Chem. Phys. Lett.* **2001**, *347*, 237.
105. Stanton, J.F. *Chem. Phys. Lett.* **1997**, *281*, 130.
106. Kowalski, K.; Piecuch, P. *J. Chem. Phys.* **2001**, *115*, 2966.
107. Kowalski, K.; Piecuch, P. *J. Chem. Phys.* **2002**, *116*, 7411.
108. Li, X.; Paldus, J. *J. Chem. Phys.* **2001**, *115*, 5759.
109. Li, X.; Paldus, J. *J. Chem. Phys.* **2001**, *115*, 5774.
110. Li, X.; Paldus, J. *J. Chem. Phys.* **2002**, *117*, 1941.
111. Piecuch, P.; Kucharski, S.A.; Kowalski, K.; Musial, M. *Comp. Phys. Commun.* **2002**, *149*, 71.
112. Schmidt, M.W.; Baldridge, K.K.; Boatz, J.A.; Elbert, S.T.; Gordon, M.S.; Jensen, J.H.; Koseki, S.; Matsunaga, N.; Nguyen, K.A.; Su, S.J.; Windus, T.L.; Dupuis, M.; Montgomery, J.A. *J. Comput. Chem.* **1993**, *14*, 1347.
113. Dunning, T.H. *J. Chem. Phys.* **1970**, *53*, 2823.
114. Arponen, J.S. *Ann. Phys.* **1983**, *151*, 311.
115. Arponen, J.S.; Bishop, R.F.; Pajanne, E. *Phys. Rev. A* **1987**, *36*, 2519.
116. Arponen, J.S.; Bishop, R.F.; Pajanne, E. *Condensed Matter Theor.* **1987**, *2*, 357.
117. Bishop, R.F.; Arponen, J.S.; Pajanne, E. In *Aspects of Many-Body Effects in Molecules and Extended Systems*; Mukherjee, D., Ed.; Lecture Notes in Chemistry, Vol. 50; Springer: Berlin, 1989; p. 79.
118. Bishop, R.F.; Arponen, J.S. *Int. J. Quantum Chem. Symp.* **1990**, *24*, 197.
119. Arponen, J.S.; Bishop, R.F. *Ann. Phys.* **1991**, *207*, 171.
120. Bishop, R.F.; Robinson, N.J.; Arponen, J.S. *Condensed Matter Theor.* **1990**, *5*, 37.
121. Bishop, R.F. *Theor. Chim. Acta* **1991**, *80*, 95.
122. Arponen, J.S. *Phys. Rev. A* **1997**, *55*, 2686.
123. Arponen, J.S.; Bishop, R.F.; Pajanne, E. *Phys. Rev. A* **1987**, *36*, 2539.
124. Piecuch, P.; Bartlett, R.J. *Adv. Quantum Chem.* **1999**, *34*, 295.
125. Bartlett, R.J.; Noga, J. *Chem. Phys. Lett.* **1988**, *150*, 29.
126. Bartlett, R.J.; Kucharski, S.A.; Noga, J.; Watts, J.D.; Trucks, G.W. In *Many-Body Methods in Quantum Chemistry*; Kaldor, U., Ed.; Lecture Notes in Chemistry, Vol. 52; Springer: Berlin, 1989; p. 124.

127. Van Voorhis, T.; Head-Gordon, M. *J. Chem. Phys.* **2000**, *113*, 8873.
128. Van Voorhis, T.; Head-Gordon, M. *Chem. Phys. Lett.* **2000**, *330*, 585.
129. Byrd, E.F.C.; Van Voorhis, T.; Head-Gordon, M. *J. Phys. Chem. B* **2002**, *106*, 8070.
130. Bartlett, R.J.; Watts, J.D.; Kucharski, S.A.; Noga, J. *Chem. Phys. Lett.* **1990**, *165*, 513.
131. Kucharski, S.A.; Bartlett, R.J. *Adv. Quantum Chem.* **1986**, *18*, 281.
132. Raghavachari, K.; Pople, J.A.; Replogle, E.S.; Head-Gordon, M. *J. Phys. Chem.* **1990**, *94*, 5579.
133. Salter, E.A.; Trucks, G.W.; Bartlett, R.J. *J. Chem. Phys.* **1989**, *90*, 1752.
134. Salter, E.A.; Bartlett, R.J. *J. Chem. Phys.* **1989**, *90*, 1767.
135. Kucharski, S.A.; Bartlett, R.J. *J. Chem. Phys.* **1998**, *108*, 5243.
136. Kucharski, S.A.; Bartlett, R.J. *J. Chem. Phys.* **1998**, *108*, 5255.
137. Pal, S. *Theor. Chim. Acta* **1984**, *66*, 151.
138. Pal, S. *Phys. Rev. A* **1986**, *33*, 2240.
139. Pal, S. *Phys. Rev. A* **1986**, *34*, 2682.
140. Ghose, K.B.; Pal, S. *Phys. Rev. A* **1987**, *36*, 1539.
141. Vaval, N.; Ghose, K.B.; Pal, S. *J. Chem. Phys.* **1994**, *101*, 4914.
142. Vaval, N.; Pal, S. *Phys. Rev. A* **1996**, *54*, 250.
143. Kumar, A.B.; Vaval, N.; Pal, S. *Chem. Phys. Lett.* **1998**, *295*, 189.
144. Vaval, N.; Kumar, A.B.; Pal, S. *Int. J. Mol. Sci.* **2001**, *2*, 89.
145. Vaval, N. *Chem. Phys. Lett.* **2000**, *318*, 168.
146. Hehre, W.J.; Stewart, R.F.; Pople, J.A. *J. Chem. Phys.* **1969**, *51*, 2657.

Chapter 5

Bond Breaking in Quantum Chemistry: A Comparison of Single- and Multi-Reference Methods

**C. David Sherrill, Antara Dutta, Micah L. Abrams,
and John S. Sears**

**Center for Computational Molecular Science and Technology,
School of Chemistry and Biochemistry, Georgia Institute of Technology,
Atlanta, GA 30332-0400**

Standard and new quantum chemical methods are evaluated for their ability to provide accurate potential energy curves for chemical reactions which break or form bonds. Comparisons to full configuration interaction benchmark results demonstrate that even high level single-reference methods such as unrestricted coupled-cluster with single, double, and perturbative triple substitutions [UCCSD(T)] can have large errors for bond breaking processes: nonparallelity errors for breaking bonds to hydrogen, which should be one of the simplest theoretical problems, are around 3-4 kcal mol⁻¹. Multi-reference methods are much more reliable but are also more computationally expensive. New, minimalist configuration interaction methods for bond breaking in larger molecules are also discussed which dramatically improve on similar earlier models.

The Bond Breaking Problem

The vast majority of quantum chemical studies focus on equilibrium properties. However, a detailed understanding of chemical reactions requires a description of their chemical dynamics, which in turn requires information about the change in potential energy as bonds are broken or formed. Even though modern electronic structure theory can provide near-spectroscopic accuracy for small molecular systems near their equilibrium geometries, the general description of potential energy surfaces away from equilibrium remains very much a frontier area of research.

Nearly all of the commonly used quantum chemical methods are ultimately based upon Hartree-Fock molecular orbital theory, which describes the motion of each electron in the average field of all the other electrons. This introduces an error because in reality the motions of electrons are correlated. Short-range electron correlation, referred to as “dynamical” correlation, is well described by the hierarchy of many-body perturbation theory and coupled-cluster methods. However, long-range electron correlations, referred to as “nondynamical” correlation, are also important and become crucial for a proper description of bond breaking processes. At the dissociation limit, the energy due to nondynamical correlation can be *larger* than the energy due to dynamical correlation (I).

The origin of this nondynamical correlation is that as bonds are broken, it is no longer true that a single electron configuration is sufficient as a zeroth-order wavefunction. It is well known that Hartree-Fock with restricted orbitals is incapable of providing qualitatively correct potential energy curves for bond breaking reactions. For the H_2 molecule, for example, the $(\sigma_g)^2$ electron configuration is appropriate at equilibrium, but at dissociation, the σ_g and σ_u^* orbitals become degenerate, necessitating an equivalent treatment of the $(\sigma_g)^2$ and $(\sigma_u^*)^2$ configurations which is not provided by Hartree-Fock theory. Although additional configurations such as $(\sigma_u^*)^2$ are added to the wavefunction via standard “single-reference” correlation methods, for larger molecules the selection of additional configurations will be imbalanced because they are generated relative to the single Hartree-Fock reference only. A completely balanced treatment of electron correlation would require, for example, all single and double excitations out of *all* near-degenerate electron configurations. Such an approach is an example of a *multi-reference* method.

Although multi-reference methods are capable of accurately describing bond breaking processes in principle, they are very difficult to formulate, implement, and apply. Typically, their computational cost is prohibitive for all but the smallest molecules. Additionally, they can require seemingly arbitrary choices of reference configurations or active spaces. Hence, continued development of methods for bond breaking has emphasized both more efficient multi-reference methods as well as generalized single-reference methods.

Within the scope of single-reference methods, there are two obvious, complementary strategies to attack the bond breaking problem. First, one may simply include more and more electron configurations (e.g., triple, quadruple substitutions) to approach the limit in which all possible configurations are included. Unfortunately, the computational cost of this strategy increases rapidly. Second, one may abandon restricted orbitals in favor of unrestricted orbitals. Unrestricted Hartree-Fock (UHF) provides qualitatively correct dissociation curves for molecules in which a single bond is broken, even though it can be quantitatively poor. By adding sophisticated treatments of electron

correlation, one might hope to obtain quantitatively good potential energy curves. However, using unrestricted orbitals introduces spin contamination, and the wavefunction is no longer an eigenfunction of the total spin operator. Any spin-dependent properties will no longer be properly predicted.

One of the most important steps in the development of new methods for bond breaking reactions is the calibration of the method against reliable benchmark results. Unfortunately, these benchmarks are very hard to obtain. In the general case, there is no simple way to obtain entire potential energy curves directly from experiment; hence, theoretical benchmarks are required. This problem may be addressed by solving the electronic Schrödinger equation exactly within the Born-Oppenheimer approximation, using the full configuration interaction (FCI) model. Because the computational cost of full CI increases factorially with the number of electrons or orbitals, it can be used only for the smallest chemical systems. Nevertheless, advances in algorithms and computer hardware have recently made it possible to obtain full CI potential energy curves for a few small molecules (2-5). In particular, Olsen and co-workers have presented very enlightening benchmark curves for several electronic states of N_2 (5, 6) and full CI energies for five points along the double dissociation of H_2O (3). A number of standard theoretical methods, including many-body perturbation theory and coupled-cluster theory, were compared to the full CI results. Benchmark curves such as these are essential for calibrating new theoretical methods meant to provide accurate potential energy curves (7-12).

At present, there remains a scarcity of high quality full CI potential energy curves. While Olsen and co-workers have focused on the most challenging cases of double and triple bond breaking, we have examined (13,14) more typical cases which should also be less challenging for standard methods. Various single- and multi-reference methods have been compared to our benchmark full CI results. We find rather large errors in even the most advanced of the standard single-reference methods. Results for the multi-reference methods considered are much improved.

Whether accurate results can be obtained for bond breaking using computationally inexpensive methods remains an open question. One new strategy, described elsewhere in this volume, is the spin-flip approach of Krylov and co-workers (12, 15, 16). This is a single-reference approach which attempts to avoid the usual pitfalls of such methods by using a high-spin ($M_s = 1$) triplet reference state to generate determinants appropriate for a ground state singlet ($M_s = 0$) potential energy curve. Of course generating a $M_s = 0$ determinant from an $M_s = 1$ determinant requires a spin flip, and hence the name of the method. The motivation for this approach is the supposition that the $M_s = 1$ triplet state is easier to describe at the Hartree-Fock level across the whole potential energy curve. At its simplest level, only single (spin-flipping) excitations are allowed

relative to the high-spin triplet reference; this is called the SF-CIS or SF-SCF method, and it is meant to give singlet potential energy curves with an accuracy roughly comparable to that of the Hartree-Fock approach, except that this accuracy is now roughly uniform across the entire curve. Improvements can be made by including various models of dynamical electron correlation (12, 16). One drawback of this approach is that the wavefunctions it generates are not spin eigenfunctions. We have recently examined (17) the effect of adding the requisite determinants to obtain spin eigenfunctions, and we find that this makes dramatic improvements.

An Assessment of Single-Reference Methods

The performance of standard single-reference electronic structure methods has not been fully assessed for bond breaking reactions because full configuration interaction benchmarks are not widely available for entire potential energy curves. In recent work (13), we have obtained full CI potential energy curves for breaking single bonds. In particular, we have used the DETCI program (18) in the PSI3 (19) package to obtain benchmark full CI curves for breaking a bond to hydrogen in BH, HF, and CH₄ using the basis sets aug-cc-pVQZ, 6-31G**, and 6-31G*, respectively. We prefer the latter Pople basis sets among standard polarized double zeta sets because they give the best predictions of molecular properties at the full CI level (20). Methods compared include Hartree-Fock theory, second-order Møller-Plesset perturbation theory (MP2) (21); coupled-cluster with single and double substitutions (CCSD) (22); and coupled-cluster with single, double, and perturbative triple substitutions [CCSD(T)] (23). We have also examined the B3LYP gradient-corrected hybrid density functional theory model (24,25). Both restricted and unrestricted orbitals have been used.

Our results were qualitatively similar for the BH, HF, and CH₄ molecules, so we will focus here on CH₄ as a representative case. The single-reference potential energy curves are compared to full CI in Figure 1, in which one C–H bond is stretched while the other geometrical parameters are held constant. One immediately notices the well-known failure of restricted Hartree-Fock (RHF) at large bond lengths; this is caused by the presence of unphysical, high-energy ionic terms in the RHF energy which may be removed by employing unrestricted orbitals or by using an appropriate multiconfigurational self-consistent-field (MCSCF) approach (26).

Unfortunately, the failure of RHF is so severe that none of the correlated methods based upon it are able to overcome it (except, of course, full CI). The MP2 curve diverges to negative infinity at the dissociation limit because of a near-degeneracy between the highest occupied and lowest unoccupied molecular

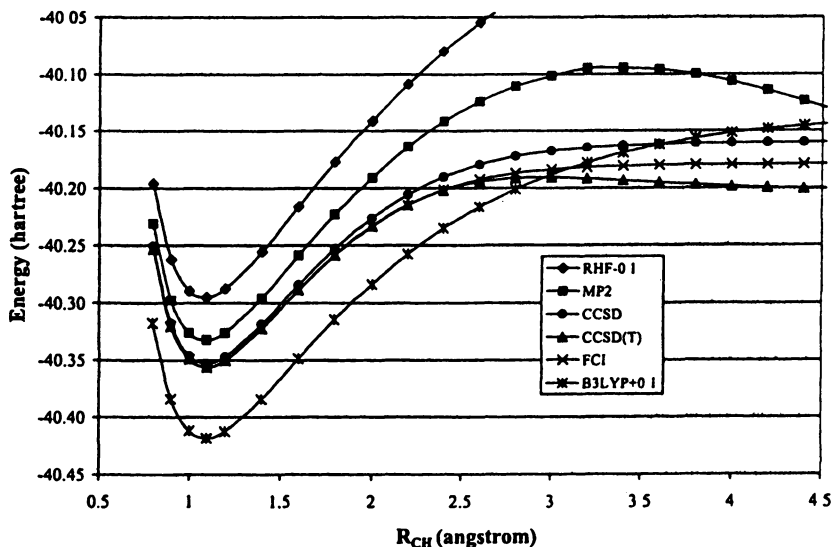


Figure 1. Potential energy curves for CH_4 in a 6-31G* basis using restricted orbitals. (Data from reference 13.)

orbitals, and the perturbative treatment of triple substitutions in CCSD(T) also causes it to fail at large bond lengths. The density functional theory method B3LYP is seen to suffer the same fate as Hartree-Fock when the orbitals are restricted: energies for large bond lengths are much too large. Of all restricted methods considered, only CCSD provides results which are qualitatively correct, but the quantitative error at large bond lengths is around 12 kcal mol^{-1} .

One might hope that highly correlated methods employing an unrestricted Hartree-Fock reference might be able to overcome these difficulties, since UHF gives a qualitatively correct (if quantitatively poor) description of bond breaking. Results for UHF references are plotted in Figure 2, where the acronyms for methods have been prefixed by 'U' to denote unrestricted orbitals. The UHF curve levels off too quickly with increasing bond length (underestimating the dissociation energy); however, the UCCSD and UCCSD(T) curves appear close to the full CI benchmark curve. Similarly, although UB3LYP provides energies much lower than full CI for this basis set, the potential energy curve has a shape close to that of full CI. Since relative energies, not total energies, are the only relevant quantity for chemical reactions, we are only concerned with how well the curves parallel the full CI results. Of the correlated methods, only UMP2 provides a curve which is qualitatively

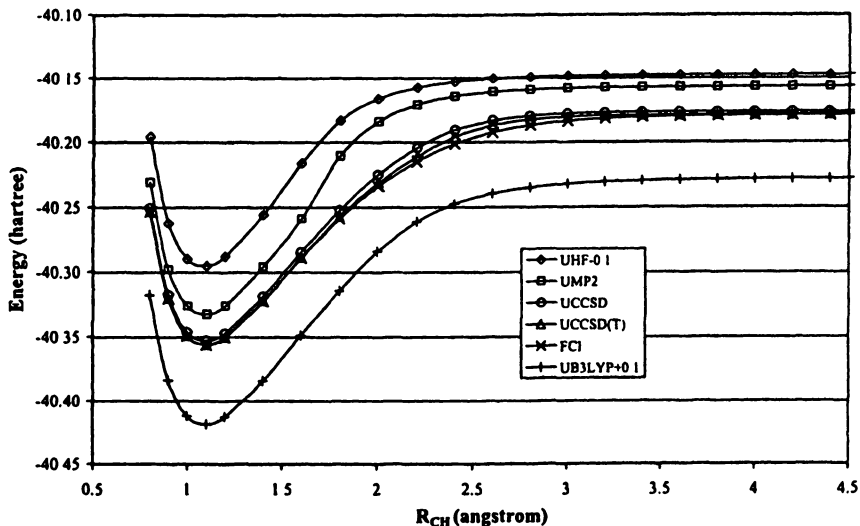


Figure 2: Potential energy curves for CH_4 in a 6-31G* basis using unrestricted orbitals. (Data from reference 13.)

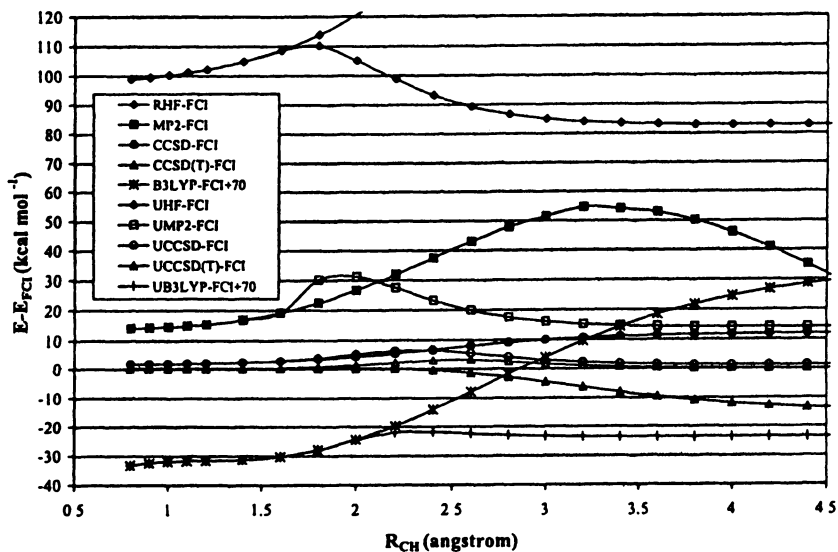


Figure 3: Errors in potential energies for CH_4 in a 6-31G* basis. B3LYP and UB3LYP error curves have been shifted up by 70 kcal mol⁻¹. (Data from reference 13.)

different from full CI. The UMP2 energy clearly rises too rapidly in the intermediate bond breaking region, between about 1.6 and 2.2 Å.

A more detailed examination of the errors in the approximate single reference methods for CH₄ is provided in Figure 3, which plots errors vs. full CI as a function of bond length. A completely flat error curve would be perfectly parallel to the full CI curve and would provide exactly the same predictions for properties such as bond length, harmonic frequency, dissociation energy, etc. Note that restricted and unrestricted curves coincide before a certain bond length which depends on the method. While all the approximate restricted methods except CCSD have very large errors near dissociation, the unrestricted methods have their largest errors in the intermediate region. This error is very large for UMP2, rising from around 15 kcal mol⁻¹ near equilibrium to more than 30 kcal mol⁻¹ in the intermediate bond breaking region. At these geometries, the UMP2 error is larger than that for restricted MP2.

Besides CCSD, the only methods with small errors are UCCSD and UCCSD(T). In order to help quantify the errors, we have computed the so-called non-parallelity error (NPE), which is the magnitude of the difference between the largest and smallest errors along the potential energy curve. A curve perfectly parallel to full CI would have a constant error across the potential energy curve, and therefore an NPE of zero. NPE values for CH₄, as well as BH and HF, are presented in Table 1. The NPEs for CCSD, UCCSD, and UCCSD(T) for CH₄ are 10.3, 5.1, and 3.2 kcal mol⁻¹, respectively. None of these errors are small enough to claim that these methods provide “chemical accuracy,” which is commonly taken to mean errors in relative energies of about 1-2 kcal mol⁻¹. This is perhaps surprising since one might expect breaking a bond to a hydrogen atom would be one of the easiest possible bond breaking problems.

Table 1 shows that the errors for CH₄ are fairly similar for the BH and HF molecules. UCCSD(T) provides the best results in all cases, yet the error never drops below 3 kcal mol⁻¹. UCCSD is the only alternative if one desires even a modest accuracy of ± 10 kcal mol⁻¹.

An Assessment of Multi-Reference Methods

By treating all near degenerate electron configurations on an equal footing, multi-reference methods are capable of handling the bond breaking problem, albeit at an increased cost in theoretical complexity and computer time. We have recently compared (14) several multi-configurational reference functions and multi-reference methods based upon them for bond breaking in a few simple molecules including the cases considered above: BH, HF, and CH₄. In this section we will discuss our general findings and examine CH₄ in particular.

Table 1: Non-parallelity error (NPE, kcal mol⁻¹) for BH, HF and CH₄ molecules.

<i>Method</i>	<i>BH</i>	<i>HF</i>	<i>CH₄</i>
RHF	-	-	-
MP2	-	-	-
CCSD	8.1	12.9	10.3
CCSD(T)	23.3	-	-
B3LYP	n/a	66.7	63.0
UHF	27.1	47.8	27.4
UMP2	17.9	25.9	17.1
UCCSD	4.7	6.0	5.1
UCCSD(T)	3.1	3.7	3.2
UB3LYP	n/a	5.9	11.4
CASSCF	9.4	18.0	6.3
CASPT2	1.8	1.6	0.7
CISD[TQ]	0.3	5.3	1.3
SOCI	0.3	5.3	0.3

NOTE: n/a denotes data not available, dashes denote very large or divergent errors.

SOURCE: Data from Refs. 13, 14.

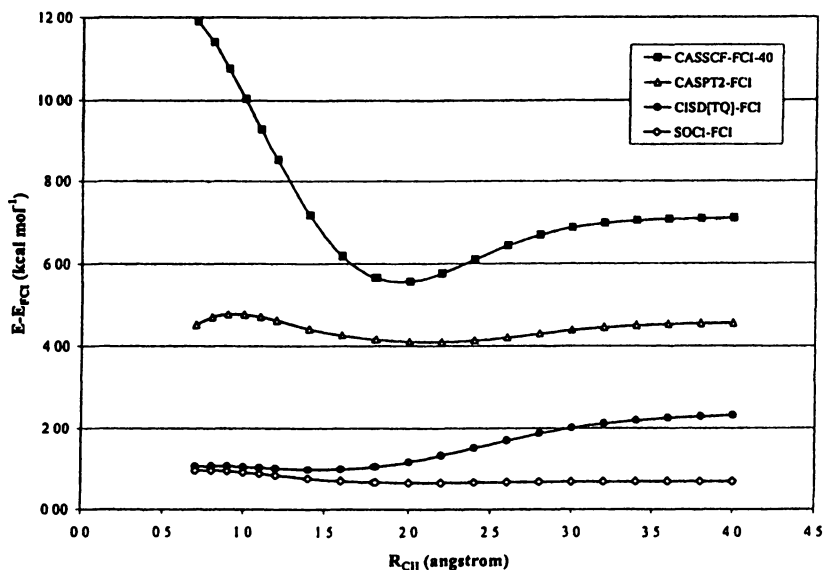


Figure 4: Errors in potential energies for CH₄ in a 6-31G* basis using multi-reference methods. (Data from reference 14.)

Figure 4 presents results for breaking a C–H bond in CH₄ obtained with several multi-reference methods. First, we have used the complete-active-space self-consistent-field (CASSCF) method (26), which includes all possible electron configurations which can be generated in a subset of orbitals termed the “active space.” We have used the space of all valence orbitals as our active space; this choice should allow CASSCF to describe any bond breaking process at least qualitatively correctly by including all configurations which could become near-degenerate. The CASSCF errors plotted in the figure have been shifted down by 40 kcal mol⁻¹ for an easier comparison with the other methods. The error is largest around equilibrium, and flattens out at large distances. This happens because the dynamical electron correlation, not described properly by CASSCF, is larger at short distances, where more electrons are closer together.

The next method considered is CASPT2 (27), which adds a second-order perturbation theory treatment of dynamical correlation on top of the qualitatively correct treatment of nondynamical correlation in CASSCF. The CASPT2 curve is much closer to full CI, as indicated by a much flatter error curve in Figure 4. The nonparallelity errors of CASSCF and CASPT2 in Table 1 are 6.3 and 0.7 kcal mol⁻¹ for CH₄, and these are seen to be fairly typical of the molecules considered (errors for HF are larger because a valence active space for that molecule includes only a single antibonding orbital). This NPE for CASSCF is roughly comparable to that of CCSD, but it should be pointed out that CASSCF is more robust for these problems and is less likely to fail for more challenging cases. The CASPT2 results are superior to any of the single-reference methods considered above.

To obtain an even greater accuracy, one might turn to multi-reference configuration interaction or multi-reference coupled-cluster methods. These approaches are typically less straightforward to apply than CASSCF or CASPT2, because in addition to the active space, one may also need to choose thresholds or reference determinants. We favor multi-reference methods that choose determinants in a simple, *a priori* fashion, such as in the restricted active space configuration interaction (RASCI) approach of Olsen *et al.* (28). Here, we have looked at a particular multi-reference CI approach which can be formulated as a RASCI, which is the so-called second-order CI (SOC1). This method generates all single and double excitations from every determinant in a CASSCF wavefunction. Unfortunately, this procedure generates a tremendous number of determinants, and few SOC1 computations have been performed. For this reason, we have also considered an approximation to SOC1 in which all determinants which would be considered more than quadruple excitations relative to the dominant Hartree-Fock reference determinant are discarded. This approach, introduced by Schaefer and co-workers (29-31), is designated CISD[TQ] because it includes all single and double substitutions but only some triples and quadruples. This wavefunction can also be formulated in the context of a RASCI.

The SOCI and CISD[TQ] curves for CH₄ are so close to full CI that they are difficult to distinguish from full CI or from each other. However, they may be examined more clearly in the error curves in Figure 4, which display very flat errors for SOCI, while CISD[TQ] errors increase gradually with increasing bond length. This suggests that some of the triple, quadruple, or higher excitations present in SOCI but neglected in CISD[TQ] are becoming important at large bond lengths. This is perhaps surprising in that, for CH₄, there should be only two dominant configurations at large bond lengths, and the CISD[TQ] wavefunction certainly includes these as well as all single and double excitations from each of them. On the other hand, the wavefunction also includes more triples and quadruples relative to the configuration dominant at equilibrium than to the antibonding one which becomes degenerate at the dissociation limit, suggesting a possible minor imbalance in the method. At any rate, the absolute errors for CISD[TQ] and SOCI are much smaller than for any other methods considered here, and their nonparallelity errors for CH₄ are very impressive at 1.3 and 0.3 kcal mol⁻¹, respectively. These methods should prove extremely reliable for any single bond breaking process where they can be afforded, and in principle, SOCI is capable of breaking any number of bonds simultaneously.

Minimalist Configuration-Interaction Approaches

As the above test cases demonstrate, the most sophisticated treatments of electron correlation are the most successful at describing bond breaking processes. However, it is important to ask whether one can formulate much simpler, less computationally demanding approaches which might still describe bond breaking accurately.

As discussed in the introduction, the spin-flip technique (12, 15, 16) is one attempt to adapt standard single-reference electronic structure methods in a simple way to be more appropriate for bond breaking. The simplest of these models, SF-SCF (also called SF-CIS), obtains singlet wavefunctions from a high-spin triplet reference by generating all single substitutions which flip a single spin from α to β . One drawback of this approach as originally formulated is that the generated set of determinants does not include all determinants necessary to form eigenfunctions of \hat{S}^2 . Recently, two of us (C.D.S. and J.S.S.) implemented the ability to obtain the spin-complete analogues of SF-SCF, denoted here SC-SF-SCF, into our group's DETCI program. One advantage of our implementation is that it decouples the orbitals used from the identity of the reference determinant. Hence, it is possible to generate spin-flipped singlet determinants relative to a triplet "reference" determinant but use, for example, closed-shell singlet orbitals. This allows us to examine the effects of orbitals separately from the selection of determinants.

Table 2: Equilibrium bond lengths and dissociation energies for the F₂ molecule with a DZP + basis set.^a

<i>Method</i>	<i>R_e</i>	<i>D_e^b</i>
RHF ^c	1.332	10.69
CCSD ^c	1.410	2.36
UCCSD ^c	1.410	0.95
SF-SCF ^d	1.567	0.28
SC-SF-SCF (singlet orbitals) ^e	1.469	1.29
SC-SF-SCF (triplet orbitals) ^e	1.448	1.37
SF-CIS(D) ^d	1.429	1.14
SF-OD ^d	1.437	1.24
VOO-CCD(2) ^f	1.417	1.51
MR-CISD ^c	1.435	1.22
Expt.	1.412	1.66

^aSpin-flip approaches used a ³Σ_u reference.

^bComputed at *r*(F-F) = 100 bohr.

^cReference 32. ^dReference 12.

^eReference 17. ^fReference 9.

Having spin complete wavefunctions dramatically improves the accuracy of the SF-SCF method. One of the most striking examples of this is for the very challenging F₂ molecule, considered in Table 2. As usual, the RHF approach is incapable of properly dissociating the molecule and gives unreasonable dissociation energies. Even single-reference CCSD methods perform very badly for this difficult case (32), giving good bond lengths but very poor dissociation energies, in contrast to the reasonable performance of CCSD for breaking single bonds to hydrogen atoms discussed above. Multi-reference CISD and the VOO-CCD(2) model (8) both give good results for this case (9, 32), considering the limited basis set used.

Although SF-SCF improves significantly over the unphysical results of RHF, nevertheless its performance is poor, overestimating *r_e* by .15 Å and predicting a dissociation energy of 0.28 eV compared to an experimental value of 1.66 eV. The spin-complete alternative, however, gives much better results: the error in the bond length is reduced by about two thirds, and the dissociation energy becomes much more reasonable around 1.3 eV. In this case, triplet orbitals are more effective than singlet orbitals, giving dissociation energies of 1.37 eV vs. 1.29 eV. Closer agreement with experiment requires a treatment of dynamical electron correlation. Since SF-CIS(D) was found to improve so dramatically over simple SF-SCF, we anticipate perturbative corrections for dynamical correlation in our spin-complete version should be even more effec-

tive. It should be noted that the most extensive spin-flip model considered for this problem, SF-OD, gives results (12) which rival MR-CISD for this case.

A perhaps more typical comparison of SF-SCF and its spin-complete alternative is presented in Figure 5, which presents potential energy curves for the HF molecule. One sees that using spin complete wavefunctions reduces the error in the SF-SCF energies by roughly 2/3 at large distances.

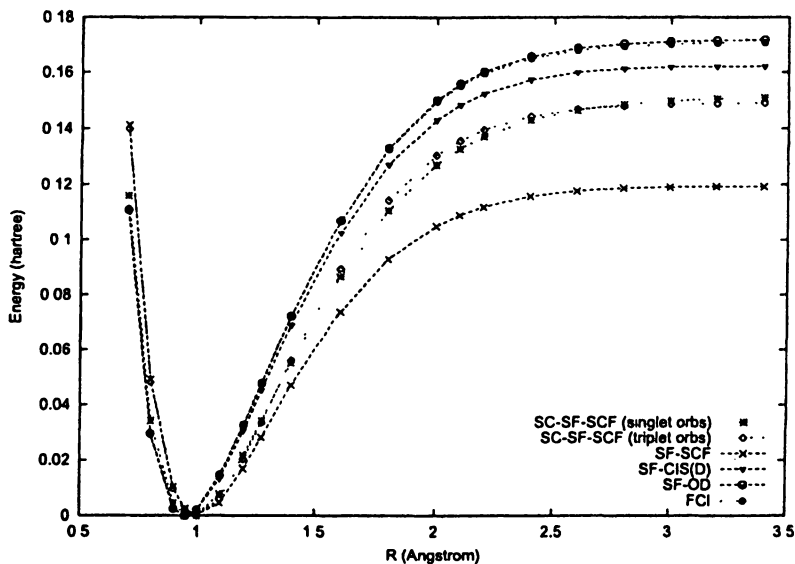


Figure 5: Potential energy curves for HF in a 6-31G basis.
(Data from reference 17.)

We anticipate that continued development of minimalist models, in conjunction with more efficient multi-reference approaches and a wider array of benchmark curves, will result in a better understanding of the theoretical challenges of bond breaking processes and increased ability of electronic structure theory to model them.

Acknowledgments

C.D.S. acknowledges a Camille and Henry Dreyfus New Faculty Award and an NSF CAREER Award (Grant No. NSF 0094088). The Center for Computational Molecular Science and Technology is funded through a Shared University Research (SUR) grant from IBM and by Georgia Tech.

References

1. Shavitt, I. in *Methods of Electronic Structure Theory*, Schaefer, H. F., Ed., pp 189–275. Plenum Press, New York, 1977.
2. van Mourik, T.; van Lenthe, J. H. *J. Chem. Phys.*, **1995**, *102*, 7479.
3. Olsen, J.; Jørgensen, P.; Koch, H.; Balková, A.; Bartlett, R. J. *J. Chem. Phys.*, **1996**, *104*, 8007.
4. Krylov, A. I.; Sherrill, C. D.; Byrd, E. F. C.; Head-Gordon, M. *J. Chem. Phys.*, **1998**, *109*, 10669.
5. Larsen, H.; Olsen, J.; Jørgensen, P.; Christiansen, O. *J. Chem. Phys.*, **2000**, *113*, 6677.
6. Larsen, H.; Olsen, J.; Jørgensen, P.; Christiansen, O. *J. Chem. Phys.*, **2001**, *114*, 10985.
7. Laidig, W. D.; Bartlett, R. J. *Chem. Phys. Lett.*, **1984**, *104*, 424.
8. Gwaltney, S. R.; Sherrill, C. D.; Head-Gordon, M.; Krylov, A. I. *J. Chem. Phys.*, **2000**, *113*, 3548.
9. Krylov, A. I. *J. Chem. Phys.*, **2000**, *113*, 6052.
10. Kowalski, K.; Piecuch, P. *J. Chem. Phys.*, **2000**, *113*, 18.
11. Kowalski, K.; Piecuch, P. *Chem. Phys. Lett.*, **2001**, *344*, 165.
12. Krylov, A. I.; Sherrill, C. D. *J. Chem. Phys.*, **2002**, *116*, 3194.
13. Dutta, A.; Sherrill, C. D. *J. Chem. Phys.*, **2003**, *118*, 1610.
14. Abrams, M. L.; Sherrill, C. D. *J. Phys. Chem. A*, **2003**, *107*, 5611.
15. Krylov, A. I. *Chem. Phys. Lett.*, **2001**, *338*, 375.
16. Krylov, A. I. *Chem. Phys. Lett.*, **2001**, *350*, 522.
17. Sears, J. S.; Sherrill, C. D.; Krylov, A. J. *J. Chem. Phys.*, **2003**, *118*, 9084.
18. Sherrill, C. D.; Schaefer, H. F. in *Advances in Quantum Chemistry*, Löwdin, P.-O., Ed., volume 34, pp 143–269. Academic Press, New York, 1999.
19. Crawford, T. D.; Sherrill, C. D.; Valeev, E. F.; Fermann, J. T.; Leininger, M. L.; King, R. A.; Brown, S. T.; Janssen, C. L.; Seidl, E. T.; Yamaguchi, Y.; Allen, W. D.; Xie, Y.; Vacek, C.; Hamilton, P.; Kellogg, C. B.; Remington, R. B.; Schaefer III, H. F. PSI 3.0, development version. PSITECH, Inc., Watkinsville, GA 30677, U.S.A., 1999.
20. Abrams, M. L.; Sherrill, C. D. *J. Chem. Phys.*, **2003**, *118*, 1604.
21. Pople, J. A.; Binkley, S.; Seeger, R. *Int. J. Quantum Chem. Symp.*, **1976**, *10*, 1.
22. Purvis, G. D.; Bartlett, R. J. *J. Chem. Phys.*, **1982**, *76*, 1910.
23. Raghavachari, K.; Trucks, G. W.; Pople, J. A.; Head-Gordon, M. *Chem. Phys. Lett.*, **1989**, *157*, 479.
24. Becke, A. D. *J. Chem. Phys.*, **1993**, *98*, 1372.
25. Stephens, P. J.; Devlin, F. J.; Chabalowski, C. F.; Frisch, M. J. *J. Phys. Chem.*, **1994**, *98*, 11623.
26. Roos, B. O.; Taylor, P. R.; Siegbahn, P. E. M. *Chem. Phys.*, **1980**, *48*, 157.
27. Andersson, K.; Roos, B. O. in *Modern Electronic Structure Theory*, Yarkony, D. R., Ed., volume 2 of *Advanced Series in Physical Chemistry*, pp 55–109. World Scientific, Singapore, 1995.

28. Olsen, J.; Roos, B. O.; Jørgensen, P.; Aa. Jensen, H. J. *J. Chem. Phys.*, **1988**, *89*, 2185.
29. Grev, R. S.; Schaefer, H. F. *J. Chem. Phys.*, **1992**, *96*, 6850.
30. Fermann, J. T.; Sherrill, C. D.; Crawford, T. D.; Schaefer, H. F. *J. Chem. Phys.*, **1994**, *100*, 8132.
31. Sherrill, C. D.; Schaefer, H. F. *J. Phys. Chem.*, **1996**, *100*, 6069.
32. Laidig, W. D.; Saxe, P.; Bartlett, R. J. *J. Chem. Phys.*, **1987**, *86*, 887.

Chapter 6

Breaking the Curse of the Non-Dynamical Correlation Problem: The Spin-Flip Method

Anna I. Krylov, Lyudmila V. Slipchenko, and Sergey V. Levchenko

Department of Chemistry, University of Southern California, Los Angeles, CA 90089-0482

The spin-flip approach to multi-reference situations (e.g., bond-breaking and diradicals) is described. Both closed and open shell singlet states are described within a single reference formalism as spin-flipping, e.g., $\alpha \rightarrow \beta$, excitations from a triplet ($M_s=1$) reference state for which both dynamical and non-dynamical correlation effects are much smaller than for the corresponding singlet state. Formally, the new theory can be viewed as an Equation-of-Motion model where excited states are sought in the basis of determinants conserving the total number of electrons but changing the number of α and β electrons.

Introduction

It is difficult to overestimate the importance of electronic structure theory in modern chemistry (1). The design and interpretation of experiments are often aided by high-level *ab initio* calculations of structural, thermochemical, and spectroscopic properties. Additional insight can be derived from the examination of wavefunctions and electron distributions which are produced in electronic structure calculations. Most importantly, high-level calculations can now be carried out almost routinely due to the availability of efficient and user-friendly electronic structure packages. However in order for electronic structure calculations to be accessible by the general chemical community, the underlying methods should belong to the class of the so called “theoretical model chemistries” (2), or, more loosely, “blackbox” methods.

As defined by Pople, “theoretical model chemistry” consists of a pair of well-defined approximations to the exact wavefunction: correlation treatment and one-electron basis set (2). Figure 1 summarizes a hierarchy of approximate methods for correlation treatment (3,4) in the ground and excited states. Both the ground state’s (left panel) and excited states’ (right panel) series converge to the exact solution, and the accuracy of the description improves with each additional step of sophistication (at the price of increased computational cost, of course). Fortunately, chemically and spectroscopically relevant answers can be obtained within computationally tractable (for moderate-size molecules) models. For example, the coupled-cluster model with single and double excitations (5) augmented by triple excitations treated perturbatively [CCSD(T)] (6) yields highly accurate structural (errors in bond lengths of 0.2-0.3 pm) and thermochemical (errors of less than 1 kcal/mol in reaction enthalpies) data (3). Excitation energies can be calculated with 0.1-0.3 eV accuracy (7) by the excited states’ counterpart of CCSD, EOM-CCSD method (8-10). Unfortunately, *the above error bars are valid only for species whose ground state wavefunction is dominated by a single Slater determinant and for excited states dominated by single electron excitations*. This restricts the applications of single-reference (SR) models to well-behaved molecules such as closed-shell species at their equilibrium geometries, leaving many chemically important situations [e.g., transition states, bond-breaking, and diradicals (11)] to the domain of multi-reference methods (12).

In order to understand the origin of the breakdown of the SR methods away from equilibrium, consider the torsional potential in ethylene (Figure 2). While at its equilibrium geometry ethylene is a well-behaved closed-shell molecule whose ground and π -valence excited states can be described accurately by SR models (except for the doubly excited Z-state), it becomes a diradical at the barrier, when the π -bond is completely broken (13). Thus, at the twisted geometry all of ethylene’s π -valence states (*N*, *T*, *V*, and *Z*) are two-configurational, *except for the high-spin components of the triplet*.

The traditional recipe for computing ethylene’s torsional potential for the ground and excited states would involve state-by-state (or state-averaged) calculations with the two-configurational SCF (TCSCF) method, the simplest variant of complete active space SCF (CASSCF) (14-16) further augmented by perturbation theory (MRPT) or configuration interaction (MRCI) corrections (12). Recently, this scheme has been reformulated (17-19) employing less expensive coupled-cluster wavefunctions instead of the exponentially expensive CASSCF one. The method, valence optimized orbitals coupled-cluster doubles (VOCCD) (18), is formulated in a SR fashion, however it still (i) relies on an active space selection (20); (ii) involves an orbital optimization step; (iii) requires subsequent inclusion of higher order corrections in a two-step procedure (19); and (iv) is not easily generalized for excited states (21). In this Chapter, we discuss an alternative strategy, the spin-flip (SF) approach, which is a multistate method (i.e., yields several states in one computation), does not require an active space selection and orbital optimization (thus, is genuinely a

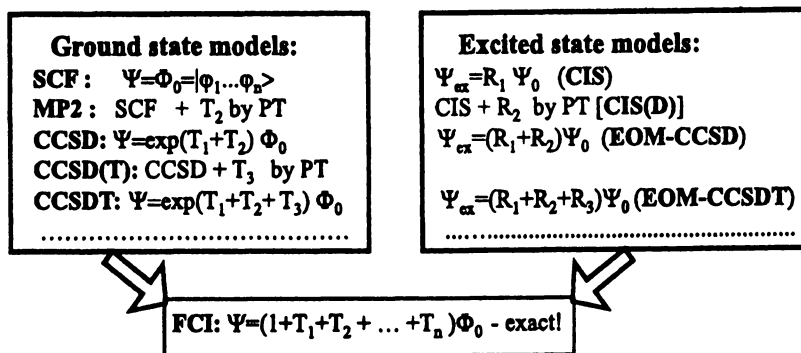


Figure 1. The hierarchy of approximations to an n -electron wavefunction. The left panel presents models of increasing complexity for ground state wavefunctions. The emerging hierarchy of excited states' methods is summarized on the right panel. The simplest possible description of an N -electron wavefunction is given by a single Slater determinant composed of spin-orbitals, i.e., states of pseudo-independent electrons moving in the field of nuclei and a mean field of other electrons [self-consistent field (SCF), or Hartree-Fock (HF) model]. The effects of electron interaction (i.e., correlation) can gradually be turned on by including single, double, and higher excitations (T_1 , T_2 , etc). This can be done perturbatively, e.g., as in the Møller-Plesset theory (MP), or explicitly, e.g., as in coupled-cluster (CC) methods. The corresponding excited states' models can be derived within the linear response (LR) or equation-of-motion (EOM) formalisms. The resulting wavefunctions have a physically appealing form: excited states are described as electronic excitations from approximate ground state wave functions (the operator R_m generates all possible m -electron excitations out of the reference determinant Φ_0). For example, the SCF analog for excited states, the configuration interaction singles (CIS) model, describes excited states as a linear combination of all singly excited determinants. Similarly to the ground state models, accuracy can systematically be improved by including higher excitations. Both series converge to the exact solution of the Schrödinger equation (in a given one-electron basis set) – full configuration interaction (FCI), which, in turn, becomes exact in the limit of the complete one-electron basis set.

robust “black-box” type SR method), and treats both non-dynamical and dynamical correlation in one scheme (i.e., is not a two-step procedure).

As mentioned above, the $M_s = \pm 1$ components of the T -state of ethylene (Figure 2) are single-determinantal at the ground state equilibrium geometry, and remain single-determinantal at all values of the twisting angle. Therefore, they can be accurately described by SR methods at all the torsional coordinates (22).

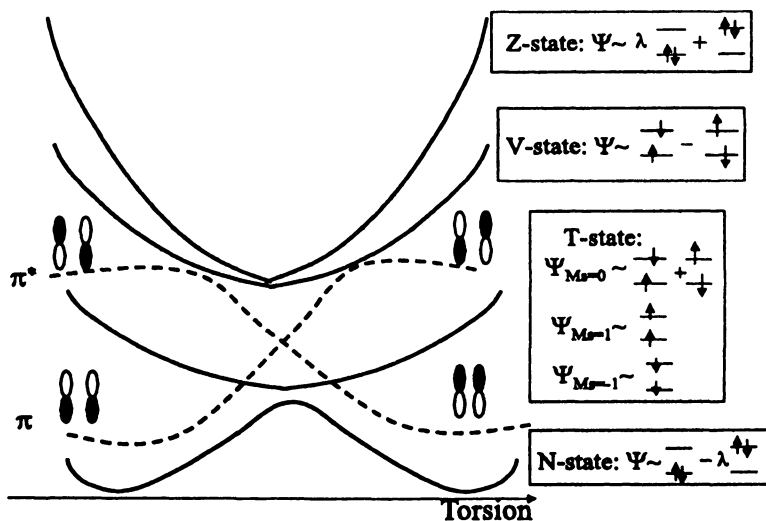


Figure 2. Around equilibrium, the ground state (N-state) wavefunction of ethylene is dominated by the π^2 configuration. However, as a degeneracy between π and π^* develops along the torsional coordinate, the importance of the $(\pi^*)^2$ configuration increases. At the barrier, where π and π^* are exactly degenerate, the qualitatively correct wavefunction for the N-state must include both configurations with equal weights. That is why the quality of the SR wavefunctions degrades as the molecule is twisted: even when the second configuration is explicitly present in a wavefunction (e.g., as in the CCSD or CISD models), it is not treated on the same footing as the reference configuration, π^2 . The singlet and triplet $\pi\pi^*$ states (the V and T states, respectively) are formally single-electron excitations from the N-state, and are well described by the SR excited states' models (despite the fact that both the singlet and the $M_s = 0$ component of the triplet are two-configurational and therefore are not accessible by the ground state SR methods). The Z-state, however, is formally a doubly excited state with respect to the N-state, and therefore SR models will not treat it accurately. Note that the high-spin $M_s = \pm 1$ components of the triplet T-state remain single-determinantal at all the torsional angles. Moreover, all the $M_s = 0$ configurations employed in the N, V, T, and Z states are formally single-electron excitations which involve a spin-flip of one electron with respect to any of the two high-spin triplet configurations.

Moreover, all the low-spin $M_s = 0$ determinants from Figure 2 are formally *single electron excitations from the high-spin triplet state involving a spin-flip of one electron*. This immediately suggests employing the EOM or LR formalism and describing the target $M_s = 0$ states as spin-flipping excitations from the well-behaved high-spin reference state. This is the essence of the SF approach (23-29).

It should be mentioned that describing ground state wavefunctions as “excited” states with respect to a reference state which is orthogonal to a target wavefunction is a well known approach. For example, the ionized states EOM-CCSD methods have proven very useful for doublet radicals whose theoretical treatment is often plagued by symmetry breaking. In this approach, the ground state CC equations are solved for a *closed shell* cation or anion, and the ground state of the corresponding doublet radical is sought in the basis of determinants which do not conserve the number of electrons e.g., either in N-1 (EOM ionization potential CC [EOMIP-CC]), or in N+1 (EOM electron affinity CC [EOMEA-CC]) electron basis (30-32). Recently, doubly-ionized/attached EOM models which target diradicals have been presented (33).

The Method

In traditional (non-SF) SR excited states models, the excited state wavefunctions are parameterized as follows (see Figure 1):

$$\Psi_{M_s=0}^{s,i} = \hat{R}_{M_s=0} \tilde{\Psi}_{M_s=0}^s, \quad (1)$$

where $\tilde{\Psi}_{M_s=0}^s$ is a closed-shell reference wavefunction, and the operator \hat{R} is an excitation operator truncated at a certain level of excitation (which should be consistent with the theoretical model employed to describe the reference $\tilde{\Psi}^s$). Note that only excitation operators that do not change the total number of α and β electrons, i.e. $M_s = 0$, need to be considered in Eq. (1).

As explained in the Introduction, this scheme breaks down both for ground and excited states when orbitals from occupied and virtual subspaces become near-degenerate, e.g. at the dissociation limit or in diradicals (see Figure 2). To overcome this problem, the SF model employs a high-spin triplet reference state which is accurately described by a SR wavefunction. The target states, closed and open shell singlets and triplets, are described as spin-flipping excitations:

$$\Psi_{M_s=0}^{s,i} = \hat{R}_{M_s=-1} \tilde{\Psi}'_{M_s=+1}, \quad (2)$$

where $\tilde{\Psi}'_{M_s=+1}$ is the $\alpha\alpha$ component of the triplet reference state, $\Psi_{M_s=0}^{s,i}$ stands for the final ($M_s = 0$) singlet and triplet states, respectively, and the operator

$\hat{R}_{M_s=-1}$ is an excitation operator that flips the spin of an electron. In order to distinguish $\hat{R}_{M_s=-1}$ excitation operators from their non-spin-flipping counterparts, we shall denote m -electron excitation operators with a spin-flip of one electron as U_m instead of R_m . As can be seen from Figure 2, all the configurations used to describe diradical-type wavefunctions (e.g., N , V , T , and Z states of ethylene) are formally single excitations with respect to the high-spin component of the triplet ($|\pi\alpha\pi^*\alpha\rangle$).

Figure 3 shows the reference high-spin configuration and the spin-flipping single and double excitations for two electrons in three orbitals system. Configuration (b) corresponds to a ground-state closed shell singlet. Configurations (c)-(e) are those which become degenerate with (b) at the dissociation limit. They are employed in a description of diradicals states, e.g., states which can be derived by distributing two electrons over two (nearly) degenerate orbitals (N , V , T , and Z states of twisted ethylene are of this type). It is easy to see that (b)-(e) are treated on an *equal footing* in our model, and that other configurations *do not introduce imbalance in treating (b)-(e)*.

Therefore, the SF ansatz (2) is sufficiently flexible to describe changes in ground state wavefunctions along a single bond-breaking coordinate. Moreover, it treats both closed-shell (e.g., N and Z) and open-shell (V and T) diradicals' states in a balanced fashion, i.e., without overemphasizing the importance of one of the configurations.

Similarly to traditional excited state theories, the description of the final states can be systematically improved by employing theoretical models of increasing complexity for the reference wavefunction as summarized in Figure 4. For example, the simplest SF model employs a Hartree-Fock wavefunction, and the operator \hat{U} is then truncated at single excitations (SF-CIS or SF-SCF) (23, 29). SF-CIS can be further augmented by perturbative corrections [SF-CIS(D) or SF-MP2] (24). A yet more accurate description can be achieved by describing the reference wavefunction by a coupled-cluster model, e.g., CCSD (28) or OO-CCD (23, 34). In this case, the excitation operator R consists of single and double excitation operators involving a flip of the spin of an electron (23). The corresponding SF equations in spin-orbital form are identical to those of traditional excited state theories i.e., CIS, CIS(D), EOM-CCSD or EOM-OO-CCD, however, they are solved in a different subspace of determinants: non-SF theories consider only $M_s=0$ excitation operators, whereas SF operates in the $M_s=-1$ subspace. The computational cost and scaling of the SF models are identical to those of the corresponding non-SF excited state theories.

Two of the SF models, SF-CISD and SF-DFT, deserve special mention. By using the SF formulation, the CI can be formulated in a rigorously size-consistent way (25, 29). For example, the SF-CISD model is (i) variational, (ii) size-consistent, and (iii) exact for two electrons. So far, this is the only approximate model [except for fully variational CCSD (35) which is prohibitively expensive to be of a practical use] that simultaneously satisfies these three highly desirable properties (2).

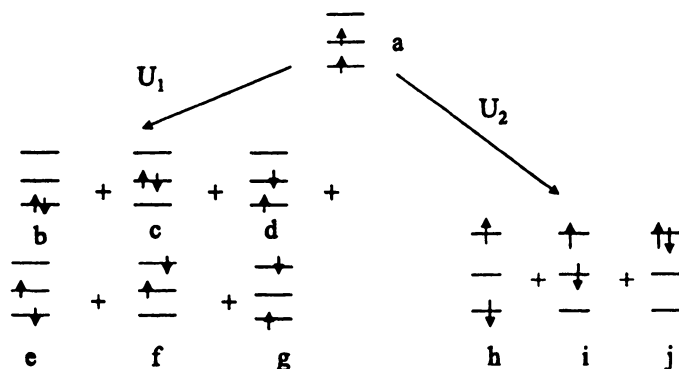


Figure 3. Two electrons in three orbitals system. Configuration (a) is the reference configuration. Single electron excitations with spin-flip produce configurations (b)-(g). Two-electron excitations with a single spin-flip produce configurations (h)-(j). Note that non-spin-flipping excitations or excitations that flip the spin of two electrons produce $M_s = \pm 1$ configurations, which do not interact through the Hamiltonian with the final $M_s = 0$ states, and thus are not present in the model.

Reference:	Method:	Wavefunction:
SCF	SF-SCF (or SF-CIS)	$U_1 \Phi_0$
MP2	SF-MP2 [or SF-CIS(D)]	$U_1 \Phi_0 + T_2$ by PT
CCSD	SF-CCSD	$(U_1 + U_2) \exp(T_1 + T_2) \Phi_0$
CCSDT	SF-CCSDT	$(U_1 + U_2 + U_3) \exp(T_1 + T_2 + T_3) \Phi_0$
.....		

Figure 4. Hierarchy of the SF models. Similar to the non-SF SR methods, the SF models converge to the exact n -electron wavefunction when the spin-flipping operator \hat{U} includes up to n -tuple excitations. For example, the SF-CCSD model is exact for two electrons

Lastly, the SF approach implemented within the time-dependent (TD) density functional theory (DFT) extends DFT to multi-reference situations with no cost increase relative to the non-SF TD-DFT. Similarly to DFT and TD-DFT, the SF-DFT model (27) is formally exact and therefore will yield exact answers with the exact density functional. With the available inexact functionals, the SF-DFT represents an improvement over its non-SF counterparts. It has been shown to yield accurate equilibrium properties and singlet-triplet energy gaps in diradicals (27).

The Spin-flip Method for Bond-breaking: the Ethylene Torsional Potential

Figure 5 shows the torsional potential calculated by the SF [SF-CIS, SF-CIS(D), and SF-OD] and non-SF (restricted and unrestricted HF and OD) methods (23, 24, 36). All curves are compared with the TC-CISD curve (24). The unbalanced treatment (within a single reference framework) of $(\pi)^2$ and $(\pi^*)^2$ configurations results in unphysical shapes of the PES, i.e., a cusp at 90° and large errors in barrier heights. The spin-unrestricted PESs are smooth; however, the barrier height is usually underestimated, even by the highly correlated methods (36). Moreover, the shape of the unrestricted PES can be quite wrong, for example, the U-OD curve is too flat around the barrier as compared against the TC-CISD one (see Figure 5). Also, the UHF based wavefunctions are heavily spin-contaminated around the barrier *even for highly correlated methods such as coupled-cluster models* (36). All the SF models produce smooth PESs. Quantitatively, SF-SCF represents a definite advantage over both the RHF and UHF results. Similarly, the SF-OD curve is closer to our reference TC-CISD curve than either R-OD or U-OD. The SF-CIS(D) curve is very close to the more expensive SF-OD one. Similar performance of the SF methods has been observed for bond-breaking in HF, BH, and F_2 (23-25).

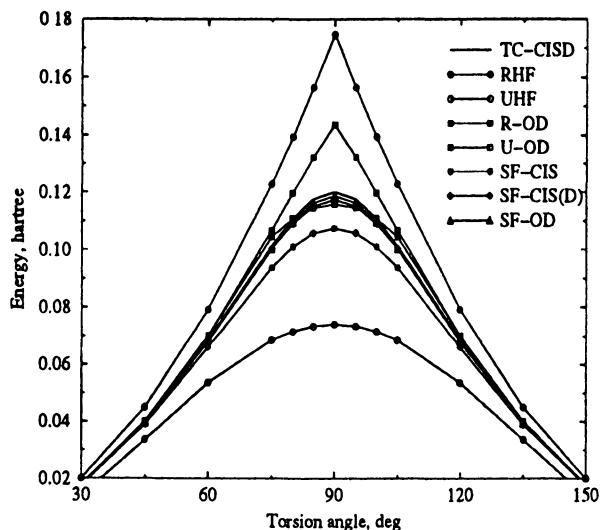


Figure 5. Ethylene torsion, DZP basis. All curves are shifted such that the energy at 0° is zero. The spin-flip curves do not exhibit an unphysical cusp and are closer to the reference TC-CISD curve than the corresponding spin-restricted and spin-unrestricted models.

The Spin-flip Method for Diradicals

Diradicals represent the most clear-cut application of the SF approach because in these systems the non-dynamical correlation derives from a single HOMO-LUMO pair (e.g., π and π^* in twisted ethylene). In this section we present results for methylene and trimethylenemethane (TMM).

Four low-lying states of methylene are diradical-type states (11) deriving from the distribution of two electrons in the two nearly degenerate orbitals, $3a_1$ ($s^x p^y$ hybrid) and $1b_1$ (out-of-plane p-orbital). The ground state of methylene is triplet \tilde{X}^3B_1 :

$$\tilde{X}^3B_1 \approx (1a_1)^2 (2a_1)^2 (1b_2)^2 (3a_1)(1b_1) \quad (3)$$

The lowest singlets are:

$$\tilde{a}^1A_1 \approx \lambda (1a_1)^2 (2a_1)^2 (1b_2)^2 (3a_1)^2 - \sqrt{1-\lambda^2} (1a_1)^2 (2a_1)^2 (1b_2)^2 (1b_1)^2 \quad (4)$$

$$\tilde{b}^1B_1 \approx (1a_1)^2 (2a_1)^2 (1b_2)^2 (3a_1)(1b_1) \quad (5)$$

$$\tilde{c}^1A_1 \approx \sqrt{1-\lambda^2} (1a_1)^2 (2a_1)^2 (1b_2)^2 (3a_1)^2 + \lambda (1a_1)^2 (2a_1)^2 (1b_2)^2 (1b_1)^2 \quad (6)$$

While the $\alpha\alpha$ ($M_s=1$) component of the \tilde{X}^3B_1 state (3) is essentially a single-reference wave function, the corresponding singlet b^1B_1 state (as well as the $M_s=0$ component of the triplet) is a linear combination of two Slater determinants with equal coefficients. Therefore, \tilde{b}^1B_1 state cannot be described within a formalism that uses a single Slater determinant reference. The character of the lowest singlet, \tilde{a}^1A_1 , varies from a single-reference ($\lambda \approx 1$) to the two-configurational ($\lambda \approx \frac{1}{\sqrt{2}}$) wave function. At the \tilde{a}^1A_1 equilibrium geometry, the effect of the second configuration is relatively small, and the \tilde{a}^1A_1 state can be reasonably well described by SR models. The second 1A_1 state, \tilde{c}^1A_1 can be described as a doubly excited state with respect to \tilde{a}^1A_1 . At its equilibrium geometry, the \tilde{c}^1A_1 state requires a two-configurational wave function. Therefore, it is not possible to describe all three singlet states of methylene by a single-reference model. The spin-flip model, however, describes all these states as spin-flipping excitations from the reference $M_s=1$ triplet \tilde{X}^3B_1 state.

For this small system, we can compare the performance of different methods against the FCI results (37) in a relatively large TZ2P basis. Calculated equilibrium geometries, vibrational frequencies, and adiabatic singlet-triplet gaps for the singlet states of methylene are shown in Table 1. The SF models describe accurately all three singlet states. SF-CIS(D) represents a qualitative improvement over SF-CIS, while the SF-CCSD and SF-OD results follow FCI closely.

Table 1: Equilibrium geometries, harmonic vibrational frequencies (cm^{-1}), and adiabatic excitation energies (eV) for singlet methylene (\bar{a}^1A_1 , \bar{b}^1B_1 , and \bar{c}^1A_1 states)^a.

Method	r_e , Å	α	$\omega_1(a_1)$	$\omega_2(a_1)$	$\omega_3(b_2)$	ΔE_{st}
\bar{a}^1A_1						
FCI/TZ2P ^b	1.1089	101.89	2899	1404	2971	0.483
SF-SCF/TZ2P	1.0945	104.07	3096	1485	3176	0.883
SF-CIS(D)/TZ2P	1.0974	102.86	3017	1443	3111	0.613
SF-OD/TZ2P	1.1043	102.37	2932	1422	3025	0.514
SF-CCSD/TZ2P	1.1040	102.45	2937	1421	3011	0.517
\bar{b}^1B_1						
FCI/TZ2P ^b	1.0748	141.56	3136	1006	3470	1.542
SF-SCF/TZ2P	1.0624	142.38	3311	1103	3611	1.875
SF-CIS(D)/TZ2P	1.0652	141.59	3243	1082	3546	1.646
SF-OD/TZ2P	1.0716	141.32	3160	1028	3424	1.564
SF-CCSD/TZ2P	1.0716	141.32	3162	1034	3420	1.565
\bar{c}^1A_1						
FCI/TZ2P ^b	1.0678	170.08	3200	666	3531	2.674
SF-SCF/TZ2P	1.0507	174.48	3446	343	3809	3.599
SF-CIS(D)/TZ2P	1.0544	173.73	3374	416	3727	2.953
SF-OD/TZ2P	1.0639	170.14	3238	672	3555	2.715
SF-CCSD/TZ2P	1.0639	170.14	3240	677	3581	2.718

^a TZ2P basis set from Ref. (37). SF models employ the \bar{X}^3B_1 ground state as the reference. The SF-CIS, SF-CIS(D), and SF-OD results are from Refs. (24, 25). ΔE_{st} are calculated at the FCI/TZ2P optimized geometries.

^b Ref. (37). One frozen core and one deleted virtual orbital.

Our next example, the TMM diradical, is a more challenging case because its frontier orbitals are exactly degenerate. The π -system of TMM is shown in Figure 6: four π -electrons are distributed over four molecular π -type orbitals. Due to the exact degeneracy between the two e' orbitals at the D_{3h} structure, Hund's rule predicts the ground state of the molecule to be a triplet $^3A'_2$ state (similar to the T -state in ethylene). This is confirmed by both the experimental and theoretical findings (38-43).

The vertical excitation energies are summarized in Figure 6 (with C_{2v} symmetry labels) (26,44). The three lowest singlet states are the diradical singlet states (similar to the N , V , and Z states of ethylene). However, excited states that derive from excitations of other π electrons are also relatively low in energy. The first closed-shell singlet, 1A_1 and the open-shell singlet 1B_2 (similar to the N and V states of ethylene, respectively) are degenerate at the D_{3h} geometry due to the degeneracy of a_2 and $2b_1$ orbitals. The second closed-shell singlet 2^1A_1 (an analog of the Z -state) is followed by a pair of degenerate triplets, 3A_1 and 3B_2 ,

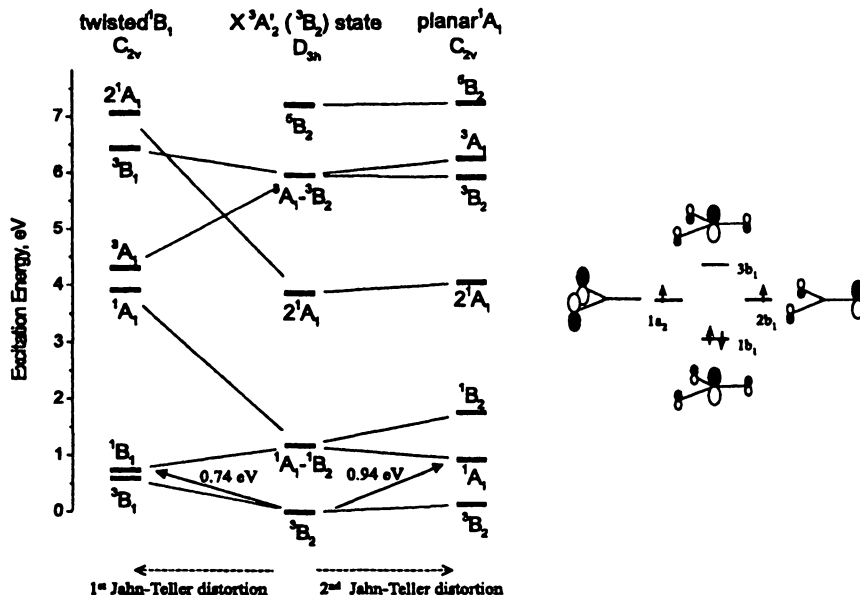


Figure 6. On the right, the π -system of TMM and the electronic configuration of the ground state are shown (C_{2v} labels are used). The left panel presents electronic states of TMM at the ground state equilibrium D_{3h} geometry, and at the two Jahn-Teller C_{2v} distorted structures (equilibrium geometries of the 1^1B_1 and 1^1A_1 states). The corresponding adiabatic singlet-triplet gaps are also shown.

obtained by excitation of one electron from the doubly occupied $1b_1$ orbital to the a_2 or $2b_1$ degenerate orbitals. Finally, there is a quintet 5B_2 state in which all π -orbitals are singly occupied. We do not discuss low-lying states derived from electron excitations beyond the TMM's π -system. Several such states appear between the pair of degenerate triplets and the quintet state. The SF-OD model should be augmented by higher excitations to achieve a quantitatively accurate description of these states.

In accordance with the Jahn-Teller theorem, the degeneracy between the degenerate states (closed-shell and open-shell singlets, and a pair of triplets) can be lifted in lower symmetry. The closed-shell singlet is stabilized at the planar C_{2v} geometry, with one short CC bond. The open-shell singlet prefers an equilibrium structure with one long CC bond and a twisted methylene group. The real minimum of the open-shell singlet is a C_2 structure with a 79.0° twisted methylene group; however, the energy difference between this structure and the C_{2v} twisted one (the dihedral angle equals 90.0°) is only 0.001 eV (0.03 kcal/mol). The second 1A_1 state prefers D_{3h} equilibrium geometry. The adiabatic singlet-triplet energy separations for the three lowest singlet states are 0.74 eV, 0.94 eV, and 3.86 eV for the 1^1B_1 , 1^1A_1 , and 2^1A_1 states, respectively (26) (at the

SF-OD level with the basis set composed of a cc-pVTZ basis on carbons and a cc-pVDZ basis on hydrogens). These energies are very close to the MRPT values (26) of 0.72 and 0.83 eV (for the 1^1B_1 and 1^1A_1 states, respectively). With regard to experiment, the lowest adiabatic state, 1^1B_1 , has not been observed in the photoelectron spectrum (40) because of unfavorable Frank-Condon factors. The experimental adiabatic energy gap (including ZPE) between the ground triplet state and the 1^1A_1 state is 0.70 eV. The estimated experimental T_e is 0.79 eV, which is 0.15 eV lower than the SF-OD estimate.

In our detailed benchmark study (26), we calculated the singlet-triplet energy separations for a large number of systems, i.e., O, C, and Si atoms, O₂, NH, NF, and OH⁺ diatomics, methylene isovalent series (CH₂, NH₂⁺, SiH₂, and PH₂⁺), benzynes, and TMM. In all these cases, the SF models performed very well. The SF-OD results are within 3 kcal/mol of the experimental or highly accurate multi-reference values. In most cases the errors are about 1 kcal/mol. Drawing from the performance of single-reference methods for well-behaved molecules, we expect that a perturbative account of triple excitations will bring the corresponding SF-CC model into the *chemical accuracy* range, i.e., < 1 kcal/mol.

Conclusions

The SF approach extends the applicability of SR methods to bond-breaking problems and to diradicals. Both closed and open shell singlet states are described within a single reference formalism as spin-flipping, e.g., $\alpha \rightarrow \beta$, excitations from the triplet ($M_s=1$) reference state for which both dynamical and non-dynamical correlation effects are much smaller than for the corresponding singlet state. Formally, the new theory can be viewed as an EOM model where the excited states are sought in the basis of determinants conserving the total number of electrons but changing the number of α and β electrons. A very attractive feature of the new approach is that it is described by equations identical to the EOMEE equations (in spin-orbital form).

This work has been supported by the Camille and Henry Dreyfus New Faculty Awards Program, the James H. Zumberge Faculty Research and Innovation Fund of the University of Southern California, the WISE Research Fund (USC), the Petroleum Research Fund administered by the American Chemical Society (types G and AC), and the National Science Foundation (CAREER award).

References

1. The Royal Swedish Academy of Sciences has awarded the 1998 Nobel Prize in Chemistry to Prof. Walter Kohn and Prof. John A. Pople. The Laureates have each made pioneering contributions in developing methods that can be

used for theoretical studies of the properties of molecules and the chemical processes in which they are involved. Citation: "to Walter Kohn for his development of the density-functional theory and to John Pople for his development of computational methods in quantum chemistry."

2. Pople, J.A. In *Energy, Structure and Reactivity: Proceedings of the 1972 Boulder Summer Research Conference on Theoretical Chemistry*; Smith, D.W., McRae, W.B., Eds.; Wiley: New York, 1973; pages 51–61.
3. Helgaker, T.; Jørgensen, P.; Olsen, J. *Molecular Electronic Structure Theory*; John Wiley & Sons, 2000.
4. Head-Gordon, M. *J. Phys. Chem.* **1996**, *100*, 13213.
5. Purvis, G.D.; Bartlett, R.J. *J. Chem. Phys.* **1982**, *76*, 1910.
6. Raghavachari, K.; Trucks, G.W.; Pople, J.A.; Head-Gordon, M. *Chem. Phys. Lett.* **1989**, *157*, 479.
7. Larsen, H.; Hald, K.; Olsen, J.; Jørgensen, P. *J. Chem. Phys.* **2001**, *115*, 3015.
8. Sekino, H.; Bartlett, R.J. *Int. J. Quant. Chem. Symp.* **1984**, *18*, 255.
9. Koch, H.; Jørgen Aa. Jensen, H.; Jørgensen, P. *J. Chem. Phys.* **1990**, *93*, 3345.
10. Stanton, J.F.; Bartlett, R.J. *J. Chem. Phys.* **1993**, *98*, 7029.
11. Salem, L.; Rowland, C. *Angew. Chem. Int. Ed. Engl.* **1972**, *11*, 92.
12. Hirao, K., Ed. *Recent Advances in Multi-reference Methods*; World Scientific, 1999.
13. Following Salem (11), we define diradicals as molecules with two electrons occupying two (near)-degenerate molecular orbitals. More loosely, Salem considers molecules with a broken bond as diradicals.
14. Roos, B.O.; Taylor, P.R.; Siegbahn, P.E.M. *Chem. Phys.* **1980**, *48*, 157.
15. Ruedenberg, K.; Schmidt, M.W.; Gilbert, M.M.; Elbert, S.T. *Chem. Phys.* **1982**, *71*, 41.
16. Schmidt, M.W.; Gordon, M.S. *Annu. Rev. Phys. Chem.* **1998**, *49*, 233.
17. Sherrill, C.D.; Krylov, A.I.; Byrd, E.F.C.; Head-Gordon, M. *J. Chem. Phys.* **1998**, *109*, 4171.
18. Krylov, A.I.; Sherrill, C.D.; Byrd, E.F.C.; Head-Gordon, M. *J. Chem. Phys.* **1998**, *109*, 10669.
19. Gwaltney, S.R.; Sherrill, C. D.; Head-Gordon, M.; Krylov, A. I. *J. Chem Phys.* **2000**, *113*, 3548.
20. Ideally, one would like to always employ a full valence active space (bonding, anti-bonding, and lone pair orbitals). Such active space is uniquely defined, and the corresponding CASSCF wave function is flexible enough to describe all the major interactions of the valence electrons, e.g., the polarization of σ electrons for the $\pi\pi^*$ ionic configurations, as in the V -state of ethylene, etc. The advantage of the VOCCD model is that it enables one to perform full valence active space calculations for much larger systems than it is possible for CASSCF. This eliminates certain arbitrariness involved in the choice of the active space.

21. Krylov, A.I.; Sherrill, C.D. Head-Gordon, M. *J. Chem. Phys.* **2000**, *113*, 6509.
22. It is hardly surprising that the high-spin T state is not affected by the π -bond breaking: indeed, since both π electrons in the T state are of the same spin, there is no π bond in this state to begin with!
23. Krylov, A.I. *Chem. Phys. Lett.* **2001**, *338*, 375.
24. Krylov, A.I.; Sherrill, C.D. *J. Chem. Phys.* **2002**, *116*, 3194.
25. Krylov, A.I. *Chem. Phys. Lett.* **2001**, *350*, 522.
26. Slipchenko, L.V.; Krylov, A.I. *J. Chem. Phys.* **2002**, *117*, 4694.
27. Shao, Y.; Head-Gordon, M.; Krylov, A.I. *J. Chem. Phys.* **2003**, *118*, 4807.
28. Levchenko, S.V.; Krylov, A.I. **2003**; manuscript in preparation.
29. Sears, J.S.; Sherrill, C.D.; Krylov, A.I. *J. Chem. Phys.* **2003**; in press.
30. Stanton, J.F.; Gauss, J. *J. Chem. Phys.* **1994**, *101*, 8938.
31. Nooijen, M.; Bartlett, R.J. *J. Chem. Phys.* **1995**, *102*, 3629.
32. Sinha, D.; Mukhopadhyaya, D.; Chaudhuri, R.; Mukherjee, D. *Chem. Phys. Lett.* **1989**, *154*, 544.
33. Wladyslawski, M.; Nooijen, M. In *ACS Symposium Series*, Vol. 828, pages 65–92, 2002.
34. In the optimized orbitals CCD (OO-CCD or OD) model, the orbitals are optimized variationally to minimize the total energy of the OO-CCD wavefunction. This allows one to drop single excitations from the wavefunction. Conceptually, OO-CCD is very similar to the Brueckner CCD (B-CCD) method. Both OO-CCD and B-CCD perform similarly to CCSD in most cases.
35. van Voorhis, T.; Head-Gordon, M. *J. Chem. Phys.* **2000**, *113*, 8873.
36. Krylov, A.I. *J. Chem. Phys.* **2000**, *113*, 6052.
37. Sherrill, C.D.; Leininger, M.L.; Van Huis, T.J.; Schaefer III, H.F. *J. Chem. Phys.* **1998**, *108*, 1040.
38. Dowd, P. *J. Am. Chem. Soc.* **1966**, *88*, 2587.
39. Baseman, R.J.; Pratt, D.W.; Chow, M.; Dowd, P. *J. Am. Chem. Soc.* **1976**, *98*, 5726.
40. Wenthold, P.G.; Hu, J.; Squires, R.R.; Lineberger, W.C. *J. Am. Chem. Soc.* **1996**, *118*, 475.
41. Cramer, C.J.; Smith, B.A. *J. Phys. Chem.* **1996**, *100*, 9664.
42. Feller, D.; Tanaka, K.; Davidson, E.R.; Borden, W.T. *J. Am. Chem. Soc.* **1982**, *104*, 967.
43. Davidson, E.R.; Borden, W.T. *J. Am. Chem. Soc.* **1977**, *99*, 2053.
44. Slipchenko, L.V.; Krylov, A.I. *J. Chem. Phys.* **2003**, *118*; in press.

Chapter 7

Economical Description of Electron Correlation

Laimutis Bytautas^{1,2} and Klaus Ruedenberg¹

¹Department of Chemistry and Ames Laboratory, U.S. Department of Energy, Iowa State University, Ames, IA 50011

²On leave from Institute of Theoretical Physics and Astronomy, Gostauto 12, Vilnius, Lithuania

Methods are presented for reducing the computational effort required to account for electron correlation in large molecules. The correlation recovery is divided into two stages: Recovery of zeroth-order dynamic correlations and dynamic correlation refinements. The former is achieved through MCSCF wavefunctions related to full valence spaces. A method is developed for the *a-priori* elimination of the configurational deadwood from such wavefunctions. Although orbital-independent, the procedure is most effective in conjunction with the use of appropriately localized molecular orbitals. Applications to the molecules HNO, OCO and NCCN show that drastic shortenings of the CI expansions (e.g., from 776,316 to 43,038 SDTQ determinants in NCCN) raise the energy by less than 1 mh. For the determination of the dynamic correlation energy, on the other hand, a model is developed that leads to an additive expression in terms of pair populations of localized orbitals multiplied by correlation energy contributions of electron pairs within and between such orbitals. This simple formula predicts the valence correlation energies of about 50 organic molecules with a mean absolute deviation of about 2 kcal/mol. Contributions of nonadjacent localized molecular orbitals are found to be near negligible.

1. Introduction

Reliable studies of chemical problems require that electron correlation be taken into account. For small systems *ab initio* results can be obtained at a high level of correlation and they accurately reproduce experimental data (1,2). Correlated studies of large systems, like DNA or periodic solids are however difficult because of the drastic increase in the computational effort for many accurate correlated methods. Although simple correlated wavefunctions such as the valence-bond approach (3) have yielded noteworthy predictions, such as providing simple rules for the occurrence of unpaired π -electron density near graphitic edges (4,5), most quantitative studies of chemical interest require sophisticated *ab-initio* approaches. The least expensive correlated approach appears to be density functional theory (6-8) and it is the only widely used method so far for extended systems. Unfortunately, even its most current functionals encounter difficulties in properly describing certain structures and properties of interest, such as the band gap or ionization potential in polyacetylene (9). Møller-Plesset (MP2) perturbation theory or coupled-cluster theory (10) are considered to be more accurate (11). However, MP2 scales formally as N^5 and coupled cluster singles and doubles (CCSD) method scales as N^6 , where N is the number of basis functions. The most widely used variational approach, the configuration interaction (CI) method (12,13), scales even more steeply with N .

Since these algorithmic scalings are considerably in excess of what one would conjecture from physical reasoning (14), some recent work has explored ways of reducing the computational effort. Sæbø and Pulay (15,16) have shown the usefulness of localized orbitals for efficient correlated methods. Most often these orbitals are utilized in the context of MP2 or coupled-cluster theories (16-18). Since the level of treatment of electron correlation between such orbitals is usually associated with the spatial distance between them (16-20), the arbitrariness in specifying this distance may cause discontinuities when mapping geometry changes. Within the context of variational methods, Buenker and Peyerimhoff (21-23) rather early developed a method for generating effective truncated CI expansions by iterative single-plus-double excitations from reference spaces, and there have been further advances along these lines (24-32). It has also been recognized for a long time that it is essential to account for up to at least quadruply substituted configurations in correlation energy calculations (33,34).

In the approach pursued here, the recovery of correlation is perceived as a two-stage process: First, the determination of a zeroth-order approximation in form of a MCSCF wavefunction that is in some way related to the full valence space and determines the molecular orbitals; then, the determination of refinements that recover the remaining dynamic correlation. Section 2 of this paper deals with the elimination of all configurational deadwood from full valence spaces. In Section 3, a simple approach for obtaining an accurate estimate of the dynamic correlation is discussed.

In section 2, a method is described for selecting a priori only those configurations that are needed to achieve milli-hartree accuracy in the full valence space (35). It involves an appropriate ordering of the configurations and a truncation criterion based on a reliable truncation error estimate. The most effective reduction of CI expansions is obtained by using appropriately localized MO's rather than natural orbitals. The selection method does not involve an explicit judgment regarding inter-orbital distances. The method is contingent upon a recent determinantal code for performing direct CI calculations with arbitrary configuration selections (36,37). While the presented applications are limited to molecules at equilibrium geometries and to SDTQ-CI expansions, we expect that the method can be extended to reaction path following and to the inclusion of quintuple and sextuple excitations. The selection procedure can also be applied beyond full-valence CI spaces.

In Section 3, we discuss a method for the accurate estimation of the dynamic electron correlation energy. We find that, for equilibrium geometries of singlet ground states, the total, mostly-dynamic correlation energy can be predicted by an extremely simple formula that contains bonding information and correlation strengths between localized molecular orbitals (38). Due to the short-range character of the dynamic correlation the main contributions to the dynamic correlation energy come from the intra-orbital electron correlations, and from the inter-orbital electron correlations between adjacent orbital pairs.

2. A Priori Elimination of Configurational Deadwood from Full Valence Spaces in Large Molecules

2.1 Formulation of objective

In the present section we address the problem of identifying a priori the most compact expansion for the zeroth-order wavefunction. If non-dynamic electron correlation is insignificant (39-41), this is the SCF approximation, but in the presence of non-dynamic correlation it is a limited MCSCF (42-47) expansion. There is some freedom in the zeroth-order wavefunction in as much as it may be expedient for it to include also some dynamic correlation. Zeroth order MCSCF functions that are in some way based on *full* configuration spaces generated by the *formal minimal valence basis orbitals* (FORS = full optimized reaction space model) have proven particularly useful for the reliable description of chemical processes on potential energy surfaces (44-47). But even with the severe orbital restriction of this model, such configuration spaces still rapidly outgrow current computational capabilities with increasing molecular size and this leads to the problem of reducing the dimensions of full valence configuration spaces for large systems.

The number N_o of occupied valence SCF orbitals in a molecule is typically less than the total number N_{mb} of orbitals in the minimal valence basis sets of all atoms. The full valence MCSCF wavefunction is the optimal expansion in terms of all configurations that can be generated from N_{mb} molecular orbitals. Closely related is the full MCSCF wavefunction of all configurations that can be generated from N_e orbitals, where N_e is the number of valence electrons, i.e. each occupied valence orbital has a correlating orbital, as first postulated by Boys (48) and also presumed in perfect pairing models (49,50). We shall call these two types of full spaces FORS 1 and FORS 2. In both, the inner shell remains closed.

A standard way of reducing the size of the resulting configuration spaces is to include only those valence orbitals as configuration generators that are considered to be "active" in the electronic rearrangements occurring in a particular reaction. This option, which has proven extremely fruitful, always exists and we shall not elaborate on it further. Rather, the focus of our interest will be the fact that full valence spaces, even if reduced as just mentioned, typically contain large amounts of "deadwood", i.e. configurations whose omission will result in a deterioration of the energy by less than, say, 1 mh or even 0.1 mh. Our aim is to identify and select the minimum number of "live" configurations *a priori*, i.e. without having to do the full-space calculation.

A well-established effective approach to generating a rapidly converging configurational expansion consists of dividing the molecular orbitals into strongly and weakly occupied ones. In the simplest cases, the former are those occupied in the SCF wavefunction and the latter are the remaining orbitals. The configurations can then be generated by single, double, triple, quadruple etc. excitations from the strongly to the weakly occupied molecular valence orbitals. In this configurational grouping the contributions are known to rapidly decrease with increasing excitation level, so that excitations beyond the sextuple level are rarely needed, and up to quadruple excitations ("SDTQ-CI") are very often satisfactory. We shall adopt this approach here.

The number of quadruple, quintuple and sextuple excitations is however still a very large number for a zeroth-order wavefunction and even these configuration spaces still contain more dead than live wood. Our goal is therefore the development of a method for *a priori* identifying and selecting the latter. It will be achieved by

- (i) Identifying a set of molecular orbitals that yields a rapid convergence for the full configurational expansion (full configuration spaces are invariant under nonsingular transformations of the generating orbitals),
- (ii) Predicting for the full expansion at each excitation level, the sequence of configurations in the order of decreasing importance.
- (iii) Predicting the cut-off in this full expansion such that the corresponding truncation will result in an energy error of less than a given threshold, typically less than 1 mh.

In the following, we discuss the method that has been developed for SDTQ-CI type wavefunctions (35). Quintuple and sextuple excitations will be the subject of future investigations.

The method has been tested for the FORS 1 and FORS 2 wavefunctions of the molecules HNO, OCO and NCCN, i.e. by calculating the “live parts” of the following MCSCF wavefunctions: SDTQ-[12/9] and -[12/12] for HNO; SDTQ-[16/12] and -[16/16] for OCO; SDTQ-[18/16] and [18/18] for NCCN. All configurational expansions were expressed in terms of determinants and calculated with the direct full CI and general CI codes of Ivanic and Ruedenberg (36,37). Dunning’s triple-zeta cc-pVTZ AO bases (51) were used on all atoms. The calculations were performed with the GAMESS molecular program system (52).

2.2 Orbital determination

Strongly and Weakly Occupied Approximate FORS Molecular Orbitals

The first step is the determination of a good approximation to the FORS orbital space without a full valence space MCSCF calculation. The following procedure has proved successful (35). First, the SCF wavefunction is determined. Then, the SD-CI wavefunction is calculated in the determinantal space of *all* single and double excitations from the occupied to the virtual SCF orbitals. Finally, the natural orbitals of this wavefunction are found. If the FORS wavefunction is to be based on M molecular orbitals, then the M natural orbitals with the highest occupation numbers are being chosen as first approximations to FORS configuration space generators. The MCSCF improvement of these M orbitals will be performed at the very end, after completion of the configurational truncation procedure.

Next, the M identified SD-CI natural orbitals are separated into two groups, the strongly and the weakly occupied NOs. In the systems considered here, this distinction was straightforward since all occupation numbers were either larger than 1.90 or smaller than 0.1. One could therefore have chosen the occupied SCF orbitals as the strongly occupied FORS MOs and determined “virtual natural orbitals” by diagonalizing only that sub-block of the SD-CI first-order density matrix that is spanned by the virtual SCF orbitals. Then, the $(M - M_{\text{SCF}})$ virtual NOs with the highest occupation numbers would be the weakly occupied FORS MOs. We found however that, even in these systems, the NOs from the full SD-CI density matrix yielded somewhat better configurational convergence properties.

Split-Localized FORS Molecular Orbitals

There exists a widespread presumption that configurations generated from natural orbitals will yield the most rapid configurational convergence. For the

configuration spaces considered here, certain types of localized orbitals are however found to be considerably more effective in this respect. They are those obtained by *localizing the strongly and the weakly occupied FORS orbitals separately without mixing the two kinds of orbitals*. We shall call them *split-localized* FORS molecular orbitals. While the strongly occupied ones (SOLMOs) are typically extremely similar to the standard localized SCF orbitals, each of the weakly occupied ones (WOLMOs) is located in the same region as one of the SOLMOs but with one nodal surface cutting through the center of the latter. They correspond to what Frank Boys used to call “main oscillatory orbitals” (48). For a bonding SOLMO the corresponding WOLMO is the anti-bonding orbital; for a lone-pair SOLMO the WOLMO is simply the lowest correlating orbital. The latter occur only for N-electrons-in-N-orbitals wavefunctions.

For such localizations to be effective in the present context, those orbital symmetry constraints that would prevent maximal localization in larger molecules must be abandoned. For instance, in the NCCN molecule, C_{2v} symmetry can be preserved during the localization process, but not left-right mirror symmetry. We have used Raffanetti’s (53) version of the Edmiston-Ruedenberg localization method (54).

Figure 1 illustrates for four molecular wavefunctions that split-localized MOs generate CI expansions whose configurational convergence is markedly faster than that of the CI expansions generated by natural orbitals. Plotted are the truncation errors due to CI truncations versus the number of determinants in the truncated CI expansions.

2.3. Truncation of a known CI expansion

Ordering of Configurations

The first step in our truncation procedure is the *ordering* of the determinants according to the importance of their contribution to the CI expansion. The second step will be the *deletion* of all determinants after a certain truncation determinant. As mentioned above, a CI wavefunction can be arranged in terms of increasing levels of excitation relative to the reference determinant $|\Phi_0\rangle$.

$$|\Psi\rangle = c_0 |\Phi_0\rangle + \sum_{i,a} c_i^a |\Phi_i^a\rangle + \sum_{i_1,ab} c_{i_1}^{ab} |\Phi_{i_1}^{ab}\rangle + \sum_{i_1,abc} c_{i_1}^{abc} |\Phi_{i_1}^{abc}\rangle + \dots \quad (2.1)$$

where, e.g., $|\Phi_i^a\rangle$ represents the determinant formed by replacing the SCF spin-orbital ϕ_i by the virtual spin-orbital ϕ_a . A configurational selection based on the magnitudes of the c-coefficients, with appropriate complementation to generate eigenvalues of S^2 , typically yields an effective ordering according to energy contributions.

O : Natural Orbitals

● : Split-Localized MO's

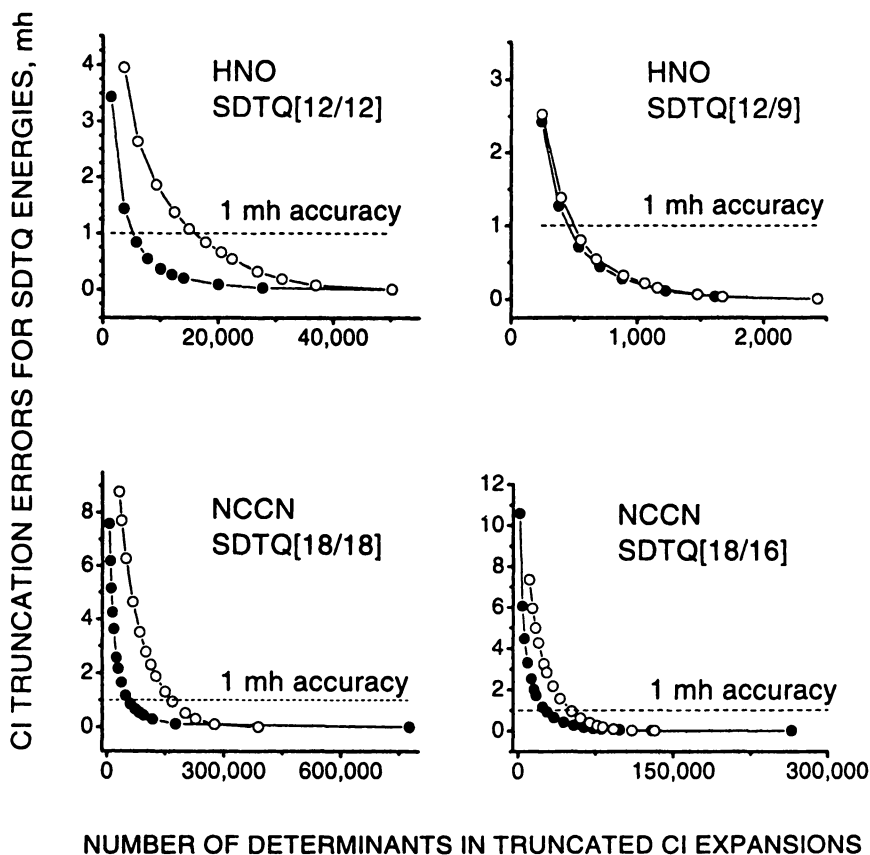


Figure 1. Rate of convergence of SDTQ-CI truncated expansions for FORS 1 and FORS2 active spaces for HNO and NCCN molecules: (a) Open-circles correspond to CI configurations generated from SD-CI natural orbitals; (b) Filled-circles correspond to CI configurations generated from the corresponding split-localized MO's.

Alternatively, one can focus on the spatial part of the molecular orbitals and introduce the *weight of a product of space orbitals*, given that all of its spin-couplings are included in the expansion. Thus, for a given space product one can define its *space-product-weight* as

$$C_{SP}^2 = \sum_K^{N_{SP}} c_K^2, \quad (2.2)$$

where the sum runs over all N_{SP} distinct determinants differing from each other only by spin-couplings. The truncation can then be based on this ordering of the space functions and such truncated CI-expansions will automatically be eigenfunctions of S^2 . The compactness of the truncated expansion can be enhanced by dividing the weight of Eq. (2.2) by the total number of determinants corresponding to the given space-product, viz

$$\bar{C}_{SP}^2 = \sum_K^{N_{SP}} c_K^2 / N_{SP}. \quad (2.3)$$

which we shall call the “importance” of the space product. We have found the ordering of the space products according to the magnitudes of the \bar{C}_{SP}^2 to yield a slightly faster convergence of the truncated CI expansions than the ordering based on the magnitude of the largest determinantal coefficient corresponding to each selected SP.

An important result, found for the SDTQ[N/N] wavefunctions of all molecules considered, is that the split-localized molecular orbitals yield a considerably faster convergence for truncated expansions than the natural orbitals. For example, for NCCN SDTQ[18/18], millihartree accuracy is achieved by about 50,000 determinants of the ordering based on split-localized orbitals whereas about 150,000 determinants are needed for the natural-orbital-based ordering. This observation calls for the revision of a widely held bias in favor of natural orbitals.

Truncation Criterion

In order to usefully deal with truncations, a simple criterion is needed for assessing the energy error introduced by a truncation. In this context the concept of the normalization deficiency has proven to be effective. This quantity is defined as the difference between the sum of squares of the coefficients of the N_{TOT} determinants in the untruncated wavefunction expansion and the corresponding sum that includes only the N_{TR} determinants selected by the truncation:

$$\Delta c^2(N_{TR}) = \sum_k^{N_{TOT}} c_k^2 - \sum_j^{N_{TR}} c_j^2. \quad (2.4)$$

If *all* determinants of the given wavefunction are considered then the first term in equation (2.4) is of course unity. If one considers however only determinants corresponding to a given (say, quadruple) substitution level taken from a SDTQ-CI wavefunction, that will not be so. In such a case *the relative normalization deficiency (RND)* is convenient:

$$RND(N_{TR}) = \Delta c^2(N_{TR}) / \sum_k^{N_{TOT}} c_k^2, \quad (2.5)$$

The normalization deficiency turns out to be useful for the extrapolation of truncated energies because it is found to be near-proportional to the energy error introduced by the truncations considered here.

2.4. Truncation based on a priori configuration selection

Usually, SD-CI wavefunctions recover about 90-95% of the correlation energy, inclusion of triply and quadruply substituted configurations is adequate for many purposes, and inclusion of quintuply and sextuply excited configurations is sufficient for describing most chemical reactions. Since the explosion of the number of configurations typically starts with the quadruple excitations, our first priority is the predictive deletion of deadwood from this group.

Let us therefore assume that a preliminary full SDT[N/M]-CI calculation is made. We then examine the triply excited configurations, order them by space products according to the magnitudes of the \bar{C}_{sp}^2 given by equation (2.3), and truncate them such that the resulting energy error is not larger than ~ 0.1 mh. Next, the a-priori truncation of the quadruply excited configurations is accomplished using again the tools described in the preceding section, *except that the unknown exact CI coefficients are replaced by estimated CI coefficients*. In the spirit of coupled-cluster theory, these estimates are obtained by approximating the coefficients of the quadruply excited terms by products of coefficients of doubly excited terms in the prior SDT calculation. Specifically, we have found that the weights as defined by Eq. (2.2) for the quadruply substituted space products can be effectively estimated by the following simple expressions

$$(C(Q_{EST}))^2 = (C_{abcd}^{ijkl})^2 = \sum_{ALL-COMBINATIONS}^M (C_{ab}^{ij})^2 \cdot (C_{cd}^{kl})^2 \quad (2.6)$$

where the sum goes over all M products of double orbital excitations that will result in the same quadruple orbital excitation and the quantities in brackets on the RHS are obtained by application of Eq. (2.3) to the doubly excited space products in the prior SDT wavefunction.

The first step is to estimate the *importance*, in the sense of Eq. (2.3), of each quadruply excited space product in the quadruples sum of Eq. (2.1). In accordance with Eq. (2.6), we estimate it as

$$\left(\bar{C}_{abcd}^{ijkl}\right)^2 = \frac{1}{M} \sum_{ALL-COMBINATIONS}^M \left(\bar{C}_{ab}^{ij}\right)^2 \cdot \left(\bar{C}_{cd}^{kl}\right)^2, \quad (2.7)$$

and order the quadruply substituted orbital products in accordance with these importance measures.

Next, SDTQ-CI calculations are performed for a few truncated quadruple expansions with quadruple truncation degrees in the expected range (around 10% of all quadruple space products). Furthermore, using our estimation formula (2.6), the quadruple normalization deficiencies of these wavefunctions relative to the full SDTQ wavefunction are readily estimated as

$$\Delta c^2(N_{TR})_{EST} = \sum_k^{N_{TR}} C(Q_{EST})_k^2 \sum_j^{N_{TR}} C(Q_{EST})_j^2, \quad (2.8)$$

Considering now the calculated energies of the truncated expansions as functions of the estimated normalization deficiencies, one finds that, in all cases, the energies approach the full-SDTQ value for the limit $\Delta c^2(N_{TR}) \rightarrow 0$ from above along a linear or weakly quadratic curve. By means of an extrapolation of this curve one can then determine the degree of truncation necessary for the error not to exceed the desired threshold, say 1 mh, without having to calculate a CI wavefunctions larger than the truncated one.

The effectiveness of the method is exhibited by Figure 2 in which the energy errors of truncated expansions are plotted versus the numbers of determinants in these expansions. For each of the four systems shown, one curve displays this relationship for the expansions generated by the just discussed *a priori* truncations, whereas the other curve is obtained *a posteriori* by starting with the full SDTQ calculation in the same orbital basis and, then, simply truncating the determinantal expansion based on the ordering established by the exact coefficients of the determinants. There is practically no difference in the number of determinants needed to achieve an accuracy of 1 mh.

Since the triply and quadruply excited configurations are truncated separately, it is usually possible to shorten the CI expansion somewhat further, if this should be desirable, by applying the procedure described in Section 2.3 to the total calculated truncated SDTQ-CI wavefunction obtained as described in this section. Thus, for the SDTQ[18/18] wavefunction of NCCN, an accuracy of 1 mh is achieved with 49,033 determinants by the estimation method, and with 43,038 determinants by the just mentioned additional improvement, reducing the truncation from 6.32% to 5.54% of the 776,316 determinants of the full SDTQ-CI expansion.

O: a posteriori ordering ●: a priori ordering

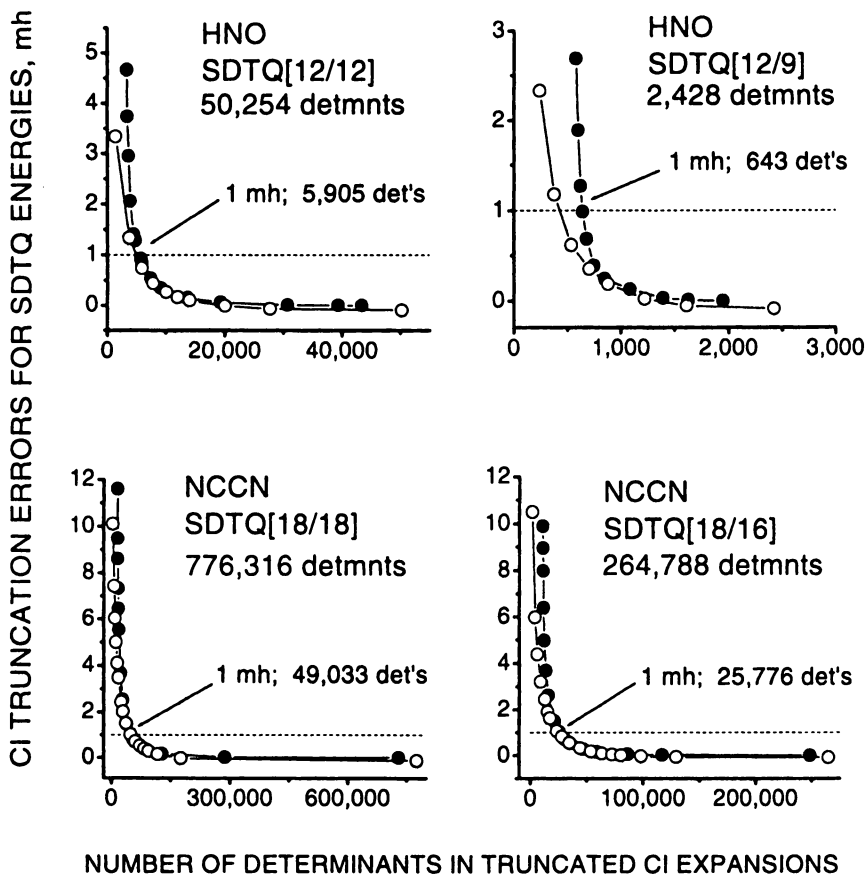


Figure 2. Rate of convergence of truncated SDTQ-CI expansions based on a priori and a posteriori ordering and error assessment. Filled circles: Truncations based on anticipated a priori estimates. Open circles: Truncations determined a posteriori from the full wavefunctions.

2.5. Orbital optimization of the truncated SDTQ-CI expansions

The final step is the orbital optimization for the truncated SDTQ-CI expansion. We used the Jacobi-rotation-based MCSCF method of Ivanic and Ruedenberg (55) for that purpose. Table 1 contains the results for the FORS 1 and FORS2 wavefunctions of HNO and NCCN, obtained using cc-pVTZ basis sets (51). In all cases, the configurations were based on split-localized orbitals. For each case, four energies are listed corresponding to (i) whether the full or the truncated SDTQ-CI expansion was used and (ii) whether the split-localized orbitals were those deduced from the SD naturals orbitals or were eventually MCSCF optimized. It is seen that

- (i) The energy gain by orbital optimization is the same for the full and the truncated expansions.
- (ii) Orbital optimization leads to a slight decrease in the truncation error.
- (iii) Less than 10% of the full SDTQ-CI expansion is needed to achieve chemical accuracy except for HNO [12/9] where 25% are needed.

3. Dynamic Correlation Energy Estimate and Analysis Based on Localized Orbitals

We now turn to the problem of simplifying the recovery of the dynamic correlation energy. We consider the simplest situation, viz., where the zeroth-order wavefunction can be chosen as the SCF approximation. A challenging disparity exists between the energetic smallness of these refinements and the complexity and magnitude of the computational efforts required for their variational determination. In order to reduce this disproportion, various semiempirical approaches have been proposed (56-61), notably in particular the introduction of semiempirical elements into MP2 theory which has led to the successful Gn methods (62-64).

We have explored whether, on the basis of sound theoretical and physical reasoning, a semiempirical formula can be derived that would directly provide an accurate estimate of the dynamic correlation energy as a whole. Two known rigorous results are suggestive in this context: (i) The dynamic correlation energy can be expressed as the expectation value of a perturbing correlation operator (65-67) and (ii) the correlation energy is known to be expressible (10) as sum of contributions of occupied orbital pairs, viz.

$$E_c = \sum_{ij} \varepsilon_{ij}, \quad \text{where} \quad \varepsilon_{ij} = \sum_{ab} c_{ij}^{ab} \langle \Phi_0 | \hat{H} | \Phi_{ij}^{ab} \rangle \quad (3.1)$$

where Φ_0 is the SCF determinant and the c_{ij}^{ab} are the CI coefficients of the double excitations Φ_{ij}^{ab} in the actual wavefunctions as in Eq. (2.1).

Table 1. Energies of full and truncated SDTQ-CI FORS-1 and FORS-2 calculations with and without MCSCF orbital optimization for the molecules HNO and NCCN (values in Hartrees unless noted otherwise).

Molecule/Model	No of Dets	SD-NO Based on	MCSCF Optimized	Energy lowering Due to MCSCF (mh)
<u>FORS-1: SDTQ[N/N_y]</u>				
<u>HNO [12/9]</u>				
SDTQ-FULL	2,428	-129.96819	-129.97152	3.33
SDTQ-TRUNC.	643	-129.967711	-129.97105	3.94
Trunc. Error (mh):		+1.08	+0.47	
<u>NCCN [18/16]</u>				
SDTQ-FULL	264,788	-184.92838	-184.93753	9.15
SDTQ-TRUNC.	25,776	-184.92725	-184.93663	9.38
Trunc. Error (mh):		+1.13	+0.93	
<u>FORS2: SDTQ[N/N]</u>				
<u>HNO [12/12]</u>				
SDTQ-FULL	50,254	-130.04370	-130.04855	4.85
SDTQ-TRUNC.	5,905	-130.04276	-130.04774	4.98
Trunc. Error (mh):		+0.94	+0.81	
<u>NCCN [18/18]</u>				
SDTQ-FULL	776,316	-184.96822	-184.97746	9.24
SDTQ-TRUNC.	49,033	-184.96709	-184.97650	9.41
Trunc. Error (mh):		+1.13	+0.94	

By postulating the correlation operator to be a sum of two-electron operators and assuming the occupied orbitals to be localized, we were able to show that the correlation energy can in fact be approximately expressed in terms of the bilinear expression

$$E_c = \sum_i P_{ii} E_{ii} + \sum_{i < k} 2 P_{ij} E_{ij}, \quad (3.2)$$

where the P_{ij} are *electron pair populations* and the E_{ij} are *correlation contributions per electron pair* for the localized orbitals ϕ_i and orbital pairs ϕ_i, ϕ_j respectively. For SCF wavefunctions, one has $P_{ii} = 1$ and $P_{ij} = 0$ when $i \neq j$.

We have then found that the values of the intra- and inter-orbital energy contributions can be empirically determined in such a way that, for about 50 molecules with E_C ranging from 26 to about 650 kcal/mol, the total *ab-initio* valence correlation energies are reproduced within near-chemical accuracy of the theoretically calculated values. For one set of molecules, the *ab-initio* values had been obtained by valence CCSD(T) calculations in a cc-pVTZ basis (57); for another set, they were obtained by extrapolation to the complete basis (68).

In fact, this close fit could be achieved with the following additional simplifying assumptions: The intra-orbital correlation energy contributions are the same for all lone pairs on all atoms and so are those for all bond orbitals. The inter-orbital pairs are divided in the following five categories:

- Type LL: Both localized MOs are lone-pair orbitals on the same atom.
 Type LB: One localized MO is a lone-pair orbital, the other is a bond orbital going from the same atom to some other atom.
 Type BB1: Both localized orbitals are bond orbitals originating from the same atom but bonding this atom to two different atoms.
 Type BB2: Both localized orbitals are bonding orbitals between the same two atoms, i.e. they correspond to two different bonds in a multiple bond.
 Type VV: Any two localized MOs that are separated by only one other localized MO ("vicinal" localized MOs).

For all orbital pairs within one group, regardless of the molecule and the atom, the interorbital energy contributions are then taken to have the same value. Thereby Eq. (3.2) further simplifies to

$$E_C = E_L N_L + E_B N_B + 4E_{LL} N_{LL} + 4E_{LB} N_{LB} + 4E_{BB1} N_{BB1} + 4E_{BB2} N_{BB2} + 4E_{VV} N_{VV} \quad (3.3)$$

where N_L , N_B , N_{LL} , N_{LB} , . . . denote the *number* of orbitals or orbital pairs of the various types in the molecule under consideration.

The seven group correlation contributions E_L , E_B , E_{LL} , E_{LB} , . . . were then determined by a least-mean-squares fit of E_C to the *ab initio* valence correlation energies of the afore-mentioned sets of molecules. They were found to have the following values (38):

Energies in mh	E_L	E_B	E_{LL}	E_{LB}	E_{BB2}	E_{BB1}	E_{VV}
cc-pVTZ set of 48 mol's	29.5	35.05	6.39	6.67	6.32	3.49	0.04
CBS-limit set of 18 mol's	33.0	41.68	8.49	6.75	6.12	3.10	0.09

It may be noted that, due to the pair-population factor 4 between doubly occupied orbitals, the total correlation contribution from a pair of neighboring orbitals is about of the same order of magnitude as the intra-orbital correlation contributions. On the other hand, the smallness of the vicinal contributions (*in spite of typically having a large weight N_{vv} in the LMSQ fitting!*) justifies the neglect of contributions from orbital pairs that are separated by two or more other localized orbitals. The exhibited distance dependence of the listed orbital interactions is consistent with the findings of other researchers for conceptually related quantities (16,69,70). Even the numerical values of the individual energy contributions are in rough agreement with the values found by the quite different *ab-initio* assessment of such interactions by Stoll (70).

The operation of Eq. (3.3) is illustrated by the results given in Table 2 out of 48 molecules of the cc-pVTZ set. They are listed in order of increasing correlation energy. The first column of the table lists the molecule. The next 6 columns show how many orbitals and orbital pairs of the various types are in each molecule, i.e. the numbers N_L , N_B , N_{LL} , N_{LB} . . . etc. The seventh column lists the CCSD(T)/triple-zeta correlation energy and the eight column lists the difference between the latter and the prediction by Eq. (3.3). The mean absolute deviation over the entire set of cc-pVTZ data set is 3.14 kcal/mol. For the 18 molecules of the CBS-limit data set it is found to be 1.57 kcal/mol. The maximum absolute deviations for the two data sets are 11.29 kcal/mol and 4.64 kcal/mol, respectively. Since the errors do not increase with the size of the molecule, the errors in the estimates of the individual contributions must fluctuate randomly within any one molecule, i. e. there does not seem to exist a systematic error. The *relative* accuracy of the predictions increases thus with the size of the system. It should be kept in mind that CCSD(T) results can in fact deviate from full CI results by amounts comparable to the mean absolute deviation associated with Eq. (3.3).

As a further test, we have also used the CBS-limit formula (3.3) to predict the correlation energy of diamond (per carbon atom). We found the value of 164 mh while the "experimental value" is quoted as 174 mh (38). The only other previous predictions based on more elaborate theories have yielded the values 161 mh (70), 162 mh (71) and 150 mh (72).

Eq. (3.3) represents the correlation energy with respect to the SCF determinant, and if non-dynamic correlation were negligible all the total correlation energy would be dynamic and could be so calculated. In reality various systems possess however different amounts of non-dynamic correlation energy. This fact could be a source of error in the fittings that produced the numerical values in Eq. (3.3). Another source of error could be the differences in molecular environment for various types of atoms. Thus, better results might be achieved if the non-dynamic part of correlation energy is determined by an MCSCF calculation, and the remaining dynamic correlation energy is estimated

Table 2. Numbers of orbitals and orbital-pairs and comparison of valence correlation energies (mh) estimated by Eq. (3.3) with CCSD(T) values from reference (57) for selected systems.

System	Number of orbitals and orbital pairs respectively						Correlation energy	
	L	B	LL	BL	BB2	BB1	CCSD(T)	Error ^{a)}
H ₂	0	1	0	0	0	0	39.4	5.2
CH ₄	0	4	0	0	0	6	224.6	0.9
NH ₃	1	3	0	3	0	3	255.3	-1.0
HOH	2	2	1	4	0	1	275.5	0.4
FH	3	1	3	3	0	0	280.3	0.1
HC≡CH	0	5	0	0	3	6	338.2	3.4
H ₂ C=CH ₂	0	6	0	0	1	10	375.5	-0.3
N≡N	2	3	0	6	3	0	390.4	-9.6
H ₂ C=NH	1	5	0	3	1	7	404.0	-4.4
H ₃ C-CH ₃	0	7	0	0	0	12	416.3	2.5
H ₂ C=O	2	4	1	4	1	5	422.9	-4.4
H ₃ C-NH ₂	1	6	0	3	0	9	443.6	-2.8
H ₃ C-OH	2	5	1	4	0	7	461.7	-3.5
H-N=O	3	3	1	7	1	2	462.7	2.8
H ₃ C-F	3	4	3	3	0	6	463.8	-6.5
H ₂ N-NH ₂	2	5	0	6	0	6	473.5	-5.5

H ₂ C=C=CH ₂	0	8	0	0	2	14	528.4	0.4
(C ₃ H ₄) _{cyc}	0	8	0	0	1	16	533.4	1.1
(C ₃ H ₆) _{cyc}	0	9	0	0	0	18	569.5	-0.7
H ₂ C=C=O	2	6	1	4	2	9	573.9	-5.6
F-C≡CH	3	5	3	3	3	6	581.7	0.3
(C ₂ NH ₅) _{cyc}	1	8	0	3	0	15	599.1	-3.7
(N ₂ CH ₂) _{cyc}	2	6	0	6	1	10	600.4	2.9
H ₃ C-CH ₂ -CH ₃	0	10	0	0	0	18	606.3	2.5
F-C≡N	4	4	3	6	3	3	612.2	-1.8
O=C=O	4	4	2	8	2	4	619.8	-11.1
HC≡C-C≡CH	0	9	0	0	6	12	643.9	7.9
H ₂ C=C=C=CH ₂	0	10	0	0	3	18	684.1	3.9
N≡C-C≡N	2	7	0	6	6	6	704.5	3.3
(C ₄ H ₆) _{cyc}	0	11	0	0	1	22	724.6	2.2
F-NH-F	7	3	6	9	0	3	751.9	2.4
(C ₄ NH ₅) _{cyc}	1	12	0	3	2	23	909.2	2.0
(C ₄ OH ₄) _{cyc}	2	11	1	4	2	21	928.4	2.4
(N ₂ C ₂ OH ₂) _{cyc}	4	9	1	10	2	15	989.3	-1.9
(C ₆ H ₆) _{cyc}	0	15	0	0	3	30	1024.9	-1.9

^{a)} Error = E_{corr}[CCSD(T)] - E_{corr}[model].

by an expression analogous to Eq. (3.2). Indeed, it has been recently reported (73) that additivity rules for nondynamic and dynamic correlation energy can be successfully used in planar chain heteroatomic polyenes.

The set of molecules for which the relationship of Eq. (3.3) has been tested with the reported accuracy, has certain simplifying features in common: They all have standard bonding coordinations around each atom and the shortfall of the SCF energy is entirely due to dynamic correlations. Modifications are to be expected for systems where these premises are not satisfied. Even with these limitations, however, the molecules in Table 2 represent a variety of atom and bond combinations. It is therefore remarkable that, for all of them, the correlation energy can be recovered by a simple system-independent formula that allows for a physically meaningful interpretation.

Theoretical derivations and detailed discussions of further aspects of this approach are given elsewhere (38).

4. Conclusions

A two-pronged approach has been discussed for dealing with electron correlation in large systems: (i) An extension of zeroth-order full-valence type MCSCF calculations to larger systems by radical *a priori* truncations of SDTQ-CI expansions based on split-localized orbitals in the valence space and (ii) the recovery of the remaining dynamic correlation by means of a theoretically-based simple semi-empirical formula.

The truncation procedure for full-valence-space and N-electrons-in-N-orbitals SDTQ MCSCF wavefunctions is based on choosing "split-localized" molecular orbitals as configuration generators since they lead to the greatest number of "deadwood configurations" that can be deleted. A quite accurate estimation method of identifying the latter has been developed so that the truncation can be performed *a priori*. The method has been shown to be effective in applications to the molecules HNO, OCO and NCCN where, for instance, the energies of the full SDTQ[N/N] calculations are recovered to better than 1 mh by truncated expansions that require only 11.8%, 10.9% and 6.3%, respectively, of the number of determinants in the full calculations. Similar trends are observed for the FORS 1 model.

A close estimate of the dynamic correlation energy was obtained by a simple formula in terms of pair populations and correlation contributions within and between localized molecular orbitals. The orbital and orbital-pair correlation strengths rapidly decrease with the distance between the orbitals in a pair. For instance, the total valence correlation energy of diamond per carbon atom, estimated as 164 mh, is the result of 84 mh from intra-orbital contributions, 74.5 mh from inter-orbital "closest neighbors" contributions, and 6.1 mh from inter-orbital vicinal contributions. The rapid decay of the orbital correlation contributions with the distance between the localized orbitals explains the *near-*

linear scaling of the total correlation energy with the number of electrons, a feature that had been observed quite early (74,75).

The present approach will be generalized in two respects. On the one hand, the a priori truncation method will be extended to quintuply and sextuply excited configurations. On the other hand, the truncation method as well as the dynamic correlation estimate will be extended to systems where the number of strongly occupied orbitals exceeds the number of SCF orbitals, entailing zeroth-order wavefunctions that are dominated by several determinants. It will then be possible to combine the two approaches.

Acknowledgements

The authors wish to thank Dr. M.W. Schmidt for his help with the GAMESS program. The present work was supported by the Division of Chemical Sciences, Office of Basic Energy Sciences, U.S. Department of Energy under Contract No. W-7405-Eng-82 with Iowa State University through the Ames Laboratory.

References

1. Klopper, W.; Bak, K. L.; Jørgensen, P.; Olsen, J.; Helgaker, T.; *J. Phys. B: At. Mol. Opt. Phys.*, **1999**, *32*, R103.
2. Sherrill, C. D.; Schaefer III, H. F.; *The Configuration Interaction Method: Advances in Highly Correlated Approaches. Adv. Quant. Chem.*, **1999**, vol. 34, p. 143.
3. Pauling, L.; Wheland, G. W.; *J. Chem. Phys.*, **1933**, *1*, 362.
4. Klein, D. J.; Bytautas, L.; *J. Phys. Chem. A*, **1999**, *103*, 5196.
5. Ivanciuc, O.; Bytautas, L.; Klein, D. J.; *J. Chem. Phys.*, **2002**, *116*, 4735.
6. Kohn, W.; *Rev. Mod. Phys.*, **1999**, *71*, 1253.
7. Parr, R. G. and Yang, W.; *Density-Functional Theory of Atoms and Molecules*, Oxford University Press, **1989**.
8. D. Cremer; *Mol. Phys.*, **2001**, *99*, 1899.
9. Jones, R. O.; Gunnarsson O.; *Rev. Mod. Phys.*, **1989**, *61*, 689.
10. Szabo, A.; Ostlund, N. S.; *Modern Quantum Chemistry. Introduction to Advanced Electronic Structure Theory*, McGraw-Hill, Inc. **1989**.
11. Ayala, P. Y.; Kudin, K. N.; Scuseria, G. E., *J. Chem. Phys.*, **2001**, *115*, 9698.
12. Davidson, E. R.; *Configuration Interaction description of electron correlation, in The World of Quantum Chemistry*, ed. Daudel, R. and Pullman, B.; D. Reidel, Dordrecht; **1974**.
13. Shavitt, I.; *Mol. Phys.*, **1998**, *94*, 3.
14. Head-Gordon, M.; *J. Phys. Chem.*, **1996**, *100*, 13213.
15. Pulay, P.; *Chem. Phys. Lett.*, **1983**, *100*, 157.

16. Saebø, S.; Pulay, P.; *Annu. Rev. Phys. Chem.*, **1993**, *44*, 213.
16. Hampel, C.; Werner, H.-J.; *J. Chem. Phys.*, **1996**, *104*, 6286.
17. Schütz, M.; Hetzer, G.; Werner, H.-J.; *J. Chem. Phys.*, **1999**, *111*, 5691.
18. Reynolds, G.; Martinez, T. J.; Carter, E. A.; *J. Chem. Phys.*, **1996**, *105*, 6455.
19. Walter, D.; Carter, E. A.; *Chem. Phys. Lett.*, **2001**, *346*, 177.
20. Buenker, R. J.; Peyerimhoff, S.; *Theor. Chim. Acta*, **1968**, *12*, 183.
21. Buenker, R. J.; Peyerimhoff, S.; *Theor. Chim. Acta*, **1974**, *35*, 33.
22. Buenker, R. J.; Peyerimhoff, S.; *Theor. Chim. Acta*, **1975**, *39*, 217.
23. Friesner, R. A.; Murphy, R. B.; Beachy, M. D.; Ringnalda, M. N.; Pollard, W. T.; Dunietz, B. D.; Cao, Y.; *J. Phys. Chem. A*, **1999**, *103*, 1913.
24. Dunietz, B. D.; Friesner, R. A.; *J. Chem. Phys.*, **2001**, *115*, 11052.
25. Gershgorin, Z.; Shavitt, I.; *Int. J. Quant. Chem.*, **1968**, *2*, 751.
26. Huron, B.; Malrieu, J. P.; Rancurel, P.; *J. Chem. Phys.*, **1973**, *58*, 5745.
27. Cave, R. J.; Xantheas, S. S.; Feller, D.; *Theor. Chim. Acta*, **1992**, *83*, 31.
28. Harrison, R. J.; *J. Chem. Phys.*, **1991**, *94*, 5021.
29. Hanrath, M.; Engels, B.; *Chem. Phys.*, **1997**, *225*, 197.
30. Palmieri, P.; Tarroni, R.; Mitrushenkov, A. O.; Rettrup, S.; *J. Chem. Phys.*, **1998**, *109*, 7085.
31. Maynau, D.; Evangelisti, S.; Guihéry, N.; Calzado, C. J.; Malrieu, J. P.; *J. Chem. Phys.*, **2002**, *116*, 10060.
32. Davidson, E. R.; Silver, D. W.; *Chem. Phys. Lett.*, **1977**, *52*, 403.
33. Sherrill, C. D.; Schaefer III, H. F.; *J. Phys. Chem.*, **1996**, *100*, 6069.
34. Bytautas, L.; Ivanic, J.; Ruedenberg, K.; *J. Chem. Phys.*, (to be submitted).
35. Ivanic, J.; Ruedenberg, K.; *Theor. Chem. Acc.*, **2001**, *106*, 339.
36. Ivanic, J.; Ruedenberg, K.; *Theor. Chem. Acc.*, **2002**, *107*, 220.
37. Bytautas, L.; Ruedenberg, K.; *Mol. Phys.*, **2002**, *100*, 757.
38. Pulay, P.; Hamilton, T. P.; *J. Chem. Phys.*, **1988**, *88*, 4926.
39. Gordon, M. S.; Schmidt, M. W.; Chaban, G. M.; Glaesemann, K. R.; Stevens, W. J.; Gonzalez, C.; *Chem. Phys.*, **1999**, *110*, 4199.
40. Schmidt, M. W.; Gordon, M. S.; *Ann. Rev. Phys. Chem.*, **1998**, *49*, 233.
41. Roos, B. O.; *Adv. Chem. Phys.*, **1987**, *69*, 399.
42. Andersson, K.; Malmqvist, P.-A.; Roos, B. O.; *J. Chem. Phys.*; **1992**, *96*, 1218.
43. Ruedenberg, K.; Schmidt, M. W.; Gilbert, M. M.; Elbert, S. T.; *Chem. Phys.*, **1982**, *71*, 41.
44. Ruedenberg, K.; Schmidt, M. W.; Gilbert, M. M.; *Chem. Phys.*, **1982**, *71*, 51.
45. Ruedenberg, K.; Schmidt, M. W.; Gilbert, M. M.; Elbert, S. T.; *Chem. Phys.*, **1982**, *71*, 65.
46. Lam, B.; Schmidt, M. W.; Ruedenberg, K.; *J. Phys. Chem.*, **1985**, *89*, 2221.
47. Foster, J. M.; Boys, S. F.; *Rev. Mod. Phys.*, **1960**, *32*, 300.
48. Hurley, A. C.; Lennard-Jones, J.; Pople, J. A.; *Proc. R. Soc. London, Ser. A*, **1953**, *220*, 446.

49. Goddard, W. A.; Harding, L. B.; *Annu. Rev. Phys. Chem.*, **1978**, *29*, 363.
50. Dunning Jr., T. H.; *J. Chem. Phys.*, **1989**, *90*, 1007.
51. Schmidt, M. W.; Baldridge, K. K.; Boatz, J. A.; Elbert, S. T.; Gordon, M. S.; Jensen, J. H.; Koseki, S.; Matsunaga, N.; Nguyen, K. A.; Su, S. J.; Windus, T. L.; Montgomery, J. A.; *J. Comp. Chem.*, **1993**, *14*, 1347.
52. Raffanetti, R. C.; Ruedenberg, K.; Janssen, C. L.; Schaefer, H. F.; *Theor. Chim. Acta*, **1993**, *86*, 149.
53. Edmiston, C.; Ruedenberg, K.; *Rev. Mod. Phys.*, **1963**, *35*, 457.
54. Ivanic, J.; Ruedenberg, K.; *J. Comp. Chem.*, (accepted).
55. Cremer, D.; *J. Comp. Chem.*, **1982**, *3*, 165.
56. Rościszewski, K.; *Int. J. Quant. Chem.*, **1996**, *58*, 471.
57. Martin, J. M. L.; *J. Chem. Phys.*, **1992**, *97*, 5012.
58. Martin, J. M. L.; *J. Chem. Phys.*, **1994**, *100*, 8186.
59. Maksić, Z. B.; Barić, D.; Petanjek, I.; *J. Phys. Chem. A*, **2000**, *104*, 10873.
60. Maksić, Z. B.; Smith, D. M.; Barić, D.; *Chem. Phys.*, **2001**, *269*, 11.
61. Pople, J. A.; Head-Gordon, M.; Fox, D. J.; Raghavachari, K.; Curtiss, L. A.; *J. Chem. Phys.*, **1989**, *90*, 5622.
62. Curtiss, L.A.; Ragavachari, K.; Trucks, G.W.; Pople, J.A.; *J. Chem. Phys.*, **1991**, *94*, 7221.
63. Pople, J. A., *Rev. Mod. Phys.*, **1999**, *71*, 1267.
64. Essén, H., *Int. J. Quant. Chem.*, **1986**, *30*, 89.
65. Roos, B. O.; Szulkin, M.; Jaszuński, M.; *Theor. Chim. Acta*, **1987**, *71*, 375.
66. Savin, A.; Flad, H.-J.; *Int. J. Quant. Chem.*, **1995**, *56*, 327.
67. Feller, D.; Peterson, K. A.; *J. Chem. Phys.*, **1998**, *108*, 154.
68. Ayala, P. Y.; Scuseria, G. E.; *Chem. Phys. Lett.*, **2000**, *322*, 213.
69. Stoll, H.; *Phys. Rev. B*, **1992**, *46*, 6700.
70. Stollhoff, G.; Bohnen, K. P.; *Phys. Rev. B*, **1988**, *37*, 4678.
71. Fahy, S.; Wang, X. W.; Louie, S. G.; *Phys. Rev. B*, **1990**, *42*, 3503.
72. Smith D. M.; Barić D.; Maksić, Z. B.; *J. Chem. Phys.*, **2001**, *115*, 3474.
73. Clementi, E.; *J. Chem. Phys.*, **1963**, *38*, 2248.
74. Clementi, E.; *J. Chem. Phys.*, **1963**, *39*, 175.

Chapter 8

Correlation Consistent Basis Sets with Relativistic Effective Core Potentials: The Transition Metal Elements Y and Hg

Kirk A. Peterson

Department of Chemistry, Washington State University, Pullman,
Washington 99164-4630 and the Environmental Molecular Sciences
Laboratory, Pacific Northwest National Laboratory, Richland, WA 99352

Gaussian basis sets for the elements Y and Hg appropriate for valence electron correlation have been developed using a correlation consistent prescription with accurate relativistic effective core potentials. The resulting sequences of basis sets are denoted cc-pVnZ-PP (correlation consistent polarized relativistic valence $n\zeta$) and range in size from $n = D-5$. In each case systematic convergence towards the complete basis set limit is clearly observed for both the Hartree-Fock and correlation energies. In the case of Hg, all-electron basis sets are also reported both with and without the inclusion of scalar relativity via the Douglas-Kroll-Hess Hamiltonian. The accuracy of the resulting basis sets is demonstrated in benchmark calculations on YC, HgH⁺, and Hg₂. Predictions are made for r_e and D_e for YC and D_e for HgH⁺. In all three cases, the results appear to be the most accurate to date and agree very well with experiment.

Introduction

One of the major advances in the *ab initio* calculation of molecular electronic structure over the last 15 years has been the development of Gaussian basis sets that exhibit systematic convergence towards the apparent complete basis set (CBS) limit. Motivated in part by the atomic natural orbital basis sets of Almlöf and Taylor (1), Dunning introduced the idea of correlation consistent basis sets for the first row atoms (2). In this scheme a set of *spdfg...* correlation functions were included with a *sp* primitive Hartree-Fock (HF) set based on the criteria that each function should contribute nearly equal amounts of incremental correlation energy in configuration interaction (CI) calculations on the atoms. For the first row atoms this resulted, for example, in the smallest basis set including just one *d*-type polarization function, while the next set in the series included both 2 *d*-type functions as well as 1 *f*-type correlation function. In the latter case the 2nd *d*-type function and 1st *f*-type function each contributed very similar amounts of correlation energy to the total energy of the atom in CI calculations and about an order of magnitude less than the first *d*-type function. The resulting family of basis sets, denoted cc-pVnZ with $n = D, T, Q, 5$ (and sometimes 6), resulted in very regular convergence of the total energies of atoms and molecules towards their CBS limits. Numerous subsequent studies have investigated how best to exploit this regular convergence for the accurate calculation of thermochemistry and spectroscopic properties of molecules. Determination of the CBS limit also facilitates the estimation of the errors intrinsic to the correlation method chosen to describe the many electron wave function. Over the last several years, Dunning and co-workers have extended these basis sets to include the 2nd row atoms Al – Ar (3) and the 3rd row main group atoms Ga – Kr (4). Extensions of these sets for describing anions (5) and weakly bound systems (6), as well as the description of core electron correlation effects (7,8), have also been reported.

By their construction, the correlation consistent basis sets are all-electron sets, i.e., all of the electrons in each atom are explicitly described by basis functions. In many respects this is advantageous, but this approach can also lead to very large basis sets for heavier elements in order to adequately describe the low-lying core electrons. In addition, both scalar and spin-orbit relativistic effects must also be treated using all-electron methods, which can lead to relatively high computational costs. On the other hand, a nearly effortless way to accurately recover relativistic effects involves the use of relativistic effective core potentials (ECPs) or pseudopotentials (PPs). In addition to yielding accurate scalar and spin-orbit relativistic effects, the resulting basis sets can be much smaller due to the absence of the core electrons. While PPs are generally accompanied by their own basis sets, these are generally of only double- or triple-zeta quality and do not allow for a systematic expansion towards the CBS limit like the all-electron correlation consistent basis sets. Recently there have

been a few studies involving correlation consistent-like basis sets developed in conjunction with relativistic PPs. Bauschlicher (9) has developed sequences of basis sets for use with both large- and small-core PPs of the Stuttgart variety for the In atom and reported their use in thermochemical studies (10). More recently Martin and Sundemann (11) developed a series of basis sets with correlation consistent polarization functions for Ga – Kr and In – Xe that utilized large-core Stuttgart-Dresden-Bonn PPs (with some small-core studies also for In). Their SDB-cc-pVnZ ($n=T, Q$) basis sets were then used in several small molecule benchmark calculations. Lastly, Schwerdtfeger and co-workers (12,13) have reported a series of cc-like basis sets for Hg that use the same accurate small-core PP as in the present work. Their basis sets were derived from a single HF set and all exponents were optimized at the MP2 level of theory.

In the present work, correlation consistent basis sets have been developed for the transition metal atoms Y and Hg using small-core quasirelativistic PPs, i.e., the ns and $(n-1)d$ valence electrons as well as the outer-core $(n-1)sp$ electrons are explicitly included in the calculations. This can greatly reduce the errors due to the PP approximation, and in particular the pseudo-orbitals in the valence region retain some nodal structure. Series of basis sets from double-through quintuple-zeta have been developed and are denoted as cc-pVnZ-PP (correlation consistent polarized valence $n-\zeta$ with pseudopotentials). The methodology used in this work is described in Sec. II, while molecular benchmark calculations on YC, HgH^+ , and Hg_2 are given in Sec. III. Lastly, the results are summarized in Sec. IV.

Methodology

The development of correlation consistent basis sets can generally be divided into 3 - 4 steps:

- Optimization of a series of correlation functions for the total correlated energy of the atom using a large HF base set – this establishes the identity and quantity of angular momentum functions that will be included in each correlation consistent basis set.
- Optimization of a series of spd HF sets that systematically converge to the HF limit.
- Determination of how to best include correlating functions for angular momenta that correspond to occupied atomic orbitals, i.e., uncontract or add additional functions.
- Optimization of augmenting functions for the description of electron affinities, weak interactions, or core-valence correlation effects.

This procedure has recently been carried out by the present author for all of the post-*d* elements Ga – Rn using accurate small-core relativistic PPs (14,15). Only a few modifications to the above schema was required due to the presence of a PP (see below). On the other hand, as discussed previously by several authors (c.f., Refs. (16-18)), the development of accurate basis sets for transition metals must involve addressing a number of issues that do not generally exist for main group elements. In particular, most of the transition metal elements have several important low-lying electronic states that contribute to bonding in molecules containing these elements, namely configurations of the type $ns^2(n-1)d^{m-2}$, $ns(n-1)d^{m-1}$, and $(n-1)d^m$, where m is the number of valence electrons. Optimization of basis functions for just one of these configurations can introduce significant bias into the resulting exponents, especially since the ns orbital generally has a very different radial extent than the $(n-1)d$ orbitals. In addition, the valence p orbitals are generally unoccupied for the atoms, but can be important for bonding in molecular systems. Lastly, the spatial region of the semi-core $(n-1)sp$ shell is very similar to that of the $(n-1)d$ shell, which can lead to strong core-valence correlation effects. In the case of all-electron basis sets for the 1st row transition metals, Bauschlicher and Taylor (16), Bauschlicher (17), and Pou-Amerigo et al. (18) have carefully addressed these issues for correlated calculations within the framework of atomic natural orbital basis sets. Each of these studies was based on large spd Hartree-Fock basis sets optimized by Partridge (19) for the $4s^23d^{m-2}$ states of the atoms. Several diffuse p functions were then added in an even tempered fashion to describe the $4p$ orbital, as well as an additional diffuse d -type function. The latter of these was to primarily account for a possible bias in the original HF d set (optimized explicitly for the $4s^23d^{m-2}$ state) against the $4s3d^{m-1}$ configuration. Correlating functions of dfg symmetry were then added to these sets, and these were optimized for the average of up to three electronic states of the atoms. In the work of Pou-Amigo et al. (18), ionic states and calculations with small external electric fields applied to the neutral atoms were also used in the averaging procedure. More recently, these ideas have been extended by Bauschlicher (20) and Ricca and Bauschlicher (21) to basis sets for Ti and Fe, respectively, with correlation consistent-type polarization functions. Martin and Sundemann (11) have also reported sets of state-averaged ($2f1g$) functions to be added to existing small-core Stuttgart PP basis sets for all three rows of the transition metal elements. A different averaging scheme has been reported by Noro et al. (22) for the first row transition metals, whereby the exponents were optimized to produce natural orbitals that closely reproduced large basis set results in state averaged calculations of the $4s^23d^{m-2}$ and $4s3d^{m-1}$ states.

The present work represents a preliminary attempt to incorporate many of these strategies in conjunction with the use of small-core relativistic effective core potentials for obtaining compact series of correlation consistent basis sets

for the transition metals. All of the exponent optimizations in this work were carried out using a BFGS algorithm (23) using double-sided numerical derivatives. The actual exponent (ζ) optimizations were performed in the space of $\ln(\zeta)$ and the gradient of $\ln(\zeta)$ was generally converged to better than 1×10^{-6} . The MOLPRO program suite (24) was employed for all calculations and only the pure spherical harmonic components of the *dfg...* angular momentum functions were used. Unless otherwise noted, only the valence electrons (5s and 4d for Y and 6s and 5d for Hg) were correlated. The Hartree-Fock base sets used in preliminary optimizations were taken from *extended* even tempered (ExtET) expansions. These are defined by modifying the usual $\zeta_k = \alpha \beta^k$ even tempered formula (25,26) to $\zeta_k = \alpha \beta^{f(k)}$, where

$$f(k) = k \left(1 + \gamma \frac{k}{n} + \delta \left(\frac{k}{n} \right)^2 \right) \quad (1)$$

for $k=0, 1, \dots, n-1$ ($k=0$ corresponds to the most diffuse exponent and n is the expansion length). The ExtET form is similar to the usual well tempered expansion scheme and requires the optimization of four parameters ($\alpha, \beta, \gamma, \delta$). The functional form of Eq.(1) is based on a cubic polynomial fit to the spacings between $\ln(\zeta_k)$ within a given basis set of fully optimized exponents. By way of contrast, the usual even tempered formula is linear in this spacing. Particularly for fully-optimized, all-electron basis sets, this spacing is a slowly increasing function of k , and are well fit by the ExtET form with the parameters γ and δ having typical values of about -1.0 for γ and $+1.0$ for δ . In the present work, (14s13p11d) ExtET sets were used as base sets in the initial optimizations of correlation functions and fully-optimized HF *spd* primitive sets.

The optimization of basis functions in the presence of an ECP does present some new issues that are explicitly addressed in the present calculations. First, since the PP attempts to force the pseudo-orbital to zero in its inner regions, unconstrained exponent optimizations at the HF level can lead to near linear dependency in the basis sets, i.e., the ratio of two neighboring exponents can be as small as 1.3 or less. This commonly occurs in existing ECP basis sets. In the present work, the exponent optimizations are constrained so that the ratio of any two exponents in the same angular symmetry must be ≥ 1.6 . This has a negligible effect on the energy. In addition, as shown by both Bladeau and co-workers (27) and Christiansen (28), single uncontracted correlating functions in ECP-based calculations are much less effective than in all-electron calculations due to the interplay of the amplitudes and derivatives of these functions near the origin and the magnitude of the pseudo-orbitals in this region. The most

straightforward solution to this problem is to just include an extra correlating function in each symmetry. While as shown below only *s* functions are significantly affected, additional *s*, *p*, and *d* functions have also been added in the present work. Hence while a double-zeta basis set typically includes only a $1s1p1d$ correlation set, the new prescription would be to include at least a $2s2p2d$ set. Lastly, in order to minimize any large gaps between the exponents of the most diffuse functions, especially for the smaller basis sets, the maximum ratio between subsequent exponents among the four most diffuse exponents was constrained to approximately equal the ratio of the first two. This constraint was enforced for both the *s* and *p* exponents in Y and only the *s* exponents in Hg. In retrospect, these latter constraints were probably unnecessary and in any event had only a minimal effect on the final exponent distributions and especially the total HF energies.

cc-pRVnZ basis sets for Y

The present basis sets for Y were developed using the 28 electron ECP of Andrae et al. (29), which leaves 11 electrons in the valence shell. A total of 3 electronic states of the neutral atom were considered in the optimizations. Specifically these corresponded to the $4d\ 5s^2$ (a^2D), $4d^2\ 5s$ (a^4F), and $4d^3$ (b^4F) states. The Hartree-Fock calculations on these states involved separate state-averaging of all degenerate components so that the orbitals were fully symmetry equivalenced. Subsequent singles and doubles CI (CISD) calculations were then carried out with these orbitals on only a single component of each state.

In order to determine the correlation consistent groupings of *dfg*... correlating functions for the yttrium atom, CISD optimizations were carried out with a $(14s13p11d)$ ExtET base set contracted to $[6s5p1d]$. For these calculations even tempered expansions were used for the correlating functions. Figure 1 shows the incremental correlation energy recovered by the addition of correlating functions in 3-state energy averaged CISD calculations (3 electrons correlated). After including up to 5 even tempered *d*-type functions, *f* functions were added to a $[6s5p1d]+(4d)$ set, *g* functions were subsequently added to a $[6s5p1d]+(4d\ 3f)$ set, *h* functions were added to a $[6s5p1d]+(4d\ 3f2g)$ set, and finally an *i* function was added to the $[6s5p1d]+(4d\ 3f2g1h)$ set. The expected correlation consistent groupings are clearly apparent from this plot, namely (1f) for DZ, (2f1g) for TZ, (3f2g1h) for QZ, and (4f3g2h1i) for SZ. In addition, including multiple angular momentum functions of the same type is energetically more important than adding a single function of the next higher type. This is opposite to the trend generally observed for main group elements. The inset to Figure 1 shows the effects of adding correlating *s*, *p*, and *d* functions to $[2s5p1d]+(4d3f2g)$, $[6s1p1d]+(4d3f2g)$, and $[6s5p1d]$ base sets, respectively. The addition of *p*-type correlating functions are calculated to recover somewhat more correlation energy than even *d*-type functions. This inset also clearly shows the effect of the underlying ECP on the correlation energy recovered by the *s*-type functions, namely the 2nd *s* function yields

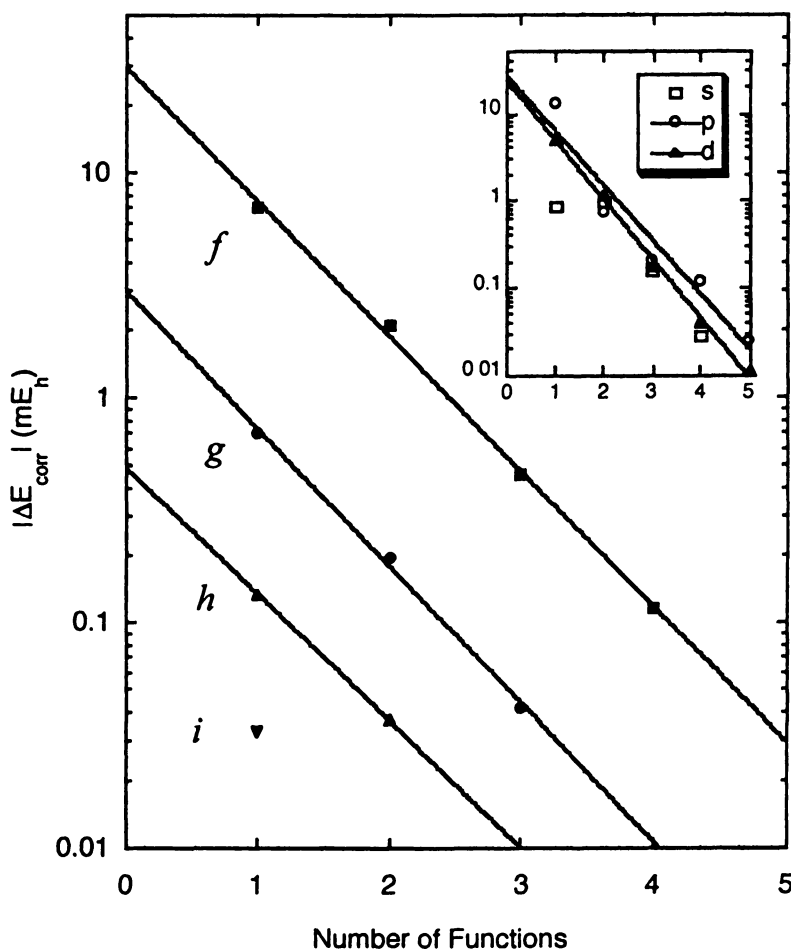


Figure 1. Contributions of correlating functions, as well as *s*, *p*, and *d* functions (inset), to the average CISD correlation energy of the $5s^2 4d^3$, $5s 4d^2$, and $4d^3$ states of yttrium. The absolute values of the incremental correlation energy lowerings, $|\Delta E_{\text{corr}}|$, are plotted in mE_h against the number of functions in the expansions for *spdfghi* functions. The solid lines are exponential fits.

essentially the same incremental correlation energy as the first. Thus the strategy of including two s -type correlating functions at the DZ level is well justified. Poor convergence of the p - and d -type functions is not observed, but in these preliminary sets two, of each are also included in the cc-pVDZ-PP basis set to remain consistent with the s correlating functions. It should also be noted at this point that when the correlating functions are optimized only for the $4d\ 5s^2$ state instead of a state-average as above, the resulting d exponents are more than 50% larger. Much smaller differences between the two approaches is observed for the higher angular momentum functions.

The next step in the development of a compact cc basis set series for Y is the optimization of spd HF sets. These optimizations were carried out for the $4d\ 5s^2$ state only, which is consistent with earlier treatments of the 1st row transition metals. The s , p , and d HF functions were optimized separately and for each series a $(14s13p11d)/[2s2p1d]$ ExtET set was used as a base set in the optimizations, i.e., $[2p1d]+ns$, $[2s1d]+np$, and $[2s2p]+nd$. Figure 2 displays the errors relative to the approximate HF limit for each series. For the ns series, the

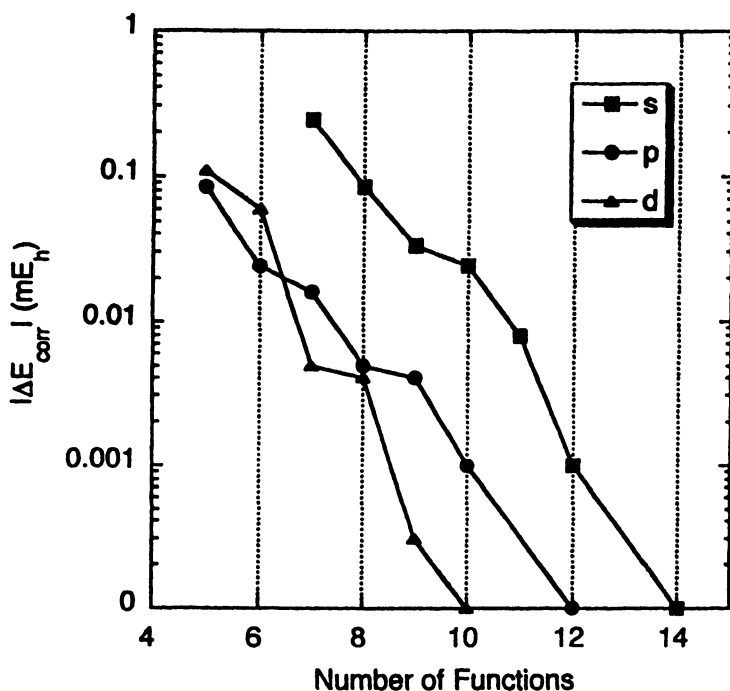


Figure 2. Hartree-Fock errors relative to a $(14s12p10d)$ base set plotted against the number of functions, m , in $(ms, 12p, 10d)$, $(14s, mp, 10d)$, and $(14s, 12p, md)$ expansions for the $5s^2\ 4d$ state of yttrium.

(7s)-(9s) sets have double- ζ exponent distributions for the 5s orbital, while larger sets have triple- ζ distributions. In the past, the decision of which *spd* HF set to use in a given cc-pVnZ basis set was based on the suitability of functions within these sets to uncontract and use for correlating functions. In principle this could also be carried out for the present cc-pVnZ-PP basis sets, but in the present work the *spd* sets were chosen primarily on their relative errors and convergence towards the HF limit. The cc-pVDZ-PP set should have a double- ζ distribution for the 5s orbital and hence the (7s) set was chosen. The (5p) and (5d) sets were then chosen for the DZ set since they had similar relative errors as shown in Figure 2. The (10s) set, which has a triple- ζ distribution for the 5s orbital and a relative error about an order of magnitude less than the (7s) set, was used in the cc-pVTZ-PP basis set and was matched with the (7p) and (7d) sets. The cc-pVQZ-PP basis set consisted of a (12s10p9d) set and the cc-pV5Z-PP used a (14s12p10d) set.

Two further modifications were used in the final versions of the cc-pVnZPP HF basis sets. First, two additional even tempered *p* functions were added to each set in order to accurately describe the unoccupied 5p orbital. Test optimizations were also carried out on the 2P state of Y and nearly identical exponents were obtained. Thus the final sets used just the even tempered exponents. Secondly, instead of adding an additional diffuse *d* function to better describe the $5s4d^2$ state as has been done in previous work, the HF *d* functions were re-optimized for a 3-state energy average. This had the effect of producing more diffuse exponents without introducing significantly larger HF errors for the $5s^24d$ state. In all cases [2s], [1p], and [1d] contraction coefficients were taken from calculations on the $5s^24d$ state, except that an additional [1p] contracted function was taken from a calculation on the $5s^25p$ state. Lastly, the *f* and *g* correlating functions were not restricted to even tempered sequences (although in the end the fully optimized exponents differed only marginally from their even tempered counterparts). The final cc-pVnZ-PP basis sets were constructed as follows:

cc-pVDZ-PP:	(7s7p5d)/[4s4p3d] + 1f
cc-pVTZ-PP:	(10s9p7d)/[6s6p4d] + 2f1g
cc-pVQZ-PP:	(12s12p9d)/[7s7p5d] + 3f2g1h
cc-pV5Z-PP:	(14s14p10d)/[8s8p6d] + 4f3g2h1i

Figure 3 shows both the HF and CISD correlation energy convergence relative to the basis set limits for the $5s^24d$, $5s4d^2$, and $4d^3$ states. The HF limit is very nearly reached at the cc-pVQZ-PP level, and the convergence of the correlation energy is also very rapid. The CBS limits for the correlation energies were obtained from the QZ and 5Z results via a 2-point n^{-3} extrapolation (30,31).

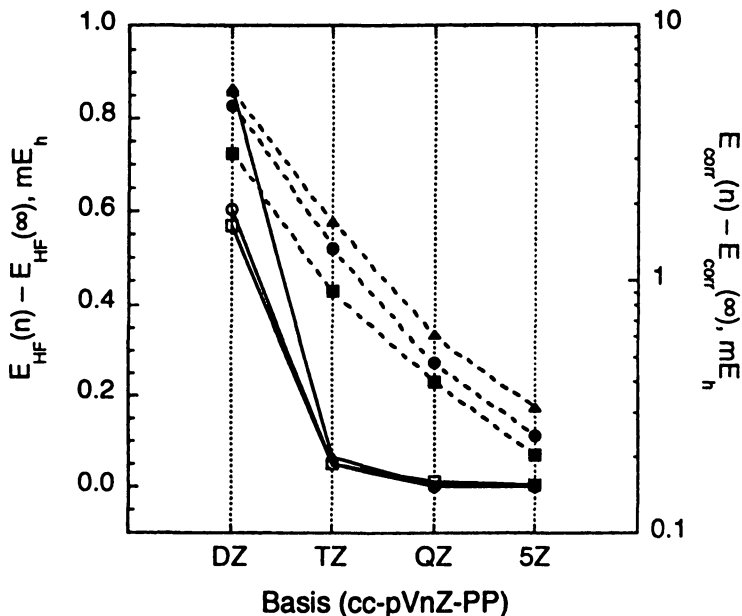


Figure 3. Basis set errors for the HF energy and CISD correlation energy with the final cc-pVnZ-PP basis sets for the (□, ■) 5s²4d, (○, ●) 5s4d², and (△, ▲) 4d³ states of yttrium. The open symbols correspond to the HF results (left axis), while the filled symbols refer to the CISD correlation energies (right axis).

Note that the correlation energy results are plotted on a log scale.

The basis sets described above are specifically designed for valence electron correlation only, i.e., the 5s and 4d electrons. As briefly mentioned above, the semi-core 4s and 4p orbitals of Y have radial extents that are expected to be very similar to the valence orbitals and hence strong core-valence correlation effects are expected. This requires a further augmentation of the cc-pVnZ-PP basis sets, and these additional functions were obtained using the weighted core-valence cc-pwCVnZ scheme as recently described for the 1st and 2nd row atoms (8). In the case of main group atoms, full shells of additional correlating functions were used, i.e., a set of [He] or [Ne] correlation consistent shells in the case of the 1st and 2nd row atoms, respectively. For the Y atom it was found that multiple functions of each angular momentum were relatively unimportant in recovering core-valence correlation energy. Hence the cc-pwCVTZ-PP basis set consisted of just the cc-pVTZ-PP set with additional 1s1p1d1f core-valence correlating functions. Note that this behavior may not be general for all of the transition metals and warrants further investigation.

All-electron basis sets for Y

In order to test the accuracy of the new ECP-based, cc-pVnZ-PP basis sets for Y, all-electron cc-pVQZ basis sets were also derived. These were based on the large (26s16p13d) HF set of Partridge, which were optimized for the $5s^2 4d$ (2D) state. This set was further augmented by 3 even tempered diffuse p functions, as well as one diffuse d function that was also obtained as an even tempered extension of the 13d set. The resulting (26s19p14d) basis was then contracted to [10s8p6d] using both nonrelativistic (NR) and DK-relativistic HF calculations. Even tempered sets of 3f2g1h correlating functions were optimized as in the cc-pVnZ-PP case for the energy average of 3 states using NR- and DK-CISD calculations. The resulting basis sets are denoted by cc-pVQZ-NR and cc-pVQZ-DK.

cc-pVnZ-PP basis sets for Hg

The cc-pVnZ-PP basis sets for Hg were developed using the 60 electron quasirelativistic ECP of Häussermann et al. (32). This PP has a $[Kr4d^{10}3f^{14}]$ core and leaves 20 electrons in the valence shell, the 8 electrons in the $5s5p$ orbitals and the 12 electrons in the $6s$ and $5d$ orbitals. The initial optimization of correlating functions was carried out for the $6s^2 5d^{10}$ ground state with the (12s10p9d) basis set of Häussermann et al. with the addition of 2 even tempered p functions. Figure 4 plots the incremental correlation energy contributions of each type of correlating function at the CISD level of theory. These quantities were obtained in a similar manner as in Y, i.e., up to 5 even tempered f functions were added to a [6s6p5d] base set, then up to 4 g functions were added to a [6s6p5d4f] set, etc. The series of d functions were added to a [6s6p1d4f3g] set, while [2s6p5d4f3g] and [6s2p5d4f3g] sets were used for the s and p series, respectively. The results are qualitatively similar to Y except that the magnitudes of the correlation energy contributions are much greater due to more electrons being correlated in Hg compared to Y. In the case of the $fghi$ correlating functions, the correlation consistent groupings are again easily observed in Figure 4, but in the case of Hg, addition of the first h function and the first i function is energetically more important than the 2nd g (and 3rd f) or 2nd h (and 3rd g and 4th f) functions, respectively. In the case of the spd functions, only the d -type correlating functions exhibit near exponential convergence towards the CBS limit. Further investigation of the somewhat erratic convergence for the p functions revealed that much better convergence was achieved by removing the restriction to even tempered expansions. The behavior of the 1st two correlating s functions is very similar to Y and can also be attributed to the presence of the ECP.

The optimization of HF primitive sets then proceeded much like the Y case, i.e., a (14s13p11d) ExtET base set was used in HF optimizations on the d^{10} state of Hg to generate s sets from (7s) – (14s), p sets from (4p – 12p), and d sets

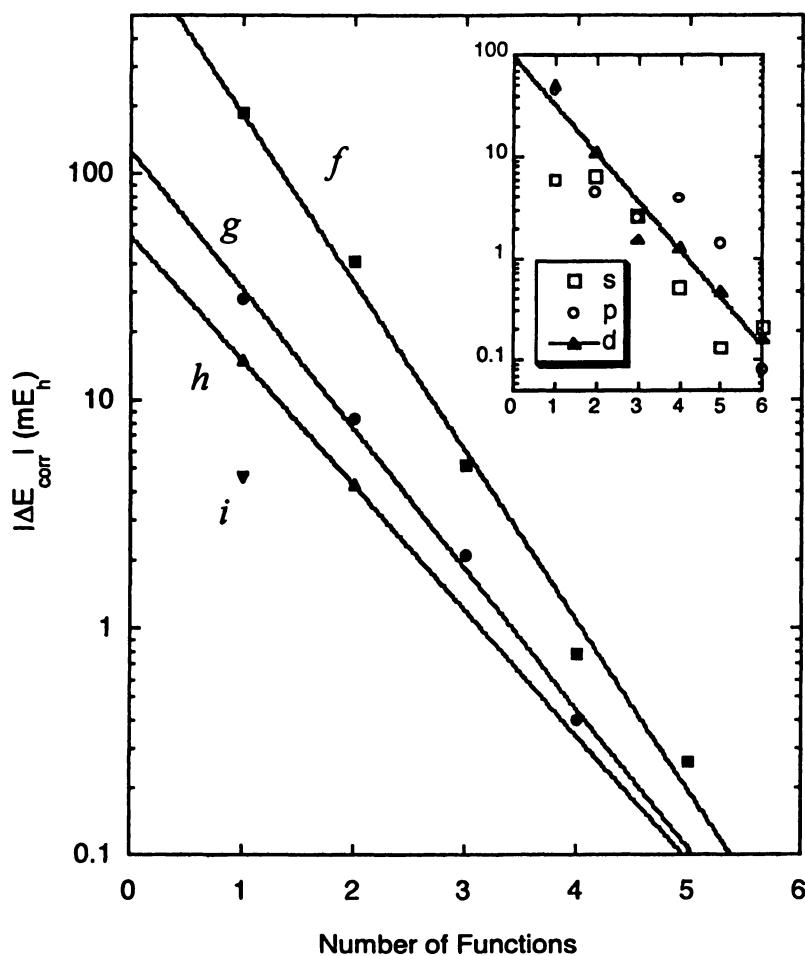


Figure 4. Contributions of correlating functions, as well as s, p, and d functions (inset), to the CISD correlation energy of the $5d^{10}$ state of mercury. The absolute values of the incremental correlation energy lowerings, $|\Delta E_{\text{corr}}|$ are plotted in mE_h against the number of functions in the expansions for spdf... functions. The solid lines are exponential fits.

from $(5d-11d)$. The errors for each of these sets relative to a $(14s12p11d)$ fully optimized set, which is expected to be within $0.01 mE_h$ of the Hartree-Fock limit, are shown in Figure 5. As with Y, the choice of which HF set to use in a given cc-pVnZ-PP basis set was determined mostly by the size of the HF error. The other consideration was whether the most diffuse exponents followed a smooth progression from one set to another. For Hg, a $(7s5p6d)$ set was chosen

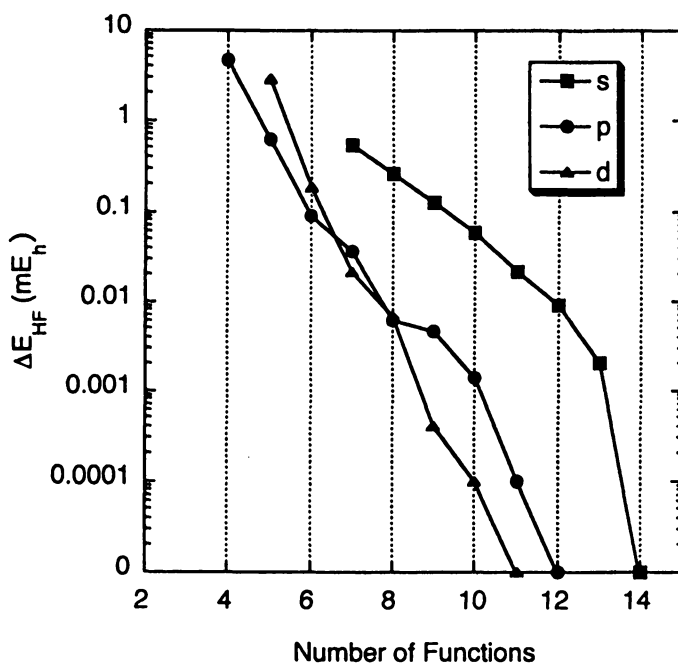


Figure 5. Hartree-Fock errors relative to a $(14s12p10d)$ base set plotted against the number of functions, m , in $(ms, 12p, 10d)$, $(14s, mp, 10d)$, and $(14s, 12p, md)$ expansions for the $5d^{10}$ state of mercury.

for the DZ basis set since these all have similar HF errors and the $(7s)$ set has a double- ζ description of the $6s$ orbital. For the TZ set, a $(10s7p7d)$ primitive set was chosen since the $(10s)$ set has a triple- ζ description of the $6s$ orbital and the $(7p)$ and $(7d)$ sets have comparable HF errors. For the QZ and 5Z basis sets, the $(12s10p9d)$ and $(14s12p11d)$ primitive sets, respectively, were decided to be good choices. These primitives were then augmented in each case by 2 diffuse p functions optimized for 3P state of Hg. The original p exponents were then

relaxed in HF optimizations for the 1S state in the presence of these two fixed exponents. The final cc-pVnZ-PP basis sets were then obtained by first generally contracting each HF set to $[2s2p1d]$, where the contraction coefficients for the 2nd contracted p function were taken from 3P calculations, then uncontracting spd correlating functions from the HF primitive set, and finally optimizing the appropriate correlation consistent groups of even tempered fg ... correlating functions (see Figure 4) in CISD calculations. Explicitly these consisted of:

cc-p VDZ-PP:	$(7s7p6d1f)/[4s4p3d1f]$
cc-p VTZ-PP:	$(10s9p7d2fg)/[6s6p5d2fg]$
cc-p VQZ-PP:	$(12s12p9d3f2g1h)/[7s7p6d3f2g1h]$
cc-pV5Z-PP:	$(14s14p11d4f3g2h1i)/[8s8p7d4f3g2h1i]$

Figure 6 displays the HF and CISD correlation energy errors with respect to their estimated CBS limits for both the 1S state and 3P states of Hg. Systematic convergence is observed for both states at the HF and CISD levels of theory. In addition, the errors for each basis set at the CISD level are essentially identical for both states.

Lastly, in order to accurately describe both the polarizability of Hg, as well as core-valence correlation effects arising from the $5s$ and $5p$ electrons, two augmentations of the cc-pVnZ-PP basis sets were developed. In the case of main group elements, additional diffuse functions are generally optimized for the atomic negative ions. This is not possible for Hg and hence aug-cc-pVnZ-PP basis sets were generated from the cc-pVnZ-PP ones by a simple even tempered extension of each angular momentum in the set. Calculations of the dipole polarizability of the Hg atom at the CCSD(T) level of theory with these augmented basis sets yield very good results: 34.77 (aug-cc-pVDZ-PP), 34.85 (aug-cc-pVTZ-PP), 34.82 (aug-cc-pVQZ-PP), 34.79 a.u. (aug-cc-pV5Z-PP) compared to the accurate static experimental value, 33.92 a.u. (33). The inclusion of $5s5p$ correlation with a aug-cc-pwCVTZ-PP basis set (see below) is predicted to decrease the CCSD(T) values by 0.65 a.u. Applying this to the valence-only aug-cc-pV5Z-PP result yields a best calculated value of 34.1 a.u., which is in excellent agreement with experiment.

In the case of core-valence correlation effects, correlating functions were optimized at the CISD level of theory using the weighted core-valence scheme (8). In this case a cc-pwCVTZ-PP set consisted of the cc-pVTZ-PP basis set with the addition of $2s2p2d1f$ core-valence correlating functions.

All-electron basis sets for Hg

In order to benchmark the ECP results for Hg, all-electron correlation consistent basis sets were also developed both with and without the inclusion of

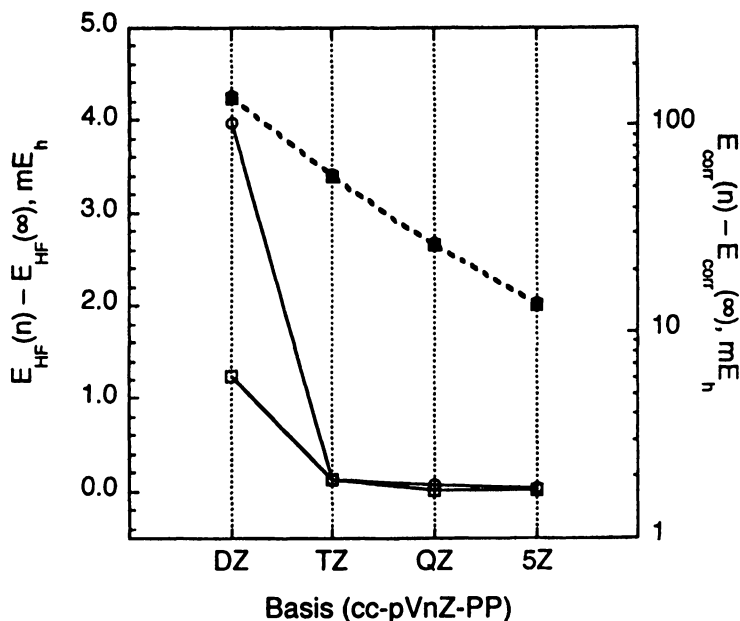


Figure 6. Basis set errors for the HF energy and CISD correlation energy with the final cc-pVnZ-PP basis sets for the (\square , \blacksquare) 1S and (\circ , \bullet) 3P states of mercury. The open symbols correspond to the HF results (left axis), while the filled symbols refer to the CISD correlation energies (right axis). Note that the correlation energy results are plotted on a log scale.

scalar relativistic effects. For these basis sets, however, only a single HF primitive set was optimized and this was used with the same number of correlating functions as in the cc-pVnZ-PP basis sets. To further reduce the computational cost for the primitive set optimizations, ExtET sets were used. For the nonrelativistic basis sets, a (29s21p19d13f) HF set was optimized, which was the same size as the previous well tempered basis set of Huzinaga and Klobukowski (HK) (34). This was sufficient to give a triple- ζ exponent distribution for the Hg 6s orbital with an estimated HF basis set error of less than $0.1 mE_h$. After adding 3 diffuse p functions obtained by an even tempered extension of this 21p set, the final HF energy for Hg (1S) was $-18408.991298 E_h$, which is lower than that of HK by $0.8 mE_h$. In an analogous manner, an ExtET HF set was also optimized for the Hg atom including scalar relativity by using the Douglas-Kroll-Hess (DK) Hamiltonian (35,36). In this case it was found necessary to increase the basis set to include (32s) and (23p) sets in order to obtain the same relative accuracy as the nonrelativistic case. The HF-DK total energy with this (32s26p19d13f) set (including the 3 diffuse p functions that

were also added in this case as above) was $-19604.012598 E_h$. The final basis sets, cc-pVnZ-NR and cc-pVnZ-DK for nonrelativistic and DK-relativistic, respectively, were obtained by adding correlating functions in the same groupings as in the cc-pVnZ-PP sets and were optimized in either nonrelativistic or DK-relativistic CISD calculations. In most cases, the *spd* correlating functions were just uncontracted from the HF sets, except that for the VDZ basis sets optimal CISD exponents were used due to the lack of appropriate functions in the HF set. The final contracted basis set sizes were (identical sizes for both NR and DK versions):

```
cc-pVDZ: [8s8p5d2f]
cc-pVTZ: [10s10p7d3f1g]
cc-pVQZ: [11s10p8d4f2g1h]
cc-pV5Z: [11s11p9d5f3g2h1i]
```

For both the DZ and TZ sets a contracted function was included for the 6*p* orbital, but this was deleted in the QZ and 5Z sets due to near linear dependence. The 6*s* contraction was also deleted from the 5Z set for the same reason. Figure 7 plots the correlation energies for both nonrelativistic and DK-relativistic CISD calculations. The CBS limits using a n^{-3} extrapolation of the QZ and 5Z correlation energies are -391.8 and -418.0 m E_h for NR and DK, respectively.

Diffuse augmented basis sets were also developed for both the NR and DK cases by simple even tempered extensions. Valence electrons correlated CCSD(T) dipole polarizabilities calculated with the inclusion of DK scalar relativity are 35.08 and 35.07 a.u. for aug-cc-pVQZ-DK and aug-cc-pV5Z-DK, respectively. These values are about 0.3 a.u. larger than the PP values and therefore somewhat further away from experiment.

Molecular Benchmarks

$X^4\Pi_{YC}$

The yttrium monocarbide molecule was only recently observed under high resolution by Simard et al. (37) using jet-cooled optical spectroscopy. The ground electronic state was determined to be an $\Omega=5/2$ state, which was consistent with the ab initio calculations of Shim et al. (38) who predicted a $^4\Pi$ ground state for YC in CASSCF calculations. The experimental work of Simard et al. yielded estimates for both the bond length and harmonic frequency of YC. In addition to their CASSCF calculations, Shim et al. (38) also reported results from mass spectrometric equilibrium experiments, which resulted in a bond dissociation energy of $D_0 = 99.0 \pm 3.3$ kcal/mol. The results from the present work are shown in Table I. An open-shell coupled cluster singles and doubles

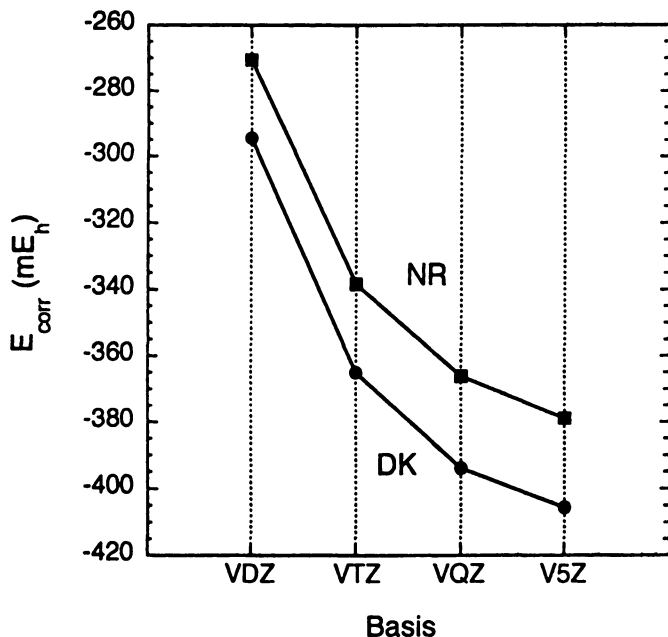


Figure 7. All-electron correlation energies from non-relativistic (NR) and DKrelativistic CISD calculations on the Hg atom using *cc-pVnZ-NR* and *cc-pVnZDK* basis sets, respectively.

method with perturbative triples was used that was based on restricted open-shell Hartree-Fock (ROHF) orbitals, R/UCCSD(T) (33,39). Potential energy functions were obtained by fitting 7 points to polynomials in simple displacement coordinates, ($r-r_e$), and the spectroscopic constants were obtained by the usual Dunham analysis. The atomic energies were obtained using orbitals with full symmetry equivalencing. As shown in Table I, the energetics and spectroscopic constants obtained using the new *cc-pVnZ-PP* basis sets exhibit very regular convergence towards their respective CBS limits. The core-valence correlation effect on r_e obtained at the R/UCCSD(T)/*cc-pRwCVTZ* level of theory is substantial, -0.032 \AA , but is much more modest for the dissociation energy, $+0.69 \text{ kcal/mol}$. When these effects are added to the R/UCCSD(T)/CBS results, the best predicted values for $^4\Pi \text{ YC}$ are $r_e = 2.024 \text{ \AA}$, $\omega_e = 701 \text{ cm}^{-1}$, $\omega_e x_e = 3.2 \text{ cm}^{-1}$, and $D_e = 78.8 \text{ kcal/mol}$. Of these quantities, only the harmonic frequency is in reasonable agreement with the available experimental results (37). The predicted bond length is smaller by 0.025 \AA , while the calculated dissociation energy is smaller than the quoted experimental result by 21 kcal/mol . These large discrepancies cannot be attributed to an

Table I. CCSD(T) spectroscopic constants calculated for the $^4\Pi$ state of YC using the new ECP-based cc-pVnZ-PP (VnZ-PP) and all-electron cc-pVQZ (-NR and -DK) basis sets for Y and cc-pVnZ for C

<i>Basis Set</i>	E_e (E_h)	r_e (\AA)	ω_e (cm^{-1})	$\omega_e x_e$ (cm^{-1})	α_e (cm^{-1})	D_e (kcal/mol)
VDZ-PP	-75.726 302	2.0779	668.6	3.75	0.0023	67.56
VTZ-PP	-75.759 918	2.0611	684.8	3.47	0.0021	73.90
VQZ-PP	-75.770 148	2.0572	687.1	3.45	0.0021	76.26
V5Z-PP	-75.773 510	2.0565	688.0	3.39	0.0021	77.15
CBS ^a	-75.777 04	2.0557	688.9	3.34	0.0020	78.09
wCVTZ(7) ^b	-75.762 658	2.0577	685.1	3.53	0.0021	74.31
wCVTZ(17)	-76.088 016	2.0262	696.9	3.37	0.0022	75.00
CBS+CV ^c		2.0241	700.7	3.18	0.0021	78.8
VQZ-NR	-3369.643 638	2.0575	680.0	3.53	0.0021	79.44
VQZ-DK	-3420.572 946	2.0600	686.2	3.43	0.0021	76.11
Expt. ^d		2.050	686±20			100±3

^a Obtained via a 2-point $1/n^3$ extrapolation of the VQZ-PP and V5Z-PP total energies

^b cc-pwCVTZ-PP (Y) and cc-pCVTZ (C) core-valence basis sets with valence-only (7) and all-electrons (17) correlated.

^c Obtained by addition of the CBS results of (a) with the core-valence effects of (b).

^d Refs. (37) and (38). The bond length is a r_0 value. Use of the ab initio α_e yields $r_e = 2.049 \text{ \AA}$.

inadequate correlation treatment; large scale MRCI calculations were also undertaken and these results were entirely consistent with the R/UCCSD(T) values. As evidenced by the all-electron DK results shown in Table I, errors due to the PP approximation are also very small, e.g., only -0.003 \AA in r_e and $\sim 0.15 \text{ kcal/mol}$ in D_e . Further experimental investigations of YC would clearly be desirable.

$X^1\Sigma^+ \text{HgH}^+$

Recent calculations on the mercury hydride cation include the relativistic Fock-space coupled cluster calculations of Visscher et al. (40) and Mosyagin et al. (41), the generalized RECP-CCSD calculations of Mosyagin et al. (41), and the quasirelativistic PP MRCI calculations by Häussermann et al. (32). While several of these calculations were very sophisticated, basis sets of only approximately triple-zeta quality were used and the effects of $5s5p$ correlation in Hg were not investigated. In the present work, the CCSD(T) method has been used with the new cc-pVnZ-PP and aug-cc-pVnZ-PP basis sets for Hg to calculate near-equilibrium potential energy functions (calculated analogously to YC) and spectroscopic constants. Table II summarizes these results together with both valence-only (12 electrons) and core-valence (20 electrons) correlation calculations with the cc-pRwCVTZ basis set (cc-pVTZ on H). Very rapid convergence towards the CBS limit is observed for all of the derived spectroscopic constants, as well as D_e , as the basis set is expanded from DZ to 5Z. As expected, the extra diffuse functions provided by the aug-cc-pVnZ-PP sets offer little overall improvement for HgH^+ but do result in slightly faster convergence towards the CBS limits. Correlation of the $5s$ and $5p$ electrons of Hg results in a shortening of the HgH bond by 0.008 \AA with a concomitant increase in the harmonic frequency of 28 cm^{-1} . The dissociation energy is increased by 1.6 kcal/mol . At the CCSD(T)/CBS level of theory with corrections due to $5s5p$ correlation, the calculated spectroscopic constants are in excellent agreement with experiment with deviations of just -0.001 \AA , -8 cm^{-1} and -1.4 cm^{-1} for r_e , ω_e , and $\omega_e x_e$, respectively. The predicted dissociation energy, however, differs from the uncertain experimental value by about 9 kcal/mol . At this level of theory, the theoretical value is expected to be the more accurate quantity. All electron calculations on HgH^+ both with (DK) and without (NR) the effects of scalar relativity are shown in Table III. At the CCSD(T)/CBS level of theory, scalar relativity is predicted by the DK approximation to reduce the bond length by 0.18 \AA and increase the harmonic frequency by 334 cm^{-1} . Relativity also destabilizes the bond in HgH^+ by over 17 kcal/mol or nearly 40%. The DK results of Table III also demonstrate the

Table II. CCSD(T) spectroscopic constants calculated for the $X^1\Sigma^+$ state of HgH^+ using the new ECP-based cc-pVnZ-PP (VnZ-PP) and aug-cc-pVnZ (AVnZ-PP) basis sets for Hg. The cc-pVnZ and aug-cc-pVnZ basis sets were used throughout for H

Basis Set	E_e (E_h)	r_e (\AA)	ω_e (cm^{-1})	$\omega_e x_e$ (cm^{-1})	α_e (cm^{-1})	D_e (kcal/mol)
VDZ-PP	-153.105 334	1.6073	2018.4	43.3	0.205	57.07
VTZ-PP	-153.205 324	1.5982	1999.9	40.8	0.207	59.99
VQZ-PP	-153.242 135	1.5987	2003.2	40.8	0.206	61.00
V5Z-PP	-153.256 701	1.6001	1995.1	40.3	0.205	61.34
AVDZ-PP	-153.132 726	1.6110	1996.7	42.4	0.203	59.04
AVTZ-PP	-153.215 076	1.6020	1986.1	40.6	0.206	60.65
AVQZ-PP	-153.245 954	1.6008	1990.9	40.7	0.207	61.34
AV5Z-PP	-153.258 507	1.6009	1991.6	40.1	0.205	61.54
CBS ^a	-153.271 68	1.6009	1992.3	39.5	0.202	61.78
wCVTZ(12) ^b	-153.211 992	1.5974	1997.9	40.3	0.208	60.09
wCVTZ(20)	-153.502 982	1.5894	2026.0	40.3	0.210	61.68
CBS+CV		1.5929	2020.4	39.5	0.204	63.37
Expt. ^c		1.5944	2027.7	40.9	0.206	72

^a Obtained via a 2-point $1/n^3$ extrapolation of the VQZ-PP and V5Z-PP total energies

^b cc-pwCVTZ-PP core-valence basis set for Hg with valence-only (12) and all-electrons (20) correlated.

^c Ref. (49).

high accuracy of the PP used in the current work. At the CBS limit the ECP-based spectroscopic constants differ from their all-electron DK values by just -0.0015 \AA , -4.4 cm^{-1} , and -0.16 kcal/mol for r_e , ω_e , and D_e respectively.

$X^1\Sigma_g^+ \text{Hg}_2$

The Hg dimer has been the subject of numerous experimental and theoretical studies. In particular, the high resolution experiments of Koperski et al. (42-44) have resulted in accurate molecular parameters for the weakly bound ground state, including the equilibrium bond distance and binding energy. Recent *ab initio* studies include the work of Jordan and co-workers (45), Schwerdtfeger et al. (13), and Dolg and Flad (46). In each of these cases the

Table III. Spectroscopic constants of $X^1\Sigma^+$ HgH⁺ from all-electron CCSD(T) calculations both with (DK) and without (NR) the approximate inclusion of scalar relativistic effects^a

<i>Basis Set</i>	E_e (E_h)	r_e (\AA)	ω_e (cm^{-1})	$\omega_e x_e$ (cm^{-1})	α_e (cm^{-1})	D_e (kcal/mol)
AVQZ-NR	-18409.671 498	1.7849	1651.5	32.9	0.155	44.07
AV5Z-NR	-18409.683 530	1.7846	1657.1	34.2	0.153	44.23
CBS-NR	-18409.696 15	1.7842	1662.8	34.5	0.151	44.42
AVQZ-DK	-19604.682 494	1.6025	1994.1	41.0	0.205	61.50
AV5Z-DK	-19604.693 772	1.6024	1995.3	40.4	0.204	61.72
CBS-DK	-19604.705 60	1.6024	1996.7	39.6	0.202	61.94
$\Delta\text{Rel (CBS)}$		-0.182	333.9	5.1	0.052	17.5

^a The CBS limits were obtained via 2-point $1/n^3$ extrapolations of the QZ and 5Z total energies.

relativistic PP of Häussermann et al. was used with relatively large 1-particle basis sets in order to minimize the basis set superposition error (BSSE). In addition, Kunz et al. (47) have reported all-electron calculations on Hg₂ employing the Douglas-Kroll-Hess Hamiltonian. In each of these studies, high level electron correlation methods were employed such as CCSD(T) and good agreement with experiment was generally obtained, but the basis sets used did not allow an extrapolation to the complete basis set limit, which limited the accuracy attainable in these studies.

The results using the new aug-cc-pVnZ-PP basis sets at the CCSD(T) level of theory are shown in Table IV. In each case the spectroscopic constants were obtained from fits of 10 points spanning the range from 6.4 – 8.2 a_0 and the results of fits to both total energies and interaction energies obtained by the application of the function counterpoise method (CP) for the removal of BSSE are shown. In both cases, systematic convergence towards the CBS limit is observed for all quantities. At the CBS limit both the CP-corrected and uncorrected values are nearly identical, which provides a good check of the extrapolation procedure. As also shown in Table IV, correlation of the 5s and 5p electrons of Hg results in a significant shortening of the Hg-Hg bond, -0.035 \AA , and an increase in the binding energy of about 14 cm^{-1} . Previous workers (45,46,48) have also investigated the effects of correlating the 5s and 5p electrons, but their results for the bond shortening due to core-valence correlation were all much too large, -0.1 \AA at the MP4 level (46) to -0.07 \AA at the MP2 level (48). In each case these large values can probably be attributed to

Table IV. Spectroscopic constants calculated for the $X^1\Sigma_g^+$ state of Hg_2 at the CCSD(T) level of theory using the new ECP-based aug-cc-pVnZ-PP (AVnZ-PP) basis sets

<i>Basis Set</i>	E_e (<i>E_h</i>)	r_e (<i>Å</i>)	ω_e (<i>cm⁻¹</i>)	$\omega_e x_e$ (<i>cm⁻¹</i>)	D_e (<i>cm⁻¹</i>)	r_e (CP) ^{a)} (<i>Å</i>)	ω_e (CP) ^{a)} (<i>cm⁻¹</i>)	$\omega_e x_e$ (CP) ^{a)} (<i>cm⁻¹</i>)	D_e (CP) ^{a)} (<i>cm⁻¹</i>)
AVDZ-PP	-305.827 496	3.9022	17.68	0.20	381.95	4.2064	12.28	0.22	171.38
AVTZ-PP	-305.992 071	3.8643	17.06	0.21	311.01	3.9099	16.21	0.22	277.42
AVQZ-PP	-306.054 972	3.7816	18.23	0.23	344.53	3.8047	17.77	0.23	326.49
AV5Z-PP	-306.080 520	3.7566	18.74	0.23	359.58	3.7715	18.43	0.23	348.15
CBS ^{b)}	-306.107 33	3.7310	19.28	0.23	376.06	3.738	19.1	0.23	372.1
AwCVTZ (24) ^{c)}						3.9049	16.25	0.22	278.58
AwCVTZ (40)						3.8697	16.73	0.22	292.25
CBS+CV						3.704	19.8	0.23	391.3
CBS+CV+SO ^{d)}						3.687	19.8	0.23	399
Expt ^{e)}						3.69±0.01	19.6±0.3	0.25±0.05	380±15
Selected other work									
Ref. (46) ^{f)}		3.729	19.4	0.24	379				
Ref. (45)		3.718	19.4	0.24	379				
Ref. (13) ^{g)}						3.743	18.4	.28	328

^{a)} Derived from fits to the counterpoise-corrected interaction energies.

^{b)} Obtained via 2-point $1/n^3$ extrapolations of the QZ and 5Z total energies and CP-corrected interaction energies.

^{c)} aug-cc-pwCVTZ-PP core-valence basis set for Hg with valence-only (24) and all-electrons (40) correlated.

^{d)} CBS plus core-valence effects of (c) with the addition of spin-orbit effects from Ref. (46) (2-electron SO-PP values)

^{e)} Ref. (42-44).

^{f)} Includes 5s5p core-valence and spin-orbit corrections These values were cited in Ref. (13).

^{g)} Includes spin-orbit corrections.

defects in the basis set, i.e., sufficient core-valence correlating functions were not included. After applying our core-valence corrections to the CCSD(T)/CBS limit results, excellent agreement with experiment is obtained with all quantities being nearly within the experimental uncertainties. As shown by Dolg and Flad (46), however, the spin-orbit effects on the spectroscopic constants are not negligible. While there seems to be some uncertainty in the exact magnitude of this effect, addition of SO corrections from their work does seem to slightly improve the agreement with experiment for the equilibrium bond length. Larger corrections have also been used (13), however, but application of these quantities would result in a r_e too short compared to experiment. On the other hand, the CBS limit bond length is over 0.03 Å shorter than the aug-cc-pV5Z-PP result, from which one might suspect that the 2-point extrapolation scheme may be overshooting the actual valence correlated CBS limit.

The results from all-electron calculations on Hg_2 are shown in Table V. At the valence correlated (5d6s) CBS limit, scalar relativity is calculated to result in a bond length contraction of 0.165 Å and a destabilization of the bond by 51 cm^{-1} or ~12%. The bond length contraction is in nearly exact agreement with the small basis set PP results of Schwerdtfeger et al., but in their work the bond was actually slightly stabilized (+23 cm^{-1}) by scalar relativity at the MP2 level of theory. With their basis set, however, MP2 overestimates the binding energy of Hg_2 by nearly a factor of 3.5 compared to QCISD(T), hence it is much less reliable than the present results. In fact, as shown by Dolg and Flad (46) even MP4 yields a binding energy nearly a factor of 2 too large compared to CCSD(T) or QCISD(T), which could explain the poor results for the effects of $5s5p$ correlation. On comparing the present all-electron CCSD(T)-DK/CBS results to the valence-only CCSD(T)/CBS PP results, the binding energies are very similar in both cases, differing by only ~7 cm^{-1} . The bond lengths and harmonic frequencies differ, however, by more than expected amounts, i.e., -0.025 Å and -0.6 cm^{-1} , respectively. Given the excellent agreement between PP and all-electron results in the case of HgH^+ , the origin of these differences are not clear at this time. As mentioned above, the all-electron DK dipole polarizabilities are also somewhat too large, which may also be reflecting residual errors in the 2nd-order DK approximation. Perhaps 3rd-order DK calculations could determine if the problem lies in the present all-electron treatment of scalar relativity.

Summary

New correlation consistent basis sets have been developed for Y and Hg in conjunction with accurate small-core relativistic pseudopotentials. A few all-electron basis sets have also been optimized both with and without the inclusion

Table V. Spectroscopic constants of $X^1\Sigma_g^+$ Hg₂ from all-electron CCSD(T) calculations both with (DK) and without (NR) the approximate inclusion of scalar relativistic effects^a

<i>Basis Set</i>	E_e (E_h)	r_e (\AA)	ω_e (cm^{-1})	D_e (cm^{-1})	r_e (CP) (\AA)	ω_e (CP) (cm^{-1})	D_e (CP) (cm^{-1})
AVQZ-NR	-36818.818 355	3.9395	17.40	405.81	3.9577	16.87	387.00
AV5Z- NR	-36818.842 764	3.9108	17.74	419.00	3.9193	17.60	411.22
CBS-NR	-36818.868 38	3.880	18.2	433.7	3.881	18.5	438.0
AVQZ-DK	-39208.927 041	3.7636	18.35	351.60	3.7867	17.87	335.94
AV5Z-DK	-39208.949 988	3.7373	18.88	366.58	3.7518	18.24	356.24
CBS-DK	-39208.974 07	3.715	19.7	383.0	3.713	18.5	378.9
ΔRel (CBS)		-0.165	1.5	-51	-0.168	0.0	-59

^a The CBS limits were obtained via 2-point $1/n^3$ extrapolations of the QZ and 5Z total energies and CP-corrected interaction energies

of scalar relativity. Molecular benchmark calculations were reported for the electronic ground states of YC, HgH^+ , and Hg_2 . In each case systematic convergence to the CBS limit was observed for the calculated energetics and spectroscopic constants. After the accurate inclusion of core-valence correlation effects, excellent agreement with experiment was observed where experimental information was available (HgH^+ and Hg_2) and accurate predictions for the molecular parameters of YC were made. For the more strongly bound YC and HgH^+ molecules, the CBS limit results obtained in PP calculations with the cc-pVnZ-PP basis sets were nearly identical with all-electron results using the DK approximation. In the case of the Hg dimer, the CCSD(T)/CBS equilibrium bond distance from all-electron calculations was somewhat shorter than the PP result and seemingly further from experiment.

The basis sets reported in this work can be obtained from the author on request.

Acknowledgements

This research was performed in the William R. Wiley Environmental Molecular Sciences Laboratory (EMSL) at the Pacific Northwest National Laboratory (PNNL). Operation of the EMSL is funded by the Office of Biological and Environmental Research in the U.S. Department of Energy (DOE). PNNL is operated by Battelle Memorial Institute for the U.S. DOE under Contract DEAC06-76RLO 1830. This work was supported by the Division of Chemical Sciences in the Office of Basis Energy Sciences of the U.S. DOE.

References

1. Almlöf, J.; Taylor, P. R. *J Chem Phys.* **1987**, *86*, 4070.
2. Dunning, T. H., Jr. *J. Chem. Phys.* **1989**, *90*, 1007-1023.
3. Woon, D. E.; Dunning, T. H., Jr. *J. Chem. Phys.* **1993**, *98*, 1358-1371.
4. Wilson, A. K.; Peterson, K. A.; Woon, D. E.; Dunning, T. H., Jr. *J. Chem. Phys.* **1999**, *110*, 7667-7676.
5. Kendall, R. A.; Dunning, T. H., Jr.; Harrison, R. J. *J. Chem. Phys.* **1992**, *96*, 6796-6806.
6. Woon, D. E.; Dunning, T. H., Jr. *J. Chem. Phys.* **1994**, *100*, 2975.
7. Woon, D. E.; Dunning, T. H., Jr. *J. Chem. Phys.* **1995**, *103*, 4572-4585.
8. Peterson, K. A.; Dunning, T. H., Jr. *J. Chem. Phys.* **2002**, *117*, 10548-10560.
9. Bauschlicher, C. W., Jr. *Chem. Phys. Lett.* **1999**, *305*, 446-450.
10. Bauschlicher, C. W., Jr. *J. Phys. Chem. A* **1999**, *103*, 6429-6432.

11. Martin, J. M. L.; Sundermann, A. *J. Chem. Phys.* **2001**, *114*, 3408-3420.
12. Wesendrup, R.; Kloo, L.; Schwerdtfeger, P. *Int. J. Mass Spectrom.* **2000**, *201*, 17-21.
13. Schwerdtfeger, P.; Wesendrup, R.; Moyano, G. E.; Sadlej, A. J.; Greif, J.; Hensel, F. *J. Chem. Phys.* **2001**, *115*, 7401-7412.
14. Peterson, K. A. *J. Chem. Phys.* **2003**, *119*, 11099-11112.
15. Peterson, K. A.; Figgen, D.; Goll, E.; Stoll, H.; Dolg, M. *J. Chem. Phys.* **2003**, *119*, 11113-11123.
16. Bauschlicher, C. W., Jr.; Taylor, P. R. *Theor. Chim. Acta* **1993**, *86*, 13-24.
17. Bauschlicher, C. W., Jr. *Theor. Chim. Acta* **1995**, *92*, 183-198.
18. Pou-Amerigo, R.; Merchan, M.; Nebot-Gil, I.; Widmark, P.-O.; Roos, B. O. *Theor. Chim. Acta* **1995**, *92*, 149-181.
19. Partridge, H. *J. Chem. Phys.* **1989**, *90*, 1043-1047.
20. Bauschlicher, C. W., Jr. *Theor. Chem. Acc.* **1999**, *103*, 141-145.
21. Ricca, A.; Bauschlicher, C. W., Jr. *Theor. Chem. Acc.* **2001**, *106*, 314-318.
22. Noro, T.; Sekiya, M.; Koga, T.; Matsuyama, H. *Theor. Chem. Acc.* **2000**, *104*, 146-152.
23. Press, W. H.; Teukolsky, S. A.; Vetterling, W. T.; Flannery, B. P. *Numerical Recipes in FORTRAN: the Art of Scientific Computing*, 2nd ed.; Cambridge University Press: Cambridge, 1992.
24. MOLPRO is a package of *ab initio* programs written by H.-J. Werner and P.J. Knowles with contributions from J. Almlöf, R.D. Amos, A. Bernhardsson, A. Berning, P. Celani, D.L. Cooper, M.J.O. Deegan, A.J. Dobbyn, F. Eckert, S.T. Elbert, C. Hampel, G. Hetzer, T. Korona, R. Lindh, A.W. Lloyd, S.J. McNicholas, F.R. Manby, W. Meyer, M.E. Mura, A. Nicklass, P. Palmieri, K.A. Peterson, R.M. Pitzer, P. Pulay, G. Rauhut, M. Schütz, H. Stoll, A.J. Stone, R. Tarroni, P.R. Taylor, T. Thorsteinsson. *Molpro2000* (2000).
25. Schmidt, M. W.; Ruedenberg, K. *J. Chem. Phys.* **1979**, *71*, 3951-3962.
26. Feller, D. F.; Ruedenberg, K. *Theor. Chim. Acta* **1979**, *52*, 231-251.
27. Blaudeau, J.-P.; Brozell, S. R.; Matsika, S.; Zhang, Z.; Pitzer, R. M. *Int. J. Quantum Chem.* **2000**, *77*, 516-520.
28. Christiansen, P. A. *J. Chem. Phys.* **2000**, *112*, 10070-10074.
29. Andrae, D.; Häussermann, U.; Dolg, M.; Stoll, H.; Preuss, H. *Theor. Chim. Acta* **1990**, *77*, 123-141.
30. Helgaker, T.; Klopper, W.; Koch, H.; Noga, J. *J. Chem. Phys.* **1997**, *106*, 9639-9645.
31. Halkier, A.; Helgaker, T.; Jørgensen, P.; Klopper, W.; Koch, H.; Olsen, J.; Wilson, A. K. *Chem. Phys. Lett.* **1998**, *286*, 243-252.
32. Häussermann, U.; Dolg, M.; Stoll, H.; Preuss, H.; Schwerdtfeger, P.; Pitzer, R. M. *Mol. Phys.* **1993**, *78*, 1211-1224.
33. Goebel, D.; Hohm, U. *J. Phys. Chem.* **1996**, *100*, 7710-7712.
34. Huzinaga, S.; Klobukowski, M. *Chem. Phys. Lett.* **1993**, *212*, 260-264.

35. Douglas, M.; Kroll, N. M. *Ann. Phys. (New York)* **1974**, *82*, 89-155.
36. Jansen, G.; Hess, B. A. *Phys. Rev. A* **1989**, *39*, 6016-6017.
37. Simard, B.; Hackett, P. A.; Balfour, W. J. *Chem. Phys. Lett.* **1994**, *230*, 103-109.
38. Shim, I.; Pelino, M.; Gingerich, K. A. *J. Chem. Phys.* **1992**, *97*, 9240-9248.
39. Rittby, M.; Bartlett, R. J. *J. Phys. Chem.* **1988**, *92*, 3033-3036.
40. Visscher, L.; Eliav, E.; Kaldor, U. *J. Chem. Phys.* **2001**, *115*, 9720-9726.
41. Mosyagin, N. S.; Titov, A. V.; Eliav, E.; Kaldor, U. *J. Chem. Phys.* **2001**, *115*, 2007-2013.
42. Koperski, J.; Atkinson, J. B.; Krause, L. *Chem. Phys. Lett.* **1994**, *219*, 161-168.
43. Koperski, J.; Atkinson, J. B.; Krause, L. *Can. J. Phys.* **1994**, *72*, 1070-1077.
44. Koperski, J.; Atkinson, J. B.; Krause, L. *J. Mol. Spectrosc.* **1997**, *184*, 300-308.
45. Munro, L. J.; Johnson, J. K.; Jordan, K. D. *J. Chem. Phys.* **2001**, *114*, 5545-5551.
46. Dolg, M.; Flad, H.-J. *J. Phys. Chem.* **1996**, *100*, 6147-6151.
47. Kunz, C. F.; Hättig, C.; Hess, B. A. *Mol. Phys.* **1996**, *89*, 139-156.
48. Schwerdtfeger, P.; Li, J.; Pyykkö, P. *Theor. Chim. Acta* **1994**, *87*, 313-320.
49. Huber, K. P.; Herzberg, G. *Molecular Spectra and Molecular Structure IV. Constants of Diatomic Molecules*; Van Nostrand: Princeton, 1979.

Chapter 9

Multilevel Methods for Thermochemistry and Thermochemical Kinetics

Benjamin J. Lynch and Donald G. Truhlar

Department of Chemistry and Supercomputer Institute, University of Minnesota, Minneapolis, MN 55455-0431

This chapter presents an overview of the performance of current multilevel methods for computational thermochemistry and thermochemical kinetics. Multilevel methods extrapolate to the exact solution of the electronic Schrödinger equations by using calculations carried out with two or more levels, where a level is a combination of a specific form for the many-electron wave function and a specific one-electron basis set. This chapter compares the performance for thermochemistry and thermochemical kinetics of several multilevel methods, including scaling-all-correlation (SAC), complete basis set (CBS) methods, multi-coefficient correlation methods (MCCM), and Gaussian-3 extended (G3X) methods. It also compares these methods to hybrid density functional theory, and additional calculations are presented to test the importance of diffuse basis functions on hydrogen. In order of decreasing cost, the G3SX(MP3), MCG3/3, MC-QCISD/3, CBS-4, mPW1PW91/MG3S, and SAC/3 methods are shown to provide especially good performance-to-cost tradeoffs.

Introduction

Computational thermochemistry and computational thermochemical kinetics are based on the Born-Oppenheimer approximation and the use of quantum-mechanical electronic structure theory to calculate potential energy surfaces. The electronic structure methods may be based on interacting-electron wave functions or on density functional theory. The present overview is primarily concerned with the former approach. The starting point is Hartree-Fock (HF) theory. In HF theory, the electrons occupy a set of molecular orbitals, which are an orthogonal set of one-electron functions typically constructed from linear combinations of atom-centered basis functions. In HF theory, each electron moves in the average field of the other electrons, and so the correlated motion of the electrons is ignored. This is sometimes called a single-configuration method, and explicitly correlated wave functions based on an HF starting point are called single-reference methods. The error in energy due to the HF approximation is called the correlation energy (I). Neglect of the correlation energy leads to many systematic errors in the predicted thermochemical and dynamical properties at the HF level. The cost and poor performance of HF calculations have engendered the development of a variety of more cost-efficient semi-empirical methods. Two very popular semi-empirical methods related to HF theory are AM1 (2,3) and PM3 (4). These methods remove the most expensive parts of a minimum-basis-set HF calculation, and they introduce 15 empirical parameters for each element. The empirical parameters effectively estimate the parts of HF theory that are ignored, and they also implicitly account for effects due to extended basis sets and correlation energy. Methods like AM1 and PM3 tend to outperform minimum-basis-set HF for most problems of chemical interest.

Although semi-empirical methods like AM1 and PM3 are fairly accurate, especially considering their low cost, we need to pursue higher levels of theory to attain chemical accuracy (~ 1 kcal/mol) in calculating quantities such as bond strengths, electron affinities, ionization potentials, and reaction barrier heights. To achieve higher accuracy, we can use larger basis sets and explicitly account for electron correlation. Full configuration interaction (FCI) accounts for *all* electron correlation energy within the limitations of the one-electron basis set. This type of calculation is prohibitively expensive for all but the smallest of systems, and it is even more expensive to converge the calculation with respect to the size of the one-electron basis set. Therefore we introduce empirical parameters or we extrapolate, or both. For example, we can employ partial treatments of electron correlation, and then use empirical parameters to extrapolate from two or more incomplete levels of calculation to the exact solution. Such calculations, based on two or more levels, are called multilevel methods. All of the multilevel methods presented here include explicitly correlated, extended basis set, post-HF calculations, and so the empirical

parameters in these methods need only to account for high-level electron correlation and the remaining basis set effects. By using extended-basis-set post-HF calculations as our starting point, we can attain higher accuracy than is possible with AM1 and PM3 semi-empirical methods. A disadvantage though, is that the popular post-HF methods scale as N^5 , N^6 , or N^7 (for large N) as the number of atoms N is increased (5), and the coefficient of N^α becomes larger as the number of basis functions on each atom is increased. (We will give the scaling exponent α for various methods in section 3.)

One of the first methods to take advantage of the systematic nature of the errors in explicitly correlated *ab initio* methods and extrapolate toward complete configuration interaction (CCI, which is the combination of FCI with a converged one-electron basis set) is the scaling external correlation (6) (SEC) method. This method scales the correlation energy calculated from a multi-reference wave function. Although it has been shown to be very accurate, the calculation of the correlation energy from a multi-reference wave function is computationally expensive and technically difficult. The scaling-all-correlation (7-11) (SAC) method was therefore developed as a simplified method that only requires the correlation energy to be calculated with a single-reference wave function. Though it is less accurate than SEC, SAC is much more cost-efficient.

MCCM methods (11-18) are the general class of methods that use a linear combination of explicitly correlated *ab initio* calculations with two or more basis sets and two or more levels of electron correlation. The linear combinations extrapolate the correlation energy and the basis set to the CCI limit. One example of an MCCM is MCG3/3 (18), which has been shown (18) to calculate bond energies with less than $1/10^{\text{th}}$ the error of CCSD(T)/aug-cc-pVTZ (19,20) at less than $1/100^{\text{th}}$ the cost. (All "costs" in this paper are based on gradient calculations as explained below.) This comparison is especially striking because the CCSD(T) method is sometimes called "the gold standard," due to its high accuracy. Furthermore, the accuracy of MCG3/3 in calculating reaction barrier heights is only achieved by *ab initio* methods that are about 100 times more expensive (18).

Increasing either the basis set or the explicit level of correlation greatly increases the cost of *ab initio* calculations. If high-level correlation effects could be accurately estimated with a small basis, and large-basis-set effects could be estimated with a low level of correlation, then a large-basis high-level-correlation calculation would be unnecessary. Methods such as Gaussian-2 (21-23) (G2), Gaussian-3 (24,25) (G3), and G3 extended (26) (G3X) use such an additive approximation to reduce the cost of explicitly correlated calculations. In particular, starting with a modest *ab initio* calculation, various high-level and larger-basis-set contributions are estimated separately and assumed additive. Furthermore, an empirical correction, called the high-level-correction (HLC), is added to account for missing higher-level effects and nonadditivity, which may also be considered a higher-level effect. As an example, consider the G3 and G3X methods. In these methods the 6-31 G(d) basis is used to calculate the

energy with quadratic configuration interaction with double and single excitations and quasiperturbative connected triples (QCISD(T)) (27), and larger-basis-set effects are added on by calculations with lower levels of electron correlation. This effectively approximates a large-basis-set calculation at the QCISD(T) level of theory. Finally, a HLC that is a function of the number of valence electron pairs and unpaired electrons is added in an attempt to extrapolate to CCI. The G2, G3, and G3X methods all have the disadvantage of discontinuous potential energy surfaces because of the form of the HLC. In response to this problem, the MCCM-style methods G3S (15) and G3SX (26) were developed. These are similar to G3 and G3X, but they scale various energy components (as in SAC and MCG3) rather than assuming separability and correcting systematic errors with a HLC. The same group (26) has also developed less expensive methods in which MP3 or MP2 calculations are substituted for more expensive calculations in certain steps; we will consider two such methods, namely G3SX(MP3), and G3 SX(MP2).

The CBS methods of Petersson and coworkers (22,25,28-30) extrapolate the basis set and add empirical terms to extrapolate to experiment. Two especially powerful versions of the CBS approach are CBS-4 (30) and CBS-Q (30). For CBS-Q, the empirical terms are based on the overlap matrix and the spin contamination (which arises in some partial treatments of the electron correlation). CBS-4 also includes these terms plus a term based on the number of electrons in the system.

A qualitatively different approach to the problem of treating electron correlation is provided by the Kohn-Sham implementation of density functional theory (DFT) (31,32) and the empirically more successful hybrid DFT (32-34). Although this is not the primary focus of the current paper, hybrid DFT results will be presented for comparison to the multilevel methods. In hybrid DFT, the correlation energy and a portion of the exchange energy are accounted for by a density functional. Very useful hybrid DFT functionals include B3LYP (35,36), mPW1PW91 (37), MPW1K (38), and PBE1PBE (39,40) which are functionals based on the density and magnitude of the local gradient of the density. (We note that mPW1PW91, MPW1K, and PBE1PBE are sometimes called MPW25, MPW42.8, and PBE0, respectively.) Like other methods that do not explicitly account for electron interactions, hybrid DFT is not systematically improvable. Increasing the basis set can often improve the quality of the results (41,42); however, just as for *ab initio* methods, there is no guarantee that it will.

Section 2 describes the methods used and the experimental test data used for comparison. Section 3 presents results and discussion, and Section 4 gives conclusions.

Methods and Test Data

All electronic structure calculations in this paper were performed with GAUSSIAN98 (43). All calculations use the spin-restricted formalism for closed

shells and the spin-unrestricted formalism for open-shell systems. The four basis sets explicitly discussed and used in calculations are 6-31G(d)(44), 6-31G(2df,p) (44), MG3 (14,45), and MG3S (42). We note that the MG3 basis is identical to 6-311++G(3d2f,2df,2p) (44,46) for atoms H through Si, but is an improved version of this basis for atoms P–Cl; it includes a diffuse s function on H and a diffuse sp shell on Li through Cl, and it is a modification (14) of the G3Large basis (24) of Curtiss et al. MG3S is the same except the diffuse functions on H atoms are deleted (42). Several other basis sets are used as part of the multilevel techniques, and they are as described in the original papers.

For all results in this paper, spin-orbit coupling corrections have been added to open-shell calculations from a compendium given elsewhere (10); we note that this consistent treatment sometimes differs from the original methods employed by other workers, e.g., standard G3 calculations include spin-orbit contributions only for atoms. In the SAC and MCCM calculations presented here, core correlation energy and relativistic effects are not explicitly included but are implicit in the parameters (i.e., we use parameters called versions 2s and 3s in the notation of previous papers (11,16,18)).

The hybrid DFT methods used here are B3LYP (35,36), PBE1PBE (39,40,47), mPW1PW91 (37), and MPW1K (38). The *ab initio* methods discussed in this article include HF, MP4SDQ (44), and QCISD(T) (27). We consider only one pure DFT method, namely BLYP (48,49).

The cost function used in all tables and figures is the sum of the time to calculate an energy, gradient, or Hessian (as stated in each case) for the two molecules, 1-phosphinopropane and 2,2-dichloro-1-ethanol, with a single 500MHz R14000 processor on a Silicon Graphics Origin 3800 with the GAUSSIAN98 (43) electronic structure package normalized by dividing by the sum of the times for MP2/6-31 G(2df,p) gradient calculations on the same two molecules with the same program on the same computer. The test molecules were chosen to give a balanced cost at a variety of levels and sizes of basis sets. The cost for calculations with basis sets such as aug-cc-pVTZ (20) will be dominated by the cost of 1-phosphinopropane, which has nine hydrogen atoms, because aug-cc-pVTZ includes a very large number (23) of basis functions for each hydrogen atom. The cost of calculations using the MG3 or MG3S basis set will tend to be dominated by the cost of 2,2-dichloro-1-ethanol, which has two second-row atoms, because these basis sets weigh more heavily on 2nd row atoms rather than hydrogen.

The test set used for most comparisons in the present paper is Database/3 (18), which was introduced elsewhere. It consists of 109 atomization energies (AEs), 44 forward and reverse reaction barrier heights (BHs) of 22 reactions, 13 electron affinities (EAs), and 13 ionization potentials (IPs). There are a total of 513 bonds among the 109 molecules used for AEs, where double or triple bonds are only counted as a single bond. Note that all ionization potentials and electron affinities are adiabatic (not vertical), i.e., the geometry is optimized for the ions

as well as the neutrals. Our tests in the present paper will also include 2 data for LiH (see below) and 22 values $\Delta E_{\text{reaction}}$, which are the zero-point-exclusive energies of reaction for the 22 reactions in the database. All mean unsigned and root-mean-squared errors in the tables and text are unweighted averages over the specified data.

Database/3 and the other data used in this paper consist entirely of zero-point-exclusive data, which allows for direct comparisons with calculated Born-Oppenheimer potential energy surfaces, i.e., the sum of the electronic energies and nuclear repulsion. Although the G3X and CBS families of methods have standard geometry and frequency calculations associated with them, in this paper only the potential energy surfaces are required to compare with Database/3. The geometries used are optimized QCISD/MG3 geometries for all calculations in this paper.

One additional system, namely LiH, is discussed in this paper. The heat of formation and electron affinity of LiH are taken from the G3/99 (50) data set. The zero-point-exclusive atomization energy (D_0) was obtained from the heat of formation using the method described elsewhere (10). The electron affinity is converted into a zero-point exclusive electron affinity by removing the neutral and anionic zero-point energies calculated at the mPW1PW91/MG3 level and scaled (18) by 0.9758.

Discussion

Diffuse functions are often omitted on hydrogen because hydrogen has a lower electronegativity than many elements of general interest (C, N, O, F, S, Cl), and there is very little electron density around hydrogen. Hydrogen is the most numerous atom type in many systems of interest (e.g., amino acids and carbohydrates), and for methods to be cost-effective it is important not to use too many basis functions on such a common atom. The MCG3/3 and MC-QCISD/3 methods have no diffuse functions on hydrogen for any component of the calculation, and they perform very well compared to multilevel methods that use diffuse functions on hydrogen for one or more components (CBS-4, CBS-Q, G3X, G3SX, MCG3/2, MC-QCISD/2). It is desirable to test the limits of this observation, and the calculations presented next are designed to do this. If diffuse functions are required for systems where hydrogen is bonded to a less electronegative atom, then a metal hydride system, such as LiH (which is not in Database/3) may be poorly treated. Tables 1 and 2 test this hypothesis. Table 1 presents calculations of the electron affinity (EA) and atomization energy (AE) of LiH by methods that do not include diffuse functions on H, and Table 2 presents calculations of these same quantities by methods that do include diffuse functions on H. It can be seen in Table 1 that MCG3/3 and MC-QCISD/3 perform very well on the LiH AE and EA. On average they outperform MCG3/2

Table 1. Atomization energies and electron affinities (kcal/mol) for LiH at QCISD/MG3 geometries for methods that do not involve diffuse functions on hydrogen.

Method	AE ^a	EA ^b	MUE ^c
Experiment	57.4	7.9	...
QCISD(T)/MG3S	55.9	6.6	1.4
MCG3/3	58.0	7.9	0.3
MP4SDQ/MG3S	55.4	6.5	1.7
MC-QCISD/3	57.8	6.9	0.8
MC-UT/3	57.3	6.5	0.7
MC-CO/3	54.5	5.9	2.4
B3LYP/MG3S	58.3	9.7	1.4
PBE1PBE/MG3S	52.7	9.6	3.2
mPW1PW91/MG3S	53.2	9.7	3.0
MPW1K/MG3S	52.8	9.6	3.1
BLYP/MG3S	57.9	7.5	0.5
SAC/3	49.8	5.2	5.1
AM1	58.7	-15.1	12.1

^a atomization energy

^b electron affinity

^c mean unsigned error in AE and EA

Table 2. Atomization energies and electron affinities (kcal/mol) for LiH at QCISD/MG3 geometries for methods that involve diffuse functions on hydrogen.

Method	AE ^a	EA ^b	MUE ^c
Experiment	57.4	7.9	...
QCISD(T)/MG3	55.9	6.8	1.3
G3SX	57.9	7.8	0.4
G3X	57.3	8.8	0.5
CBS-Q	57.6	6.8	0.7
G3SX(MP3)	58.0	7.8	0.3
G3SX(MP2)	57.6	7.2	0.5
G3X(MP3)	57.0	9.5	1.0
MCG3/2	58.1	9.0	0.9
MP4SDQ/MG3	55.4	6.7	1.6
CBS-4	55.3	9.5	1.8
MC-QCISD/2	57.5	8.6	0.4
B3LYP/MG3	58.3	9.8	1.4
mPW1PW91/MG3	53.1	9.8	3.1

^a atomization energy

^b electron affinity

^c mean unsigned error in AE and EA

and MC-QCISD/2, both of which have a component calculation that involves diffuse functions on hydrogens (and therefore these methods are in Table 2). On the whole, the accurate multilevel methods in Table 1 (MCG3/3, MC-QCISD/3) and the hybrid DFT methods mPW1PW91 and B3LYP do not have systematically higher errors than the methods in Table 2. Therefore, since metal hydrides are seemingly a “worst case” for omitting diffuse functions on H, it appears to be confirmed that diffuse functions on hydrogen have little importance for most thermochemical calculations. Tables 3, 4, and 5, which are discussed next include errors on the two LiH test cases in the “All data” rows.

Table 3 shows the errors for the multilevel methods that scale (N) as N^7 , where N is the number of atoms (in this table and in Table 4 the methods are arranged in order of decreasing cost for gradient calculations). Table 3 also shows one single-level method, namely QCISD(T)/MG3S. All of the multilevel methods in Table 3 have similar mean unsigned errors, in the range (all errors quoted in the text are mean unsigned errors for all data) of 0.84–1.20 kcal/mol. However they have gradient costs varying by over an order of magnitude, from 45 to 460. Thus they have a broad range of performance-to-cost ratios. G3SX is both the most expensive and the most accurate among these methods. However if gradient calculations are required, MCG3/3 and G3SX(MP3) are only about one tenth the cost of G3SX, and the increase in MUE is less than 15% as compared to G3SX. The MCG3/3 method not only has a relatively low cost for gradients, it also has a relatively low cost for energies. Furthermore, the single-level method in Table 3 is not competitive in terms of either cost or accuracy.

Table 4 gives the errors for the multilevel methods with much lower costs. These methods are ideal for geometry optimizations or frequency calculations on many systems and for energy calculations on very large systems. These methods are, however, still much more accurate than any *ab initio* method of similar cost. To illustrate this Table 4 also gives the results for a single-level N^6 method for comparison. We also note that MC-QCISD/3 has an error only 27% larger than CBS-Q, but a gradient cost 14 times less. The CBS-4 method has an error 44% larger than MC-QCISD, but a gradient cost 2 times smaller. SAC/3 method has a mean unsigned error 2.5 times larger than CBS-4, but the cost is 9 times lower yet. If one considers larger systems, eventually the N^5 methods become the winner because in the limit of large N their cost rise more slowly than the other methods in Tables 3 and 4.

Table 5 gives the errors for a DFT method, four hybrid DFT methods, and AM1. Although hybrid DFT is very affordable, it lacks the accuracy of multi-coefficient semi-empirical methods based on explicitly correlated wave functions. Nevertheless the mPW1PW91/MG3S and AM1 methods have performance/cost characteristics that put them near the envelope of best performance in Figure 1. AM1 is valuable for larger systems where the other methods in the figure are not affordable.

Figure 1 is a scatter plot of the MUE over Database/3 versus the cost of a gradient for all methods in tables 3–5. Notice that the abscissa spans seven decades of cost.

Table 3. Mean Unsigned Errors (kcal/mol), Root-Mean-Square Errors, and Times at QCISD/MG3 Geometries for Methods with N^7

Quantity	Item	QCISD(T) MG3S	G3SX	G3X	CBS-Q	G3SX(MPS)	G3SX(MP2)	G3X(MP3)	MCG3/3
MUE	Atomization energies (109)	15.06	0.87	0.86	1.42	0.95	1.23	1.02	1.04
	Error per bond (513)	3.2	0.18	0.18	0.30	0.20	0.26	0.22	0.22
	Barrier heights (44)	1.37	0.81	1.07	0.87	0.94	0.92	1.26	1.01
	ΔE_{RXN} (22)	0.98	0.55	0.88	0.86	0.63	0.84	0.97	0.90
	Electron affinities (13)	3.72	1.06	1.27	1.12	1.00	1.42	1.60	0.92
	Ionization potentials (13)	2.78	1.07	1.81	1.26	1.34	1.54	2.11	0.95
	All Database/3 data (179) ^a	9.98	0.88	1.01	1.25	0.98	1.19	1.20	1.01
	All data (203) ^b	8.92	0.84	0.99	1.20	0.94	1.15	1.17	0.99
RMSE	All Database/3 data (179)	13.70	1.24	1.39	1.75	1.33	1.68	1.64	1.38
	All data (203)	12.87	1.20	1.37	1.70	1.29	1.63	1.61	1.33
Cost	Energy	50	13.5	13.5	3.8	8.1	5.3	7.9	3.3
	Gradient	3100	460	450	79	66	56	54	45
	Hessian	200000	29000	29000	4600	3500	3200	2700	2600

^a based on rows 1, 3, 5, and 6.

^b Database/3 plus 22 values of ΔE and atomization energy and electron affinity of LiH

Table 4. Mean Unsigned Errors (kcal/mol), Root-Mean-Square Errors, and Times at QCISD/MG3 Geometries for Methods with N^6 and N^5 Scaling

Quantity	Item	MP4SDQ/ MG3S	MC-QCISD/3	MC-UT/3	MC-CO/3	CBS-4	SAC/3
MUE	Atomization energies (109)	21.91	1.73	2.17	3.23	2.78	6.48
	Error per bond (513)	4.66	0.37	0.46	0.69	0.59	1.38
	Barrier heights (44)	3.95	1.33	2.69	3.23	1.64	3.64
	ΔE_{RXN} (22)	1.28	0.90	0.69	1.38	0.64	2.30
	Electron affinities (13)	4.92	1.38	1.42	2.11	2.11	7.82
	Ionization potentials (13)	3.00	1.95	1.94	2.09	2.28	8.64
	All Database/3 data (179) ^a	14.89	1.62	2.22	3.07	2.41	6.04
	All data (203) ^b	13.29	1.53	2.04	2.88	2.21	5.63
RMSE	All Database/3 data (179)	19.68	2.09	3.17	4.23	3.27	7.53
	All data (203)	18.49	2.01	3.00	4.03	3.10	7.18
Cost scaling		6	6	6	5	6	5
Cost	Energy	4.9	1.9	1.7	1.7	1.0	0.078
	Gradient	27	5.5	5.0	4.9	2.7	0.31
	Hessian	1700	140	110	100	110	6.3

^a based on rows 1, 3, 5, and 6

^b Database/3 plus 22 values of ΔE and atomization energy and electron affinity of LiH.

Table 5. Mean Unsigned Errors (kcal/mol), Root-Mean-Square Errors, and Times for hybrid DFT and DFT Methods and AM1 at QCISD/MG3 Geometries

Quantity	Item	mPW1PW91/ MG3S	PBE1PBE/ MG3S	B3LYP/ MG3S	MPW1K/ MG3S	BLYP/ MG3S	AM1
MUE	Atomization energies (109)	3.56	4.36	4.23	11.02	7.05	26.70
	Error per bond (513)	0.89	0.93	0.90	2.34	1.50	5.67
	Barrier heights (44)	3.56	4.19	4.25	1.63	7.42	9.09
	ΔE_{RXN} (22)	1.15	1.26	2.16	1.31	2.60	9.53
	Electron affinities (13)	2.62	2.78	2.29	3.71	2.63	17.61
	Ionization potentials (13)	3.72	3.24	4.72	3.53	4.87	16.01
	All Database/3 data (179) ^a	3.88	4.12	4.13	7.64	6.66	20.93
	All data (203) ^b	3.58	3.80	3.89	6.86	6.16	19.61
RMSE	All Database/3 data (179)	4.91	5.40	5.73	10.32	8.57	28.98
	All data (203)	4.65	5.12	5.46	9.69	8.13	27.58
Cost scaling		4	4	4	4	4	3
Cost	Energy	1.2	1.2	1.2	1.2	1.2	2×10^{-3c}
	Gradient	1.7	1.7	1.7	1.7	1.7	4×10^{-3c}
	Hessian	12.7	12.7	12.7	12.7	12.7	4×10^{-3c}

^abased on rows 1, 3, 5, and 6.

^bDatabase/3 plus 22 values of ΔE and atomization energy and electron affinity of LiH

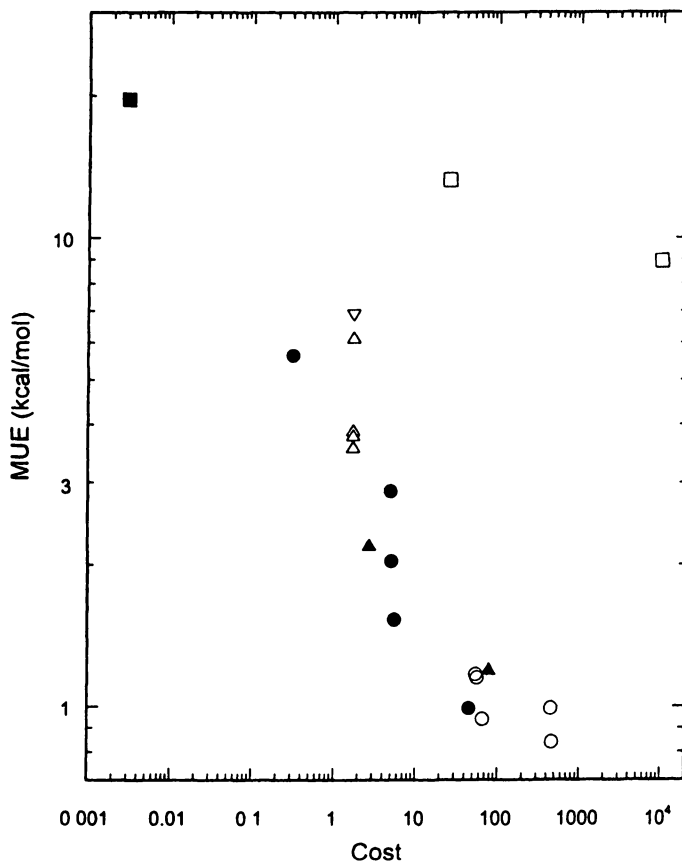


Figure 1. Mean unsigned error over all 203 data vs. gradient cost for AM1 (■), ab initio (□), CBS (▲), G3 (○), MCCM (●), DFT (▽), and hybrid DFT (△) methods. The figure includes all the methods that are included in Tables 3-5.

Conclusions

The comparisons in this paper indicate that diffuse functions on hydrogen atoms have little effect on the performance of multilevel methods. Furthermore, tests against 209 data show that multilevel methods provide very attractive performance levels for a given cost for applications requiring thermochemical calculations. We also note that some multilevel methods have performance-to-cost ratios that rise above the rest of the crowd of even the very select group of highly efficient methods considered here. Among N^7 methods, G3SX(MP3) and MCG3/3 methods have very favorable costs and only mild loss in accuracy as compared to the most accurate levels. MC-QCISD/3 has the best performance among N^6 methods, with a MUE over all data of 1.5 kcal/mol. Another N^6 method with notable performance is CBS-4, which has an error over all data of 2.2 kcal/mol.

Acknowledgement

This work was supported in part by the U. S. Department of Energy, Office of Basic Energy Sciences.

Literature Cited

1. Löwdin, P.-O. *Adv. Chem. Phys.* **1959**, *2*, 207.
2. Dewar, M. J. S.; Zuebis, E. G.; Healy, E. F.; Stewart, J. J. P. *J. Am. Chem. Soc.* **1985**, *107*, 3902.
3. Stewart, J. J. P. *J. Comp. Chem.* **1989**, *10*, 221.
4. Stewart, J. J. P. *J. Comp. -Aided Molecular Design*, *4*, 1.
5. Raghavachari, K.; Anderson, J. B. *J. Phys. Chem. A* **1996**, *100*, 12960.
6. Brown, F. B.; Truhlar, D. G. *Chem. Phys. Lett.* **1985**, *117*, 307.
7. Gordon, M. S.; Truhlar, D. G. *J. Am. Chem. Soc.* **1986**, *108*, 5412.
8. Rossi, I.; Truhlar, D. G. *Chem. Phys. Lett.* **1995**, *234*, 64.
9. Corchado, J. C.; Truhlar, D. G. *ACS Symp. Ser.* **1998**, *712*, 106.
10. Fast, P. L.; Corchado, J.; Sanchez, M. L.; Truhlar, D. G. *J. Phys. Chem. A* **1999**, *103*, 3139.
11. Tratz, C. M.; Fast, P. L.; Truhlar, D. G. *Phys. Chem. Comm.* **1999**, *2*, 14.
12. Fast, P. L.; Corchado, J. C.; Sanchez, M. L.; Truhlar, D. G. *J. Phys. Chem. A* **1999**, *103*, 5129.
13. Fast, P. L.; Sanchez, M. L.; Corchado, J. C.; Truhlar, D. G. *J. Chem. Phys.* **1999**, *110*, 11679.
14. Fast, P. L.; Sanchez, M. L.; Truhlar, D. G. *Chem. Phys. Lett.* **1999**, *306*, 407.

15. Curtiss, L. A.; Raghavachari, K.; Redfern, P. C.; Pople, J. A. *J. Chem. Phys.* **2000**, *112*, 1125.
16. Fast, P. L.; Truhlar, D. G. *J. Phys. Chem. A* **2000**, *104*, 6111.
17. Curtiss, L. A.; Redfern, P. C.; Rassolov, V.; Kedziora, G.; Pople, J. A. *J. Chem. Phys.* **2001**, *114*, 9287.
18. Lynch, B. J.; Truhlar, D. G. *J. Phys. Chem. A*, submitted.
19. Raghavachari, K.; Trucks, G. W.; Pople, J. A.; Head-Gordon, M. *Chem. Phys. Lett.* **1989**, *157*, 479.
20. Kendall, R. A.; Dunning, T. H., Jr.; Harrison, R. J. *J. Chem. Phys.* **1992**, *96*, 6796.
21. Curtiss, L. A.; Raghavachari, K.; Trucks, G. W.; Pople, J. A. *J. Chem. Phys.* **1991**, *94*, 7221.
22. Irikura, K. K., Frurip, David J., Eds. *Computational Thermochemistry: Prediction and Estimation of Molecular Thermodynamics*; ACS Symp. Ser., **1998**; *677*, 1998, Washington.
23. Pople, J. A. *Rev. Mod. Phys.* **1999**, *77*, 1267.
24. Curtiss, L. A.; Raghavachari, K.; Redfern, P. C.; Rassolov, V.; Pople, J. A. *J. Chem. Phys.* **1998**, *109*, 7764.
25. *Quantum-Mechanical Prediction of Thermochemical Data*; Cioslowski, J., Ed.; *Understanding Chemical Reactivity Series Vol. 22*; Kluwer: Dordrecht, **2001**.
26. Curtiss, L. A.; Redfern, P. C.; Raghavachari, K.; Pople, J. A. *J. Chem. Phys.* **2001**, *114*, 108.
27. Pople, J. A.; Head-Gordon, M.; Raghavachari, K. *J. Chem. Phys.* **1987**, *87*, 5968.
28. Nyden, M. R.; Petersson, G. A. *J. Chem. Phys.* **1981**, *75*, 1843.
29. Montgomery, J. A., Jr.; Ochterski, J. W.; Petersson, G. A. *J. Chem. Phys.* **1994**, *101*, 5900.
30. Ochterski, J. W.; Petersson, G. A.; Montgomery, J. A., Jr. *J. Chem. Phys.* **1996**, *104*, 2598.
31. Kohn, W.; Sham, L. J. *J. Phys. Rev.* **1965**, *140*, A1133.
32. Kohn, W.; Becke, A. D.; Parr, R. G. *J. Phys. Chem.* **1996**, *100*, 12974.
33. Becke, A. D. *J. Chem. Phys.* **1993**, *98*, 5648.
34. Becke, A. D. *J. Chem. Phys.* **1996**, *104*, 1040.
35. Stephens, P. J.; Devlin, F. J.; Chabalowski, C. F.; Frisch, M. J. *J. Phys. Chem.* **1994**, *98*, 11623.
36. Stephens, P. J.; Devlin, F. J.; Ashvar, C. S.; Bak, K. L.; Taylor, P. R.; Frisch, M. J. *ACS Symp. Ser.* **1996**, *629*, 105.
37. Adamo, C.; Barone, V. *J. Chem. Phys.* **1998**, *108*, 664.
38. Lynch, B. J.; Fast, P. L.; Harris, M.; Truhlar, D. G. *J. Phys. Chem. A* **2000**, *104*, 4811.
39. Ernzerhof, M.; Scuseria, G. E. *J. Chem. Phys.* **1999**, *110*, 5029.
40. Adamo, C.; Cossi, M.; Barone, V. *Theochem* **1999**, *493*, 145.
41. Bauschlicher, C. W., Jr.; Partridge, H. *Chem. Phys. Lett.* **1995**, *240*, 533.

42. Lynch, B. J.; Zhao, Y.; Truhlar, D. G. *J. Phys. Chem. A*, in press.
43. Frisch, M. J. T., G. W.; Schuelegel, H. B.; Scuseria, G. E.; Robb, M. A.; Cheeseman, J. R.; Zakrzewski, V. G.; Montgomery, J. A.; Stratmann, R. E.; Burant, J. C.; Dapprich, S.; Millam, J. M.; Daniels, A. D.; Kudin, K. N.; Strain, M. C.; Farkas, O.; Tomasi, J.; Barone, V.; Cossi, M.; Cammi, R.; Mennucci, B.; Pomelli, C.; Adamo, C.; Clifford, S.; Ochterski, J.; Petersson, G. A.; Ayala, P. Y.; Cui, Q.; Morokuma, K.; Malick, K.; Rabuck, A. D.; Raghavachari, K.; Foresman, J. B.; Cioslowski, J.; Ortiz, J. V.; Baboul, A. G.; Stefanov, B. B.; Liu, G.; Liashenko, A.; Piskorz, P.; Komaromi, I.; Gomperts, R.; Martin, R. L.; Fox, D. J.; Keith, T.; Al-Laham, M. A.; Peng, C. Y.; Nanayakkara, A.; Challacombe, M.; Gill, P. M. W.; Johnson, B. G.; Chen, W.; Wong, M. W.; Andres, J. L.; Gonzalez, C.; Head-Gordon, M.; Replogle, E. S.; Pople, J. A. GAUSSIAN98; Gaussian, Inc.: Pittsburgh, PA, 2001.
44. Hehre, W. J.; Radom, L.; Schleyer, P. v. R.; Pople, J. A. *Ab Initio Molecular Orbital Theory*; Wiley: New York, 1986.
45. Curtiss, L. A.; Redfern, P. C.; Raghavachari, K.; Rassolov, V.; Pople, J. A. *J. Chem. Phys.* **1999**, *110*, 4703.
46. McLean, A. D.; Chandler, G. S. *J. Chem. Phys.* **1980**, *72*, 5639.
47. Perdew, J. P.; Burke, K.; Ernzerhof, M. *Phys. Rev. Lett.* **1996**, *77*, 3865.
48. Becke, A. D. *Phys. Rev. A* **1988**, *38*, 3098.
49. Lee, C.; Yang, W.; Parr, R. G. *Phys. Rev. B* **1988**, *37*, 785.
50. Curtiss, L. A.; Raghavachari, K.; Redfern, P. C.; Pople, J. A. *J. Chem. Phys.* **2000**, *112*, 7374.

Chapter 10

A Nonlocal Energy Functional Derived from the Fluctuation–Dissipation Theorem

Katharine L. C. Hunt

Department of Chemistry, Michigan State University,
East Lansing, MI 48824

In the Born-Oppenheimer approximation, the electronic energy of a molecule is a functional of the electron density and the nonlocal charge-density susceptibility. The electron-electron interaction energy differs from the Coulomb energy of a classical charge distribution with the same averaged charge density $\langle \hat{\rho}_e(\mathbf{r}) \rangle$, because of correlations between spontaneous, quantum mechanical fluctuations in the charge density. By the fluctuation-dissipation theorem, these correlations are related to the imaginary part of the charge-density susceptibility. Use of the virial theorem for the kinetic energy of the electrons yields a functional for E that is simple and exact, but non-variational.

The electronic energy E of a molecule depends on the nuclear coordinates $\{\mathbf{R}_N\}$, the nuclear charges $\{Z_N\}$, the average electronic charge density $\langle \hat{\rho}_e(\mathbf{r}) \rangle$ and the charge-density susceptibility $\chi(\mathbf{r}, \mathbf{r}'; i\omega)$ at imaginary frequencies (1). By definition, $\chi(\mathbf{r}, \mathbf{r}'; \omega)$ gives the change in the electronic charge density at point \mathbf{r} , due to the application of a perturbing potential of frequency ω at \mathbf{r}' (2). The total electronic energy of a molecule with a fixed nuclear configuration $\{\mathbf{R}_N\}$ is (1)

This chapter is adapted with permission from reference 1. Copyright 2002 American Institute of Physics.

$$\begin{aligned}
E = & 1/2 \sum_N Z_N \int d\mathbf{r} \langle \hat{\rho}_e(\mathbf{r}) \rangle / |\mathbf{r} - \mathbf{R}_N| \\
& + 1/4 \int d\mathbf{r} d\mathbf{r}' \langle \hat{\rho}_e(\mathbf{r}) \rangle \langle \hat{\rho}_e(\mathbf{r}') \rangle / |\mathbf{r} - \mathbf{r}'| \\
& + (\hbar/4\pi) \int_{-\varepsilon} d\mathbf{r} d\mathbf{r}' \int_0^\infty d\omega \chi(\mathbf{r}, \mathbf{r}'; i\omega) / |\mathbf{r} - \mathbf{r}'| \\
& + (1/2) \sum_{N,\alpha} Z_N R_{N\alpha} \int d\mathbf{r} \langle \hat{\rho}_e(\mathbf{r}) \rangle (R_{N\alpha} - r_\alpha) / |\mathbf{r} - \mathbf{R}_N|^3. \quad (1)
\end{aligned}$$

The sum over N runs over all of the nuclei in the molecule, and the sum over α runs over the Cartesian coordinates x , y , and z . The subscript $-\varepsilon$ on the integral containing $\chi(\mathbf{r}, \mathbf{r}'; i\omega)$ indicates that an infinitesimal region around $\mathbf{r} = \mathbf{r}'$ is excluded from the range of integration.

The potential energy $\langle V \rangle$ of the electrons is the quantum mechanical average of the total Coulomb energy V_{eN} of electron-nuclear interactions and the instantaneous Coulomb energy V_{ee} of electron-electron interactions. The expectation value of the electron-nuclear interaction energy $\langle V_{eN} \rangle$ is identical to the Coulomb energy of interaction between the nuclei and a classical charge distribution with the charge density $\langle \hat{\rho}_e(\mathbf{r}) \rangle$. In contrast, the electron-electron interaction energy $\langle V_{ee} \rangle$ differs from the internal Coulomb energy of the static charge distribution $\langle \hat{\rho}_e(\mathbf{r}) \rangle$, because the electronic charge density fluctuates spontaneously about its average value, and the fluctuations are correlated. In addition, self-interaction effects, which are contained in the internal Coulomb energy of the full static charge distribution, must be removed to obtain $\langle V_{ee} \rangle$. Exchange and correlation are included in the energy E primarily through their contributions to the difference between the averaged product of the charge densities $\langle \hat{\rho}_e(\mathbf{r}, t) \rangle \langle \hat{\rho}_e(\mathbf{r}', t) \rangle$ and the product of the averages $\langle \hat{\rho}_e(\mathbf{r}, t) \rangle \langle \hat{\rho}_e(\mathbf{r}', t) \rangle$. The averaged product determines $\langle V_{ee} \rangle$, while the product of the averages determines the static electronic Coulomb energy. Exchange and correlation also affect the average charge density $\langle \hat{\rho}_e(\mathbf{r}) \rangle$, hence affecting $\langle V_{eN} \rangle$.

For an individual molecule, fluctuations of the instantaneous electronic charge density away from its quantum mechanical average are characterized by the fluctuation-dissipation theorem (3, 4). The molecule is assumed to be in equilibrium with a radiation bath at temperature T ; then in the final step of the derivation, the limit is taken as $T \rightarrow 0$. The fluctuation correlations, which are defined by

$$\begin{aligned}
\langle \delta \hat{\rho}_e(\mathbf{r}, t) \delta \hat{\rho}_e(\mathbf{r}', t) \rangle & \equiv \left[\langle \hat{\rho}_e(\mathbf{r}, t) - \langle \hat{\rho}_e(\mathbf{r}, t) \rangle \rangle \langle \hat{\rho}_e(\mathbf{r}', t) - \langle \hat{\rho}_e(\mathbf{r}', t) \rangle \rangle \right] \\
& = \langle \hat{\rho}_e(\mathbf{r}, t) \hat{\rho}_e(\mathbf{r}', t) \rangle - \langle \hat{\rho}_e(\mathbf{r}, t) \rangle \langle \hat{\rho}_e(\mathbf{r}', t) \rangle, \quad (2)
\end{aligned}$$

persist at $T = 0$ due to quantum “zero-point” effects. The fluctuation-dissipation theorem relates the correlation $\langle \delta\hat{\rho}_e(\mathbf{r},t) \delta\hat{\rho}_e(\mathbf{r}',t) \rangle$ to the imaginary part of the nonlocal charge-density susceptibility, $\chi''(\mathbf{r},\mathbf{r}';\omega)$.

In this work, the electronic kinetic energy is expressed in terms of the potential energy and derivatives of the potential energy with respect to nuclear coordinates, by use of the virial theorem (5-8). Thus, the results are valid for all bound electronic states. However, the functional derived for E does not obey a variational principle with respect to $\langle \hat{\rho}_e(\mathbf{r}) \rangle$, even though $\chi(\mathbf{r},\mathbf{r}';\omega)$ is in principle a functional of $\langle \hat{\rho}_e(\mathbf{r}) \rangle$, as implied by the Hohenberg-Kohn theorem (9-12).

The derivation (1) of Eq. (1) is related to the treatment of van der Waals energies within density functional theory, given by Kohn, Meir, and Makarov (13). However, in Ref. 13, the fluctuation-dissipation theorem was applied only to the *long-range* exchange-correlation effects, after the short-range exchange-correlation energy had been separated out. In addition, the exchange-correlation energy ϵ_{xc} as determined by Kohn, Meir, and Makarov (13) incorporates the difference between the exact electronic kinetic energy and the kinetic energy of a system of non-interacting electrons. This accords with the standard definition of ϵ_{xc} in density-functional theory, but it differs from the approach used here. In the current approach, the fluctuation-dissipation theorem is used to determine both short- and long-range fluctuation correlations $\langle \delta\hat{\rho}_e(\mathbf{r},t) \delta\hat{\rho}_e(\mathbf{r}',t) \rangle$, and the virial theorem is applied to the kinetic energy of the system with the full electron-electron interactions.

The result in Eq. (1) is also related to adiabatic-coupling functionals for the energy, derived by integration over a coupling constant λ that “turns on” the electron-electron interactions as it varies from 0 to 1 (14-23). This approach was introduced in the context of density functional theory by Langreth and Perdew (14) and used shortly thereafter by Harris and Griffin (15) and by Gunnarson and Lundqvist (16). In related work, Görling and Levy (17) have developed a coupling-constant perturbation expansion for the correlation energy; and Levy, March, and Handy have suggested a generalized, two-point adiabatic connection (19).

Nonlocal Charge-density Susceptibilities

The charge-density susceptibility is a linear response function; it is nonlocal because a perturbing potential applied at any point \mathbf{r} affects the charge density throughout the molecule. Quantum mechanically, $\chi(\mathbf{r}, \mathbf{r}';\omega)$ is specified by (2)

$$\chi(\mathbf{r}, \mathbf{r}';\omega) = -[\langle g | \rho_e(\mathbf{r}) G(\omega) \hat{\rho}_e(\mathbf{r}') | g \rangle + \langle g | \hat{\rho}_e(\mathbf{r}') G(-\omega) \hat{\rho}_e(\mathbf{r}) | g \rangle], \quad (3)$$

where $G(\omega)$ is the resolvent operator,

$$G(\omega) = (1 - \wp_0)(H_0 - E_0 - \hbar\omega)^{-1}(1 - \wp_0), \quad (4)$$

\wp_0 denotes the ground-state projection operator $|g\rangle\langle g|$, H_0 is the Hamiltonian for the unperturbed molecule, and E_0 is the ground-state energy. For real frequencies ω , $\chi(\mathbf{r}, \mathbf{r}'; \omega)$ gives the functional derivative of the charge density at point \mathbf{r} with respect to a variation of frequency ω in the applied potential at \mathbf{r}' .

The relation $\nabla \nabla': \alpha(\mathbf{r}, \mathbf{r}'; \omega) = -\chi(\mathbf{r}, \mathbf{r}'; \omega)$ connects $\chi(\mathbf{r}, \mathbf{r}'; \omega)$ to the non-local polarizability density $\alpha(\mathbf{r}, \mathbf{r}'; \omega)$ (24, 25). In earlier work, it has been proven that the following properties all depend on $\alpha(\mathbf{r}, \mathbf{r}'; \omega)$:

- infrared intensities (26),
- intramolecular dielectric functions (27),
- Sternheimer electric field shielding tensors (26),
- electronic reorganization terms in vibrational force constants (28, 29),
- softness kernels (30, 31),
- induction energies for interacting molecules (32, 33), and
- van der Waals dispersion energies (34).

Each of these properties can be expressed equivalently in terms of $\chi(\mathbf{r}, \mathbf{r}'; \omega)$. In the current work, $\chi(\mathbf{r}, \mathbf{r}'; \omega)$ contains exchange and correlation contributions to $\langle V_{ee} \rangle$; it also contains terms that (in effect) remove the self-energy (35-37) from the final result for $\langle V_{ee} \rangle$.

Static charge-density susceptibilities have been computed *ab initio* by Li *et al* (38). The frequency-dependent susceptibility $\chi(\mathbf{r}, \mathbf{r}'; \omega)$ can be calculated within density functional theory, using methods developed by Ando (39), Zangwill and Soven (40), Gross and Kohn (41), and van Gisbergen, Snijders, and Baerends (42). In *ab initio* work, $\chi(\mathbf{r}, \mathbf{r}'; \omega)$ can be determined by use of time-dependent perturbation techniques, pseudo-state methods (43-49), quantum Monte Carlo calculations (50-52), or by explicit construction of the linear response function in coupled cluster theory (53). Then the imaginary-frequency susceptibility can be obtained by analytic continuation from the susceptibility at real frequencies, or by a direct replacement $\omega \rightarrow i\omega$, where possible (for example, in pseudo-state expressions).

Working within the coupling-constant formalism, Hult, Rydberg, Lundqvist, and Langreth (20) have used applied the fluctuation-dissipation relation for values of λ intermediate between 0 and 1. They have obtained ϵ_{xc} in terms of a λ -dependent susceptibility, with an integration over the coupling constant. In the current work, $\chi(\mathbf{r}, \mathbf{r}'; \omega)$ corresponds to the $\lambda = 1$ value of the susceptibility.

In its underlying physics, the use of susceptibilities to obtain E is related to the use of a generalized dielectric response function to determine the energy of a

free electron gas, in the classic work of Nozières and Pines (54). On the intramolecular scale, a nonlocal dielectric function $\epsilon_v^{-1}(\mathbf{r}, \mathbf{r}'; \omega)$ characterizes the screening of applied potentials; that is, the contribution to the effective potential φ_{eff} at point \mathbf{r} due to the application of an external perturbation φ_{ex} at \mathbf{r}' is given by $\epsilon_0 \epsilon_v^{-1}(\mathbf{r}, \mathbf{r}'; \omega) \varphi_{\text{ex}}(\mathbf{r}'; \omega)$. The nonlocal dielectric function $\epsilon_v^{-1}(\mathbf{r}, \mathbf{r}'; \omega)$ is related to $\chi(\mathbf{r}, \mathbf{r}'; \omega)$ by (27)

$$\epsilon_0 \epsilon_v^{-1}(\mathbf{r}, \mathbf{r}'; \omega) = \delta(\mathbf{r} - \mathbf{r}') + (4\pi\epsilon_0)^{-1} \int d\mathbf{r}'' |\mathbf{r} - \mathbf{r}''|^{-1} \chi(\mathbf{r}'', \mathbf{r}'; \omega). \quad (5)$$

The fluctuation-dissipation relation has previously been applied to van der Waals interactions between pairs of molecules or multiplets by Linder and co-workers (55-57), Langbein (4), and Hunt (24, 34). The relation yields the dispersion energy of large or weakly overlapping molecules (55-57), for which point multipole representations of the potential break down. Langhoff has treated both covalent bonding and van der Waals interactions, using electronic susceptibilities (58). Hunt (34) has used the fluctuation-dissipation relation to prove Feynman's "conjecture" (59, 60) that the dispersion force between non-overlapping atoms in S states stems from the attraction of the nucleus in each atom to the perturbed charge distribution of the same atom, and to generalize the result to nonoverlapping molecules of arbitrary symmetry (34). Dispersion effects on the dipoles (61, 62) and polarizabilities (63, 64) of interacting molecules have also been derived within the fluctuation-dissipation framework.

Electronic Potential Energy

The total electronic potential energy of a molecule depends on the averaged electronic charge density and the nonlocal charge-density susceptibility. The molecule is assumed to be in equilibrium with a radiation bath at temperature T , so that the probability distribution over electronic states is determined by the partition function at T . The electronic potential energy is given exactly by

$$\begin{aligned} \langle V \rangle = & \sum_N \sum_i Z_N e \int d\mathbf{r} \langle \delta(\mathbf{r} - \mathbf{r}_i) \rangle / |\mathbf{r} - \mathbf{R}_N| \\ & + 1/2 e^2 \sum_i \sum_{j \neq i} \int d\mathbf{r} d\mathbf{r}' \langle \delta(\mathbf{r} - \mathbf{r}_i) \delta(\mathbf{r}' - \mathbf{r}_j) \rangle / |\mathbf{r} - \mathbf{r}'|, \end{aligned} \quad (6)$$

where the sums over i and j run over electrons, while the sum over N runs over all of the nuclei, with charges $\{Z_N\}$ located at positions $\{\mathbf{R}_N\}$; e is the charge on an electron, with $e < 0$. In this equation, the angular brackets denote thermally averaged expectation values of the operator or operator products. Thus, $\langle \delta(\mathbf{r} - \mathbf{r}_i) \delta(\mathbf{r}' - \mathbf{r}_j) \rangle$ represents the thermally weighted average of the expectation value of $\delta(\mathbf{r} - \mathbf{r}_i) \delta(\mathbf{r}' - \mathbf{r}_j)$ in each of the electronic states. When the limit as $T \rightarrow 0$ is

taken subsequently, this average becomes the ground-state expectation value of the operator. (In this case the operator is the product of Dirac delta functions of the positions of electrons i and j .) No self-energy terms are included in Eq. (6).

In terms of the electronic charge density operator $\hat{\rho}_e(\mathbf{r})$,

$$\hat{\rho}_e(\mathbf{r}) = e \sum_i \delta(\mathbf{r} - \mathbf{r}_i), \quad (7)$$

$\langle V \rangle$ has the form

$$\begin{aligned} \langle V \rangle = & \sum_N Z_N \int d\mathbf{r} \langle \hat{\rho}_e(\mathbf{r}) \rangle / |\mathbf{r} - \mathbf{R}_N| \\ & + 1/2 \int d\mathbf{r} d\mathbf{r}' \langle \hat{\rho}_e(\mathbf{r}) \hat{\rho}_e(\mathbf{r}') \rangle / |\mathbf{r} - \mathbf{r}'| \\ & - 1/2 e^2 \sum_i \int d\mathbf{r} d\mathbf{r}' \langle \delta(\mathbf{r} - \mathbf{r}_i) \delta(\mathbf{r}' - \mathbf{r}_i) \rangle / |\mathbf{r} - \mathbf{r}'|. \end{aligned} \quad (8)$$

The third term in Eq. (8) is the negative of the self-energy Σ_{ee} . The self-energy is divergent (35-37), but the divergence is precisely canceled by an opposing divergence in the integral containing $\langle \hat{\rho}_e(\mathbf{r}) \hat{\rho}_e(\mathbf{r}') \rangle$.

The statistical average of the product $\langle \hat{\rho}_e(\mathbf{r}) \hat{\rho}_e(\mathbf{r}') \rangle$ is identical to the single-time correlation $\langle \hat{\rho}_e(\mathbf{r}, t) \hat{\rho}_e(\mathbf{r}', t) \rangle$. From Eq. (2), this quantity can be expressed as the sum of the fluctuation correlation $\langle \delta \hat{\rho}_e(\mathbf{r}, t) \delta \hat{\rho}_e(\mathbf{r}', t) \rangle$ and the product of the average charge densities, $\langle \hat{\rho}_e(\mathbf{r}, t) \rangle \langle \hat{\rho}_e(\mathbf{r}', t) \rangle$, which are independent of time. Thus

$$\begin{aligned} \langle V \rangle = & \sum_N Z_N \int d\mathbf{r} \langle \hat{\rho}_e(\mathbf{r}) \rangle / |\mathbf{r} - \mathbf{R}_N| \\ & + 1/2 \int d\mathbf{r} d\mathbf{r}' \langle \hat{\rho}_e(\mathbf{r}) \rangle \langle \hat{\rho}_e(\mathbf{r}') \rangle / |\mathbf{r} - \mathbf{r}'| - \Sigma_{ee} \\ & + 1/4 \int d\mathbf{r} d\mathbf{r}' \langle \delta \hat{\rho}_e(\mathbf{r}, t) \delta \hat{\rho}_e(\mathbf{r}', t) + \delta \hat{\rho}_e(\mathbf{r}', t) \delta \hat{\rho}_e(\mathbf{r}, t) \rangle / |\mathbf{r} - \mathbf{r}'|. \end{aligned} \quad (9)$$

The second term in Eq. (9) for $\langle V \rangle$ gives the classical Coulomb energy of a continuous, static charge distribution with charge density $\langle \hat{\rho}_e(\mathbf{r}) \rangle$. The integrand has a singularity at $\mathbf{r} = \mathbf{r}'$, but the singularity is integrable.

By Fourier transformation,

$$\begin{aligned} \langle V \rangle = & \sum_N Z_N \int d\mathbf{r} \langle \hat{\rho}_e(\mathbf{r}) \rangle / |\mathbf{r} - \mathbf{R}_N| \\ & + 1/2 \int d\mathbf{r} d\mathbf{r}' \langle \hat{\rho}_e(\mathbf{r}) \rangle \langle \hat{\rho}_e(\mathbf{r}') \rangle / |\mathbf{r} - \mathbf{r}'| - \Sigma_{ee} \\ & + 1/4 \int d\mathbf{r} d\mathbf{r}' \int_{-\infty}^{\infty} \int_{-\infty}^{\infty} \exp[-i(\omega + \omega') t] \\ & \times \langle \delta \hat{\rho}_e(\mathbf{r}, \omega) \delta \hat{\rho}_e(\mathbf{r}', \omega') + \delta \hat{\rho}_e(\mathbf{r}', \omega') \delta \hat{\rho}_e(\mathbf{r}, \omega) \rangle / |\mathbf{r} - \mathbf{r}'|. \end{aligned} \quad (10)$$

The fluctuation-dissipation theorem (3) relates correlations of the spontaneous fluctuations in the charge density to the imaginary part of the charge-density susceptibility, $\chi''(\mathbf{r}, \mathbf{r}'; \omega)$, where $\chi(\mathbf{r}, \mathbf{r}'; \omega) = \chi'(\mathbf{r}, \mathbf{r}'; \omega) + i\chi''(\mathbf{r}, \mathbf{r}'; \omega)$:

$$\begin{aligned} & 1/2 \langle \delta\hat{\rho}_e(\mathbf{r}, \omega) \delta\hat{\rho}_e(\mathbf{r}', \omega') + \delta\hat{\rho}_e(\mathbf{r}', \omega') \delta\hat{\rho}_e(\mathbf{r}, \omega) \rangle \\ & = (\hbar/2\pi) \chi''(\mathbf{r}, \mathbf{r}'; \omega) \delta(\omega + \omega') \coth(\hbar\omega/2kT). \end{aligned} \quad (11)$$

Although $\chi(\mathbf{r}, \mathbf{r}'; \omega)$ is a linear response tensor, Eq. (11) is exact—its use does not imply that the calculation itself is limited to linear response.

The averaged potential energy $\langle V \rangle$ includes contributions from fluctuations in the charge density at all real frequencies. The fluctuation-dissipation theorem restricts the contributing frequencies to $\omega = -\omega'$, but allows for all real ω . The effects on the energy are contained in the term $\langle V \rangle_{fl}$, defined by

$$\langle V \rangle_{fl} = (\hbar/4\pi) \int d\mathbf{r} d\mathbf{r}' \int_{-\infty}^{\infty} \chi''(\mathbf{r}, \mathbf{r}'; \omega) \coth(\hbar\omega/2kT) / |\mathbf{r} - \mathbf{r}'|. \quad (12)$$

The ω -integral in $\langle V \rangle_{fl}$ is evaluated analogously to integrals appearing in the van der Waals interaction energy (4, 24, 55-57), dispersion dipoles (61, 62), and dispersion polarizabilities (63, 64). By itself, $\chi''(\mathbf{r}, \mathbf{r}'; \omega)$ is not analytic as a function of ω ; however, the full susceptibility $\chi(\mathbf{r}, \mathbf{r}'; \omega)$ is analytic throughout the upper complex ω half-plane (65); and by parity arguments (4), $\chi''(\mathbf{r}, \mathbf{r}'; \omega)$ can be replaced in the integrand by $(-i) \chi(\mathbf{r}, \mathbf{r}'; \omega)$. Both the imaginary part of the susceptibility $\chi''(\mathbf{r}, \mathbf{r}'; \omega)$ and $\coth(\hbar\omega/2kT)$ are odd in ω , while the real part $\chi'(\mathbf{r}, \mathbf{r}'; \omega)$ is even in ω . The frequency integral can then be evaluated by complex contour integration, where the contour runs along the real axis from $\omega = -W$ to $\omega = -\epsilon$, around an infinitesimal semicircle of radius ϵ to $\omega = \epsilon$, then along the real axis to $\omega = W$ (4). The contour is closed by a semi-circle of radius W in the upper half-plane, and the limit is taken as $W \rightarrow \infty$. By causality (4, 65), the poles of $\chi(\mathbf{r}, \mathbf{r}'; \omega)$ are confined to the lower complex half-plane, so the only enclosed poles are those of $\coth(\hbar\omega/2kT)$, at $\hbar\omega_n = 2, \pi i n kT$, for each integer n (4). (The contribution from the pole at $n = 0$ is multiplied by 1/2.) In the limit as $T \rightarrow 0$, the poles become infinitesimally close, and the sum over the residues at these poles becomes a Riemann sum for the integral

$$\langle V \rangle_{fl} = (\hbar/2\pi) \int d\mathbf{r} d\mathbf{r}' \int_0^{\infty} \chi(\mathbf{r}, \mathbf{r}'; i\omega) / |\mathbf{r} - \mathbf{r}'|. \quad (13)$$

While the $T \rightarrow 0$ limit has been taken formally, it should be noted that the electronic fluctuation correlations at room temperature are essentially equivalent to those at $T = 0$ for normal, nondegenerate systems. (Thermal photons at room temperature are generally unable to excite electronic transitions!)

With the result for $\langle V \rangle_n$ from Eq. (13), the potential energy becomes

$$\begin{aligned} \langle V \rangle &= \sum_N Z_N \int d\mathbf{r} \langle \hat{\rho}_e(\mathbf{r}) \rangle / |\mathbf{r} - \mathbf{R}_N| \\ &+ 1/2 \int d\mathbf{r} d\mathbf{r}' \langle \hat{\rho}_e(\mathbf{r}) \rangle \langle \hat{\rho}_e(\mathbf{r}') \rangle / |\mathbf{r} - \mathbf{r}'| - \Sigma_{ee} \\ &+ (\hbar/2\pi) \int d\mathbf{r} d\mathbf{r}' \int_0^\infty \chi(\mathbf{r}, \mathbf{r}'; i\omega) / |\mathbf{r} - \mathbf{r}'|. \end{aligned} \quad (14)$$

The self-energy Σ_{ee} is divergent, but there is a canceling divergence in the χ term, so that the net result for $\langle V \rangle$ is finite.

Electronic Kinetic Energy

A virial theorem (5-8) applied to the electronic coordinates gives the kinetic energy $\langle T \rangle$ in terms of $\langle V \rangle$ and expectation values of the first derivative of V with respect to nuclear coordinates (66-72). For bound electronic states $|f\rangle$

$$2\langle f | T | f \rangle = \left\langle f \left| \sum_{i,\alpha} \mathbf{r}_{i\alpha} \partial V / \partial \mathbf{r}_{i\alpha} \right| f \right\rangle, \quad (15)$$

where the summation over i and α runs over all electrons i and over the Cartesian coordinates $\alpha = x, y,$ and z . The Born-Oppenheimer approximation is used in this work, so $|f\rangle$ represents an electronic state that depends parametrically on the nuclear coordinates. The Coulomb potential for the interaction between charged particles is a homogeneous function of degree -1 , with respect to the coordinates of *all* of the interacting particles. By Euler's theorem,

$$\sum_{i,\alpha} \mathbf{r}_{i\alpha} \partial V / \partial \mathbf{r}_{i\alpha} + \sum_{N,\alpha} \mathbf{R}_{N\alpha} \partial V / \partial \mathbf{R}_{N\alpha} = -V, \quad (16)$$

with the nuclear coordinates denoted by $\{\mathbf{R}_N\}$. Equation (16) applies both to the classical potential function and to V in operator form. Then, from Eqs. (15) and (16),

$$\langle f | T | f \rangle = -(1/2) \langle f | V | f \rangle - (1/2) \sum_{N,\alpha} \mathbf{R}_{N\alpha} \langle f | \partial V / \partial \mathbf{R}_{N\alpha} | f \rangle. \quad (17)$$

By the Hellmann-Feynman theorem, the expectation value $\langle f | -\partial V / \partial \mathbf{R}_{N\alpha} | f \rangle$ is the force on nucleus N in the α direction. The force on each nucleus vanishes for a molecule in its equilibrium nuclear configuration; the force also vanishes for an isolated atom. In these cases the virial theorem becomes $\langle T \rangle = -(1/2) \langle V \rangle$. In other cases, however, the second term on the right in Eq. (17) is non-vanishing.

With Eq. (17) for $\langle T \rangle$, it is not necessary to use a gradient expansion (73) or generalized gradient expansion (74-77) for the kinetic energy. On the other

hand, the virial theorem applies to the exact wave function, but it does not apply to approximate wave functions, in general. Hence, the functional for E obtained by use of Eq. (17) is non-variational.

A general result for E follows from $E = \langle T \rangle + \langle V \rangle$, with Eq. (17) for $\langle T \rangle$ and Eq. (14) for $\langle V \rangle$. At this stage, the result differs from Eq. (1), because of its explicit inclusion of the self-energy.

Self-Energy

Self-energies (35-37) are present in the individual terms in Eq. (14), but not in the sum of the terms. Σ_{ee} is an explicit self-energy, introduced in order to express the electron-electron interaction energy in terms of the charge-density operator. Self-energy effects have not been removed from the static Coulomb term in Eq. (14), since it contains the full product $\langle \hat{\rho}_e(\mathbf{r}) \rangle \langle \hat{\rho}_e(\mathbf{r}') \rangle$, rather than the product weighted by $(n_e - 1)/n_e$. (In fact, the static Coulomb term is contained in the functional for a one-electron system.) Both of these self-energy contributions are canceled precisely by the term containing $\chi(\mathbf{r}, \mathbf{r}'; i\omega)$. To prove this, it is convenient to work with a sum-over-states representation of $\chi(\mathbf{r}, \mathbf{r}'; i\omega)$,

$$\chi(\mathbf{r}, \mathbf{r}'; i\omega) = (2/\hbar) \Sigma'_j \langle \mathbf{g} | \hat{\rho}_e(\mathbf{r}) | j \rangle \langle j | \hat{\rho}_e(\mathbf{r}') | \mathbf{g} \rangle \omega_{j\mathbf{g}} (\omega_{j\mathbf{g}}^2 + \omega^2)^{-1}, \quad (18)$$

where the prime on the summation indicates that the ground-state has been omitted from the sum over states j . The transition frequency $\omega_{j\mathbf{g}}$ satisfies $\omega_{j\mathbf{g}} = (E_j - E_{\mathbf{g}})/\hbar$. In obtaining Eq. (18), it has been assumed that all states are real and that damping is negligible for frequencies along the imaginary axis.

With Eq. (18) for $\chi(\mathbf{r}, \mathbf{r}'; i\omega)$, the last term on the right hand side in Eq. (14) can be integrated analytically, to yield

$$\begin{aligned} & (\hbar/2\pi) \int d\mathbf{r} d\mathbf{r}' \int_0^\infty \chi(\mathbf{r}, \mathbf{r}'; i\omega) / |\mathbf{r} - \mathbf{r}'| \\ & = (1/2) \int d\mathbf{r} d\mathbf{r}' \Sigma'_j \langle \mathbf{g} | \hat{\rho}_e(\mathbf{r}) | j \rangle \langle j | \hat{\rho}_e(\mathbf{r}') | \mathbf{g} \rangle / |\mathbf{r} - \mathbf{r}'|. \end{aligned} \quad (19)$$

From the closure relation $\Sigma'_j |j\rangle \langle j| = 1 - |\mathbf{g}\rangle \langle \mathbf{g}|$, the sum over the product of transition matrix elements involving $\hat{\rho}_e(\mathbf{r})$ and $\hat{\rho}_e(\mathbf{r}')$ separates into two terms, one containing the ground-state expectation value of $\hat{\rho}_e(\mathbf{r}) \hat{\rho}_e(\mathbf{r}')$ and the other containing the product of the expectation values of $\hat{\rho}_e(\mathbf{r})$ and $\hat{\rho}_e(\mathbf{r}')$, both in the ground state. These terms can be further separated into those containing self interactions vs. those containing interactions between distinct electrons. Then

$$\begin{aligned}
(\hbar/2\pi) \int d\mathbf{r} d\mathbf{r}' \int_0^\infty \chi(\mathbf{r}, \mathbf{r}'; i\omega) / |\mathbf{r} - \mathbf{r}'| = & \\
+ (e^2/2) \int d\mathbf{r} d\mathbf{r}' \langle \mathbf{g} | \sum_i \sum_{j \neq i} \delta(\mathbf{r} - \mathbf{r}_i) \delta(\mathbf{r}' - \mathbf{r}_j) | \mathbf{g} \rangle / |\mathbf{r} - \mathbf{r}'| & \\
- (e^2/2) \int d\mathbf{r} d\mathbf{r}' \langle \mathbf{g} | \sum_i \delta(\mathbf{r} - \mathbf{r}_i) | \mathbf{g} \rangle & \\
\times \langle \mathbf{g} | \sum_{j \neq i} \delta(\mathbf{r}' - \mathbf{r}_j) | \mathbf{g} \rangle / |\mathbf{r} - \mathbf{r}'| & \quad (20) \\
+ (e^2/2) \int d\mathbf{r} d\mathbf{r}' \sum_i \langle \mathbf{g} | \delta(\mathbf{r} - \mathbf{r}_i) \delta(\mathbf{r}' - \mathbf{r}_i) | \mathbf{g} \rangle / |\mathbf{r} - \mathbf{r}'| & \\
- (e^2/2) \int d\mathbf{r} d\mathbf{r}' \sum_i \langle \mathbf{g} | \delta(\mathbf{r} - \mathbf{r}_i) | \mathbf{g} \rangle \langle \mathbf{g} | \delta(\mathbf{r}' - \mathbf{r}_i) | \mathbf{g} \rangle / |\mathbf{r} - \mathbf{r}'|. &
\end{aligned}$$

The third term on the right in Eq. (20) cancels the divergent self energy \sum_{ee} in $\langle V \rangle$. The final term on the right equals $(-1/n_e)$ times the internal Coulomb energy of the charge distribution $\langle \hat{\rho}_e(\mathbf{r}) \rangle$ [the second term in Eq. (14)]; thus it removes the self-interactions from the static Coulomb energy.

For precise cancellation of the self energy, the closure relation must be satisfied by the expansion basis. Thus for numerical work, a different approach is needed to remove the canceling divergences in the expression for $\langle V \rangle$. If an infinitesimal region around $\mathbf{r} = \mathbf{r}'$ is removed from the range of integration, at least one of the two delta functions $\delta(\mathbf{r} - \mathbf{r}_i)$ and $\delta(\mathbf{r}' - \mathbf{r}_i)$ must vanish, for any value of \mathbf{r}_i . Consequently $\sum_{ee} \rightarrow 0$ and the third term in Eq. (20) also vanishes. Equation (1) for E follows immediately, with the deleted region denoted by the subscript $-\varepsilon$ on the range of integration. Deletion of the infinitesimal region has a negligible effect on the static Coulomb energy and a negligible effect on the fourth term in Eq. (20). This technique is analogous to the use of a “cut-out” propagator in dielectric theory (79, 80), to exclude self-polarization contributions to the dielectric function.

Summary

Equation (1) gives the final result for the electronic energy as a functional of the electronic charge density and the charge-density susceptibility. This result follows immediately from Eqs. (14), (17), and deletion of an infinitesimal region around $\mathbf{r} = \mathbf{r}'$ from the range of integration. Although the fluctuation-dissipation theorem has been used in the derivation of Eq. (1) for E , the same result follows by analytic integration of $\chi(\mathbf{r}, \mathbf{r}'; i\omega)$, using Eq. (18). Within the non-relativistic Born-Oppenheimer approximation, the functional is exact. The functional is nonlocal because it contains $\chi(\mathbf{r}, \mathbf{r}'; i\omega)$. It differs from the nonlocal density functionals in use for computations (23, 71, 78, 81-94), including the average-density (95) and weighted-density approximations (96-100).

This approach gives a compact expression for the electronic energy, in terms of the molecular properties; in this form, the result is useful for analytical work. The result may also be useful for determining contributions to the correlation energy from widely separated regions within a single molecule, or in interacting molecules, complementing the adiabatic coupling (14-23, 101-105) and "seamless" density functional (106-108) approaches. Earlier expressions for the van der Waals energy of large, nonoverlapping molecules (24, 34, 55-58) required integration over four spatial variables, vs. the integrations over two variables, \mathbf{r} and \mathbf{r}' , in Eq. (1).

Use of Equation (1) in numerical work requires a means of generating $\chi(\mathbf{r}, \mathbf{r}'; i\omega)$ as well as the average charge density. Direct variational methods are not applicable to the expression for E itself, due to use of the virial theorem. However, both $\rho_c(\mathbf{r})$ and $\chi(\mathbf{r}, \mathbf{r}'; i\omega)$ (39-42, 109-112) are computable with density-functional methods, thus permitting individual computations of E from Eq. (1) and investigations of the effects of various approximations for $\chi(\mathbf{r}, \mathbf{r}'; i\omega)$. Within coupled-cluster theory, $\chi(\mathbf{r}, \mathbf{r}'; i\omega)$ can be generated directly (53) from the definition in Eq. (3); then Eq. (1) yields the coupled-cluster energy in a new form, as an expectation value.

Acknowledgments

This work has been supported in part by the National Science Foundation, through Award Number CHE-9817297.

References

1. Hunt, K. L. C. *J. Chem. Phys.* **2002**, *116*, 5440.
2. Linder, B. *Adv. Quantum Chem.* **1972**, *6*, 203.
3. Callen, H. B.; Welton, T. A. *Phys. Rev.* **1951**, *83*, 34.
4. Langbein, D. *Theory of van der Waals Attraction*; Springer-Verlag: Berlin, 1974, Ch. 3.
5. Slater, J. C. *J. Chem. Phys.* **1933**, *1*, 687; **1972**, *57*, 2389.
6. Fock, V. Z. *Phys.* **1950**, *63*, 855.
7. Parr, R. G.; Brown, J. E. *J. Chem. Phys.* **1968**, *49*, 4849.
8. Sham, L.J. *Phys. Rev. A* **1970**, *1*, 969.
9. Hohenberg, P.; Kohn, W. *Phys. Rev.* **1964**, *136*, B864.
10. Kohn, W.; Sham, L. *Phys. Rev.* **1965**, *140*, A1133.
11. March, N. H. *Electron Density Theory of Atoms and Molecules*; Academic: New York, 1992.
12. Dreizler, R. M.; Gross, E. K. U. *Density Functional Theory: An Approach to the Quantum Many-Body Problem*; Springer-Verlag: Berlin, 1990.
13. Kohn, W.; Meir, Y.; Makarov, D. E. *Phys. Rev. Lett.* **1998**, *80*, 4153.

14. Langreth, D.; Perdew, J. *Solid State Commun.* **1975**, *17*, 1425; *Phys. Rev. B* **1977**, *15*, 2884.
15. Harris, J.; Griffin, A. *Phys. Rev. B* **1975**, *11*, 3669.
16. Gunnarson, O.; Lundqvist, B. I. *Phys. Rev. B* **1976**, *13*, 4275.
17. Levy, M.; Perdew, J. P. *Phys. Rev. A* **1985**, *32*, 2010.
18. Görling, A.; Levy, M. *Phys. Rev. B* **1993**, *47*, 13105.
19. Levy, M.; March, N. H.; Handy, N. C. *J. Chem. Phys.* **1996**, *104*, 1989.
20. Hult, E.; Rydberg, H.; Lundqvist, B. I.; Langreth, D. C. *Phys. Rev. B* **1999**, *59*, 4708.
21. The first use of a coupling constant in this manner is attributed to W. Pauli; e.g., see Pines, D. *The Many-Body Problem, Frontiers in Physics*; Benjamin: New York, 1961; p. 43.
22. Andersson, Y.; Hult, E.; Rydberg, H.; Apell, P.; Lundqvist, B. I.; Langreth, D. C. in *Electronic Density Functional Theory: Recent Progress and New Directions*; Dobson, J. F.; Vignale, G.; Das, M. P., Eds.; Plenum: New York, 1997; p. 243.
23. Mazin, I. I.; Singh, D. J. *Phys. Rev. B* **1998**, *57*, 6879.
24. Hunt, K. L. C. *J. Chem. Phys.* **1983**, *78*, 6149.
25. Hunt, K. L. C. *J. Chem. Phys.* **1984**, *80*, 393.
26. Hunt, K. L. C. *J. Chem. Phys.* **1989**, *90*, 4909.
27. Jenkins, O. S.; Hunt, K. L. C. to be published.
28. Handler, G. S.; March, N. H. *J. Chem. Phys.* **1975**, *63*, 438.
29. Hunt, K. L. C. *J. Chem. Phys.* **1995**, *103*, 3552.
30. Berkowitz, M.; Parr, R. G. *J. Chem. Phys.* **1988**, *88*, 2554.
31. Liu, P.-H.; Hunt, K. L. C. *J. Chem. Phys.* **1995**, *103*, 10597.
32. Liang, Y. Q.; Hunt, K. L. C. *J. Chem. Phys.* **1991**, *95*, 2549; **1993**, *98*, 4626.
33. Li, X.; Hunt, K. L. C. *J. Chem. Phys.* **1996**, *105*, 4076.
34. Hunt, K. L. C. *J. Chem. Phys.* **1990**, *92*, 1180.
35. Perdew, J. P.; Zunger, A. *Phys. Rev. B* **1981**, *23*, 5048.
36. Perdew, J. P. *Lect. Notes Phys.* **1983**, *187*, 127.
37. See also Goedecker, S.; Umrigar, C. J. *Phys. Rev. A* **1997**, *55*, 1765.
38. Li, X.; Hunt, K. L. C.; Ahuja, C.; Harrison, J. F. to be published.
39. Ando, T. *Z Phys. B* **1977**, *26*, 263.
40. Zangwill, A.; Soven, P. *Phys. Rev. A* **1980**, *21*, 1561.
41. Gross, E. K. U.; Kohn, W. *Phys. Rev. Lett.* **1985**, *55*, 2850; **1986**, *57*, 923.
42. van Gisbergen, S. J. A.; Snijders, J. G.; Baerends, E. J. *Phys. Rev. Lett.* **1997**, *78*, 3097.
43. Bishop, D. M.; Pipin, J. *J. Chem. Phys.* **1989**, *91*, 3549; **1992**, *97*, 3375; **1993**, *99*, 4875; **1995**, *103*, 5868.
44. Bishop, D. M.; Pipin, J. *Int. J. Quantum Chem.* **1993**, *45*, 349; **1993**, *47*, 129.
45. Thakkar, A. J. *J. Chem. Phys.* **1981**, *75*, 4496.
46. Meath, W. J.; Kumar, A. *Int. J. Quantum Chem. Symp.* **1990**, *24*, 501.
47. Kumar, A.; Meath, W. J.; Bundgen, P.; Thakkar, A. J. *J. Chem. Phys.* **1996**, *105*, 4927.
48. Bundgen, P.; Thakkar, A. J.; Kumar, A.; Meath, W. J. *Mol. Phys.* **1997**, *90*, 721.

49. Bundgen, P.; Thakkar, A. J.; Grein, F.; Ernzerhof, M.; Marian, C. M.; Nestmann, B. *Chem. Phys. Lett.* **1996**, *261*, 625.
50. Ceperley, D. M.; *Phys. Rev. B* **1978**, *18*, 3126.
51. Ceperley, D. M.; Alder, B. J. *Phys. Rev. Lett.* **1980**, *45*, 566.
52. Moroni, S.; Ceperley, D. M.; Senatore, G. *Phys. Rev. Lett.* **1995**, *75*, 689.
53. Piecuch, P. personal communication.
54. Nozières, P.; Pines, D. *Nuovo Cimento* **1958**, *9*, 470.
55. Linder, B.; Lee, K. F.; Malinowski, P.; Tanner, A. C. *Chem. Phys.* **1980**, *52*, 353.
56. Malinowski, P.; Tanner, A. C.; Lee, K. F.; Linder, B. *Chem. Phys.* **1981**, *62*, 423; *Int. J. Quantum Chem.* **1982**, *21*, 753.
57. Wozniak, S.; Raof, K. F.; Linder, B. *J. Chem. Phys.* **1983**, *79*, 220.
58. Langhoff, P. W. *J. Phys. Chem.* **1996**, *100*, 2974.
59. Feynman, R. P. *Phys. Rev.* **1939**, *56*, 340.
60. Hirshfelder, J. O.; Eliason, M. A. *J. Chem. Phys.* **1967**, *47*, 1164.
61. Galatry, L.; Gharbi, T. *Chem. Phys. Lett.* **1980**, *75*, 427.
62. Hunt, K. L. C.; Bohr, J. E. *J. Chem. Phys.* **1985**, *83*, 5198.
63. Hunt, K. L. C.; Zilles, B. A.; Bohr, J. E. *J. Chem. Phys.* **1981**, *75*, 3079.
64. Hunt, K. L. C.; Bohr, J. E. *J. Chem. Phys.* **1986**, *84*, 6141.
65. Landau, L. D.; Lifschitz, E. M. *Electrodynamics of Continuous Media*; Addison-Wesley: Oxford, 1960.
66. Janak, J. F. *Phys. Rev. B* **1974**, *9*, 3985.
67. Bartolotti, L. J.; Parr, R. G. *J. Chem. Phys.* **1980**, *72*, 1593.
68. Averill, F. W.; Painter, G. S. *Phys. Rev. B* **1981**, *24*, 6795.
69. Levy, M. *Phys. Rev. A* **1982**, *26*, 1200.
70. Levy, M.; Perdew, J. P. *Phys. Rev. A* **1985**, *32*, 2010.
71. March, N. H.; Santamaria, R. *Int. J. Quantum Chem.* **1991**, *39*, 585.
72. Hessler, P.; Park, J.; Burke, K. *Phys. Rev. Lett.* **1999**, *82*, 378.
73. Parr, R. G.; Yang, W. *Density Functional Theory of Atoms and Molecules*; Oxford University Press: Oxford, 1989.
74. Perdew, J. P.; Burke, K.; Ernzerhof, M. *Phys. Rev. Lett.* **1996**, *77*, 3865.
75. Ziesche, P.; Kurth, S.; Perdew, J. P. *Comput. Mater. Sci.* **1998**, *11*, 122.
76. Perdew, J. P.; Kurth, S.; Zupan, A.; Blaha, P. *Phys. Rev. Lett.* **1999**, *82*, 2544.
77. Freed, K. F.; Levy, M. *J. Chem. Phys.* **1982**, *77*, 396.
78. Rydberg, H.; Lundqvist, B. I.; Langreth, D. C.; Dion, M. *Phys. Rev. B* **2000**, *62*, 6997.
79. Böttcher, C. J. F. *Theory of Electric Polarization*; Elsevier: Amsterdam, 1973).
80. Logan, D. E., *Mol. Phys.* **1981**, *44*, 1271.
81. Perdew, J. P.; Ernzerhof, M.; Zupan, A.; Burke, K. *J. Chem. Phys.* **1998**, *108*, 1522.
82. Lein, M.; Gross, E. K. U.; Perdew, J. P. *Phys. Rev. B* **2000**, *61*, 13431.
83. Palumbo, M.; Onida, G.; Del Sole, R.; Corradini, M.; Reining, L. *Phys. Rev. B* **1999**, *60*, 11329.

84. March, N. H. *Phys. Rev. A* **1997**, *56*, 1025.
85. Filatov, M.; Thiel, W. *Int. J. Quantum Chem.* **1997**, *62*, 603; *Phys. Rev. A* **1998**, *57*, 189.
86. Alvarellos, J. E.; Tarazona, P.; Chacon, E. *Phys. Rev. B* **1986**, *33*, 6579.
87. Garcia-Gonzalez, P.; Alvarellos, J. E.; Chacon, E. *Phys. Rev. B* **1996**, *53*, 9509; **1998**, *57*, 4857.
88. Lee, A. M.; Colwell, S. M. *J. Chem. Phys.* **1994**, *101*, 9704.
89. Van Leeuwen, R.; Baerends, E. J. *Int. J. Quantum Chem.* **1994**, *52*, 711.
90. Wilson, L. C.; Levy, M. *Phys. Rev. B* **1990**, *41*, 12930.
91. Wilson, L. C. *Chem. Phys.* **1994**, *181*, 337.
92. Lee, C. T.; Fitzgerald, G.; Yang, Y. T. *J. Chem. Phys.* **1993**, *98*, 2971.
93. Fan, L. Y.; Ziegler, T. *J. Chem. Phys.* **1991**, *94*, 6057; **1991**, *95*, 7401.
94. Langreth, D. C.; Mehl, M. J. *Phys. Rev. Lett.* **1981**, *47*, 446.
95. Gunnarsson, O.; Jonson, M.; Lundqvist, B. I. *Phys. Lett.* **1976**, *59 A*, 177.
96. Gunnarsson, O.; Jonson, M.; Lundqvist, B. I. *Solid State Commun.* **1977**, *24*, 765; *Phys. Rev. B* **1979**, *20*, 3136.
97. Alonso, J. A.; Girifalco, L. A. *Phys. Rev. B* **1978**, *17*, 3735.
98. Singh, D. J. *Phys. Rev. B* **1993**, *48*, 14099.
99. Sadd, M.; Teter, M. P. *Phys. Rev. B* **1996**, *54*, 13643.
100. Charlesworth, J. P. A. *Phys. Rev. B* **1996**, *53*, 12666.
101. Lundqvist, B. I.; Andersson, Y.; Shao, H.; Chan, S.; Langreth, D. C. *Int. J. Quantum Chem.* **1995**, *56*, 247.
102. Andersson, Y.; Langreth, D. C.; Lundqvist, B. I. *Phys. Rev. Lett.* **1996**, *76*, 102.
103. Dobson, J. F.; Dinte, B. P. *Phys. Rev. Lett.* **1996**, *76*, 1780.
104. Hult, E.; Andersson, Y.; Lundqvist, B. I.; Langreth, D. C. *Phys. Rev. Lett.* **1996**, *77*, 2029.
105. Andersson, Y.; Hult, E.; Apell, P.; Langreth, D. C.; Lundqvist, B. I. *Solid State Commun.* **1998**, *106*, 235.
106. Dobson, J. F.; Wang, J. *Phys. Rev. Lett.* **1999**, *82*, 2123.
107. Dobson, J. F.; Wang, J. *Phys. Rev. B* **2000**, *62*, 10038.
108. Dobson, J. F.; Dinte, B. P.; Wang, J.; Gould, T. *Aust. J. Phys.* **2000**, *53*, 575.
109. Gross, E. K. U.; Dobson, J. F.; Petersilka, M. *Density Functional Theory II: Topics in Current Chemistry* **1996**, *181*, 81.
110. Runge, E.; Gross, E. K. U. *Phys. Rev. Lett.* **1984**, *52*, 997.
111. Petersilka, M.; Gossmann, U. J.; Gross, E. K. U. *Phys. Rev. Lett.* **1996**, *76*, 1212.
112. Vignale, G.; Kohn, W. *Phys. Rev. Lett.* **1996**, *77*, 2037.

Chapter 11

The Protonation Site of Aniline Revisited: A ‘Torture Test’ for Electron Correlation Methods

A. Daniel Boese¹, Jan M. L. Martin¹, Frank De Proft²,
and Paul Geerlings²

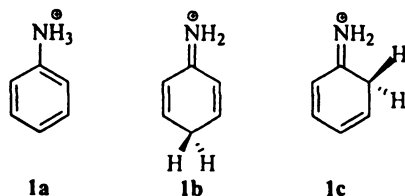
¹Department of Organic Chemistry, Weizmann Institute of Science,
IL-76100 Rehovot, Israel
(email: comartin@wicc.weizmann.ac.il)

²Eenheid Algemene Chemie, Faculteit Wetenschappen, Vrije Universiteit
Brussel, Pleinlaan 2, 1050 Brussels, Belgium
(email: fdeprof@vub.ac.be)

The site of protonation of aniline is revisited using many high level ab initio wave function methodologies and several DFT exchange-correlation functionals. The results indicate that the prediction of the protonation site and the relative energy of the N-, *o*-, and *p*-protonated species depend critically on the method and basis set used. At the highest level of theory (W1c), aniline is predicted to be a nitrogen base with a proton affinity of 211.0 kcal/mol, in very good agreement with experiment, the *p*- and *o*-protonated forms lying respectively 1.1 and 6.2 kcal/mol higher in energy. Despite yielding errors of less than 5 kcal/mol in all cases, all density functional methods considered wrongly predict protonation at the para site.

Introduction

It is a well established fact that the preferred site of protonation of aniline in solution is the nitrogen atom, due to the higher stabilization upon solvation of the N-protonated species with respect to the ring protonated ion (1). In the gas phase however, the situation is less clear, and the preferred site of protonation has been the subject of many experimental and theoretical studies. Based on proton transfer equilibria at 600 K and upon correlation of the proton affinities with σ_p^+ constants for *p*-substituents, Lau and Kebarle concluded that the preferred site of protonation is on the aromatic ring (2). This was confirmed by mass spectroscopic studies involving the collision-activated dissociation of partially deuterated aniline ions, suggesting preferential ring protonation under chemical ionization conditions (3–5). From the correlation of the proton affinities of a series of substituted anilines with N ionization energies, Pollack et al. concluded that the protonation in aniline occurs on the N atom (6).



Karpas et al. used the ion mobility/mass spectroscopy method to show that under atmospheric pressure, protonation of the aniline yields two isomeric ions, a N-protonated and a ring protonated species. Assuming that the N-protonated species is the least mobile of the two, they concluded that protonation occurs on the nitrogen (7). Smith et al. showed that the kinetically favored site of protonation is N (8). The structure of the protonated species was studied by Nold and Wesdemiotis using neutralization-reionization mass spectrometry. Fast atom bombardment ionization was shown to yield predominantly the N-protonated isomer, whereas chemical ionization with a variety of reagents yielded the ring protonated species (9). Minimal basis set Hartree-Fock and semi-empirical calculations have shown that aniline is a nitrogen base, the energy difference between the N and carbon protonated forms being 1–3 kcal/mol (6,10). Sjöberg, Murray, Brinck and Politzer used the average local ionization energy and showed that the para carbon is the most reactive toward electrophiles (11). The absolute minimum in the molecular electrostatic potential of the molecule however is found near the nitrogen atom as was concluded by Ritchie (12). Based on MP2 computations on HF optimized structures, Hillebrand et al. concluded that aniline is protonated on the nitrogen atom (13). Roy, De Proft and Geerlings used DFT based reactivity indices, such as the relative

nucleophilicity, to study the site of protonation of aniline and a series of *m*- and *p*-substituted anilines (14). They also concluded that the nitrogen atom is the site of protonation. These systems were also revisited by Roy et al. in a study addressing the non-negativity of Fukui functions. It was confirmed by Fuentealba, Perez and Contreras that the electrophilic Fukui function indeed predicted the correct protonation site (15). In contrast, Russo et al. concluded that the orbital Fukui function indices, associated with the hardest orbitals, point to the para carbon as the preferred site of protonation (16). Moreover, they performed proton affinity calculations at the B3LYP, BP, MP4 and G2(MP2) levels of theory. All methods indeed predict that the nitrogen and para carbon of the aromatic ring are the thermodynamic most favorable protonation sites. However, the DFT methods and MP4 point to the *p*-carbon as the preferred protonation site, whereas G2(MP2) yields N-protonation: the difference with the *p*-protonated form is only 0.7 kcal/mol. At the G3(MP2) level, N-protonation is favored by 1.2 kcal/mol over ring protonation; this energy difference increases to 10.1 kcal/mol when applying the IPCM continuum method with an ϵ value of 78.3 (water) (17). Water clusters of protonated substituted anilines generated by an electrospray ion source were investigated using a Fourier transform ion cyclotron resonance mass spectrometer by Lee, Cox, Goddard III and Beauchamp (18). From these studies, it was concluded that the preferred site of protonation in the nitrogen atom.

From all this theoretical and experimental work, it can be concluded that the energy difference between the N-protonated form **1a** and the *p*-protonated species **1b** is very small. (The *o*-protonated structure **1c** lies somewhat higher in energy.) Moreover, the relative stability of the two species changes when using different calculation levels and can even change when the basis set is altered for a given methodology. In this contribution, the definitive relative stability of the different protonated aniline species is theoretically established and the performance of the different methods is critically investigated.

Methods

All calculations were carried out on a Compaq GS160 minisupercomputer at Brussels Free University and on a Linux farm consisting of dual-CPU 2GHz and 2.4Ghz Pentium Xeon workstations at the Weizmann Institute of Science.

The coupled cluster calculations involved in W1c theory were carried out using MOLPRO 2002.3. (19) (For the open-shell calculations on the constituent atoms, the definition of the open-shell CCSD and CCSD(T) energies in Ref. (20) was employed.) The density functional calculations were carried out using a modified version of Gaussian 98 rev. All (21), as were the Gn theory (22–24) and CBS-*n* (25) calculations.

Aside from the well-known LDA (local density approximation (26, 27)), BLYP (Becke-Lee-Yang-Parr (28, 29)) and B3LYP (29, 30) functionals, we considered the more recent B97-1 functional (which is a reparametrization (31) of Becke's 1997 hybrid functional), the B97-2 functional (32) (a variation of B97-1 which includes a kinetic energy density term), and the HCTH-407 (33) functional of Boese and Handy (arguably the best GGA functional in existence at the time of writing). The rationale behind the W1c (Weizmann-1 cheap) approach is extensively discussed elsewhere. (34,35) For the sake of self-containedness of the paper, we briefly summarize the steps involved for the specific system discussed here:

- the geometry is optimized at the B3LYP level with a Dunning correlation consistent (36) cc-pVTZ basis set;
- the zero-point energy was obtained from B3LYP/cc-pVTZ harmonic frequencies scaled by 0.985, and rigid rotor-harmonic oscillator (RRHO) thermal corrections were derived from the B3LYP/cc-pVTZ rotational constants and harmonic frequencies;
- CCSD(T)/cc-pVnZ+aug(N) ($n=D,T$) calculations are carried out using a conventional (disk-based) algorithm, where aug(N) stands for the use of the diffuse function augmented aug-cc-pVnZ basis set on the nitrogen atom;
- an integral-direct (37) CCSD/cc-pVQZ+aug(N) is carried out;
- the SCF energy is extrapolated to the infinite basis limit using $E_{\infty} = E_L + (E_L - E_{L-1})/((L/L-1)^{\alpha}-1)$, where $\alpha = 5$ and $L = \{3,4\}$ for {VTZ,VQZ} respectively;
- the CCSD valence correlation energy is extrapolated using the same expression, but using $\alpha = 3.22$;
- the (T) contribution is extrapolated in the same manner but using $L = \{2,3\}$ for {VDZ,VTZ};
- the inner-shell correlation and scalar relativistic contributions are obtained using the Martin-Sundermann-Fast-Truhlar (MSFT) (38) bond-additivity model

The 'ultrafine' pruned (99,590) integration grid was used in all DFT calculations.

Table I: Computed total atomization energy at 0 K of aniline and proton affinities at 298 K for protonation at different sites. Proton affinities for N-protonation of aniline. All values are given in kcal/mol.

	TAE ₀	PA ₂₉₈ N-prot. ^a	PA ₂₉₈ para	PA ₂₉₈ ortho	N-prot. para vs.	para vs. ortho
Expt. (39)	1467.7±0.7	210.9				
W1c	1468.7	211.0	209.9	204.9	1.1	5.1
G1	1462.7	210.8	209.2	204.3	1.6	4.9
G2	1464.0	211.4	210.0	205.1	1.4	4.9
G2MP2	1463.0	211.5	209.9	205.0	1.6	4.9
G3	1467.0	211.4	209.8	204.8	1.6	5.0
G3B3	1467.3	211.4	209.9	204.8	1.5	5.1
CBS-Q	1468.8	210.5	207.9	204.2	2.7	3.6
CBS-QB3	1466.2	211.4	208.3	203.2	3.1	5.1
SVWN3	1738.2	203.1	204.3	199.6	-1.2	4.7
BLYP	1459.7	209.9	212.5	208.5	-2.7	4.1
B3LYP	1461.2	211.0	212.8	208.3	-1.8	4.5
B97-1	1468.7	212.5	214.0	209.5	-1.5	4.4
B97-2	1472.2	213.7	215.0	210.6	-1.4	4.5
HCTH/407	1465.0	212.6	214.9	210.8	-2.3	4.1
HF/VDZ+		215.1	219.8	214.1	-4.8	5.8
HF/VTZ+		215.6	220.7	214.7	-5.1	5.9
HF/VQZ+		215.4	220.5	214.6	-5.2	5.9
HF limit		215.3	220.5	214.5	-5.2	5.9
CCSD/VDZ+		213.9	214.3	209.1	-0.5	5.3
CCSD/VTZ+		213.2	213.5	208.0	-0.4	5.5
CCSD/VQZ+		212.6	212.9	207.4	-0.2	5.5
CCSD limit		212.3	212.5	207.0	-0.1	5.5
MP2/VTZ+		210.0	203.8	198.8	6.2	5.0
CCSD/VTZ+		213.2	213.5	208.0	-0.4	5.5
CCSD(T)/VTZ+		212.1	211.4	206.3	0.7	5.1
CCSD[T]/VTZ+		211.9	211.7	206.6	0.3	5.1

^a includes correction for internal rotation of the -NH₃⁺ group (RT/2, +0.3 kcal/mol)

Results and Discussion

All relevant results are gathered in Table I.

The relative energies apparently exhibit a rather weak basis set dependence: the equilibrium between the N- and *p*-protonated forms is driven by electron correlation, while the ortho-para equilibrium is apparently quite well reproduced even at the HartreeFock level. We may safely argue that the W1c results are converged with respect to the basis set.

The W1c total atomization energy at 0 K of aniline, 1468.7 kcal/mol, is in satisfying agreement with the value obtained from heats of formation in the NIST WebBook (39), 1467.7±0.7 kcal/mol. (Most of the uncertainty derives from the heat of vaporization of graphite.) The various contributions to this result are (in kcal/mol): SCF limit 1144.4, valence CCSD correlation energy limit 359.0, connected triple excitations 31.7, inner shell correlation 7.6, scalar relativistic effects -1.2, atomic spin-orbit coupling -0.5 kcal/mol. Extrapolations account for 0.6, 12.1, and 2.5 kcal/mol, respectively, out of the three first contributions.

As the MSFT (38) additivity model predicts only very weak core correlation and scalar relativistic contributions to the proton affinity, we have not attempted their explicit (and very expensive) calculation.

The B3LYP B97-*n*, and HCTH/407 compare quite well to experiment and W1c: it should be recalled that all four functionals were wholly or partially fitted to atomization energies. The B97-1 result in fact is identical to W1c, while the 'pure DFT' HCTH/407 functional does surprisingly well.

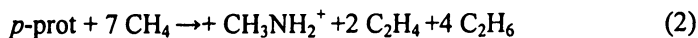
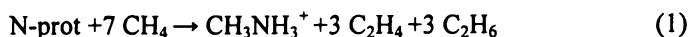
The relative energies of the three protonated species are well reproduced by all methods from the G_n family. This can largely be explained by (a) the fact that all these methods involved CCSD(T) or QCISD(T) steps (and apparently triple excitations are quite important here); (b) the relatively rapid basis set convergence noted above, which means that it is not really an issue that the CCSD(T) and QCISD(T) steps are carried out in relatively small basis sets. CBS-QB3 likewise reproduces the relative energetics quite well.

As has been pointed out in the past (e.g. concerning the linear-cyclic equilibrium in C₆ and C₁₀ carbon clusters (40)), Hartree-Fock underestimates the resonance stabilization of aromatic relative to non-aromatic systems (in the case at hand, between the N- and *p*-protonated isomers) and MP2 overcorrects. The structures are found to be nearly isoenergetic at the CCSD level; inclusion of connected triple excitations favors the N-protonated ion. The direction of the effect of connected quadruples is somewhat unclear, and a CCSD(TQ) or CCSDT(Q) calculation impossible on systems this size, but the contribution will anyhow be much smaller in absolute magnitude than that of connected triple excitations, particularly for systems like these which are dominated by a single reference determinant. We may therefore infer that at the full CI limit, the N-protonated species will be slightly more stable than its *p*-protonated counterpart.

On the other hand, the PAs at the para and ortho positions are manifestly more sensitive to the electron correlation treatment than the PA at the nitrogen. From the point of view of the \mathcal{T}_1 diagnostic (a measure for the importance of nondynamical correlation), aniline ($\mathcal{T}_1=0.0113$) and N-anilinium ($\mathcal{T}_1=0.0096$) are very similar (and basically purely single-reference), while the *p*- and *o*-protonated species exhibit very mild multireference character (0.0149 and 0.0157, respectively). Since protonation at these sites thus involves a noticeable change in \mathcal{T}_1 , the PA is expected to be more sensitive to the correlation method.

Let us now turn to the density functional methods. All of them correctly predict the para-ortho ordering, but considering that this is the case even for a Hartree-Fock treatment this is a somewhat hollow victory. Without exception, all functionals wrongly predict *p*-protonation. Arguably, this small energy difference falls within the error margin of any type of calibration for (semi-) 'empirical' DFT functionals.

In an attempt at finding the 'root cause' of this failure of DFT, we first estimate the conjugation stabilization of the cations by means of isodesmic reaction energies at the CCSD(T)/cc-pVTZ+aug(N) and B3LYP/cc-pVTZ+aug(N) levels. (The same qualitative trends are exhibited by other DFT methods.) The isodesmic reactions



have stabilization energies of 65.9 and 67.0 kcal/mol at the CCSD(T) level of theory, respectively. This result is somewhat counterintuitive, since one might expect the conjugation energy of the (aromatic) N-protonated aniline to be the greater of the two. Still, B3LYP overestimates reaction (1) by 3.2 and (2) by 3.8 kcal/mol, hence favoring the *p*-protonated aniline by an additional 0.6 kcal/mol. Nevertheless, this does not fully account for the 2.5 kcal/mol discrepancy between B3LYP and CCSD(T) for the energy difference between N- and *p*-protonated aniline.

A second potential source of error may be overstabilization of the 'tautomeric' form of aniline, 2,5-cyclohexadien-1-imine. At the CCSD(T)/cc-pVTZ+aug(N) level, the energy difference is 23.9 kcal/mol. This, incidentally, implies a very high proton affinity for the tautomeric form of 235.3 kcal/mol. However, while B3LYP overestimates the tautomerization energy by 3.5 kcal/mol compared to CCSD(T), it does so even more (4.9 kcal/mol) for the imine proton affinity, which is enough to tip the scales to the wrong protonation site. Considering the proton affinities of some small model compounds at the B3LYP/cc-pVTZ+aug(N) and CCSD(T)/cc-pVTZ+aug(N) levels, we find an overestimate by B3LYP of 1.7 kcal/mol for CH_2NH , and 3.1 kcal/mol for vinyl imine. The 'Schiff base tautomer' of aniline has two conjugated branches similar to vinyl imine, and exhibits an even larger overestimate. (Similar findings are seen with other exchange-correlation functionals.)

Overall, we see that imperfect cancellation between two (apparently systematic) errors leads to DFT consistently predicting the wrong protonation site.

Conclusions

In this contribution, the protonation site of aniline has been revisited. From our results, it can be inferred that at the full CI limit, the N-protonated species will be slightly more stable than the *p*-protonated one. For this problem, W1c theory was found to be converged in basis set and pointed to an N-protonation of the base, the *p*- and *o*-protonated forms lying respectively 1.1 and 6.2 kcal/mol higher in energy. The resonance stabilization of N-protonated relative to the *p*-protonated species is underestimated by Hartree-Fock theory, whereas MP2 overestimates it. At the CCSD level both forms are nearly isoenergetic, the inclusion of connected triples favoring protonation on the nitrogen. Furthermore, considering the \mathcal{T}_1 diagnostic, aniline and the N-protonated conjugate acid are classified as having essentially single-reference character, while the *p*-protonated and *o*-protonated forms exhibit very mild multireference character. Finally, all the DFT methods considered severely overestimate the proton affinity of 2,5-cyclohexadien-1-imine at nitrogen, hence erroneously predicting protonation of aniline at the para site rather than on the nitrogen.

Acknowledgments

JMLM is a member of the Helen and Martin Kimmel Center for Molecular Design. ADB acknowledges a postdoctoral fellowship from the Feinberg Graduate School. Research at the Weizmann Institute was partially supported by the Minerva Foundation, Munich, Germany.

Supporting Information

B3LYP/cc-pVTZ geometries and vibrational frequencies, as well as total energies at all levels of theory, are available on the World Wide Web at <http://theochem.weizmann.ac.il/web/papers/aniline.html>

Literature Cited

1. McMurry, J. *Organic Chemistry*, Fifth Edition, Brooks/Cole, 2000.
2. Lau, Y. K.; Kebarle, P. *J. Am. Chem. Soc.* **1976**, *98*, 7452.

3. Wood, K. V.; Burinsky, D. J.; Cameron, D.; Cooks, R. G. *J. Org. Chem.* **1983**, *48*, 5236.
4. Pachuta, S. J.; Isern-Flecha, I.; Cooks, R. G. *Org. Mass. Spectrom.* **1986**, *21*, 1.
5. Maquestiau, A.; Van Haverbeke, Y.; Misprouve, H.; Flammang, R.; Harris, J. A.; Howe, I.; Benon, J. H. *Org. Mass. Spectrom.* **1980**, *15*, 144.
6. Pollack, S. K.; Devlin III, J. L.; Summerhays, K. D.; Taft, R. W.; Hehre, W. J. *J. Am. Chem. Soc.* **1977**, *99*, 4583.
7. Karpas, Z.; Berant, Z.; Stimac, R. M. *Struct. Chem.* **1990**, *1*, 201.
8. Smith, R. L.; Chyall, L. J.; Beaseley, B. J.; Kentamaa, H. I. *J. Am. Chem. Soc.* **1995**, *117*, 201.
9. Nold, M. J.; Wesdemiotis, C. J. *Mass. Spectrom.* **1996**, *31*, 1169.
10. Dewar, M. J. S.; Dieter, K. M. *J. Am. Chem. Soc.* **1986**, *108*, 8075.
11. Sjoberg, P.; Murray, J. S.; Brinck, T.; Politzer, P. *Can. J. Chem.* **1990**, *68*, 1440.
12. Ritchie, J. P. *J. Mol. Struct. (Theochem)* **1992**, *225*, 297.
13. Hillebrand, C.; Klessinger, M.; Eckert-Maksić, M.; Maksić, Z. B. *J. Phys. Chem.* **1996**, *100*, 9698.
14. Roy, R. K.; De Proft, F.; Geerlings, P. *J. Phys. Chem. A* **1998**, *102*, 7035.
15. Fuentealba, P.; Perez, P.; Contreras, R. *J. Chem. Phys.* **2000**, *113*, 2544.
16. Russo, N.; Toscano, M.; Grand, A.; Mineva, T. *J. Phys. Chem. A* **2000**, *104*, 4017.
17. Bagno, A.; Terrier, F. *J. Phys. Chem. A* **2001**, *105*, 6537.
18. Lee, S.-W.; Cox, H.; Goddard III, W. A.; Beauchamp, J. L. *J. Am. Chem. Soc.* **2000**, *122*, 9201.
19. MOLPRO is a package of ab initio programs written by H.-J. Werner and P. J. Knowles, with contributions from J. Almlöf, R. D. Amos, A. Berning, D. L. Cooper, M. J. O. Deegan, A. J. Dobbyn, F. Eckert, S. T. Elbert, C. Hampel, R. Lindh, A. W. Lloyd, W. Meyer, A. Nicklass, K. Peterson, R. Pitzer, A. J. Stone, P. R. Taylor, M. E. Mura, P. Pulay, M. Schütz, H. Stoll, and T. Thorsteinsson.
20. Watts, J. D.; Gauss, J.; Bartlett, R. J.; *J. Chem. Phys.* **1993**, *98*, 8718.
21. Frisch, M. J.; Trucks, G. W.; Schlegel, H. B.; Scuseria, G. E.; Robb, M. A.; Cheeseman, J. R.; Zakrzewski, V. G.; Montgomery, Jr., J. A.; Stratmann, R. E.; Burant, J. C.; Dapprich, S.; Millam, J. M.; Daniels, A. D.; Kudin, K. N.; Strain, M. C.; Farkas, O.; Tomasi, J.; Barone, V.; Cossi, M.; Cammi, R.; Mennucci, B.; Pomelli, C.; Adamo, C.; Clifford, S.; Ochterski, J.; Petersson, G. A.; Ayala, P. Y.; Cui, Q.; Morokuma, K.; Salvador, P.; Dannenberg, J. J.; Malick, D. K.; Rabuck, A. D.; Raghavachari, K.; Foresman, J. B.; Cioslowski, J.; Ortiz, J. V.; Baboul, A. G.; Stefanov, B. B.; Liu, G.; Liashenko, A.; Piskorz, P.; Komaromi, I.; Gomperts, R.; Martin, R. L.; Fox, D. J.; Keith, T.; Al-Laham, M. A.; Peng, C. Y.; Nanayakkara, A.; Challacombe, M.; Gill, P. M. W.; Johnson, B. G.; Chen, W.; Wong, M. W.;

- Andres, J. L.; Gonzalez, C.; Head-Gordon, M.; Replogle, F. S.; Pople, J. A.; Gaussian 98, Revision A.]] (Gaussian, Inc., Pittsburgh, PA, 1998).
22. Curtiss, L. A.; Raghavachari, K.; Trucks, G. W.; Pople, J. A.; *J. Chem. Phys.* **1991**, *94*, 7221.
 23. Curtiss, L. A.; Raghavachari, K.; Redfern, P. C.; Rassolov, V.; Pople, J. A.; *J. Chem. Phys.* **1998**, *109*, 7764.
 24. Curtiss, L. A.; Redfern, P. C.; Raghavachari, K.; Pople, J. A.; *J. Chem. Phys.* **2001**, *114*, 108.
 25. Montgomery, Jr., J. A.; Frisch, M. J.; Ochterski, J. W.; Petersson, G. A.; *J. Chem. Phys.* **1999**, *110*, 2822 and references therein.
 26. Slater, J. C.; *Phys. Rev.* **1951**, *81*, 385.
 27. Vosko, S.H.; Wilk, L.; Nusair, M.; *Can J. Phys.* **1980**, *58*, 1200.
 28. A. D. Becke, *Phys. Rev. A* **1988**, *38*, 3098.
 29. Lee, C.; Yang, W.; Parr, R. G.; *Phys. Rev. B* **1988**, *37*, 785.
 30. Becke, A. D.; *J. Chem. Phys.* **1993**, *98*, 5648.
 31. Hamprecht, F. A.; Cohen, A. J.; Tozer, D. J.; Handy, N. C.; *J. Chem. Phys.* **1998**, *109*, 6264.
 32. Wilson, P. J.; Bradley, T. J.; Tozer, D. J.; *J. Chem. Phys.* **2001**, *115*, 9233.
 33. Boese, A. D.; Handy, N. C.; *J. Chem. Phys.* **2001**, *114*, 5497.
 34. Martin, J. M. L.; de Oliveira, G. *J. Chem. Phys.* **1999**, *111*, 1843.
 35. Martin, J. M. L.; Parthiban, S. in: *Quantum-mechanical prediction of thermochemical data* (ed. J. Cioslowski), *Understanding Chemical Reactivity*, vol. 22 (Kluwer Academic Publishers, Dordrecht, 2001), pp. 31–65.
 36. Dunning Jr., T.H.; Peterson, K.A.; Woon, D.E.; “Correlation consistent basis sets for molecular calculations”, in *Encyclopedia of Computational Chemistry*, ed. P. von Ragué Schleyer, (Wiley & Sons, Chichester, 1998), pp. 88–115.
 37. Schütz, M.; Lindh, R.; Werner, H.-J.; *Mol. Phys.* **1999**, *96*, 719
 38. Martin, J. M. L.; Sundermann, A.; Fast, P. L.; Truhlar, D. G.; *J. Chem. Phys.* **2000**, *113*, 1348
 39. Afeefy, H.Y.; Liebman, J.F.; Stein, S.F.; “Neutral Thermochemical Data”, and Hunter, E.P.; Lias, S. G.;, “Proton Affinity Data”, in NIST Chemistry WebBook, NIST Standard Reference Database Number 69, Mallard, W.G.; Linstrom, P.G.; Eds.; February 2000, National Institute of Standards and Technology, Gaithersburg, MD, 20899; <http://webbook.nist.gov>.
 40. Martin, J. M. L.; Taylor, P. R. *J. Phys. Chem.* **1996**, *100*, 6047

Chapter 12

Equilibrium Structure of the Silicon Trimer

John F. Stanton

Institute for Theoretical Chemistry, Departments of Chemistry and
Biochemistry, The University of Texas at Austin, Austin, TX 78712
email: jfstanton@mail.utexas.edu

Recent microwave data for the potential interstellar molecule Si_3 is used together with high-level coupled-cluster calculations to extract an accurate equilibrium structure. Observed rotational constants for several isotopomers have been corrected for effects of vibration-rotation interaction; subsequent least-squares refinements of structural parameters provide the equilibrium structure. This combined experimental-theoretical approach yields the following parameters for this C_{2v} molecule: $r_e(\text{SiSi}) = 2.173 \pm 0.002 \text{ \AA}$ and $\theta_e(\text{SiSiSi}) = 78.1 \pm 0.2^\circ$.

In addition to its undeniable importance in various areas of materials science, silicon is one of the most abundant elements in the universe. Consequently, molecules containing one or more silicon atoms are expected to be present in the interstellar medium. Indeed, the blue-green emission of SiC_2 from N-type stars and comets was first observed in 1926 (1,2). Laboratory observation allowed these features to be assigned to this interesting molecular species three decades later (3). SiC_2 has since been found in the interstellar gas by radioastronomy (4), and is a popular subject in *ab initio* investigations due to its extreme nonrigidity (5). To date, nine silicon-containing molecules have been detected in the interstellar medium (6), a list that should continue to grow.

Laboratory study of discharge products has proven to be an extremely useful means for detecting potential interstellar molecules (7). As an illustrative example, two isomers of the cyclic SiC₃ molecule are generated in a silane-diacetylene discharge, and the respective microwave spectra were recorded in 1999 (8,9). The rotational constants were then used to guide an astronomical search, and the more stable of the two isomers was found (10) immediately in the evolved carbon star IRC + 10216. A later high-level *ab initio* study established an accurate thermodynamic energy difference between the cyclic forms as well as precise equilibrium geometries for both (11).

The purpose of this report is to demonstrate the ease with which highly accurate equilibrium structures can be determined by combining laboratory microwave data with the results of *ab initio* calculations. In this procedure, the effects of vibration-rotation interaction are calculated and removed from the observed rotational constants, A_0 , B_0 and C_0 . The resulting values correspond to approximate rigid-rotor constants A_e , B_e and C_e and are thus inversely proportional to the principal moments of inertia. A subsequent least-squares fitting of the independent structural parameters to the corrected constants yields the equilibrium structure, provided that the number of available and independent rotational constants is greater than or equal to the number of internal degrees of freedom in the totally symmetric subspace (which is the same as the number of totally symmetric vibrational modes).

Determination of the equilibrium structure for a polyatomic molecule by means of the method outlined in the preceding paragraph was apparently first carried out by Meyer, Pulay and Boggs a quarter-century ago (12). The same approach has been used by Allen and collaborators in the last decade (13,14). In recent years, the availability of analytic second derivative methods at highly correlated levels of theory (15) has made the determination of accurate anharmonic force fields for polyatomic molecules a relatively routine procedure. When the goal is to calculate vibration-rotation contributions to rotational constants, it is simpler still since only cubic force constants of the type ϕ_{ij} are needed (16), where i is a totally symmetric normal coordinate. These are conveniently evaluated by double-sided numerical differentiation of analytic second derivatives along totally symmetric displacements. Hence, for a molecule with n internal degrees of freedom, $2n$ analytic second derivative calculations are needed in addition to that carried out at the undisplaced geometry¹. The latter calculation provides the harmonic force field, which is needed for some of the contributions to the vibration-rotation interaction Hamiltonian.

The vibration-rotation contribution to rotational constants is given (through lowest order) by the interaction constants $\alpha_i^{(A,B,C)}$ via

¹ However, if isotopomers are considered in which the point group symmetry is lowered by substitution it is necessary to calculate additional cubic constants. Isotopomers III and V in the present work are of this type, so the full cubic force field was evaluated.

$$B_0 = B_e - \sum_i \left(n_i + \frac{1}{2} \right) \alpha_i^B$$

with similar expressions for A and C . The sum runs over all vibrational modes and n_i is the vibrational quantum number. The constants α are determined entirely by the structure, quadratic and cubic force fields of the molecule in question (16). In principle, the interaction constants can be determined from high-resolution vibrational spectroscopy by measuring the vibrational state dependence of the rotational constants. However, this is rarely possible to accomplish for a polyatomic molecule; even then the procedure is often plagued by Coriolis resonances that arise when vibrational states of the molecule are nearly degenerate. Here, theory offers an advantage because it is the sum of the interaction constants for a particular axis *rather than their individual values* that is the relevant quantity. Since the difference between B_0 and B_e (or the associated differences for the other two axes) is a property of the ground state – which is not generally quasidegenerate – it should not be affected by the resonance interactions that plague the individual constants. Indeed, one can show that the sum of the constants can be written in a form in which there are no denominators involving vibrational frequencies (14). Hence, the use of theory offers tremendous advantages since it does not require rotationally-resolved spectroscopic analysis of all fundamental vibrational transitions and the Coriolis resonance problem is avoided. For these reasons, the combination of experimental rotational constants and high-level calculations of $A_0 - A_e$, $B_0 - B_e$ and $C_0 - C_e$ appears to be the most reliable means for determining equilibrium (r_e) structures of polyatomic molecules. Reviewed elsewhere (17), this procedure has been employed in recent years to determine r_e structures of the prototype organic molecules benzene (18) and cyclopropane (19), as well as a number of other systems.

In this paper, the mixed experimental-theoretical approach for determining r_e structures is applied to the silicon trimer. For reasons stated in the opening paragraph, this molecule is of obvious astrophysical interest. Furthermore, its microwave spectrum has recently been recorded (20). This should serve to direct astronomical searches for Si_3 , although the dipole moment (calculated in the present research as *ca.* 0.4 D) suggests that detection might be difficult. Previous quantum chemical studies of Si_3 have revealed that there are nearly degenerate isomers (21): a singlet with C_{2v} symmetry and a triplet with the structure of an equilateral triangle (D_{3h}). The energy difference between these forms is small, but the singlet is predicted to lie below the triplet. The electronic spectrum of Si_3 has been recorded in matrix isolation (22) and was interpreted in terms of an isosceles triangle (C_{2v}) structure, a finding that agrees with the recently recorded microwave spectrum.

Harmonic and cubic force fields of Si_3 were calculated using coupled-cluster (CC) theory (23) and a correlation-consistent basis set. Specifically, the CC singles and doubles (CCSD) method (24) was used in conjunction with the cc-pVTZ basis set (25) developed by Dunning and co-workers. The force

constants were calculated by the methods described earlier and elaborated in Ref. (26) using a local version of the ACES II program system (27). The resulting values, together with additional parameters needed to evaluate the rigid-rotor rotational constants A_e , B_e and C_e are collected in Table I.

Five isotopomers of Si_3 were studied in Ref. (20), and are labeled as follows: $^{28}\text{Si}-^{28}\text{Si}-^{28}\text{Si}$ (I); $^{28}\text{Si}-^{29}\text{Si}-^{28}\text{Si}$ (II); $^{28}\text{Si}-^{28}\text{Si}-^{29}\text{Si}$ (III); $^{28}\text{Si}-^{30}\text{Si}-^{28}\text{Si}$ (IV); $^{28}\text{Si}-^{28}\text{Si}-^{30}\text{Si}$ (V). Rotational constants for each (both corrected and uncorrected for vibration-rotation interaction) can be found towards the bottom of Table I. Structures obtained by various refinement procedures are collected in Table II. Two distinct fitting procedures were used. In the first, the structures were refined against all three rotational constants A , B and C while only A and C were used in the second procedure. Since truly planar nuclear configurations have only two independent moments of inertia ($\Delta \equiv I_a - I_b - I_c = 0$), use of B (or C) involves a redundancy if the other is included. In practice, however, vibration-rotation effects spoil the exact proportionality between rotational constants and reciprocal moments of inertia and values of Δ calculated from effective moments of inertia determined from the A_0 , B_0 and C_0 constants do not vanish. Hence refining effective (r_0) structures against all three is not without merit. Δ_0 is called the inertial defect and amounts to *ca.* 0.4 amu \AA^2 for all five isotopomers. After correcting by the calculated vibration-rotation interactions, the inertial defect is reduced by an order of magnitude in all cases.

Since Si_3 has only two independent structural parameters – the Si-Si bond length and the Si-Si-Si bond angle – the set of rotational constants for each isotopomer is sufficient to determine a structure, and this has been carried out for isotopomers I-V. Two things should be noted. First, distances and angles inferred from the independent constants A and C differ from those obtained via least-squares adjustment to all three uncorrected constants by roughly 0.02 \AA and 0.1° . However, these differences are reduced by an order of magnitude when vibration-rotation corrections are applied. The remaining difference is of course due to the fact that there is a residual inertial defect of *ca.* 0.03 amu \AA^2 for the isotopomers¹; inferred parameters would be identical for a precisely zero Δ when the third constant is rigorously redundant. Second, the structural parameters determined for all of the isotopomers are in excellent agreement, suggesting that there are no systematic problems with any of the experimental rotational

¹ In a previous study of cyclic Si_3 , a residual inertial defect of only slightly smaller magnitude was found, despite the fact that an extremely high level of calculation (surpassing that in the present study) was used to determine the vibration-rotation interaction contributions to the rotational constants. This was subsequently traced to the so-called electronic contribution, which arises from a breakdown of the assumption that the atoms can be treated as point masses at the nuclear positions. Corrections for this somewhat exotic effect were carried out in that work and reduced the inertial defect from about 0.20 to less than 0.003 amu \AA^2 . However, the associated change in the rotational constants had an entirely negligible effect on the inferred structural parameters. Hence, this issue is not considered further in this work.

Table I: Harmonic frequencies and cubic force constants (in the reduced normal coordinate representation) for the normal isotopomer (I) of Si₃ (top). Measured rotational constants and effective equilibrium values (in MHz) for the five isotopomers described in the text (bottom).

Harmonic Frequencies (cm ⁻¹)				Cubic force constants (cm ⁻¹)		
	$\omega_1(a_1)$	578		ϕ_{111}	106	
	$\omega_2(a_1)$	548		ϕ_{112}	4	
	$\omega_3(b_2)$	203		ϕ_{122}	1	
				ϕ_{222}	59	
				ϕ_{133}	106	
				ϕ_{233}	106	
Isomer	Uncorrected Constants (MHz)			Corrected Constants (MHz)		
	A_0^a	B_0^a	C_0^a	A_e	B_e	C_e
I	9506.1	4809.3	3185.9	9514.2	4817.5	3197.3
II	9287.9	4809.2	3161.0	9295.4	4817.5	3172.2
III	9452.2	4725.5	3143.0	9460.4	4733.5	3154.1
IV	9084.7	4809.1	3137.0	9091.7	4817.5	3148.1
V	9403.7	4645.8	3102.2	9412.0	4653.5	3113.1

^a From Reference (20).

Table II: Refined structural parameters for Si₃, based on the rotational constants in Table I. For the set of five isotopomers, maximum least-squares residuals for the fits to all three constants and just *A* and *C* are 6.38 and 0.70 MHz, respectively, for the uncorrected constants. Corresponding values obtained in fits to the effective equilibrium constants are 0.74 and 0.07 MHz.

Isotopomer	<u>Uncorrected</u>		<u>Corrected</u>	
	Fit to <i>A</i> ₀ , <i>B</i> ₀ , <i>C</i> ₀		Fit to <i>A</i> _e , <i>B</i> _e , <i>C</i> _e	
Refined Bond Length (Angstroms)				
I	2.1748	2.1761	2.1732	2.1734
II	2.1748	2.1761	2.1733	2.1733
III	2.1748	2.1760	2.1732	2.1734
IV	2.1747	2.1760	2.1732	2.1734
V	2.1748	2.1760	2.1732	2.1734
I-V	2.1748	2.1760	2.1732	2.1734
Refined Bond Angle (degrees)				
I	78.15	78.23	78.11	78.12
II	78.15	78.24	78.11	78.12
III	78.15	78.23	78.11	78.12
IV	78.15	78.24	78.11	78.12
V	78.14	78.23	78.11	78.12
I-V	78.15	78.23	78.11	78.12

constants. Because of the second consideration, the r_0 and r_e structures obtained by least-squares fits to all of the rotational constants are essentially the same as those determined for the individual isotopomers.

The results of this study are somewhat atypical in the sense that the inferred r_e and r_0 structures of Si₃ are nearly the same. This is a somewhat fortuitous circumstance, which cannot be attributed entirely to the fact that Si₃ appears to be only weakly anharmonic (see cubic constants in Table I), since it has a relatively low-frequency bending mode that is potentially problematic. Nonetheless, it can be stated with some certainty that the r_e structure obtained in the present research is accurate to within 0.002 Å and 0.2°. Hence, this structure can be used as a reference for benchmarking quantum chemical methods intended for high accuracy calculations on silicon clusters, as well as for comparison with structures of other silicon-containing molecules.

Acknowledgement

This work was supported by the Robert A. Welch and National Science Foundations. M.C. McCarthy and P. Thaddeus (Harvard) are thanked for a preprint of Ref. (20).

References

1. P.W. Merrill *Publ. Astron. Soc. Pac.* 38, 175 (1926).
2. R.F. Sanford *Publ. Astron. Soc. Pac.* 38, 177 (1926).
3. B. Kleman *Astrophys. J.* 123, 162 (1956).
4. P. Thaddeus, S.E. Cummins and R.A. Linke *Astrophys. J. Lett.* 283, L45 (1984).
5. S.C. Ross, T.J. Butenhoff, E.A. Rohlfing and C.M. Rohlfing *J. Chem. Phys.* 100, 4110 (1994), and references therein.
6. See: <http://cfa-www.harvard.edu/cfa/mmw/mmwlab/ismmoleculesorganic.html> for a list of interstellar species detected to date.
7. P. Thaddeus and M.C. McCarthy *Spectrochim. Acta A* 57, 757 (2001).
8. M.C. McCarthy, A.J. Apponi and P. Thaddeus *J. Chem. Phys.* 110, 10645 (1999); A.J. Apponi, M.C. McCarthy, C.A. Gottlieb and P. Thaddeus *J. Chem. Phys.* 111, 3911 (1999).
9. M.C. McCarthy, A.J. Apponi and P. Thaddeus *J. Chem. Phys.* 111, 7175 (1999).
10. A.J. Apponi, M.C. McCarthy, C.A. Gottlieb and P. Thaddeus *Astrophys. J.* 516, L103 (1999).
11. J.F. Stanton, J. Gauss and O. Christiansen *J. Chem. Phys.* 114, 2993 (2001).
12. P. Pulay, W. Meyer and J.E. Boggs *J. Chem. Phys.* 68, 5077 (1978).
13. A.L.L. East, W.D. Allen and S.J. Klippenstein *J. Chem. Phys.* 102, 8506 (1995).
14. W.D. Allen, A.L.L. East and A.G. Csaszar, in *Structures and Conformations of Nonrigid Molecules*, edited by J. Laane, M. Dakkouri, B. va der Vecken and H. Oberhammer (Kluwer, Dordrecht, 1993), p. 343; A.L.L. East, C.S. Johnson and W.D. Allen *J. Chem. Phys.* 98, 1299 (1993).
15. J. Gauss and J.F. Stanton *Chem. Phys. Lett.* 276, 70 (1997).
16. I.M. Mills, in *Modern Spectroscopy: Modern Research* edited by K.N. Rao and C.W. Matthews (Academic Press, New York, 1972), pp. 115-140.
17. J.F. Stanton and J. Gauss *Int. Rev. Phys. Chem.* 19, 61(2000).
18. J. Gauss and J.F. Stanton *J. Phys. Chem.* A104, 2865 (2000).
19. J. Gauss, D. Cremer and J.F. Stanton *J. Phys. Chem.* A104, 1319 (2000).
20. M.C. McCarthy and P. Thaddeus *Astrophys. J.*, submitted.
21. R. Fournier, S.B. Sinnott and A.E. DePristo *J. Chem. Phys.* 97, 4149 (1992); D.A. Dixon and J.L. Gole *Chem. Phys. Lett.* 188, 560 (1992); R.S. Grey and H.F. Schaefer *Chem. Phys. Lett.* 119, 111 (1985).

22. J. Fulara, P. Freivogel, M. Grutter and J.P. Maier *J. Phys. Chem.* 100, 18042 (1996).
23. For a recent review, see:
24. G.D. Purvis and R.J. Bartlett *J. Chem. Phys.* 76, 1910 (1982).
25. D.E. Woon and T.H. Dunning *J. Chem. Phys.* 98, 1358 (1993).
26. J.F. Stanton, C.L. Lopreore and J. Gauss *J. Chem. Phys.* 108, 7190 (1998).
27. J.F. Stanton, J. Gauss, J.D. Watts, W.J. Lauderdale and R.J. Bartlett *Int. J. Quantum Chem.* S26, 879 (1992).

Author Index

- Abrams, Micah L., 75
Boese, A. Daniel, 183
Bytautas, Laimutis, 103
De Proft, Frank, 183
Dutta, Antara, 75
Fan, Peng-Dong, 37
Geerlings, Paul, 183
Gill, Peter M. W., 27
Hunt, Katharine L. C., 169
Klopper, Wim, 1
Kowalski, Karol, 37
Krylov, Anna I., 89
Kümmel, Stephan, 13
Levchenko, Sergey V., 89
Lynch, Benjamin J., 153
Martin, Jan M. L., 183
O'Neill, Darragh P., 27
Perdew, John P., 13
Peterson, Kirk A., 125
Piecuch, Piotr, 37
Pimienta, Ian S. O., 37
Ruedenberg, Klaus, 103
Samson, Claire C. M., 1
Sears, John S., 75
Sherrill, C. David, 75
Slipchenko, Lyudmila V., 89
Stanton, John F., 193
Tao, Jianmin, 13
Truhlar, Donald G., 153
Wilson, Angela K., ix

Subject Index

A

Ab initio methods

equilibrium structures, 194
mean unsigned error vs. cost, 160,
164*f*

quantitative studies, 104

AM1 semi-empirical method

description, 154–155
mean unsigned errors, root-mean-
square errors, and costs, 160,
163*t*
mean unsigned error vs. cost, 160,
164*f*

Aniline. *See* Protonation site of aniline

Approximations, hierarchy of, to *n*-
electron wavefunction, 91*f*

Atomization energies (AEs)

aniline, 187*t*
lithium hydride, 159*t*
test set, 157–158

B

Barrier heights (BHs), test set with
forward and reverse reaction,
157

Basis functions. *See* Correlated basis
functions for large molecules

Basis sets. *See* Correlation consistent
basis sets

Becke's correlation functionals, spin
resolution, 21

BLYP and B3LYP functionals
exchange-correlation energy, 18*t*,
19*t*

quantum chemistry, 20

Bond breaking

assessment of multi-reference
methods, 81, 83–84

assessment of single-reference
methods, 78–81

errors in potential energies for CH₄
using multi-reference methods,
82*f*

errors in potential energy curves for
CH₄, 80*f*

extended coupled-cluster (ECC),
59–61

F₂ molecule, 85*t*

ground-state energies of nitrogen,
56*t*, 63*t*

minimalist configuration-
interaction approaches, 84–86

non-parallelity error (NPE) for BH,
HF and CH₄, 82*t*

potential energy curves for CH₄
using restricted orbitals, 79*f*

potential energy curves for CH₄
using unrestricted orbitals, 80*f*

potential energy curves for N₂
molecule, 57*f*, 64*f*

problem, 75–78

quasi-variational and quadratic
method of moments of coupled-
clusters (MMCC) methods, 54–
58

spin-flip method, 96

See also Extended coupled-cluster
(ECC) theory

Born–Oppenheimer approximation
computational thermochemistry,
154

electronic energy of molecule, 169

electronic kinetic energy, 176

C

Charge-density susceptibilities
definition, 169–170

- nonlocal, 171–173
- Chemical problems, electron correlation, 104
- Complete-active-space second-order perturbation theory (CASPT2), bond-breaking, 83
- Complete-active-space self-consistent-field (CASSCF) method, bond-breaking in CH₄, 82*f*, 83
- Complete basis set (CBS) correlation energy, 116, 117
- Gaussian basis sets converging towards CBS limit, 126
- mean unsigned errors, root-mean-square errors, and costs, 160, 162*t*
- mean unsigned error vs. cost for method, 160, 164*f*
- Complete configuration interaction (CCI), description, 155
- Computational effort. *See* Economical description of electron correlation
- Computational thermochemistry. *See* Multilevel methods for thermochemistry
- Configurational interaction singles (CIS), excited state model, 91*f*
- Configuration interaction (CI) calculations accuracy, 104 incremental correlation energy, 126 similarity-transformed Hamiltonian, 9–10 *See also* Correlation consistent basis sets
- Configuration interaction (CI) methods configurations from split-localized molecular orbitals (MOs), 109*f* convergence rate of SDTQ-CI truncated expansions, 109*f* convergence rate of truncated SDTQ-CI expansions, 113*f* correlation energies, 27–28 minimalist, for bond breaking, 84–86 orbital optimization of truncated SDTQ-CI expansions, 114, 115*t* ordering of configurations, 108, 110 truncation by a priori configuration selection, 111–112 truncation criterion, 110–111 truncation of known CI expansion, 108–111
- Configuration spaces, reducing size a priori, 106
- Consistent basis sets. *See* Correlation consistent basis sets
- Correlated basis functions for large molecules calculations of He ground-state energy in subsets, 10*f* computed equilibrium atomization energies, 7*t* Coulomb hole of He ground state, 2*f* description of electron correlation, 2 effect of adjustable parameter on number of vanishing integrals, 8, 9*f* examples of R12 calculations, 6–7 externally contracted MP2 method, 4–5 formulation of R12 theory, 3–4 Ne atom absolute pair energy, 7*t* orbital-invariant MP2-R12 method, 5–6 R12 methods, 2–9 R12 methods augmented with Gaussian geminals, 8–9 similarity-transformed Hamiltonian, 9–10 slow convergence of computed to exact wave function, 2 valence shell MP2 correlation energy in H₂O, 5*t*

- Correlation consistent basis sets
- all-electron basis sets for mercury (Hg), 138–140
 - all-electron basis sets for yttrium (Y), 135
 - all-electron correlation energies for non-relativistic (NR) and DK-relativistic CISD calculations for Hg atom, 141*f*
 - all-electron sets, 126–127
 - basis set errors for HF energy and CISD correlation energy with final cc-pVnZ-PP basis sets for ¹S and ³P states of Hg, 139*f*
 - basis set errors for HF energy and CISD correlation energy with final cc-pVnZ-PP basis sets for Y, 134*f*
 - cc-pRXnZ basis sets for Y, 130–134
 - cc-pVnZ-PP basis sets for Hg, 135–138
 - CCSD(T) (coupled cluster singles and doubles with perturbative triples) spectroscopic constants for ⁴Π state of YC, 142*t*
 - CCSD(T) spectroscopic constants for X¹Σ⁺ state of HgH⁺, 144*t*
 - contributions of correlating functions to average CISD correlation energy of 5s² 4d, 5s 4d², and 4d³ states of Y, 131*f*
 - contributions of correlating functions to CISD correlation energy of 5d¹⁰ state of Hg, 136*f*
 - final cc-pVnZ-PP basis sets, 133, 138
 - Gaussian basis sets converging toward complete basis set (CBS) limit, 126
 - Hartree–Fock (HF) base sets from extended even tempered (ExtET) expansions, 129
 - HF errors relative to base set vs. number of functions in
 - expansions for 5s² 4d state of Y, 132*f*
 - HF errors relative to basis set vs. number of functions for Hg, 137*f*
 - methodology, 127–140
 - molecular benchmarks, 140–147
 - optimization in presence of ECP, 129–130
 - post-*d* elements Ga–Rn, 128
 - pseudopotentials (PP), 126
 - relativistic effective core potentials (ECPs), 126
 - spectroscopic constants for X¹Σ⁺ HgH⁺, 145*t*
 - spectroscopic constants for X¹Σ_g⁺ state of Hg₂, 146*t*, 148*t*
 - steps in development of, 127
 - strategies for transition metals, 128–129
 - X¹Σ⁺ HgH⁺, 143–144
 - X¹Σ_g⁺ Hg₂, 144–145, 147
 - X⁴Π for yttrium monocarbide (YC), 140–143
 - See also* Mercury (Hg); Yttrium (Y)
- Correlation energy
- configuration interaction (CI) methods, 27–28
 - equations estimating, 28–29
 - high- and low-density limits, 16–17
 - parallel-spin and anti-parallel-spin, 22
 - parameterizations, 16–17
 - spin resolution of, in uniform density limit, 21–23
- Correlation recovery, two-stage process, 104
- Cost function, test molecules, 157
- Coulomb energy, electron-electron interactions, 170
- Coulomb potential, electronic kinetic energy, 176
- Coupled-cluster (CC) methods
- accuracy, 104

"black-box" character, 39, 58
 bond breaking in N₂, 54–58
 errors in approximating single-reference methods for CH₄!, 81
 extended CC (ECC) theory
 usefulness, 41–42
 extending, to potential energy surfaces (PESs), 37–38
 ground state, 91*f*
 improving T1! and T2! components by ECC theory, 58–67
 including higher excited clusters, 38–39
 method of moments of CC (MMCC) equations, 42–46
 MMCC formalism, 39–40
 MMCC methods, 40
 multi-reference CC (MRCC) formalisms, 38
 non-parallelity error (NPE), 81, 82*t*
 potential energy surfaces (PESs) involving breaking bonds, 40–41
 quasi-variational and quadratic MMCC methods, 47–58
 single-reference like approaches, 39
 theoretical considerations of MMCC, 47–54
See also Extended coupled-cluster (ECC) theory

D

Density functional theory (DFT)
 aniline protonation prediction errors, 189–190
 least expensive correlated approach, 104
 mean unsigned errors, root-mean-square errors, and costs, 160, 163*t*
 mean unsigned error vs. cost, 160, 164*f*

protonation site of aniline, 184–185
See also Self-consistent Hartree–Fock–Wigner calculations
 Density limit. *See* Exchange–correlation energy functionals
 Density parameter, definition, 14
 Diffuse functions
 atomization energies and electron affinities of lithium hydride, 159*t*
 hydrogen in metal hydride, 158, 160
 Diradicals
 degeneracy between degenerate states, 99–100
 equilibrium geometries, harmonic vibrational frequencies and adiabatic excitation energies for singlet methylene, 98*t*
 methylene and trimethylenemethane (TMM), 97
 π -system of TMM, 98, 99*f*
 spin-flip method, 97–100
 TMM electronic configuration of ground state, 99*f*
 Dissociation energies, F₂ molecule, 85*t*
 Douglas–Kroll–Hess (DK) Hamiltonian, basis sets for Hg, 139–140
 Dynamical correlation, short-range electron correlation, 76
 Dynamic electron correlation energy
 accurate estimation method, 105, 114, 120
 estimate and analysis by localized orbitals, 114–120
 group correlation contributions, 116–117
 numbers of orbitals, orbital pairs, and comparing valence correlation energies, 118*t*, 119*t*
 semi empirical formula, 114–115

simplifying assumptions, 116
sources of error, 117, 120

E

Economical description of electron correlation

accuracy by various approaches, 104
complete basis set (CBS)-limit data, 116, 117
configuration interaction (CI) from split-localized molecular orbitals (MOs), 109*f*
deletion of determinants, 108
dynamic correlation energy estimate and analysis by localized orbitals, 114–120
energies of full and truncated SDTQ-CI full optimized reaction space model (FORS1 and FORS2) calculations, 115*t*
formulation of objective, 105–107
method for accurate estimation of dynamic electron correlation energy, 105, 114–117, 120
method for selecting a priori configurations for milli-hartree accuracy, 105
numbers of orbitals, orbital-pairs and comparison of valence correlation energies, 118*t*, 119*t*
orbital determination, 107–108
orbital optimization of truncated SDTQ-CI expansions, 114, 115*t*
ordering of configurations, 108, 110
rate of convergence of SDTQ-CI truncated expansions for FORS1 and FORS2 active spaces for HNO and NCCN, 109*f*
rate of convergence of truncated SDTQ-CI expansions, 113*f*

reducing configuration spaces in large molecules, 105–114
seven group correlation contributions, 116–117
simplifying assumptions, 116
source of errors in fittings, 117, 120
split-localized FORS molecular orbitals, 107–108
strongly and weakly occupied approximate FORS molecular orbitals, 107
truncation by a priori configuration selection, 111–112
truncation criterion, 110–111
truncation of known CI expansion, 108–111
two-stage process for recovery of correlation, 104

Effective core potentials (ECP)
correlation consistent basis sets, 126–127

optimization of basis functions in presence of, 129–130

See also Correlation consistent basis sets

Electron affinities (EAs)
lithium hydride, 159*t*
test set, 157–158

Electron correlation
motion of electrons, 75–76
See also Economical description of electron correlation

Electron-electron interaction energy, self-energy, 177–178

Electron-electron interactions,
Coulomb energy, 170

Electronic charge density
electronic potential energy, 173, 174

instantaneous, 170–171

Electronic energy, total, of molecule, 169–170

Electronic kinetic energy, virial theorem, 176–177

- Electronic potential energy, total, of molecule, 173–176
- Electrons, potential energy, 170
- Equation-of-motion (EOM), excited state model, 91*f*
- Equilibrium atomization energies, R12 calculations, 6–7
- Equilibrium bond length, F₂ molecule, 85*t*
- Equilibrium structure, determination for polyatomic molecule, 194
- Ethylene
ground state wavefunction, 92*f*
spin-flip method for bond-breaking, 96
- Euler's theorem, electronic kinetic energy, 176
- Exchange-correlation energy functionals
analytic or semi-analytic many-body methods, 17
BLYP and B3LYP functionals in quantum chemistry, 18*t*, 19*t*, 20
correlation energy, 16–17
essentially-exact PW92 (Perdew and Wang) exchange-correlation energy per electron, 17, 18*t*, 19*t*
exchange energy, 16
generalized gradient approximation (GGA), 14
Gunnarsson–Lundqvist (GL) parameterization, 17, 18*t*, 19*t*
Hedin and Lundqvist (HL) parameterization, 17, 18*t*
knowledge about uniform density limit, 15–17
Moruzzi, Janak and Williams (MJW) parameterization, 17, 18*t*, 19*t*
parallel-spin and anti-parallel-spin correlation energies, 22
parallel-spin and anti-parallel-spin exchange-correlation energies, 22–23
performance of energy functionals in uniform density limit, 20–21
random phase approximation (RPA), 17, 18*t*, 19*t*
ratio of approximate to exact exchange energy per electron, 21*t*
Singwi, Sjölander, Tosi and Land (SSTL) calculation, 17
spin resolution of correlation energy in uniform density limit, 21–23
spin resolution of correlation energy of spin-unpolarized uniform electron gas, 22*t*
Vosko, Wilk and Nusair (VWN5) approximation, 17, 18*t*, 19*t*
why uniform density limit, 13–15
- Exchange energy, uniform electron density, 16
- Excited states, approximate methods, 90, 91*f*
- Explicitly correlated Gaussian (ECG) methods, small molecule accuracy, 8
- Extended coupled-cluster (ECC) theory
applicability, 61–62
components T₁ and T₂ in bond breaking region, 59–60
ground-state energies of N₂ molecule, 63*t*
improving T₁ and T₂ components by, 58–67
overlaps of wave functions, 66*f*
potential energy curves for N₂ molecule, 64*f*
triple bond breaking in N₂, 64–65
- F**
- Filatov and Thiel (FT) parameterization

exchange-correlation energy, 17, 18*t*, 19*t*
 scaling relation, 22
 Fluctuation correlations, definition, 170–171
 Fluctuation-dissipation theorem
 averaged potential energy, 175
 charge-density susceptibility, 174–175
 long-range exchange-correlation effects, 171
 nonlocal charge-density susceptibilities, 171–173
 short- and long-range fluctuation correlations, 171
 Fluorine F₂, equilibrium bond lengths and dissociation energies, 85*t*
 Force fields
 harmonic and cubic, of Si₃, 195–196
See also Silicon trimer
 FORS. *See* Full optimized reaction space model (FORS)
 Full configuration interaction (FCI)
 bond breaking model, 77
 description, 154, 155
 Full optimized reaction space model (FORS)
 convergence rate of SDTQ-CI truncated expansions for, active spaces for HNO and NCCN, 109*f*
 energies of full and truncated SDTQ-CI FORS calculations, 115*t*
 formal minimal valence basis orbitals, 105
 orbital determination, 107–108
 split-localized FORS molecular orbitals, 107–108
 strongly and weakly occupied approximate FORS molecular orbitals, 107
 types of full spaces FORS1 and FORS2, 106

See also Economical description of electron correlation
 Functionals. *See* Exchange-correlation energy functionals

G

Gaussian basis sets, convergence toward complete basis set (CBS) limit, 126
 Gaussian geminals, augmenting R12 method with, 8–9
 Gaussian methods
 mean unsigned errors, root-mean-square errors, and costs, 160, 161*t*
 mean unsigned error vs. cost for method, 160, 164*f*
 reducing cost of explicitly correlated calculations, 155–156
 Generalized gradient approximation (GGA), exchange-correlation energy, 14
 Gori–Giorgi, Sachetti and Bachelet (GSB), spin resolution of correlation energy, 22
 Ground state
 approximate methods, 90, 91*f*
 wavefunction of ethylene, 92*f*
 Gunnarsson–Lundqvist (GL) parameterization, exchange-correlation energy, 17, 18*t*, 19*t*

H

Hamiltonian, similarity-transformed, 9–10
 Hartree–Fock (HF)
 base sets from extended even tempered expansions, 129
 basis set errors for HF energy and CISD correlation energy of mercury (Hg), 139*f*

- basis set errors for HF energy and CISD correlation energy of yttrium (Y), 134*f*
 calculations for Y, 130
 correlation energy in configuration interaction (CI) calculations, 126
 errors relative to base set for Hg, 137*f*
 errors relative to base set for Y, 132*f*
 optimization of HF primitive sets for Hg, 135, 137
 optimization of *spd* HF sets, 132–133
 protonation site of aniline, 184, 188
 restricted open-shell HG (ROHF) orbitals, 140–141
See also Restricted Hartree–Fock (RHF); Unrestricted Hartree–Fock (UHF)
- Hartree–Fock (HF) model, ground state, 91*f***
- Hartree–Fock (HF) theory**
 AM1 and PM3 semi-empirical methods, 154–155
 single-reference methods, 154
See also Multilevel methods for thermochemistry
- Hartree–Fock–Wigner (HFW) method**
 digestion HFW integrals, 30–31
 errors in HFW/STO-3G energies, 33*t*
 errors in non-self-consistent field (non-SCF) and HFW energies, 32*t*
 extra computational cost for implementing, 29–30
 self-consistent scheme, 28
 standalone program, 31
See also Self-consistent Hartree–Fock–Wigner calculations
- Hedin and Lundqvist (HL)**
 parameterization, exchange–correlation energy, 17, 18*t*
- Helium ground state**
 Coulomb hole, 2*f*
 energy calculations, 10*f*
- Hellmann–Feynman theorem, electronic kinetic energy, 176**
- Hg. *See* Mercury (Hg)**
- Hohenberg–Kohn theorem, electronic kinetic energy, 171**
- Huzinaga and Klobukowski (HK), basis sets for Hg, 139**
- Hybrid density functional theory (DFT)**
 mean unsigned errors, root-mean-square errors, and costs, 160, 163*t*
 mean unsigned error vs. cost, 160, 164*f*
- Hydrogen, diffusion functions, 158, 160**
- I**
- Interelectronic distances**
 two-electron integrals, 4
 wave function, 2
- Ionization potentials (IPs), test set, 157**
- Ion mobility/mass spectroscopy method, protonation site of aniline, 184**
- L**
- Laboratory microwave data, equilibrium structures, 194**
- Large molecules**
 generating rapidly converging configurational expansion, 106
 number of occupied self-consistent field (SCF) orbitals, 106
 orbital determination, 107–108
 reducing configurational spaces, 105–114

- See also* Correlated basis functions for large molecules
- Linear response (LR), excited state model, 91*f*
- Lithium hydride
atomization energies and electron affinities, 159*t*
diffuse functions on hydrogen, 158, 160
- Local spin density (LSD)
approximation, exchange-correlation energy, 13–14
- M**
- Mercury (Hg)
all-electron basis sets for Hg, 138–140
all-electron correlation energies from non-relativistic (NR) and DK-relativistic CISD calculations, 141*f*
basis set errors for Hartree–Fock (HF) energy and CISD correlation energy, 139*f*
cc-pVnZ-PP basis sets for Hg, 135–138
CCSD(T) spectroscopic constants for $X^1\Sigma^+$ state of HgH^+ , 144*t*
contributions of correlating functions to CISD correlation energy of Hg, 136*f*
final cc-pVnZ-PP basis sets, 138
HF errors relative to base set, 137*f*
optimization of HF primitive sets, 135, 137
spectroscopic constants of $X^1\Sigma^+$ for HgH^+ , 145*t*
spectroscopic constants of $X^1\Sigma_g^+$ state of Hg_2 , 146*t*, 148*t*
 $X^1\Sigma^+$ of mercury hydride cation HgH^+ , 143–144
 $X^1\Sigma_g^+$ for Hg dimer, 144–145, 147
- Methane (CH_4)
error in potential energies for CH_4 using multi-reference methods, 82*f*
errors in potential energies, 80*f*, 81
non-parallelity error (NPE), 81, 82*t*
potential energy curves, 79*f*, 80*f*
- Method of moments of coupled-cluster (MMCC)
bond breaking in N_2 , 54–58
equations, 42–46
formalism, 39–40
ground-state formalism, 42–46
quadratic MMCC (QMMCC)
variant, 41–42
quasi-variational MMCC (QVMMCC) formalism, 41–42
QVMMCC and QMMCC methods, 47–58
theory of QVMMCC and QMMCC, 47–54
types, 40
- Methylene
equilibrium geometries, harmonic vibrational frequencies, and adiabatic excitation energies, 98*t*
spin-flip method, 97
See also Spin-flip approach
- Microwave data, equilibrium structures, 194
- Minimalist configuration-interaction approaches, bond breaking, 84–86
- Møller–Plesset, second-order (MP2) theory
accuracy, 104
computation, 28
externally contracted MP2 method, 4–5
orbital-invariant MP2-R12 method, 5–6
- Møller–Plesset theory (MP), ground state, 91*f*
- Molecules
electronic potential energy, 173–176
total electronic energy, 169–170

Monte Carlo data

- parameterizations for fitting, 16
- spin resolution of correlation energy, 22–23

Moruzzi, Janak and Williams (MJW), exchange-correlation energy, 17, 18*t*, 19*t***Multi-coefficient correlation methods (MCCM)**

- mean unsigned errors, root-mean-square errors, and costs, 160, 161*t*, 162*t*
- mean unsigned error vs. cost, 160, 164*f*

Multilevel methods for thermochemistry

- AMI and PM3 semi-empirical methods, 154–155
- atomization energies and electron affinities for LiH, 159*t*
- Born–Oppenheimer approximation, 154
- complete basis set (CBS) methods, 156
- complete configuration interaction (CCI), 155
- cost function, 157
- density functional theory (DFT), 156
- diffuse functions on hydrogen, 158, 160
- errors for DFT, hybrid DFT, and AMI methods, 160, 163*t*
- errors for multilevel methods, 160, 161*t*
- errors for multilevel methods with lower costs, 160, 162*t*
- Gaussian-2 (G2), G3 and G3 extended (G3X) methods, 155–156
- Hartree–Fock (HF) theory, 154
- hybrid DFT functionals, 156
- hybrid DFT methods, 157
- mean unsigned error vs. cost for all methods, 160, 164*f*

methods and test data, 156–158

- multi-coefficient correlation methods (MCCM), 155
- quadratic configuration interaction with double and single excitations and quasi-perturbative connected triples (QCISD(T)), 156
- scaling-all-correlation (SAC) method, 155
- scaling external correlation (SEC), 155

Multi-reference coupled-cluster (MRCC) formalisms

- bond breaking, 38
- reduced MRCCSD (single, double) method, 39
- See also* Coupled-cluster (CC) methods

Multi-reference methods

- assessment, 81, 83–84
- balanced treatment of electron correlation, 76

N

- Ne atom, absolute pair energy, 7*t*
- Nitrogen atom, protonation site of aniline, 184
- Nitrogen molecule
 - bond breaking in N₂, 54–58
 - ground-state energies, 56*t*, 63*t*
 - potential energy curves (PEC), 57*f*, 64*f*
- Nondynamical correlation, long-range electron correlation, 76
- Nonlocal charge-density susceptibilities
 - coupling-constant formalism, 172
 - dielectric response function, 172–173
 - electronic potential energy, 173–176
 - nonlocal polarizability density, 172

- quantum mechanical equation, 171–172
 static charge-density susceptibility, 172
- Non-parallelity error (NPE)**
 BH, HF, and CH₄ molecules, 82*t*
 quantifying errors, 81
- O**
- Orbital determination, full optimized reaction space model (FORS),** 107–108
- P**
- Parameterizations, correlation energy,** 16–17
- Perdew and Wang (PW), scaling relation,** 21, 22*t*
- Perdew and Wang (PW92)**
 approximation, exchange-correlation energy, 17, 18*t*, 19*t*
- Perdew and Zunger (PZ)**
 parameterization, exchange-correlation energy, 16, 18*t*, 19*t*
- PM3 semi-empirical method,** description, 154–155
- Polyatomic molecule**
 equilibrium structure, 194
See also Silicon trimer
- Potential energy curves**
 CH₄ using restricted orbitals, 79*f*
 CH₄ using unrestricted orbitals, 80*f*
 comparing spin-flip self-consistent field (SF-SCF) and spin-complete alternative, 86*f*
 errors in potential energies for CH₄, 80*f*
See also Bond breaking
- Potential energy of electrons**
 fluctuation-dissipation theorem, 175
- quantum mechanical average, 170
- Potential energy surfaces (PESs)**
 extending coupled-cluster (CC) methods to, 37–38
See also Extended coupled-cluster (ECC) theory
- Proton affinities**
 aniline, 187*t*
 calculations, 185
 protonation of aniline, 189
- Protonation site of aniline**
 computed total atomization energy and proton affinities, 187*t*
 density functional theory (DFT) reactivity indices, 184–185
 DFT predictions, 189–190
 gas phase, 184
 Hartree–Fock and semi-empirical calculations, 184
 ion mobility/mass spectroscopy method, 184
 methods, 185–186
 nitrogen atom in solution, 184
 potential sources of error, 189
 preferred, in solution, 184
 proton affinity calculations, 185
 relative energies of three protonated species, 188
 resonance stabilization of aromatic vs. non-aromatic systems, 188
- Pseudopotentials (PP), correlation consistent basis sets,** 126–127
- Q**
- Quadratic configuration interaction**
 with double and single excitations and quasi-perturbative connected triples (QCISD(T))
 approximating large-basis-set, 156
 mean unsigned errors, root-mean-square errors, and costs, 160, 161*t*, 162*t*
 single-level method, 160

Quantum chemistry, bond breaking problem, 75–78

R

R12 methods

- augmentation with Gaussian geminals, 8–9
 - computed equilibrium atomization energies, 7*t*
 - Coulomb hole in He ground state, 2*f*
 - effect of adjustable parameter on number of vanishing integrals, 8, 9*f*
 - electron correlation including interelectronic distances, 2
 - examples of R12 calculations, 6–7
 - explicitly correlated Gaussians (ECG) methods, 8
 - externally contracted MP2 method, 4–5
 - formulation of R12 theory, 3–4
 - MP2-R12 method, 4–5
 - Ne atom absolute pair energy, 7*t*
 - orbital-invariant MP2-R12 method, 5–6
 - resolution-of-identity (RI) approximation, 6
 - slow convergence of computed vs. exact wave function, 2
 - valence shell MP2 correlation energy in H₂O, 5*t*
- Random phase approximation (RPA), exchange-correlation energy, 17, 18*t*, 19*t*
- Recovery of correlation, two-stage process, 104
- Relativistic effective core potentials correlation consistent basis sets, 126–127
- See also* Correlation consistent basis sets

- Restricted active space configuration interaction (RASCI) approach, bond-breaking, 83–84
- Restricted Hartree–Fock (RHF) errors in potential energies for CH₄, 80*f*
- failure, 78–79
- Rotational constants, vibration-rotation contributions, 194–195

S

- Scaling-all-correlation (SAC) method description, 155
- mean unsigned errors, root-mean-square errors, and costs, 160, 162*t*
- Scaling external correlation (SEC), description, 155
- Schmidt, Kurth, Tao and Perdew (SKTP), scaling relation, 22
- Second-order configuration interaction (SOC) approach, bond-breaking, 83–84
- Self-consistent field (SCF), ground state model, 91*f*
- Self-consistent Hartree–Fock–Wigner calculations correlation method, 31–34
- errors in HFW/STO-3G energies, 33*t*
- errors in non-SCF and HFW energies, 32*t*
- Fock matrix, 30
- optimizing parameters, 31
- standalone program, 31
- theory, 28–31
- Wigner intracule, 28, 31
- Self-energy, electron-electron interaction energy, 177–178
- Self-interaction effects, Coulomb energy, 170
- Semi-empirical methods AM1 and PM3, description, 154–155

- Silicon**
 abundance, 193
 isomers of cyclic SiC₃ molecule, 194
- Silicon trimer**
 calculating harmonic and cubic force fields, 195–196
 harmonic frequencies and cubic force constants for normal isotopomer, 197*t*
 independent structural parameters, 196, 198
 refined structural parameters for, 198*t*
 studying and labeling five isotopomers, 196
 vibration-rotation contribution to rotational constants, 194–195
- Similarity-transformed Hamiltonian, configuration-interaction (CI) calculations, 9–10**
- Single-reference methods**
 assessment, 78–81
 Hartree–Fock starting point, 154
 potential energy curves for CH₄, 79*f*, 80*f*
 strategies for bond breaking problem, 76–77
 well-behaved molecules, 90
- Singwi, Sjölander, Tosi and Land (SSTL), exchange-correlation energy, 17**
- Spin-flip approach**
 bond breaking, 77–78, 84, 96
 configuration interaction, 84–85
 diradicals, 97–100
 ethylene torsional potential, 96
 hierarchy of spin-flip (SF) models, 95*f*
 high-spin triplet reference state, 93–94
 method, 93–95
 potential energy curves for HF, 86*f*
 two electrons in three orbitals system, 95*f*
- Spin resolution, correlation energy in uniform density limit, 21–23**
- T**
- Theoretical model chemistry, approximations to exact wavefunction, 90, 91*f***
- Theory, formulation of R12, 3–4**
- Thermochemistry. *See* Multilevel methods for thermochemistry**
- Torsional potential, ethylene, 96**
- Transition metal elements**
 development of accurate basis sets, 128
See also Mercury (Hg); Yttrium (Y)
- Trimethylenemethane (TMM)**
 electronic configuration of ground state, 99*f*
 π-system, 98, 99*f*
 spin-flip method, 99–100
See also Diradicals
- Two-electron density functional theory. *See* Self-consistent Hartree–Fock–Wigner calculations**
- U**
- Uniform density limit**
 exact constraints, 14–15
 generalized gradient approximation (GGA), 14
 knowledge about, 15–17
 local spin density (LSD) approximation, 13–14
 performance of energy functionals in, 20–21
 purpose, 13–15
 spin resolution of correlation energy in, 21–23
See also Exchange-correlation energy functionals

Unrestricted Hartree–Fock (UHF)
 bond breaking, 76–77
 description of bond breaking, 79,
 80 f

V

Valence-bond approach, predictions,
 104
 Vibration-rotation contributions,
 rotational constants, 194–195
 Virial theorem, electronic kinetic
 energy, 176
 Vosko, Wilk and Nusair (VWN5)
 approximation, exchange-
 correlation energy, 17, 18 t , 19 t

W

Wave function
 convergence of computed, to exact,
 2
 interelectronic distances, 2, 4
 Wigner (W) approximation, exchange-
 correlation energy, 18 t , 19 t , 20
 Wigner intracule

two-electron phase-space
 distribution, 28
See also Self-consistent Hartree–
 Fock–Wigner calculations

Y

Yttrium (Y)
 all-electron basis sets for Y, 135
 basis set errors for Hartree–Fock
 (HF) energy and CISD (singles
 and doubles CI) correlation
 energy, 134 f
 cc-pRVnZ basis sets for, 130–
 134
 CCSD(T) spectroscopic constants
 for $^4\Pi$ state of YC, 142 t
 CISD optimizations, 130, 132
 contributions of correlating
 functions to CISD correlation
 energy, 131 f
 final cc-pVnZ-PP basis sets, 133
 HF errors relative to base set, 132 f
 optimization of *spd* HF sets, 132–
 133
 $X^4\Pi$ for yttrium monocarbide
 (YC), 140–143